

**Environmental Biotransformation of Chiral Polychlorinated Biphenyls
and Their Metabolites**

by

Zhe Lv

A thesis submitted to the Faculty of Graduate Studies of

the University of Manitoba

in partial fulfillment of the requirements of the degree of

DOCTOR OF PHILOSOPHY

Department of Chemistry

University of Manitoba

Winnipeg

Copyright © 2013 by Zhe Lv

Abstract

This dissertation combines laboratory and field experiments to investigate the mechanisms of atropisomer enrichment for chiral polychlorinated biphenyls (PCBs) and their metabolites in organisms. Stereoselective biotransformation and bioaccumulation were identified as two major reasons for the different environmental fate of PCB atropisomers. Other affecting factors, such as presence of nanoparticles and changes in feeding ecology of organisms, also affect the fate of chiral contaminants.

In vitro incubations of rat cytochrome P-450 2B1 (CYP2B1) isozyme with chiral PCBs indicated that different biotransformation kinetics and competition among PCB congeners or between atropisomers were two main factors affecting atropisomer enrichment. Different interactions between chiral PCB congeners or atropisomers with rat CYP2B1 may occur at the molecular level. Non-racemic *meta*-hydroxylated-PCBs (5-OH-PCBs) were the major metabolites. CYP-mediated stereoselective formation of dihydroxylated PCBs from OH-PCBs was observed. Gold nanoparticles affected biotransformation activity of rat CYP2B1 and changed PCB atropisomeric composition, directly by electrostatic interaction, or indirectly by changes to the surrounding ionic strength. Thus, stereoselective metabolism of chiral PCBs and OH-PCBs by CYPs is a major mechanism for atropisomer enrichment of PCBs and their metabolites in the environment, with the degree of enrichment dependent, at least in part, on charged nanoparticles and stereoselective interference of atropisomers with each other at the enzyme level.

The atropisomer compositions of chiral PCBs were measured in the marine biota of Cumberland Sound (Canada) and Svalbard (Norway). High trophic level organisms, including harp seal, beluga, and narwhal reported for the first time, had species-specific atropisomer signatures, likely due to a combination of *in vivo* biotransformation and trophic transfer. PCB chiral signatures in Greenland sharks supported the hypothesis that some of these PCB atropisomer compositions shifted over time and space, possibly due to a change in feeding ecology. To our knowledge, this is the first report to investigate temporal trends of PCB atropisomer signatures in Arctic biota.

Acknowledgements

I would like to thank all those who have offered me help during the five years of study and research at the University of Manitoba and the University of Winnipeg. I am thankful to the following people. They played important roles in the completion of my work: my supervisor, Dr. Charles S. Wong, for his continuous support, including constant encouragement, abundance of creative ideas, excellent advice and patience; my committee members, Dr. Feiyue Wang, Dr. Annemieke Farenhorst and Dr. Sean McKenna, for their sound and critical advice; external examiner, Dr. Frank Wania; all Wong research group members; Dr. Jonathan G. C. Veinot, Dr. Guibin Ma, Dr. Rhett J. Clark, Dr. Nick Warner, Dr. Hans-Joachim Lehmler, Dr. Izabela Kania-Korwel, Dr. Gregg T. Tomy, Dr. Bruno Rosenberg, Dr. Aaron T. Fisk, Dr. Fasheng Li, Dr. Weiping Liu, Jennifer Low, Joel Smigelski and Gundars Reinfelds for helpful technical assistance, discussion and advice; funding from the Canada Research Chairs Program, Natural Sciences and Engineering Research Council of Canada, Manitoba Health Research Council, National Institute of Environmental Health Sciences, and a Chinese Government Award for Outstanding Self-Financed Students Abroad from the China Scholarship Council to myself; my wife, Yu Huang, for her love, understanding and unwavering support; my grandma Caiyun Li, my parents Jizheng Lv and Gaixiang Li, my parents-in-law Fadong Huang and Jianqin Zhang, and my aunts Runlan Lv and Fulan Lv for their love and support; my coming baby, William (Niu Niu), for his “encouragement” and others who were indirectly involved in my Ph.D. study and research.

Table of Contents

Abstract.....	I
Acknowledgements.....	III
Table of Contents.....	IV
List of Tables.....	X
List of Figures.....	XI
Chapter 1.....	1
Introduction to Polychlorinated Biphenyls and Their Chirality.....	1
1.1. Persistent Organic Pollutants.....	2
1.2. Polychlorinated Biphenyls and Their Metabolites.....	2
1.3. Chiral PCBs.....	6
1.4. Knowledge Gaps.....	8
1.5. Dissertation Hypotheses and Outline.....	9
References.....	12
Chapter 2.....	17
Factors Affecting Phase I Stereoselective Biotransformation of Chiral Polychlorinated Biphenyls (PCBs) by Rat Cytochrome P-450 2B1 Isozymes.....	17
2.1. Introduction.....	18
2.2. Materials and Methods.....	19
2.2.1. Chemicals and Regents.....	19
2.2.2. <i>In Vitro</i> Biotransformation Experiments.....	20

2.2.3. Instrumental Analysis.....	22
2.2.4. Kinetics and Statistical Analyses	23
2.2.5. Three-Dimensional Structure Modeling.....	24
2.2.6. Docking Study	25
2.3. Results and Discussion	25
2.3.1. Biotransformation Kinetics for PCB 45, 95 and 132.....	25
2.3.2. Competitive Biotransformation between Congeners	31
2.3.3. Competitive Biotransformation of Atropisomers.....	35
2.3.4. Docking Studies	36
References.....	42
Chapter 3.....	49
Disruption of Biomolecule Function by Nanoparticles: How Do Gold Nanoparticles Affect Phase I Biotransformation of Persistent Organic Pollutants?.....	49
3.1. Introduction.....	50
3.2. Materials and Methods.....	53
3.2.1. Chemicals and Reagents	53
3.2.2. Synthesis of Citrate-capped AuNPs	54
3.2.3. Characterization of Citrate-capped AuNPs.....	54
3.2.4. <i>In Vitro</i> Biotransformation Experiments.....	56
3.2.5. Chemical Extraction and Clean-up.....	56
3.2.6. Instrumentation and Measurements	56

3.2.7. Data Analyses.....	57
3.3. Results and Discussion	57
3.3.1. Stereoselective Biotransformation of PCB 95	57
3.3.2. DLS Characterization of AuNPs and Enzyme Solutions.....	62
3.3.3. Impacts of AuNPs on Buffer Conductance.....	66
3.3.4. Interactions between AuNPs and K ⁺	71
3.3.5. Influence of AuNPs on NADPH Production	75
3.3.6. The Effects of Buffer Salinity on NADPH Production and CYP Activity	79
3.3.7. Proposed Mechanism	83
References.....	85
Chapter 4.....	93
Stereoselective Formation of Mono- and Di-Hydroxylated Polychlorinated Biphenyls by Rat Cytochrome P450 2B1	93
4.1. Introduction.....	94
4.2. Materials and Methods.....	96
4.2.1. Chemicals and Regents	96
4.2.2. <i>In Vitro</i> Biotransformation Experiments.....	98
4.2.3. Chemical Extraction and Clean-up.....	98
4.2.4. Instrumentation and Measurements	100
4.2.5. Data Analyses.....	102
4.3. Results and Discussion	102

4.3.1. Stereoselective Biotransformation of Chiral PCBs.....	102
4.3.2. Stereoselective Formation of Hydroxylated PCBs	106
4.3.3. Stereoselective Biotransformation of OH-PCBs and Formation of DiOH-PCBs	110
4.3.4. Interference between the Two Atropisomers of PCB 136.....	112
4.3.5. Environmental Implications.....	117
References.....	118
Chapter 5.....	126
Temporal and Spatial Trends of Polychlorinated Biphenyl Chiral Signatures in the Greenland Shark (<i>Somniosus microcephalus</i>) and Its Arctic Food Web.....	130
5.1. Introduction.....	127
5.2. Materials and Methods.....	129
5.2.1. Sample Information	129
5.2.2. Atropisomer Analyses	132
5.2.3. Data Analyses	133
5.3. Results and Discussion	133
5.3.1. Spatial and Temporal Trends of PCBs	133
5.3.1.1. Cumberland Sound food web.....	134
5.3.1.2. Greenland sharks.....	137
5.3.2. Atropisomer Enrichment of Chiral PCBs in the Cumberland Sound Food	

Web.....	139
5.3.2.1. Zooplankton and benthic invertebrates.....	139
5.3.2.2. Pelagic fishes.....	140
5.3.2.3. Benthic fishes.....	141
5.3.2.4. Arctic char.....	141
5.3.2.5. Marine mammals.....	142
5.3.3. Temporal and Spatial Trends of PCB Chiral Signatures in Greenland	
Sharks.....	144
References.....	152
Chapter 6.....	163
Conclusions and Future Directions.....	163
6.1. Conclusions.....	164
6.2. Future Research Directions.....	167
6.2.1. Distribution of POPs in the Environment.....	167
6.2.2. Chiral Organic Pollutants.....	168
6.2.2.1. Interactions between chiral molecules.....	168
6.2.2.2. Stereospecific toxicities of chiral pollutants.....	169
6.2.2.3. Development of research material.....	169
6.2.2.4. Use of chirality as a forensics tool to detect environment change	170
Appendix 1.....	171
Chiral Polychlorinated Biphenyl Transport, Metabolism, and Distribution: A Review..	171

Appendix 2.....	214
Operation Procedures for Size and Zeta-potential Measurements of Nanoparticles by Dynamic Light Scattering.....	214
Appendix 3.....	226
GC-MS Chromatogram of Mono- and Di- Hydroxylated Metabolites.....	226
Appendix 4.....	236
PCB Concentrations and Trophic Levels of Cumberland Sound (Canada) Organisms Collected from 2007-2008.....	236
Appendix 5.....	345
PCB Concentrations in Greenland Sharks Collected from Cumberland Sound (Canada) from 1998 to 1999.....	345
Appendix 6.....	362
PCB Concentrations in Greenland Sharks Collected from Svalbard (Norway) from 2008 to 2009.....	362
Appendix 7.....	402
Enantiomer Fractions (EFs) of PCBs in Cumberland Sound (Canada) and Svalbard (Norway) Biota Collected from 1998 to 2009.....	402

List of Tables

Table 1.1 Basic physical properties of PCB homologs.....	4
Table 2.1 Parameters for Michaelis-Menten kinetics.	26
Table 3.1 Effective diameter and zeta potential of AuNPs and rat CYP2B1 mixture in incubation.....	63
Table 4.1 Initial substrate amounts for experiments to study interference between the two atropisomers of PCB136.....	99
Table 4.2 Comparison of Enantiomer Fractions (EFs) of 5-OH-PCB metabolites from different studies.....	109
Table 5.1 Comparison of PCB levels in different marine food webs.	149

List of Figures

Figure 1.1 The structure of PCB compounds.....	3
Figure 1.2 Generic phase I and II biotransformation pathway of PCBs.....	6
Figure 1.3 Conceptual flow chart of the study of chiral contaminants.....	8
Figure 2.1 Biotransformation kinetics of chiral PCBs 45, 95 and 132 with rat CYP 2B1.....	27
Figure 2.2 Competition curves of PCBs 45, 95 and 132 incubated with rat CYP2B1.	31
Figure 2.3 Inhibition kinetics for PCB 45, 95 and 132.....	33
Figure 2.4 Three-dimensional structure of rat CYP2B1 from homology modeling.	37
Figure 2.5 Ramachandran plots of the rat CYP2B1 model.	38
Figure 2.6 Docking poses of PCB 45, PCB 95 and PCB 132 with rat CYP2B1.....	39
Figure 3.1 TEM image of citrate-capped AuNPs and size distribution.....	55
Figure 3.2 Biotransformation activity of PCB 95 by rat CYP2B1 isozyme and change of EFs.	58
Figure 3.3 Effective diameter of AuNPs in potassium phosphate buffer.....	64
Figure 3.4 DLS-based particle distribution of different incubations after 30 and 60 minutes.....	67
Figure 3.5 Influence of AuNPs on the conductance of phosphate buffer solution over 20 min incubation.	68
Figure 3.6 Relationship between average conductance and K^+ concentration	70
Figure 3.7 UV-Vis Spectra of AuNPs in water as control sample (a) and phosphate buffer	

(b) (pH 7.4 and 110mM) over 20 minutes.	71
Figure 3.8 Color change of AuNPs in potassium phosphate buffer solution at room temperature.	72
Figure 3.9 UV-Vis Spectra of AuNPs in phosphate buffer in 20 minutes and effective diameter and UV-Vis adsorption λ_{\max} change of AuNPs in phosphate buffer over 20 minutes.	74
Figure 3.10 Theoretical position of the surface plasmon resonance peak (λ_{\max}) as a function of the particle diameter for AuNPs in water.	75
Figure 3.11 Selected UV-Vis spectra of NADPH formation activity by enzymatic reaction between solution A and solution B over 60 min.	76
Figure 3.12 Selected UV-Vis spectra of NADPH formation activity by enzymatic reaction between (a) solution A and cytochrome P-450 reductase (CPR) or (b) solution A and rat CYP 2B1 over 60 mins of incubation.	78
Figure 3.13 The influence of buffer salinity on NADPH production.	80
Figure 3.14 The influence of buffer salinity on CYP biotransformation activity and stereoselectivity of 100ng/mL PCB 95 or 500ng/mL PCB 95 for 30min incubation.	82
Figure 4.1 Stereoselective biotransformation of chiral PCBs and formation of hydroxylated metabolites by rat CYP2B1.	103
Figure 4.2 Stereoselective biotransformation of 4-95 and 5-95 and formation of 4,5-95 by rat CYP 2B1.	111
Figure 4.3 The two atropisomers of PCB 136 interfere with each other when biotrans-	

formed by rat CYP2B1.	113
Figure 4.4 The two atropisomers of PCB 136 interfere with each other when producing hydroxylated metabolites in biotransformation by rat CYP2B1.....	114
Figure 5.1 Location of sampling sites in Cumberland Sound, Nunavut, Canada and Svalbard, Norway.....	130
Figure 5.2 Total concentrations of PCBs in (A) organisms collected from the Cumberland Sound food web 2007-2008; and (B) Greenland sharks collected from Cumberland Sound and Svalbard at different times as stated.....	135
Figure 5.3 Temporal and spatial trends of chiral PCB concentrations in Greenland sharks collected from Cumberland Sound and Svalbard.	138
Figure 5.4 EFs for PCBs 91, 95, 136 and 149 for the organisms collected from Cumberland Sound food web.	140
Figure 5.5 Temporal and spatial trends of EFs of PCBs 91, 95, 136 and 149 in the Greenland sharks collected from Cumberland Sound and Svalbard..	145

Chapter 1

Introduction to Polychlorinated Biphenyls and Their Chirality

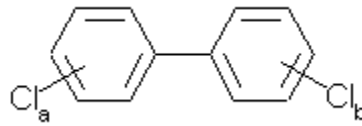
(Please See Details in Appendix 1)

1.1. Persistent Organic Pollutants

Persistent organic pollutants (POPs) are organic compounds that persist in the environment, bioaccumulate in organisms including humans, and pose a risk of causing adverse effects to organisms (1). POPs are widely distributed in air, water, soil, sediment, biota and the human body. These pollutants can stay in the environment for long periods of time due to their stable physical-chemical properties, as many environmental processes are insufficient to degrade these chemicals rapidly. They can be transported globally by atmospheric, oceanic or biologically-mediated pathways (2, 3). They are found even in polar regions, in which they have never been produced and used to any significant degree (4). Given slow removal processes and continual exposure, concentrations of some POPs build up in high trophic level organisms. These increasing concentrations can lead to levels that trigger adverse effects, which for POPs include endocrine disruption, interference with reproduction, immune system toxicity and carcinogenicity (1). Thus, it is important to understand the environmental behavior and fate of POPs in order to protect the health of organisms including humans.

1.2. Polychlorinated Biphenyls and Their Metabolites

Polychlorinated biphenyls (PCBs) are a well-known class of environmental POPs. There are 209 possible PCB congeners, which have between 1 to 10 chlorine atoms attached to a biphenyl core (Figure 1.1). Most of these congeners are colorless and odorless crystals. PCBs have low water solubility and low vapor pressure (Table 1.1) (5). They are easily dissolved in organic solvents, oils and fats. PCBs have high thermodynamic stability and cannot degrade easily. Due to these stable properties, they



$$a+b=1-10$$

Figure 1.1 The structure of PCB compounds

were widely used in dielectric fluids for transformers and capacitors, heat transfer fluids, hydraulic fluids, cutting oils and as additives in pesticides, plastics and flame retardants (6). These same stable physical-chemical properties make PCBs very difficult to remove from the environment once they are present as contaminants.

Although the production of PCBs has been widely banned since the mid-1970s, they still exist ubiquitously in the environment (water, atmosphere, soil, sediment and animals). They can bioaccumulate in organisms through food chains and lead to many toxic effects. For example, their reproductive toxicity, inhibition of growth, dermal toxicity, porphyrias (caused by a group of inherited or acquired disorders of certain enzymes in the human body which result in abdominal pain, vomiting, acute neuropathy and mental disturbances), immune system toxicity, hepatotoxicity and carcinogenicity have been observed via both *in vitro* and *in vivo* studies (6). The most infamous public health problem caused by PCBs is Yusho Disease, which first occurred in Japan in 1968. Rice bran oil contaminated with 280 kg of PCBs was accidentally used as chicken feed, resulting in a mass poisoning known as Yusho Disease in over 14,000 people. Common symptoms included dermal and ocular lesions, irregular menstrual cycles and a lowered immune response. Other symptoms included fatigue, headache, cough, and unusual skin

Table 1.1 Basic physical properties of PCB homologs (5)

PCB Isomer Group	Water Solubility (mol/m ³)	Vapour Pressure (Pa)	Henry's Law constant-K _H (Pa m ³ /mol)	Octanol-water Partition Coefficient (K _{ow})
Monochlorobiphenyl	2.12 × 10 ⁻²	1.10	5.19 × 10 ¹	5.01 × 10 ⁴
Dichlorobiphenyl	7.17 × 10 ⁻³	2.40 × 10 ⁻¹	3.35 × 10 ¹	1.26 × 10 ⁵
Trichlorobiphenyl	2.52 × 10 ⁻³	5.40 × 10 ⁻²	2.14 × 10 ¹	3.16 × 10 ⁵
Tetrachlorobiphenyl	8.90 × 10 ⁻⁴	1.20 × 10 ⁻²	1.35 × 10 ¹	7.94 × 10 ⁵
Pentachlorobiphenyl	3.03 × 10 ⁻⁴	2.60 × 10 ⁻³	8.57	2.00 × 10 ⁶
Hexachlorobiphenyl	1.05 × 10 ⁻⁴	5.80 × 10 ⁻⁴	5.51	5.01 × 10 ⁶
Heptachlorobiphenyl	3.54 × 10 ⁻⁵	1.30 × 10 ⁻⁴	3.67	1.26 × 10 ⁷
Ochtachlorobiphenyl	1.28 × 10 ⁻⁵	2.80 × 10 ⁻⁵	2.19	3.16 × 10 ⁷
Nonachlorobiphenyl	4.31 × 10 ⁻⁶	6.30 × 10 ⁻⁶	1.46	7.94 × 10 ⁷
Decachlorobiphenyl	1.52 × 10 ⁻⁶	1.40 × 10 ⁻⁶	9.19 × 10 ⁻¹	2.00 × 10 ⁸

sores. Additionally, in children, there were reports of poor cognitive development (6-8).

Therefore, there have been many studies focused on the environmental transport and fate of parent PCB compounds, as these processes and issues affect exposure. However, their transformation mechanisms and products are also of great environmental concern. Phase I (oxidation) and phase II (conjugation) reactions are two main metabolism processes of PCBs in higher organisms (e.g., mammals) (Figure 1.2). These reactions convert PCBs into more water soluble substances that can be better excreted in the urine or feces (9). Hydroxylated PCBs (OH-PCBs) and methylsulfonyl PCBs (MeSO₂-PCBs)

are the two main products of biotransformation (9). In phase I reactions, PCBs are oxidized by cytochrome P-450 (CYP) isozymes to generate PCB arene oxide intermediates and/or OH-PCBs (10,11). CYP isozymes can insert one oxygen atom from molecular oxygen into the substrate and reduce the second oxygen to form a water molecule. PCB arene oxide intermediates, if produced by CYPs, can be further biotransformed to OH-PCBs by epoxide hydroxylase (12). CYPs can also insert a hydroxyl group in a PCB substrate directly to produce OH-PCBs (Figure 1.2). In phase II reactions, PCB arene oxide intermediates can conjugate with phase II enzymes via the mercapturic acid pathway (MAP) to produce relatively hydrophilic MeSO₂-PCBs for final excretion (9). The arene oxide intermediates from phase I reactions can initially conjugate with tripeptide glutathione by either binding with glutathione-S-transferase (GST) or spontaneously. The PCB-glutathione conjugate can be further degraded by γ -glutamyltransferase and cysteinylglycine dipeptidase to remove glutamate and glycine of glutathione to produce the cysteine-PCB conjugate. This intermediate conjugation product can be further biotransformed to MeSO₂-PCBs by cysteine conjugate β -lyase, S-methyltransferase and CYPs in higher level organisms (9,13) (Figure 1.2).

OH-PCBs and MeSO₂-PCBs have been widely identified in organisms such as fishes (14,15), polar bears (15,16), and even human tissues (17). These metabolites are also of environmental concern because of their toxicities such as thyroid and estrogenic activity dysfunction in fish and birds (9,18), lung tissue distress, perturbing catalytic activity of enzymes (9), influence endocrine related processes (9), enzyme induction (19) and cell communication inhibition (20). Therefore, it is also important to understand the formation, metabolism and toxicities of these metabolites.

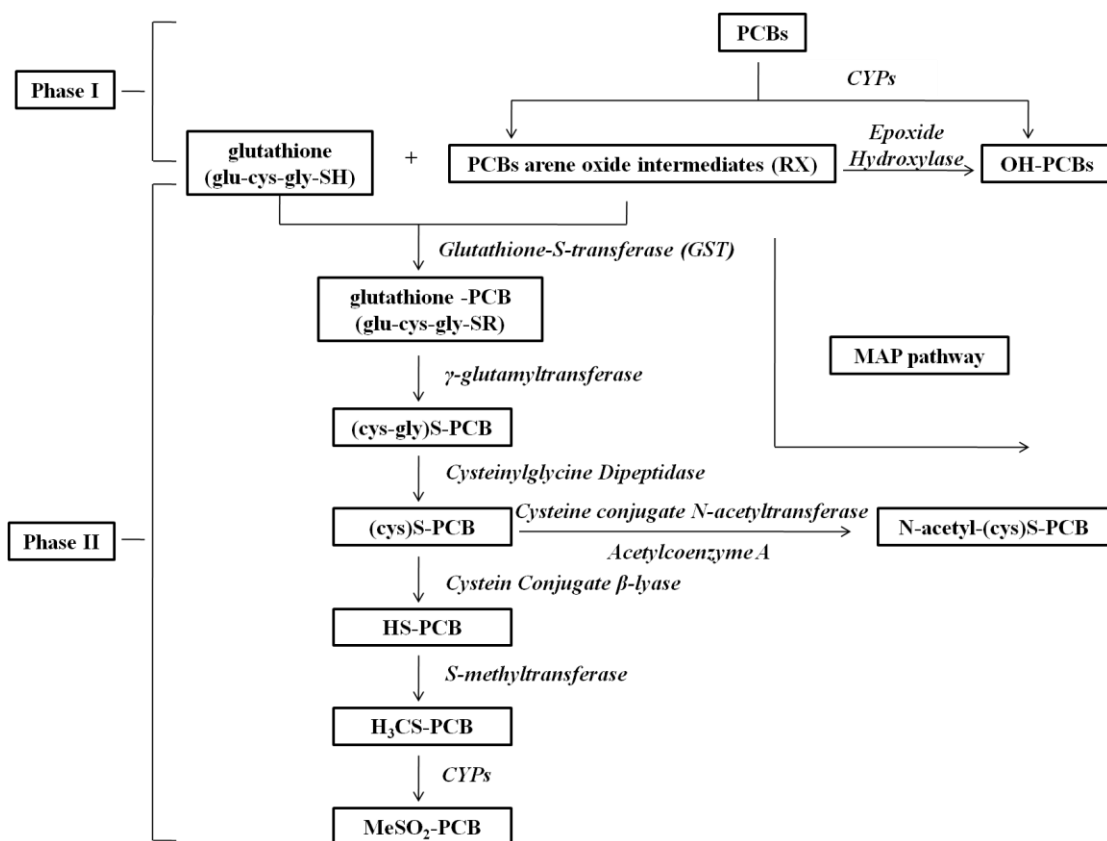


Figure 1.2 Generic phase I and II biotransformation pathways of PCBs.

(glu: glutamate; cys: cysteine; gly: glycine)

1.3. Chiral PCBs

Of the 209 PCB congeners, 78 are axially chiral, and 19 of those are stable in the environment given the presence of three or four *ortho*-chlorines hindering racemization via rotation around the phenyl-phenyl bond (21). Chiral PCBs exist as two non-superimposable mirror image forms, which are called atropisomers (stereoisomers resulting from hindered rotation about single bonds) (22). Both atropisomers have the same physical-chemical properties except for optical rotation, but often different

biological characteristics. PCBs are usually released into the environment as racemates (i.e., both atropisomers have the same concentration) because their production (e.g., biphenyl reacting with chlorine gas) is not a stereoselective process (21). However, non-racemic residues of chiral PCBs have been widely observed in the environment, especially in higher organisms (21). The different accumulation of chiral PCB atropisomers in organisms indicated their different environmental fates and toxicological effects. For example, the two atropisomers of a chiral PCB congener can stereoselectively induce CYP enzymes in organisms and affect the enzyme expression in different manner (23,24). They can also differentially disrupt Ca^{2+} signaling via activation of ryanodine receptors and thereby cause stereoselective neurotoxicity (25). In addition, atropisomer enrichments of OH-PCBs and MeSO₂-PCBs have also been detected in many organisms (26,27), indicating the different and atropisomer-specific environmental fate of these chiral PCB metabolites. These differences are important for better understanding the exposure and fate of chiral contaminants, accurate environmental risk assessment and pollution source identification. The ultimate goal of studying chiral pollutants is to improve the pollution regulation and provide useful information for new chemical design. (Figure 1.3)

Enantiomer fractions (EFs) (28) are usually used to describe atropisomer distributions, and are defined as the concentration ratio of the first-eluting atropisomer (E1) and the total concentration of both atropisomers (E1+E2) for congeners for which optical rotation is unknown, and as the concentration ratio of the (+)-atropisomer and total concentration if optical rotation is known (Equation 1.1).

$$\text{EF} = \frac{\text{E1}}{\text{E1} + \text{E2}} \text{ or } \text{EF} = \frac{(+)}{(+)+(-)} \quad [\text{Equation 1.1}]$$

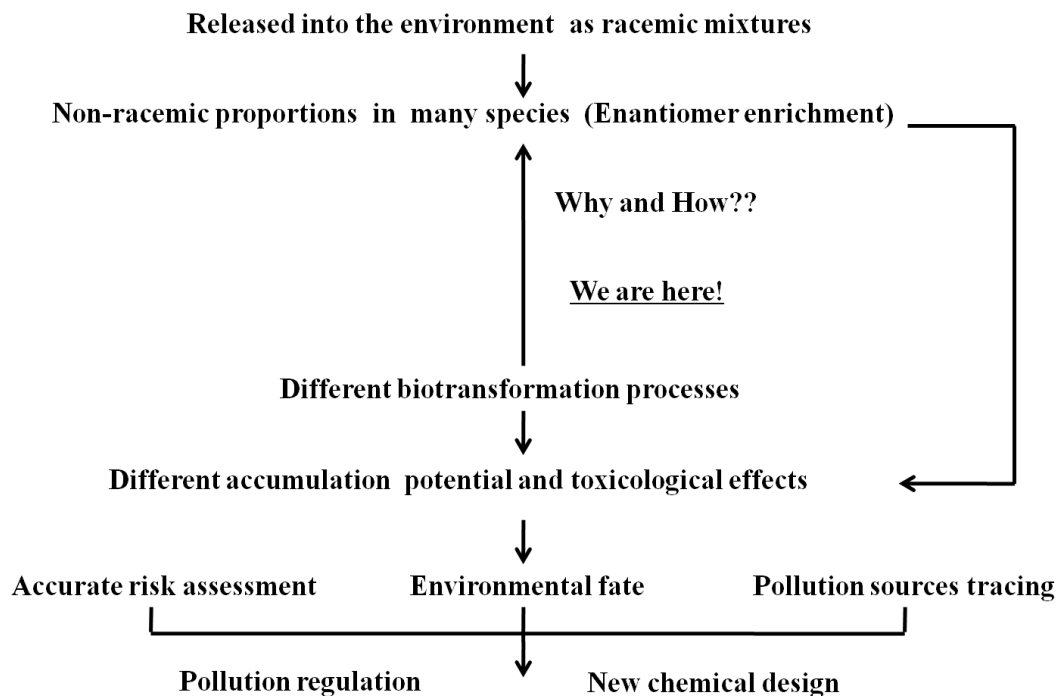


Figure 1.3 Conceptual flow chart of the study of chiral contaminants

1.4. Knowledge Gaps

The mechanisms for atropisomer enrichment of chiral PCBs and their metabolites are currently poorly understood (Figure 1.3). Previous *in vivo* studies suggested the stereoselective metabolism of chiral PCBs should play an important role in affecting the atropisomer composition (29,30). The phase I biotransformation of chiral PCBs by some CYP isozymes (e.g., rat CYP 2B1) has been proven to be a stereoselective process *in vitro* (31), which may be responsible for the observed atropisomer enrichment *in vivo*. However, the reasons for stereoselective biotransformation of chiral PCBs by CYPs are still not clear. In addition, organisms may take up non-racemic chiral PCBs from their environment such as prey and sediment. Any changes of their food web (e.g., feeding ecology change) may result in the disruption of the chiral PCB signatures in organisms,

which is also unknown. Thus, in-depth investigation of stereoselective biotransformation and bioaccumulation of chiral PCBs at the enzyme and food web levels is necessary, because such investigation can help us to better understand their metabolism and fate in environment.

1.5. Dissertation Hypotheses and Outline

The hypothesis of this dissertation is that stereoselective biotransformation and bioaccumulation are two major reasons for the observed different environmental fate of PCB atropisomers. Other affecting factors, such as presence of nanoparticles and changes in feeding ecology of organisms, also affect the fate of chiral contaminants. None are issues that have been addressed in the literature to date.

Appendix 1 is a critical review of the transport, metabolism and distribution of chiral PCBs. The author of this dissertation is a coauthor of the published and peer-reviewed manuscript, and was responsible for writing the introduction and section A1.4, plotting Figure A1.1, editing the overall manuscript and arranging the references. This review has been updated since the time in which it was published with more recent literature.

Chapter 2 discusses the mechanisms of stereoselective biotransformation of chiral PCBs by rat CYP 2B1. Biotransformation kinetics, competition modeling and docking studies are presented in this chapter. The author of this dissertation designed the experiment along with his supervisor, performed the experiment, interpreted data and wrote the manuscript.

Chapter 3 discusses how nanoparticles may disrupt the stereoselective biotransformation of chiral PCBs and the relevant mechanisms. The direct interaction of gold nanoparticles with rat CYP 2B1 isozyme is presented. The indirect influence of gold

nanoparticles on enzyme functions through changes to the surrounding ionic strength is also presented. The author of this dissertation designed these experiments along with his supervisor, performed the experiments, interpreted data and wrote the manuscript. Coauthors Dr. Guibin Ma and Dr. Jonathan G.C. Veinot were responsible for gold nanoparticle preparation.

Chapter 4 discusses the stereoselectivity of hydroxylated metabolites formation process in CYP mediated biotransformation of chiral PCBs. The stereoselective biotransformation of OH-PCBs to non-racemic dihydroxylated PCBs (diOH-PCBs) is presented. The interference of chiral PCB atropisomers of each other in phase I reactions is also discussed. The author of this dissertation designed the experiment along with his supervisor, as well as collaborators Dr. Hans-Joachim Lehmler and Dr. Izabela Kania-Korwel of the University of Iowa. They were responsible for OH- and diOH-PCB standards preparation and chiral analyses of OH- and diOH-PCBs. The author of this dissertation performed the incubation, chiral analyses of parent PCBs and achiral analyses of OH- and diOH-PCBs; interpreted data; and wrote the manuscript.

Chapter 5 discusses the temporal and spatial trends of PCB chiral signatures in Greenland sharks. Factors contributing to the PCB chiral signature change in Greenland sharks (e.g., feeding ecology change) are discussed. PCB contamination and atropisomer enrichment in organisms from Cumberland Sound food web is also presented. This study was a collaboration with Dr. Aaron T. Fisk of the University of Windsor and Dr. Gregg T. Tomy, formerly of the Department of Fisheries and Oceans, Freshwater Institute and now of the Department of Chemistry at the University of Manitoba. Fisk and Tomy were responsible for sample collection and achiral analyses, whereas chiral analyses, data

interpretation and manuscript writing by the author of this dissertation.

Chapter 6 summarizes the findings of the research presented in this dissertation and discusses future research directions in regards to the fate of chiral organic contaminants in ecosystems.

References

- (1) Eduljee, G. H. Budget and source inventories. In *Persistent Organic Pollutants: Environmental behaviour and pathways for human exposure*, Harrad, S. J., Ed. Kluwer Academic Publishers: Norwell, Massachusetts, **2001**, pp 1-29.
- (2) Blais, J.M.; Macdonald, R.W.; Mackay, D.; Webster, E.; Harvey, C.; Smol, J.P. Biologically mediated transport of contaminants to aquatic systems. *Environ. Sci. Technol.* **2007**, *41*, 1075-1084.
- (3) Krümmel, E. M.; Macdonald, R.W.; Kimpe, L. E.; Gregory, I.E.; Demers, M. J.; Smol, J. P.; Finney, B.; Blais, J. M. Delivery of pollutants by spawning salmon. *Nature* **2003**, *425*, 255-256.
- (4) Rig á, F.; Bignert, A.; Braune, B.; Stow, J.; Wilson, S. Temporal trends of legacy POPs in Arctic biota, an update. *Sci. Total Environ.* **2010**, *408*, 2874–2884.
- (5) Erickson, M.D. Polychlorinated biphenyls (PCBs) contaminated sites worldwide. In *PCBs: Recent advances in environmental toxicology and health effects*. Robertson, L.W., Hansen, L.G., Ed. The University Press of Kentucky, 2001, pp xi-xxx.
- (6) Safe, S. H. Polychlorinated biphenyls (PCBs)-environmental impact, biochemical and toxic responses, and implications for risk assessment. *Criti. Revi. Toxi.* **1994**, *24*, 87-149.
- (7) Masuda, Y. The Yusho rice oil poisoning incident. In: *Dioxin and Health*, Schecter, A., Ed., Plenum Press, New York, 1994, pp 633-659.
- (8) Holoubek, L. Polychlorinated biphenyls (PCBs) contaminated sites worldwide. Section I. Origin of PCBs and characterization of exposures. In *PCBs: Recent advances in environmental toxicology and health effects*. Robertson, L. W., Hansen,

- L.G., Ed. The University Press of Kentucky, 2001, 17-23.
- (9) Letcher, R.; Klasson-Wehler, E.; Bergman, A. Methyl sulfone and hydroxylated metabolites of polychlorinated biphenyls. *Volume 3 Anthropogenic Compounds Part K* **2000**, 315-359.
- (10) Meunier, B.; De Visser, S.P.; Shaik, S. Mechanism of oxidation reactions catalyzed by cytochrome P450 enzymes. *Chem. Rev.* **2004**, *104*, 3947-3980.
- (11) Denisov, I. G.; Makris, T. M.; Sligar, S. G.; Schlichting, I. Structure and chemistry of cytochrome P450 structure and chemistry of cytochrome P450. *Chem. Rev.* **2005**, *105*, 2253–2278.
- (12) Kawano, M.; Hasegawa, J.; Enomoto, T.; Onishi, H.; Nishiso, Y.; Matsuda, M.; Wakimoto, T. Hydroxylated polychlorinated biphenyls (OH-PCBs): Recent advances in wildlife contamination study. *Environ. Sci.* **2005**, *12*, 315–324.
- (13) Bakke, J.E.; Bergman, A.L.; Larsen, G.L. Metabolism of 2,4',5-trichlorobiphenyl by the mercapturic acid pathway. *Science* **1982**, *217*, 645-647.
- (14) Campbell, L. M.; Muir, D. C. G.; Whittle, D. M.; Backus, S.; Norstrom, R.J.; Fisk, A. T. Hydroxylated PCBs and other chlorinated phenolic compounds in Lake Trout (*Salvelinus namaycush*) blood plasma from the Great Lakes region. *Environ. Sci. Technol.* **2003**, *37*, 1720-1725.
- (15) Bergman, A.; Norstrom, R.J.; Haraguchi, K.; Kuroki, H. PCB and DDE methyl sulfones in mammals from Canada and Sweden. *Environ. Toxicol. Chem.* **1994**, *13*, 121-128.
- (16) Sandau, C. D.; Ramsay, M.; Norstrom, R. J. Implication of hydroxylated metabolites of PCBs and other halogenated phenolic compounds as endocrine disruptors in polar

- bears; Carleton University: Ottawa, ON, Canada, **2000**, 47-52.
- (17) Haraguchi, K.; Kuroki, H.; Masuda, Y. Determination of PCB methylsulfone congeners in Yusho and control patients. *Chemosphere* **1986**, *15*, 2027-2030.
- (18) Ucán-Marín, F.; Arukwe, A.; Mortensen, A.; Gabrielsen, G.W.; Fox, G.A.; Letcher, R.J. Recombinant transthyretin purification and competitive binding with organohalogen compounds in two gull species (*Larus argentatus* and *Larus hyperboreus*). *Toxicol. Sci.* **2009**, *107*, 440-450.
- (19) Kato, Y.; Haraguchi, K.; Tomiyasu, K.; Saito, H. Structure-dependent induction of CYP2B1/2 by 3-methylsulfonyl metabolites of polychlorinated biphenyl congeners in rats. *Environ. Toxicol. Phar.* **1997**, *3*, 137-144.
- (20) Kato, Y.; Kenne, K.; Haraguchi, K.; Masuda, Y.; Kimura, R.; Wängård, L. Inhibition of cell-cell communication by methylsulfonyl metabolites of polychlorinated biphenyl congeners in rat liver epithelial IAR 20 cells. *Arch. Toxicol.* **1998**, *72*, 178-182.
- (21) Wong, C.S. and Warner, N.A. Chirality as an Environmental Forensics Tool. In *Persistent Organic Pollutants*; Harrad, S., Ed.; John Wiley & Sons, Ltd, Chichester, UK. **2010**, pp 71-136.
- (22) Smith, S.W. Chiral Toxicology: It's the Same Thing... Only Different. *Toxicol. Sci.* **2009**, *110*, 4-30.
- (23) Püttmann, M.; Mannschreck, A.; Oesch, F.; Robertson, L. Chiral effects in the induction of drug-metabolizing enzymes using synthetic atropisomers of polychlorinated biphenyls (PCBs). *Biochem. Pharmacol.* **1989**, *38*, 1345-1352.
- (24) Rodman, L. E.; Shedlofsky, S. I.; Mannschreck, A.; Püttmann, M.; Swim, A. T.;

- Robertson, L. W. Differential potency of atropisomers of polychlorinated biphenyls on cytochrome P450 induction and uroporphyrin accumulation in the chick embryo hepatocyte culture. *Biochem. Pharmacol.* **1991**, *41*, 915–922.
- (25) Pessah, I.N.; Lehmler, H.-J.; Robertson, L.W.; Perez, C.F.; Cabrales, E.; Bose, D.D.; Feng, W. Enantiomeric Specificity of (–)-2, 2', 3, 3', 6, 6'-Hexachlorobiphenyl toward Ryanodine Receptor Types 1 and 2. *Chem. Res. Toxicol.* **2008**, *22*, 201-207.
- (26) Kania-Korwel, I.; Barnhart, C. D.; Stamou, M.; Truong, K. M.; El-Komy, M. H.; Lein, P. J.; Veng-Pedersen, P.; Lehmler, H.-J. 2,2',3,5',6-pentachlorobiphenyl (PCB 95) and its hydroxylated metabolites are enantiomerically enriched in female mice. *Environ. Sci. Technol.* **2012**, *46*, 11393–11401.
- (27) Zhang, Y.; Wu, J.P.; Luo, X.J.; She, Y.Z.; Mo, L.; Mai, B.X. Methylsulfonyl polychlorinated biphenyls in fish from an electronic waste-recycling site in South China: levels, congener profiles, and chiral signatures. *Environ. Toxicol. Chem.* **2012**, *31*, 2507-2512.
- (28) Harner, T.; Wiberg, K.; Norstrom, R. Enantiomer fractions are preferred to enantiomer ratios for describing chiral signatures in environmental analysis. *Environ. Sci. Technol.* **2000**, *34*, 218-220.
- (29) Kania-Korwel, I.; Garrison, A. W.; Avants, J. K.; Hornbuckle, K. C.; Robertson, L. W.; Sulkowski, W. W.; Lehmler, H.-J. Distribution of chiral PCBs in selected tissues in the laboratory rat. *Environ. Sci. Technol.* **2006**, *40*, 3704–3710.
- (30) Kania-Korwel, I.; El-Komy, M.H.; Veng-Pedersen, P.; Lehmler, H.-J. Clearance of polychlorinated biphenyl atropisomers is enantioselective in female C57Bl/6 mice. *Environ. Sci. Technol.* **2010**, *44*, 2828-2835.

(31) Warner, N. A.; Martin, J. W.; Wong, C. S. Chiral polychlorinated biphenyls are biotransformed enantioselectively by mammalian cytochrome P-450 isozymes to form hydroxylated metabolites. *Environ. Sci. Technol.* **2009**, *43*, 114–121.

Chapter 2

Factors Affecting Phase I Stereoselective Biotransformation of Chiral Polychlorinated Biphenyls (PCBs) by Rat Cytochrome P-450 2B1 Isozymes

A version of this chapter has been previously published as Lu, Z. and Wong, C. S. Factors affecting phase I stereoselective biotransformation of chiral polychlorinated biphenyls (PCBs) by rat cytochrome P-450 2B1 isozyme. *Environmental Science & Technology*. 2011, 45, 8298-8305. (DOI: 10.1021/es200673q). Copyright 2011 © American Chemical Society. Reprinted with permission.

The author of this dissertation designed the experiment along with his supervisor, performed the experiment, interpreted data and wrote the manuscript.

2.1. Introduction

Chiral environmental chemistry is an important tool for studying biotransformation processes of chiral pollutants, particularly polychlorinated biphenyls (PCBs), in the environment (1, 2). There are 78 PCBs with axial chirality, and 19 of those are stable in the environment. Chiral PCBs exist as two mirror-image atropisomers and were released as racemates. Both atropisomers have the same chemical and physical behavior, except for optical rotation. However, they have been found in non-racemic proportions in many species (1,2) and may have different biochemical weathering fates and different toxicities such as different neurotoxicities (3-6), exposure doses of precursor atropisomers (7), and propensities to form toxic OH-PCB and/or MeSO₂-PCB metabolites (8).

Some reasons for changes in PCB atropisomeric composition in organisms include differences in (9, 10): stereospecific recognition and absorption processes with receptors, enzymes (11) or cell membranes; binding abilities of atropisomers with certain proteins (e.g. plasma proteins); enzyme expression abilities of organisms (12); metabolism processes of atropisomers (1); possible atropisomerization; interactions with other endogenous or xenobiotic compounds; excretion pathways; and bioaccumulation. The prediction of environmental enantiomer distributions of chiral compounds is still not feasible because all these factors should be taken into account. Previous studies failed to predict stereoselectivity of PCBs in biota or sediment based on suspected factors including concentration, age, feeding ecology or total carbon content (13-16). However, it is logical that the factors controlling environmental stereoselectivity are at the enzyme level, as stereoselective induction (17,18) and binding abilities of cytochrome P-450 (CYP) isozymes and corresponding biotransformation processes are believed to play

important roles (1,11,19). However, these mechanisms remain poorly understood.

At the enzyme level, PCBs are metabolized in higher organisms (e.g., mammals) by phase I and phase II reactions. PCBs are initially oxidized by CYP isozymes to generate PCB arene oxide intermediates and/or OH-PCBs. These intermediates can also be biotransformed to OH-PCBs and/or conjugated with phase II enzymes to produce MeSO₂-PCBs (7, 8). Multi-*ortho*-substituted PCBs with unsubstituted vicinal *meta*, *para* H atoms, including most chiral congeners, are substrates for the CYP2B subfamily of isozymes (20-22). Warner et al. (19) recently demonstrated that rat CYP2B1 biotransformed some chiral PCBs stereoselectively, but the reasons are still not clear. In-depth investigation of stereoselective biotransformation of chiral PCBs at the enzyme level can help us better understand their metabolism in organisms.

This study tests three hypotheses for factors affecting stereoselective biotransformation of chiral PCBs 45, 95 and 132 *in vitro* with rat CYP2B1. First, different biotransformation kinetics of each atropisomer by rat CYP2B1 is one possible reason to result in their non-racemic enrichment in organisms. Second, competition between different congeners or atropisomers influences biotransformation kinetics and atropisomer distributions. Finally, stereospecific interactions of atropisomers of the same congener with rat CYP2B1 lead to changes in biotransformation kinetics and atropisomer composition. We choose these congeners for the experiment because they can be biotransformed by rat CYP 2B1 based on previous study (19) and they represent different chlorination status of PCBs.

2.2. Materials and Methods

2.2.1. Chemicals and Regents

Racemic chiral PCBs 45, 95 and 132, recovery standards PCBs 30 and 204, and internal standard PCB 159 (all purities > 99%) were purchased from Accustandard (West Haven, CT). PCB solutions were prepared in acetone. Individual PCB 132 atropisomer were isolated as previously published (46). Rat CYP2B1, insect cell control supersomes (P450 reductase and cytochrome b₅) (stored at -70 °C until use) and NADPH regeneration solutions (solution A: 31 mM NADP⁺, 66 mM glucose-6-phosphate and 66 mM MgCl₂ in water; solution B: 40 U/ml glucose-6-phosphate dehydrogenase in 5 mM sodium citrate) (stored at -20 °C until use) were purchased from BD Biosciences (San Jose, CA). Mass-labeled hydroxylated PCBs (4-hydroxy-[¹³C₁₂]-PCB 29; 4-hydroxy-[¹³C₁₂]-PCB 61; 4-hydroxy-[¹³C₁₂]-PCB 120; 4-hydroxy-[¹³C₁₂]-PCB 159; 4-hydroxy-[¹³C₁₂]-PCB 172; 4-hydroxy-[¹³C₁₂]-PCB 189) were purchased from Wellington Laboratories (Guelph, ON, Canada) as recovery standards for hydroxylated PCBs metabolite extraction (chemical purity > 98%, isotopic purity > 99%). Mass-labeled methoxy-PCBs (4-methoxy-[¹³C₁₂]-PCB 29; 4-methoxy-[¹³C₁₂]-PCB 61; 4-methoxy-[¹³C₁₂]-PCB 120; 4-methoxy-[¹³C₁₂]-PCB 159; 4-methoxy-[¹³C₁₂]-PCB 172; 4-methoxy-[¹³C₁₂]-PCB 189) were also purchased from Wellington Laboratories (Guelph, ON, Canada) (chemical purity > 98%, isotopic purity > 99%). Testosterone and its metabolite 16 α -testosterone were purchased from Steraloids (Newport RI, USA) as a positive control to correct biotransformation activities of CYP2B1 in all incubations.

2.2.2. *In Vitro* Biotransformation Experiments

Incubations were conducted in glass tubes containing 0.1 pmol rat CYP2B1 (0.01 pmol for individual PCB 132 atropisomer incubations and comparative racemate incubations), 50 μ L of solution A, 10 μ L of solution B, 10 μ L chiral PCBs and potassium

phosphate buffer (110 mM, pH 7.4) in 1 mL total volume at 37°C. Some high concentration assays contained 60 μ L acetone to increase PCB solubility. Preliminary studies indicated that the biotransformation activity of rat CYP2B1 was not affected by the presence of 1-6% (v/v) acetone. For pseudo-first order kinetics studies, three different concentrations of each congener were incubated for 0-6 minutes (0-12 minutes for low concentration PCB 45) in three separate experiments each. The incubation time for Michaelis-Menten kinetics and competition studies was 3 minutes. Incubations were terminated with 1 mL of ice-cold methanol and immediately extracted. Control assays were run under the same conditions, with 0.3 pmol insect control supersomes (0.03 pmol for individual PCB 132 atropisomer incubations and compared racemate incubations) used as a negative control containing no CYP but the same protein content, while 200 nmol testosterone and 40 pmol CYP2B1 was incubated for 30 minutes as a positive control.

Extraction, separation and instrumental analysis of PCBs have been previously reported (19,23). Briefly, PCBs 30, 204 and mass-labeled OH-PCBs were added as recovery standards to the incubation tubes after biotransformation reactions were terminated. The incubations were then acidified with HCl and washed by KCl and extracted with 6 mL of 1:1 methyl-*t*-butyl ether (MTBE)/hexane with a separating funnel. The organic phase was collected and partitioned with 6 mL of 1 M KOH to separate the OH-PCBs from the neutral organic phase. Chiral PCBs in the neutral organic fraction was purified using an acidified silica gel column (3 g, 22% H₂SO₄) and eluted with 20 mL of 15% (v/v) dichloromethane (DCM)/hexane. OH-PCBs in the aqueous fraction were then acidified by H₂SO₄ and back-extracted into MTBE/hexane (1:1). The organic phase

containing OH-PCBs was derivatized with diazomethane into their respective methoxy-PCBs (MeO-PCBs). The MeO-PCB fraction was purified using a 5 g column of the acidified silica gel and eluted with 50 mL of 1:1 DCM/hexane. Both PCB and MeO-PCB fractions were solvent exchanged to hexane and PCB 159 was used as an internal standard. Testosterone and 16 α -testosterone in the positive control samples were also acidified with HCl, washed with KCl, and extracted with 10 mL ethyl acetate (47, 48). All extraction procedures were repeated three times for each sample.

Recoveries of PCBs 30 and 204 were 85 \pm 14% and 90 \pm 12%, respectively. PCB concentrations were corrected based on the average recoveries of PCBs 30 and 204. Recoveries of mass-labeled derivatized OH-PCB standards were 39 \pm 26% (MeO-PCB 29), 34 \pm 19% (MeO-PCB 61), 115 \pm 12% (MeO-PCB 120), 105 \pm 9% (MeO-PCB 159), 107 \pm 3% (MeO-PCB 172) and 99 \pm 5% (MeO-PCB 189), similar to previous reports using the same extraction method (19). Recoveries of testosterone and 16 α -testosterone were 78 \pm 10% and 80 \pm 17%, respectively. PCB concentrations were determined using PeakFit v4.12 (Systat Software, San Jose, CA) to deconvolute chromatograms (46). All these recovery data were reported as average number \pm standard deviation.

2.2.3. Instrumental Analysis

Chiral PCBs were quantified by using an Agilent 5890 gas chromatograph equipped with an Agilent 5989 mass spectrometer (GC/MS) under electron impact ionization (70 eV) with selected ion monitoring (m/z 256, 258, 260 for PCB 30; m/z 290, 292, 294 for PCB 45; m/z 324, 326, 328 for PCB 95; m/z 358, 360, 362 for PCB 132 and PCB 159; m/z 426, 428, 430 for PCB 204). A Chirasil-Dex column (30 m \times 0.25 mm \times 0.25 μ m d_f , Varian, Palo Alto, CA) was used for quantification and atropisomer analysis of PCBs 95

and 132 (5). Cyclosil-B column (30m×0.25mm×0.25μm, J&W Scientific) was used for quantification and atropisomer analysis of PCB 45 (49). One μL samples were injected in splitless mode at 250 °C with helium as carrier gas and at a constant flow rate of 36 cm/s. Initial oven temperature was held at 40 °C for 2 min, then ramped at 15 °C/min to 160 °C, ramped at 1 °C/min to 210 °C, held for 5 min. The MeO-PCB fraction was separated by a DB-XLB column (30 m×0.25 mm×0.5 μm d_f, J&W Scientific) and initial oven temperature was held at 100 °C initial temperature for 2 min, ramped at 20 °C/min to 240 °C, held for 25 minutes, ramped at 10 °C/min to 275 °C followed by a 14 min hold (19).

Testosterone and 16α-testosterone were quantified by high performance liquid chromatography using a Waters 1525 pump (Ontario, CA), and 2487 dual wavelength absorbance detector at 254 nm, and a Symmetry C₁₈ (150×4.6 mm i.d., 5μm particle size) column. The injection volume was 20 μL and the column temperature was 25.0 °C. The mobile phase was isocratic with 0.02 M sodium dihydrogen phosphate, acetonitrile and methanol at 51:47:2, respectively, at 1.0 ml/min (50). All the biotransformation activity data were corrected by the testosterone control, which showed CYP2B1 activities of 2.3-4.1 pmol product/min/pmol CYP2B1/mL throughout our experiments.

2.2.4. Kinetics and Statistical Analyses

Enantiomer fractions (EFs) (24) (Equation 1.1) were used to describe atropisomer distributions, and are defined as the concentration ratio of the first-eluting atropisomer (E1) and the total concentration of both atropisomers (E1+E2) for PCBs 45 and 95, and as the concentration ratio of the (+)-atropisomer and total concentration for PCB 132 for which optical rotation is known.

Prism 5 (GraphPad Software, La Jolla, CA) was used for linear and nonlinear regression kinetics and statistical analyses. The Michaelis-Menten kinetic model (Equation 2.1) was used for individual congener incubations to determine the apparent half-saturation constants (apparent K_m) and the maximal biotransformation rates (V_{max}). The competition incubation data were fit using inhibition models, which include the competitive model (Equation 2.2), uncompetitive model (Equation 2.3) and mixed model (Equation 2.4), to understand better the biotransformation processes of congener mixtures (25,26):

$$V = \frac{V_{max} \times [S]}{K_m + [S]} \quad \text{[Equation 2.1]}$$

$$V = \frac{V_{max} [S]}{[S] + K_m \left(1 + \frac{[C]}{K_c}\right)} \quad \text{[Equation 2.2]}$$

$$V = \frac{V_{max} [S]}{K_m + [S] \left(1 + \frac{[C]}{\alpha K_c}\right)} \quad \text{[Equation 2.3]}$$

$$V = \frac{V_{max} [S]}{K_m \left(1 + \frac{[C]}{K_c}\right) + [S] \left(1 + \frac{[C]}{\alpha K_c}\right)} \quad \text{[Equation 2.4]}$$

where V is the biotransformation rate; $[S]$ the substrate concentration; $[C]$ the competitor concentration; K_c the equilibrium dissociation constant for the enzyme-competitor complex; and α a parameter to determine the competition mechanism. The kinetics data were normalized by negative and positive controls. Statistically significant levels were set as 0.05 for kinetic regressions.

2.2.5. Three-Dimensional Structure Modeling

Discovery Studio 2.5 (DS2.5, Accelrys Software Inc.) and Swiss-Model

(<http://swissmodel.expasy.org/>) (27-29) were used for modeling template searching, homology modeling and model refinement. The sequence of rat CYP2B1 was obtained from Swiss-Prot (accession number P00176) (30-32). BLAST Search (DS-server) in DS2.5 was used to find templates for homology modeling. Because the crystal structure of rat CYP2B1 is not available, the crystal structures of CYP2B6 from the Protein Data Bank (PDB: <http://www.rcsb.org>; PDB ID: 3IBD), was used as a template to build the three-dimensional structure of rat CYP2B1 within Swiss-Model with a sequence identity of 76.7%, which is sufficient for our study (33). The protein structure was then refined by solvation, energy minimization and molecular dynamic simulation in DS2.5. Validation of the protein model was judged by PROCHECK (<http://nihserver.mbi.ucla.edu/SAVES/>) (34) and Profiles-3D (35) in DS2.5.

2.2.6. Docking Study

The established rat CYP2B1 model was used as a receptor. *R* or *S* atropisomers of these three PCB congeners were prepared in ChemOffice 2004 (CambridgeSoft, Cambridge, MA USA) and used as ligands for docking. The binding mode for chiral PCBs to rat CYP2B1 was studied using the CDOCKER module in DS 2.5. CDOCKER is a CHARMM force field (Chemistry at Harvard Macromolecular Mechanics) based molecular dynamics simulation scheme for docking ligands in a receptor binding site. General docking steps are described elsewhere (36-39). The complex structure with the lowest CDOCKER interaction energy was used for comparison.

2.3. Results and Discussion

2.3.1. Biotransformation Kinetics for PCB 45, 95 and 132

In our incubation batches, the reaction rates were pseudo-first order for all three

congeners at different concentrations between 0-6 minutes, indicating that 3 minutes incubation time was feasible for Michaelis-Menten kinetics studies. Rat CYP2B1-mediated enzymatic PCB reactions were consistent with Michaelis-Menten kinetics (Equation 2.1, Figure 2.1A). PCB 45 had a higher biotransformation rate (V_{\max}) for incubations with the racemate than PCBs 95 and 132 (Table 2.1 and Figure 2.1A).

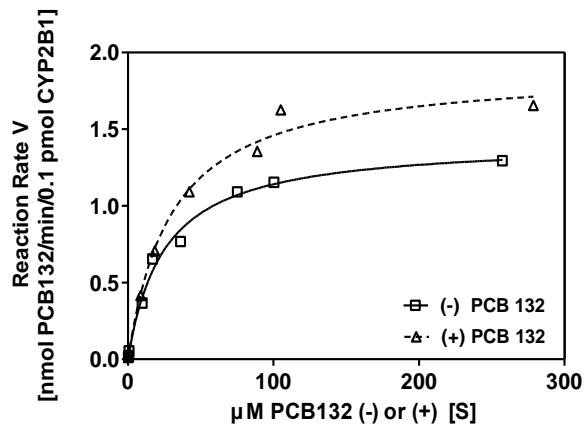
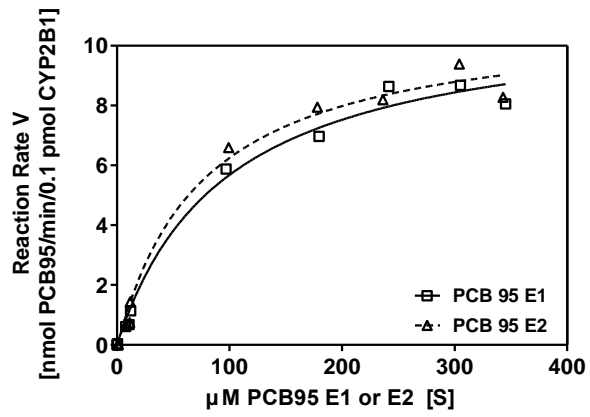
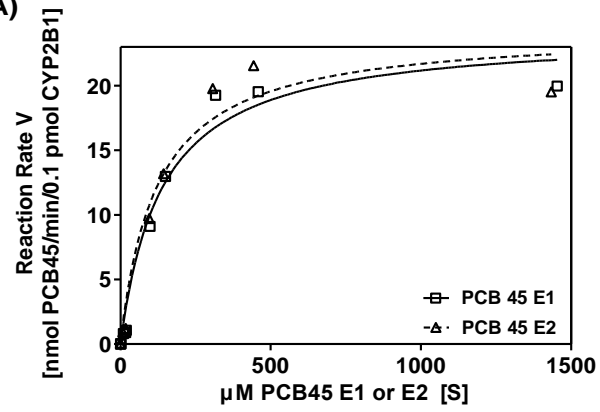
Table 2.1 Parameters for Michaelis-Menten kinetics.

Table 2.1 Parameters for Michaelis-Menten kinetics						
	PCB 45		PCB 95		PCB 132	
	E1	E2	E1	E2	(-)	(+)
$V_{\max}^{a,b}$	24.1	24.3	11.1	11.0	1.4	1.9
$K_m(\mu M)^a$	138	122	96.1	75.9	24.9	29.6
R^{2c}	0.9746	0.9651	0.9910	0.9904	0.9931	0.9918

^aIndividual congener incubation. ^bnmol/ml/min/0.1pmol CYP2B1.
^cgoodness of fit for Michaelis-Menten kinetics curves

It is well-established that less chlorinated PCBs are biotransformed more rapidly than more chlorinated congeners for several reasons. Rat CYP2B1 can directly insert a hydroxy group to PCBs 45 or 95, or generate the corresponding arene oxides more efficiently than for PCB 132, because the former congeners' unsubstituted vicinal *meta*, *para* positions. The larger molecular volume of PCB 132 (310.0 cm³/mol) (40) compared to those of PCBs 45 and 95 (268.2 and 289.1 cm³/mol, respectively) (40) may contribute to its slower biotransformation rate, because the larger molecular volume can limit access

(A)



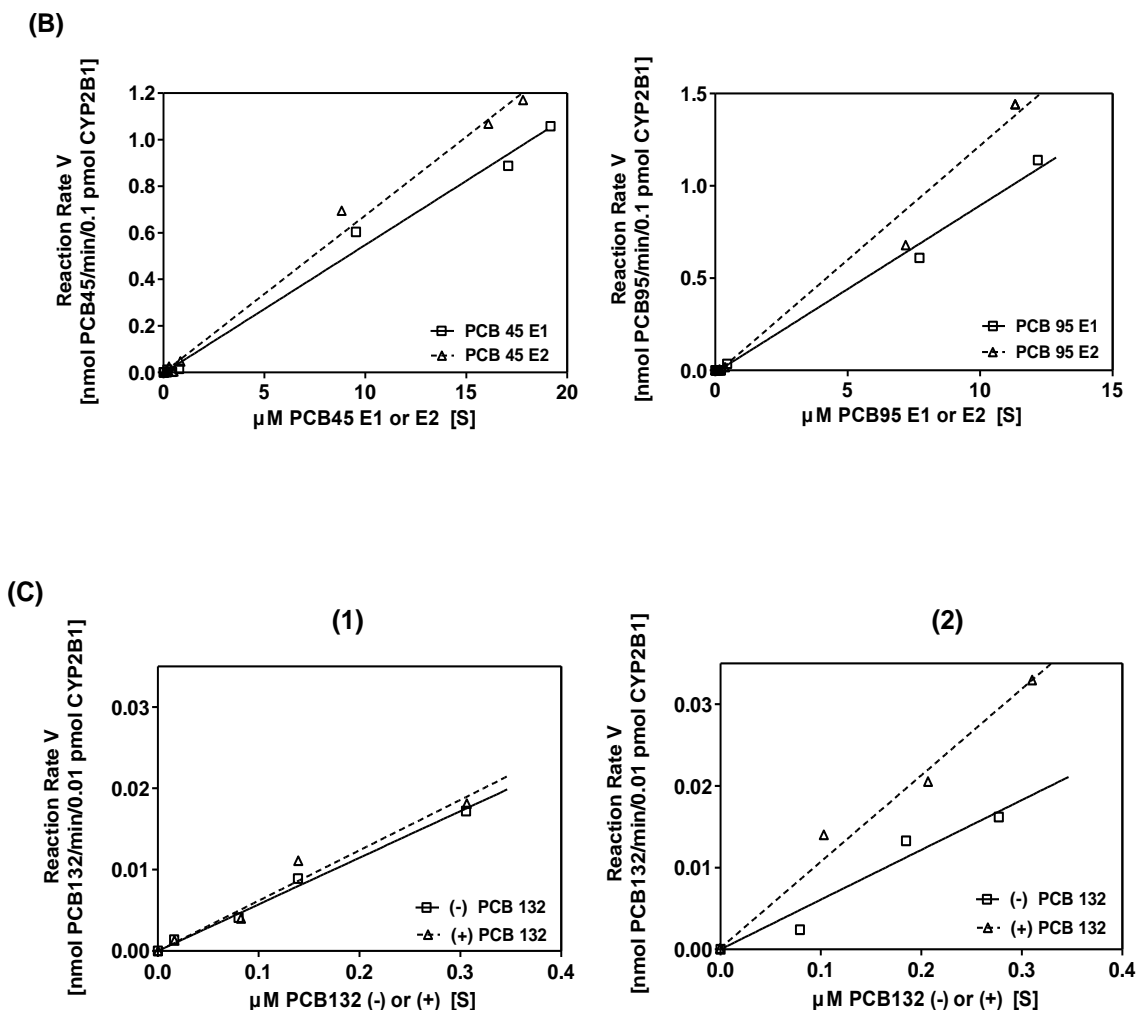


Figure 2.1 Biotransformation kinetics of chiral PCBs 45, 95 and 132 with rat CYP2B1.

(A) Michaelis-Menten kinetics for incubation of individual racemic PCB 45, PCB 95 and PCB 132 with rat CYP2B1 (see Table 2.1 for parameters); (B) Biotransformation kinetics of PCB 45 (E1: $y=0.055x-0.003, R^2=0.9937$; E2: $y=0.068x+0.0009, R^2=0.9941$) and PCB 95 (E1: $y=0.091x-0.012, R^2=0.9934$; E2: $y=0.124x-0.023, R^2=0.9864$) with rat CYP2B1 at low concentrations; (C) Biotransformation kinetics for PCB 132 incubated as a racemate [C1; (-)-PCB 132: $y=0.057x$; (+)-PCB 132: $y=0.062x$] and as individual atropisomers [C2; (-)-PCB 132: $y=0.061x$; (+)-PCB 132: $y=0.106x$]. Michaelis-Menten plots represent

multiple separate experiments, each at different concentrations, normalized to CYP2B1 activity via testosterone biotransformation (positive control). PCB 132 atropisomer plot represents two separate experiments.

to the enzyme active site and release of products. In addition, different binding positions or orientations of different congeners with rat CYP2B1 may also affect their biotransformation rates, as addressed below in our discussion of docking studies. PCB 132 had a smaller K_m value than PCB 45 and 95 (Table 2.1), indicating that PCB 132 had a higher affinity with rat CYP2B1 and saturated the isozyme at lower concentrations compared to the other congeners. The hydrophobic portion in the centre of CYP is believed to be the main interaction region between the isozyme and substrates (41). Therefore, the higher lipophilicity of PCB 132 compared to the less chlorinated congeners may also be responsible for the different binding affinities observed. Furthermore, there were no significant differences of the Michaelis-Menten kinetics parameters (V_{max} and K_m , Table 2.1 and Figure 2.1A) between the atropisomers of each congener in our experiments. This may be because our experiments were conducted with racemic mixtures, and the atropisomers of each congener can compete with each other, as discussed below.

In Michaelis-Menten kinetics, biotransformation rates (V) are proportional to substrate concentrations when $[S] \ll K_m$:

$$V = \frac{V_{max} \times [S]}{K_m} \quad [\text{Equation 2.5}]$$

At low concentrations (i.e., environmentally relevant ranges, which means the concentration of PCBs in the environment are limited by environmental conditions such

as their solubility (40), exposure history, biotransformation and bioaccumulation), the biotransformation rates of the second-eluting atropisomers of PCBs 45 and 95 were significantly faster than their respective antipodes (Figure 2.1B), with subsequent atropisomer enrichment observed. Mean EFs increased from 0.507 (negative control) to 0.533 for PCB 45 at initial concentrations less than 20 μM , and increased to 0.514 at initial concentration ranges of 20 to 450 μM . However, at enzyme saturation, EFs were racemic and identical to the negative control, as expected given the racemate had “flooded” the enzyme. Mean EFs of PCB 95 increased from 0.505 (negative control) to 0.533 at initial concentrations less than 15 μM , and to 0.520 at initial concentrations of 15 μM to 100 μM , but also stayed racemic at saturation. The results here demonstrate that the biotransformation stereoselectivity observed in this study depended on substrate concentration. This means that the concentration of chiral PCBs and enzyme kinetics should be taken into account when predicting EFs *in vitro* and/or *in vivo*.

These observations are consistent with previous reports of preferential depletion of E2-PCB 45 and E2-PCB 95. For instance, Warner et al. (19) found non-racemic atropisomer compositions of PCBs 45 and 95 after incubation with rat CYP2B1. Atropisomer enrichment of PCB 95 (EF>0.5) in adipose tissue, liver and skin of rats was observed *in vivo* (42), consistent with our observation that stereospecific biotransformation kinetics of PCB 95 were responsible. However, the stereoselectivity of PCB 132 by CYP2B1 contrasted with prior *in vitro* work (19) for reasons that are not clear, possibly from different incubation conditions (e.g., shorter incubation time in this study).

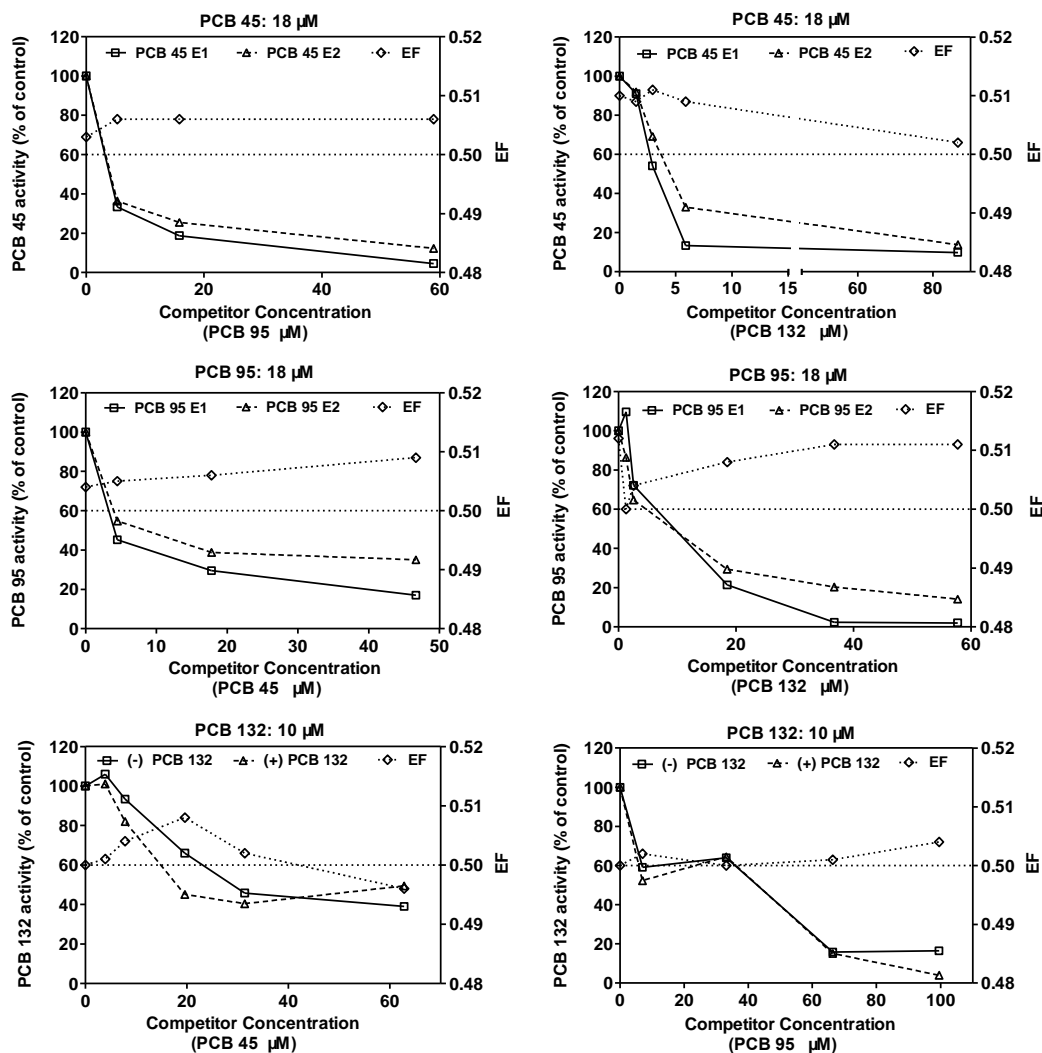


Figure 2.2 Competition curves of PCBs 45, 95 and 132 incubated with rat CYP2B1. Racemic PCBs 45 and 95 were each incubated at 18 μM with variable concentrations of racemates of the other congeners, while PCB 132 was incubated at 10 μM .

2.3.2. Competitive Biotransformation between Congeners

Potential competition and/or inhibition effects from different endogenous or xenobiotic compounds should also be considered when predicting the stereoselective biotransformation of chiral pollutants. Our results indicate that competition existed in

incubations of pairwise racemic PCB mixtures within environmentally relevant concentration ranges. Biotransformation rates decreased when competitor concentrations increased, with some resultant shifts in EFs (Figure 2.2). A reversal in EFs for PCB 132 with PCB 45 as competitor was not significant. Warner et al. (19) found that the atropisomer enrichment was more apparent in single congener incubations with human CYP2B6, compared to incubations with multiple congeners. Our study confirmed that the *in vitro* biotransformation kinetics and EFs of PCBs 45, 95 and 132 can be changed by the presence of other congeners.

In this study, to simplify the understanding of complex competition biotransformation process (two congeners and thus 4 atropisomers present as major substrates), we used inhibition models to describe possible congener competition by treating two atropisomers of one congener as one compound. (Note that OH-PCB products were at much lower concentrations and therefore not likely to compete for CYP2B1 with the much higher parent congeners present.) There are three different inhibition mechanisms for CYP-mediated reactions: reversible inhibition, quasi-irreversible inhibition and irreversible inhibition (26). Reversible inhibition is the most common inhibition type, and encompasses competitive inhibition, non-competitive inhibition, uncompetitive inhibition and mixed inhibition (26). The mixed-model (Equation 2.4) is identical to noncompetitive inhibition when $\alpha=1$. When α is very large (e.g., >10), inhibitor (competitor) binding prevents substrate binding, and the mixed-model is identical to the competitive inhibition model (Equation 2.2). The mixed model becomes nearly identical to the uncompetitive model (Equation 2.3) when α is very small but non-zero. To determine the mode of inhibition, we fit our

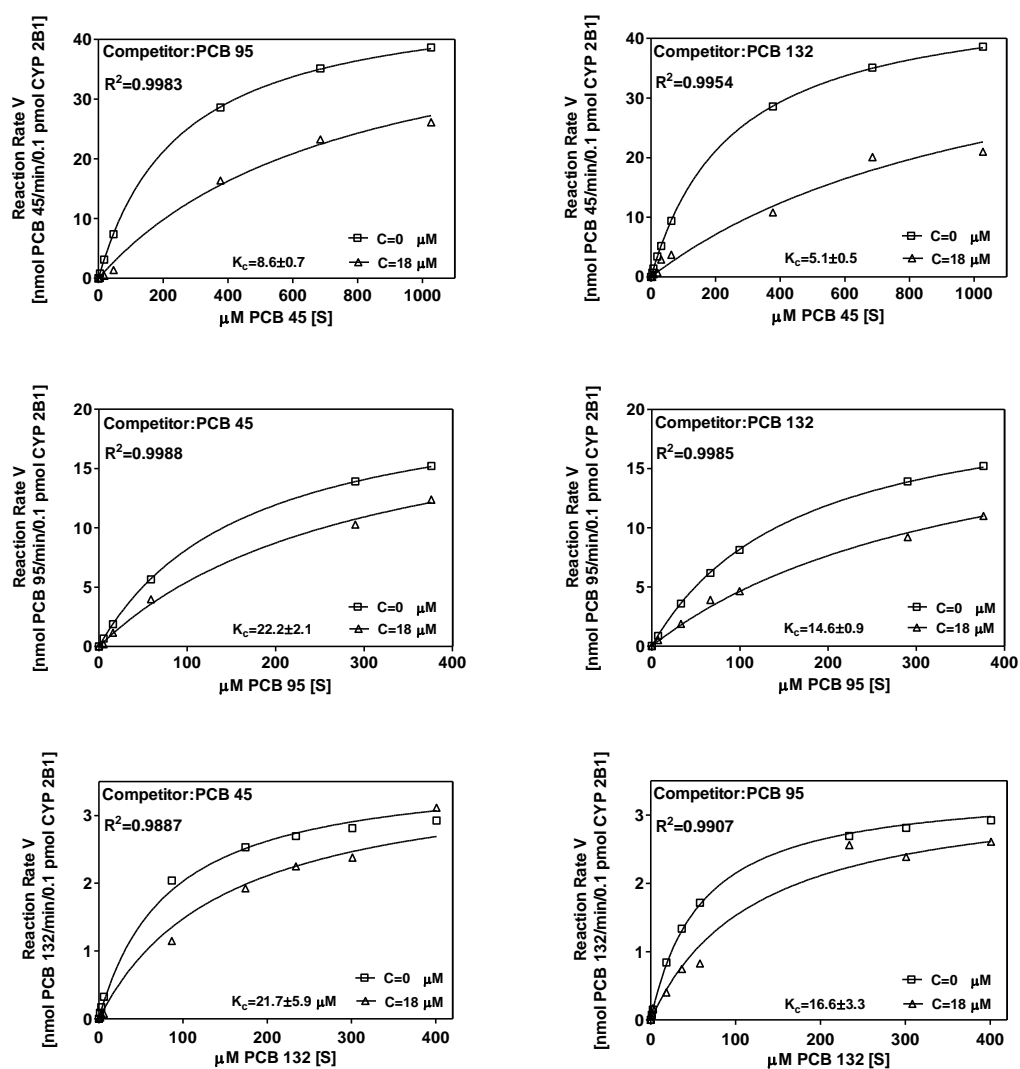
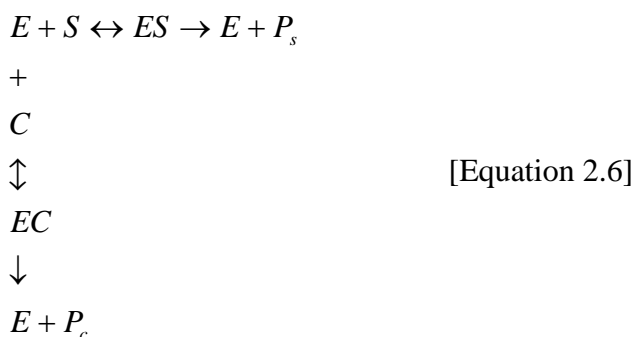


Figure 2.3 Inhibition kinetics for PCB 45, 95 and 132. K_c is the equilibrium dissociation constant for the enzyme-competitor complex; C the abbreviation of competitor; R^2 the global goodness of fit of nonlinear kinetic regression.

biotransformation rate data to different inhibition models. The competitive inhibition model had similar goodness-of-fit as the mixed inhibition model, with α value in all

mixed models greater than unity, suggesting that competitive inhibition is a suitable model to simulate competitive biotransformation in these incubations. A possible reason for this observation is that the dominant step of biotransformation is the binding processes of CYP isozymes with PCBs, so that a competitor can be approximately treated as an inhibitor in this case.

The competitive biotransformation reaction scheme can be expressed in Equation 2.6 (competitive inhibition scheme in box) (26):



where E is the enzyme, S the substrate, ES the enzyme-substrate complex, P_s the product of the substrate, C the competitor, EC the enzyme-competitor complex and P_c the product of the competitor. In our experiments, competitive biotransformation had no effect on V_{max} and can increase substrate K_m values. The competitive inhibition constant (K_c) (Equation 2.7) was used to evaluate the competition ability between each congener (26):

$$K_c = \frac{[E][C]}{[EC]} \qquad \text{[Equation 2.7]}$$

where [E] is the enzyme concentration, [C] the competitor concentration and [EC] the enzyme-competitor complex concentration. The value of K_c (Table 2.1) indicates the strength of enzyme-competitor interaction affinity when [E] and [C] are constant, with smaller K_c values suggesting increasing competition (e.g. for PCB 45, K_c was 8.6 μM when the competitor was PCB 95, but was 5.1 μM when the competitor was PCB 132,

Figure 2.3). Our results suggest that the degree of competition was dependent on the PCB chlorination pattern, with PCB 132 having the highest competition ability (PCB 132>PCB 95>PCB 45). This result is consistent with the K_m values of these congeners from our Michaelis-Menten kinetics studies.

2.3.3. Competitive Biotransformation of Atropisomers

Our incubation studies using racemic PCB 132 and its individual atropisomers indicates that competition between (-)-PCB 132 and (+)-PCB 132 may exist (Figure 2.1C). This experiment was performed at very low substrate concentrations, given the limited atropisomer-enriched PCB 132 available. In the racemic incubation, the atropisomers of PCB 132 had similar biotransformation rates, consistent with our pseudo-first order kinetics and Michaelis-Menten kinetics results at this concentration range. The assay was linear with regard to protein concentration from 0 to 0.01 to 0.1 pmol CYP2B1 when the concentration of PCB 132 was from 0 to 0.4 μ M. In contrast, the biotransformation rate of (+)-PCB 132 when incubated by itself was faster than its reaction rate in the racemic mixture incubation under the same conditions (Figure 2.1C). However, there was no difference in biotransformation rates for (-)-PCB 132 incubated either individually or as a racemate (Figure 2.1C). It is possible that (-)-PCB 132 can inhibit the biotransformation of (+)-PCB 132 in the racemic mixture incubations, because (-)-PCB 132 had higher affinity (smaller K_m , although not significantly different) for rat CYP2B1 compared to (+)-PCB 132 (Table 2.1 and Figure 2.1A). Alternatively, the atropisomers may inhibit each other at similar levels, as there was some (+)-PCB 132 present in the atropisomer-enriched (-)-PCB 132 (EF=0.256). This (+)-PCB 132 may inhibit the reaction rate of (-)-PCB 132 in individual incubations.

Our results indicate that the prediction of EFs based on environmental concentrations and physiological conditions of organisms, as previously attempted (13-16) is not possible for PCBs and by extension other chiral contaminants, because the various substrates (which may also include achiral compounds) compete with each other, including at the stereoisomer level. More study is needed to characterize such dynamics to develop predictive models of environmental stereoselectivity.

2.3.4. Docking Studies

Stereoselective interaction with enzymes of chiral organic pollutants was supported by molecular docking studies (43). Different interactions between PCB congeners and atropisomers with rat CYP2B1 are a possible reason for the different biotransformation kinetics observed. To test this hypothesis, we developed a three-dimensional structure of rat CYP2B1 (Figure 2.4) based on its amino acid sequence and the known structures of homologous isozyme CYP2B6. The PROCHECK statistics shown in the Ramachandran map (44) (Figure 2.5) indicated that 92.7% of model residues were in the most favored regions, 7.1% in the additional allowed regions, 0.2% in the generously allowed regions, and none in the disallowed conformations. The Profiles-3D score of this model was 206.3, higher than the expected value of 205.4, indicating that the protein sequence had a good fit with the current 3D environment. These results suggested that the overall protein structure of this CYP2B1 model is reasonable.

The three target congeners partially overlapped when docked in the model CYP2B1 structure (Figure 2.6), suggesting that competition between different congeners could be due to disruption of their respective binding to the isozyme. All three congeners had different CDOCKER interaction energies (nonbonded interactions including van der

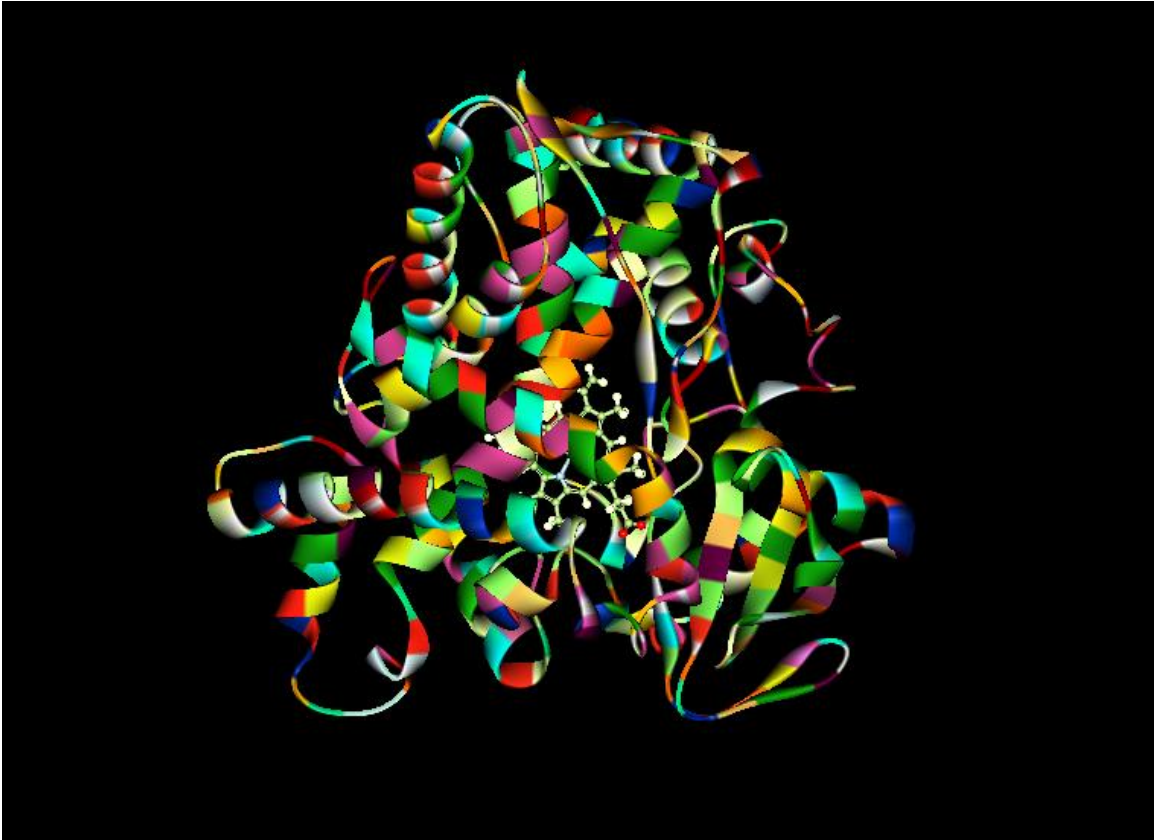


Figure 2.4 Three-dimensional structure of rat CYP2B1 from homology modeling.

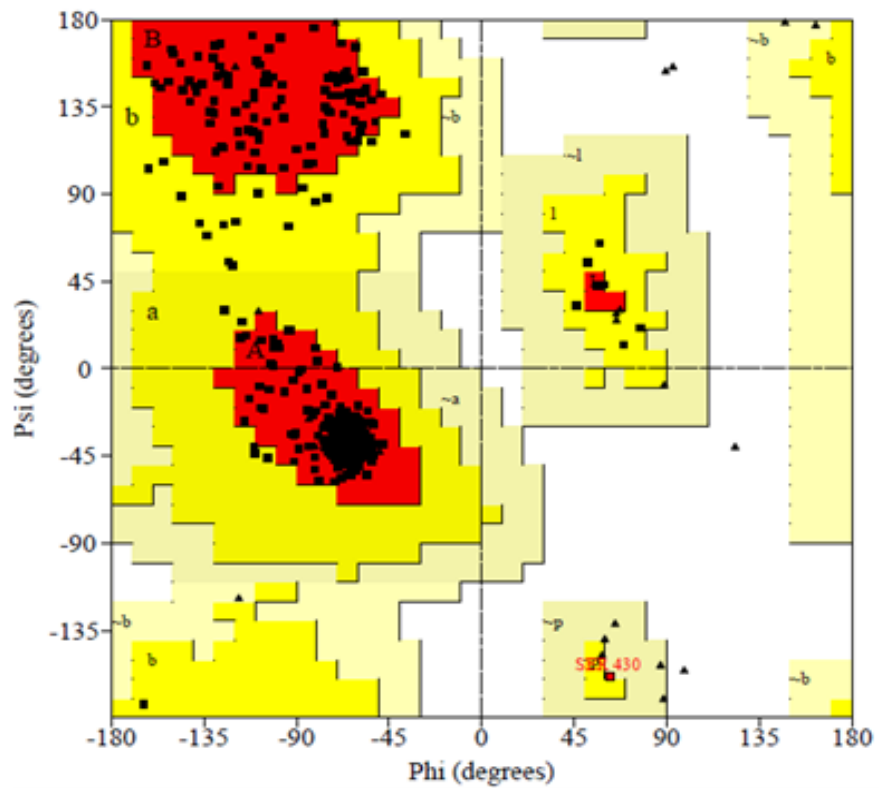


Figure 2.5 Ramachandran plots of the rat CYP2B1 model. The different colored areas indicate “disallowed” (white), “generously allowed” (light yellow, ~a, ~b, ~l, ~p), “additional allowed” (yellow, a, b, l, p), and “most favored” (red, A, B, L) regions.

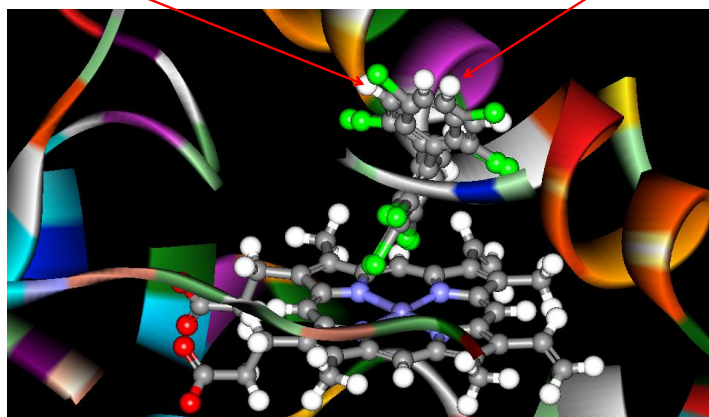
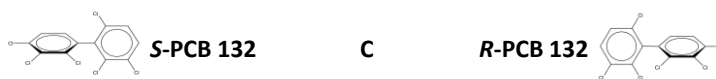
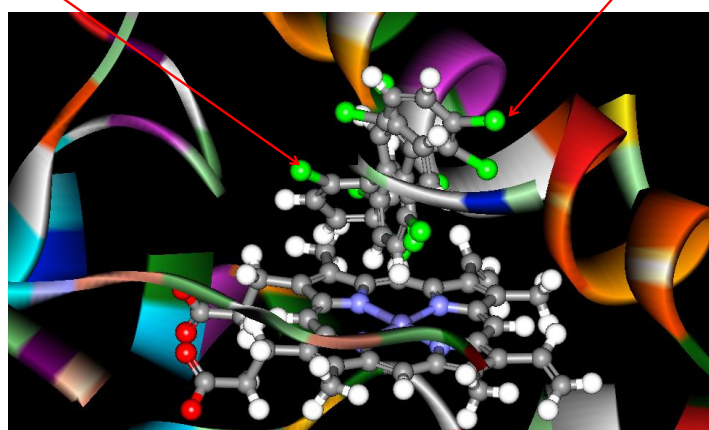
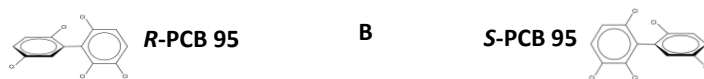
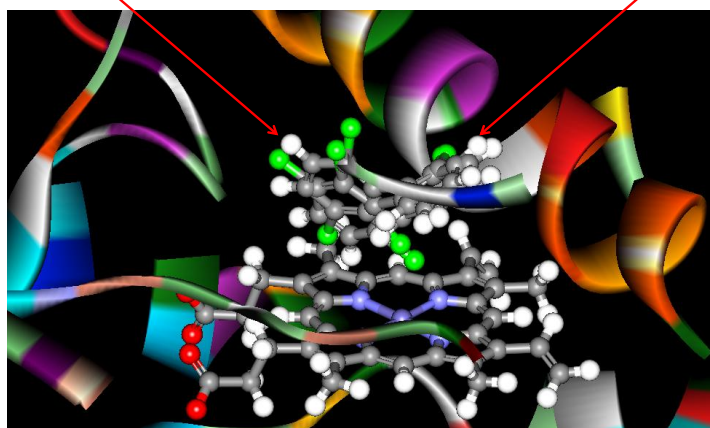
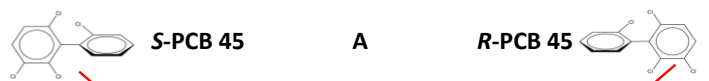


Figure 2.6 Docking poses of PCB 45 (A), PCB 95 (B) and PCB 132 (C) with rat CYP2B1. Cl atoms are in green, H atoms in white. CDOCKER interaction energies (kcal/mol) for each atropisomer are *R*-PCB 45: -28.0871; *S*-PCB 45: -32.8571; *R*-PCB 95: -32.0503; *S*-PCB 95: -32.1662; *R*-PCB 132: -34.6296; *S*-PCB 132 : -40.0324.

Waals and electrostatics forces) after docking. The lowest interaction energy, for PCB 132, was consistent with its lowest K_m values (Table 2.1), which indicates highest binding affinities. The individual atropisomers of each congener were also docked in different positions with rat CYP2B1, with different CDOCKER interaction energies. This observation is consistent with our experiments showing that individual atropisomers had different biotransformation kinetics of each congener, at least at low concentration ranges, and is also consistent with the competition observed between atropisomers in incubations of racemic mixtures, such as PCB 132.

Our study found that *S*-PCB 132 had a lower CDOCKER interaction energy than *R*-PCB 132, suggesting that *S*-PCB 132 had higher binding affinity with rat CYP2B1 consistent with our K_m value for (-)-PCB 132 (Figure 2.1A). This observation suggests that the first-eluting enantiomer, (-)-PCB 132, on Chirasil-Dex is the *S* configuration. However, this conclusion contrasts previous literature, which suggested that (-)-PCB 132 is the *R* configuration given indirect evidence from the configurations of their methylsulfonyl metabolites (45). One possible explanation for this discrepancy is that K_m values were not only affected by interaction energies but also competition from the antipode, which existed in our incubations (Figure 2.1C). This competition can influence the binding processes and change K_m values. Another explanation is that congeners or

atropisomers may not actually dock with the isozymes in the best conformation at the lowest energy, resulting in differences between modeling and experimental results. Validation of absolute stereochemistry is needed.

In addition, based on these molecular docking results and previous kinetics results, it is reasonable to assume that the *S* configurations of PCBs 45 and 95 preferentially bind and react with CYP2B1 compared to their antipodes. We suggest that the second-eluting atropisomers of PCB 45 on Cyclosil-B and PCB 95 on Chirasil-Dex are the *S* atropisomers, based on CDOCKER interaction energies and K_m values. However, the biotransformation kinetics of each atropisomer may not only be affected by binding affinities but also by other factors (*II*), e.g., how the compound enters the CYP, how products are released, and possible binding sequestration. Again, verification is necessary in future work.

Our results indicate that the prediction of reaction rates and EFs at the enzyme level, based on current information, is still not available. Uncertain factors include: whether chiral PCBs can induce some specific isozymes (e.g. CYP2B1) *in vitro* and/or *in vivo*; whether induction is also stereoselective; whether other enzymes catalyze chiral PCB metabolism; and whether other xenobiotics or endogenous compounds or their isomers also affect biotransformation. In addition, the stereoselective biotransformation of chiral PCBs *in vivo* is much more complex than that *in vitro*. Uptake, transportation and excretion processes must also be considered in addition to metabolism in attempting to predict stereoselectivity *in vivo*.

References

- (1) Lehmler, H.-J.; Harrad, S.J.; Hühnerfuss, H.; Kania-Korwel, I.; Lee, C.M.; Lu, Z.; Wong, C.S. Chiral Polychlorinated Biphenyl Transport, Metabolism, and Distribution: A Review. *Environ. Sci. Technol.* **2009**, *44*, 2757-2766.
- (2) Wong, C.S. and Warner, N.A. Chirality as an Environmental Forensics Tool. In *Persistent Organic Pollutants*; Harrad, S., Ed.; John Wiley & Sons, Ltd, Chichester, UK. 2009; pp 71-136.
- (3) Wong, P.W.; Brackney, W.R.; Pessah, I.N. *Ortho*-substituted polychlorinated biphenyls alter microsomal calcium transport by direct interaction with ryanodine receptors of mammalian brain. *J. Biol. Chem.* **1997**, *272*, 15145-15153.
- (4) Wong, P.W.; Joy, R.M.; Albertson, T.E.; Schantz, S.L.; Pessah, I.N. *Ortho*-substituted 2,2',3,5',6-pentachlorobiphenyl (PCB 95) alters rat hippocampal ryanodine receptors and neuroplasticity *in vitro*: evidence for altered hippocampal function. *Neurotoxicology* **1997**, *18*, 443-456.
- (5) Pessah, I.N.; Lehmler, H.-J.; Robertson, L.W.; Perez, C.F.; Cabrales, E.; Bose, D.D.; Feng, W. Enantiomeric Specificity of (-)-2, 2', 3, 3', 6, 6'-Hexachlorobiphenyl toward Ryanodine Receptor Types 1 and 2. *Chem. Res. Toxicol.* **2008**, *22*, 201-207.
- (6) Lehmler, H.-J.; Robertson, L.W.; Garrison, A.W.; Kodavanti, P.R.S. Effects of PCB 84 enantiomers on [³H]-phorbol ester binding in rat cerebellar granule cells and ⁴⁵Ca²⁺ -uptake in rat cerebellum. *Toxicol. Lett.* **2005**, *156*, 391-400.
- (7) Safe, S.H. Polychlorinated biphenyls (PCBs): environmental impact, biochemical and toxic responses, and implications for risk assessment. *CRC Crit. Rev. Toxicol.* **1994**, *24*, 87-149.

- (8) Letcher, R.; Klasson-Wehler, E.; Bergman, A. Methyl sulfone and hydroxylated metabolites of polychlorinated biphenyls. *Handbook of Environmental Chemistry Volume 3 Anthropogenic Compounds Part K* **2000**, 315-359.
- (9) Brocks, D.R. Drug disposition in three dimensions: an update on stereoselectivity in pharmacokinetics. *Biopharm. Drug Dispos.* **2006**, *27*, 387-406.
- (10) Smith, S.W. Chiral Toxicology: It's the Same Thing... Only Different. *Toxicol. Sci.* **2009**, *110*, 4-30.
- (11) Kania-Korwel, I.; Hrycay, E.G.; Bandiera, S.M.; Lehmler, H.-J. 2, 2', 3, 3', 6, 6'-hexachlorobiphenyl (PCB 136) atropisomers interact enantioselectively with hepatic microsomal cytochrome P450 enzymes. *Chem. Res. Toxicol.* **2008**, *21*, 1295-1303.
- (12) Warner, N.A.; Norstrom, R.J.; Wong, C.S.; Fisk, A.T. Enantiomeric fractions of chiral polychlorinated biphenyls provide insights on biotransformation capacity of arctic biota. *Environ. Toxicol. Chem.* **2005**, *24*, 2763-2767.
- (13) Wong, C.S.; Garrison, A.W.; Smith, P.D.; Foreman, W.T. Enantiomeric composition of chiral polychlorinated biphenyl atropisomers in aquatic and riparian biota. *Environ. Sci. Technol.* **2001**, *35*, 2448-2454.
- (14) Chu, S.; Covaci, A.; Vijver, K.V.; Coen, W.D.; Blust, R.; Schepens, P. Enantiomeric signatures of chiral polychlorinated biphenyl atropisomers in livers of harbour porpoises (*Phocoena phocoena*) from the southern North Sea. *J. Environ. Monit.* **2003**, *5*, 521-526.
- (15) Wong, C.S.; Garrison, A.W.; Foreman, W.T. Enantiomeric composition of chiral polychlorinated biphenyl atropisomers in aquatic bed sediment. *Environ. Sci.*

Technol. **2001**, *35*, 33-39.

- (16) Kobližková, M.; Dušek, L.; Jarkovský, J.; Hofman, J.; Bucheli, T.D.; Klánová, J.
Can physicochemical and microbial soil properties explain enantiomeric shifts of
chiral organochlorines? *Environ. Sci. Technol.* **2008**, *42*, 5978-5984.
- (17) Rodman, L.E.; Shedlofsky, S.I.; Mannschreck, A.; Püttmann, M.; Swim, A.T.;
Robertson, L.W. Differential potency of atropisomers of polychlorinated biphenyls
on cytochrome P450 induction and uroporphyrin accumulation in the chick embryo
hepatocyte culture. *Biochem. Pharmacol.* **1991**, *41*, 915-922.
- (18) Püttmann, M.; Mannschreck, A.; Oesch, F.; Robertson, L. Chiral effects in the
induction of drug-metabolizing enzymes using synthetic atropisomers of
polychlorinated biphenyls (PCBs). *Biochem. Pharmacol.* **1989**, *38*, 1345-1352.
- (19) Warner, N.A.; Martin, J.W.; Wong, C.S. Chiral polychlorinated biphenyls are
biotransformed enantioselectively by mammalian cytochrome P-450 isozymes to
form hydroxylated metabolites. *Environ. Sci. Technol.* **2009**, *43*, 114-121.
- (20) Ngui, J.S. and Bandiera, S.M. Induction of Hepatic CYP2B Is a More Sensitive
Indicator of Exposure to Aroclor 1260 than CYP1A in Male Rats. *Toxicol. Appl.
Pharmacol.* **1999**, *161*, 160-170.
- (21) Letcher, R.J.; Norstrom, R.J.; Lin, S.; Ramsay, M.A.; Bandiera, S.M.
Immunoquantitation and microsomal monooxygenase activities of hepatic
cytochromes P4501A and P4502B and chlorinated hydrocarbon contaminant levels
in polar bear (*Ursus maritimus*). *Toxicol. Appl. Pharmacol.* **1996**, *137*, 127-140.
- (22) Routti, H.; Letcher, R.J.; Arukwe, A.; van Bavel, B.; Yoccoz, N.G.; Chu, S.;
Gabrielsen, G.W. Biotransformation of PCBs in relation to phase I and II

- xenobiotic-metabolizing enzyme activities in ringed seals (*Phoca hispida*) from Svalbard and the Baltic Sea. *Environ. Sci. Technol.* **2008**, *42*, 8952-8958.
- (23) Sandau, C.D.; Ayotte, P.; Dewailly, E.; Duffe, J.; Norstrom, R.J. Analysis of hydroxylated metabolites of PCBs (OH-PCBs) and other chlorinated phenolic compounds in whole blood from Canadian Inuit. *Environ. Health Perspect.* **2000**, *108*, 611-616.
- (24) Harner, T.; Wiberg, K.; Norstrom, R. Enantiomer fractions are preferred to enantiomer ratios for describing chiral signatures in environmental analysis. *Environ. Sci. Technol.* **2000**, *34*, 218-220.
- (25) Edwards, P.R.; Hryciak, E.G.; Bandiera, S.M. Differential inhibition of hepatic microsomal alkoxyresorufin O-dealkylation activities by tetrachlorobiphenyls. *Chem. Biol. Interact.* **2007**, *169*, 42-52.
- (26) Bisswanger, H. Enzyme kinetics: principles and methods. WILEY-VCH Verlag GmbH & Co. KGaA, Weinheim **2008**, 91-119.
- (27) Arnold, K.; Bordoli, L.; Kopp, J.; Schwede, T. The SWISS-MODEL workspace: a web-based environment for protein structure homology modelling. *Bioinformatics* **2006**, *22*, 195.
- (28) Peitsch, M.C. Protein modeling by E-mail. *Nat. Biotechnol.* **1995**, *13*, 658-660.
- (29) Kiefer, F.; Arnold, K.; Kunzli, M.; Bordoli, L.; Schwede, T. The SWISS-MODEL Repository and associated resources. *Nucleic Acids Res.* **2009**, *37*, D387-D392.
- (30) Nelson, D.R.; Koymans, L.; Kamataki, T.; Stegeman, J.J.; Feyereisen, R.; Waxman, D.J. P450 superfamily: update on new sequences, gene mapping, accession numbers and nomenclature. *Pharmacogenetics* **1996**, *6*, 1-42.

- (31) Rosales-Hernández, M.C.; Mendieta-Wejbe, J.E.; Trujillo-Ferrara, J.G.; Correa-Basurto, J. Homology modeling and molecular dynamics of CYP1A1 and CYP2B1 to explore the metabolism of aryl derivatives by docking and experimental assays. *Eur. J. Med. Chem.* **2010**, *45*, 4845-4855.
- (32) Honma, W.; Li, W.; Liu, H.; Scott, E.E.; Halpert, J.R. Functional role of residues in the helix B' region of cytochrome P450 2B1. *Arch. Biochem. Biophys.* **2005**, *435*, 157-165.
- (33) Cavasotto, C.N. and Phatak, S.S. Homology modeling in drug discovery: current trends and applications. *Drug Discov. Today* **2009**, *14*, 676-683.
- (34) Laskowski, R.A.; MacArthur, M.W.; Moss, D.S.; Thornton, J.M. PROCHECK: a program to check the stereochemical quality of protein structures. *J. Appl. Cryst.* **1993**, *26*, 283-291.
- (35) Liathy, R.; Bowie, J.U.; Eisenberg, D. Assessment of protein models with three-dimensional profiles. *Nature* **1992**, *356*, 83-85.
- (36) Wu, G.; Robertson, D.H.; Brooks III, C.L.; Vieth, M. Detailed analysis of grid - based molecular docking: A case study of CDOCKER—A CHARMM - based MD docking algorithm. *J. Comput. Chem.* **2003**, *24*, 1549-1562.
- (37) Vieth, M.; Hirst, J.D.; Kolinski, A.; Brooks III, C.L. Assessing energy functions for flexible docking. *J. Comput. Chem.* **1998**, *19*, 1612-1622.
- (38) Mattila, K. and Renkonen, R. Modelling of Bet v 1 Binding to Lipids. *Scand. J. Immunol.* **2009**, *70*, 116-124.
- (39) Koska, J.; Spassov, V.Z.; Maynard, A.J.; Yan, L.; Austin, N.; Flook, P.K.; Venkatachalam, C.M. Fully Automated Molecular Mechanics Based Induced Fit

- Protein– Ligand Docking Method. *J.Chem.Inf.Model* **2008**, *48*, 1965-1973.
- (40) Mackay, D.; Shiu, W.Y.; Ma, K.C.; Lee, C. *Physical-chemical Properties and Environmental Fate for Organic Chemicals on CD-ROM*. CRC/Taylor & Francis: **2006**.
- (41) Al-Gailany, K.A.S.; Houston, J.B.; Bridges, J.W. The role of substrate lipophilicity in determining type 1 microsomal P450 binding characteristics. *Biochem. Pharmacol.* **1978**, *27*, 783-788.
- (42) Kania-Korwel, I.; Garrison, A.W.; Avants, J.K.; Hornbuckle, K.C.; Robertson, L.W.; Sulkowski, W.W.; Lehmler, H.-J. Distribution of chiral PCBs in selected tissues in the laboratory rat. *Environ. Sci. Technol.* **2006**, *40*, 3704-3710.
- (43) Wang, C.; Zhang, N.; Li, L.; Zhang, Q.; Zhao, M.; Liu, W. Enantioselective interaction with acetylcholinesterase of an organophosphate insecticide fenamiphos. *Chirality* **2010**, *22*, 612-617.
- (44) Ramachandran, G.N.; Ramakrishnan, C.; Sasisekharan, V. Stereochemistry of polypeptide chain configurations. *J. Mol. Biol.* **1963**, *7*, 95-99.
- (45) Norström, K.; Eriksson, J.; Haglund, J.; Silvari, V.; Bergman, Å. Enantioselective Formation of Methyl Sulfone Metabolites of 2,2',3,3',4,6'-Hexachlorobiphenyl in Rat. *Environ. Sci. Technol.* **2006**, *40*, 7649-7655.
- (46) Asher, B.J.; D'Agostino, L.A.; Way, J.D.; Wong, C.S.; Harynuk, J.J. Comparison of peak integration methods for the determination of enantiomeric fraction in environmental samples. *Chemosphere* **2009**, *75*, 1042-1048.
- (47) Baltes, M.; Dubois, J.; Hanocq, M. Ethyl acetate extraction procedure and isocratic high-performance liquid chromatographic assay for testosterone metabolites in cell

- microsomes. *J. Chromatogr.* **1998**, 706, 201-207.
- (48) Baldwin, W.S. and LeBlanc, G.A. *In vivo* biotransformation of testosterone by phase I and II detoxication enzymes and their modulation by 20-hydroxyecdysone in *Daphnia magna*. *Aquat. Toxicol.* **1994**, 29, 103-117.
- (49) Wong, C.S.; Hoekstra, P.F.; Karlsson, H.; Backus, S.M.; Mabury, S.A.; Muir, D.C.G. Enantiomer fractions of chiral organochlorine pesticides and polychlorinated biphenyls in standard and certified reference materials. *Chemosphere* **2002**, 49, 1339-1347.
- (50) Ng, B.H. and Yuen, K.H. Determination of plasma testosterone using a simple liquid chromatographic method. *J. Chromatogr. B* **2003**, 793, 421-426.

Chapter 3

Disruption of Biomolecule Function by Nanoparticles: How Do Gold Nanoparticles Affect Phase I Biotransformation of Persistent Organic Pollutants?

A version of this chapter has been previously published as Lu, Z., Ma, G. B. Veinot, J.G.C., Wong, C. S. Disruption of biomolecule function by nanoparticles: How do gold nanoparticles affect phase I biotransformation of persistent organic pollutants? *Chemosphere*. 2013, 93, 123-132. (DOI: 10.1016/j.chemosphere.2013.05.004). Copyright 2013 © Elsevier. Reprinted with permission.

The author of this dissertation designed these experiments along with his supervisor, performed the experiments, interpreted data and wrote the manuscript. Dr. Guibin Ma and Dr. Jonathan G.C. Veinot were responsible for gold nanoparticle preparation.

3.1.Introduction

The fate of persistent organic pollutants (POPs) is of environmental concern due to their persistence, bioaccumulation and toxicities. Oxidative metabolism of POPs to more polar metabolites by cytochrome P-450 isozymes (CYPs) in phase I biotransformation is a significant detoxification mechanism (1). Factors affecting this process include the characteristics of different substrates and CYPs, the solution chemistry, and the involvement of other xenobiotics. The classic catalytic cycle of CYPs consists of substrate binding to the isozyme's active site; electron transfer, catalyzed by cytochrome P-450 reductase (CPR), from reduced nicotinamide adenine dinucleotide phosphate (NADPH) through flavin adenine dinucleotide and flavin mononucleotide to the CYP's heme group; and oxidation of substrates with formation of water (2-5). In this cycle, the kinetics and dynamics of substrate binding and electron transfer are important. Any alteration of these two processes will dramatically change biotransformation rates and selectivity of CYPs.

Engineered nanoparticles have attracted increasing attention because of their multiple applications, special physical-chemical properties compared to the bulk material, unclear environmental fate, and potential toxicities (6). Based on their structural characteristics and the fact that they could be taken up by hepatocytes (7), nanoparticles may be able to disrupt the functions of CYPs by affecting the factors mentioned above. However, the mechanisms behind disruption of CYPs, other biomolecules, and cellular processes in general is not necessarily obvious, given the potential complexity of interactions between nanoparticles, and ions and molecules in their environs. For example, aggregation, sorption, uptake by organisms, and interaction with biomolecules

or other xenobiotics are likely to be the main aqueous fate processes of nanoparticles affecting their transport, transformation, bioavailability and toxicity (6,8). Changes in environmental mobility of nanoparticles resulting from aggregation can significantly affect cellular uptake, reactivity and toxicity of these contaminants (9). For example, graphite, gold and polyamidoamine dendrimer nanoparticles smaller than 12 nm can penetrate the blood-brain barrier (10), and 20-60 nm polystyrene nanoparticles have greater intracellular distribution concentration and inhibition ability of CYPs than that of larger particles (11). Some nanoparticles are powerful adsorbents because of their unique structure and electronic characteristics (8). Thus, they can interact with organic pollutants and metal ions, thereby changing the environmental behavior of all contaminants involved in these interactions and thereby alleviating or amplifying their toxicities (8). In addition, nanoparticles can interact with proteins through electrostatic interactions, hydrophobic interactions, and specific chemical interactions. These interactions may result in either the loss of functional structure of the protein and consequent inhibition of activity, or immobilization of the protein and potential improvement of its activity and selectivity (12). Moreover, many studies have demonstrated that solution chemistry, especially ionic strength, is one of the key factors affecting the aggregation of nanoparticles (10). However, the reverse issue--namely the influence of nanoparticle aggregation on solution ionic strength--is less well understood. These potential effects are important, because changes of ionic strength may change the microenvironment of biomolecules and consequently indirectly affect their functions.

In the present study, gold nanoparticles (AuNPs), rat CYP2B1 isozyme and polychlorinated biphenyl (PCB) were chosen as probe substances to analyze such

potential direct and indirect influences of nanoparticles on the biotransformation of POPs, a representative model enzymatic process. Our overall hypothesis is that these nanoparticles will directly interact with CYPs and also change the ionic strength in the microenvironment near them. The function of CYPs is thereby changed, and more generally those of other biomolecules with functions that depend on ionic strength.

AuNPs have been used extensively in chemistry, biology, engineering and biomedicine due to their optical and structural properties (13). They have also been considered as toxicologically relevant substances (10). Bioaccumulation and biomagnification of AuNPs in food webs were observed previously (14). At the cellular level, studies have reported conflicting data regarding toxicity of AuNPs (10, 15). AuNPs were shown to be non-toxic for cells or in blood (10,16,17). However, other studies suggested different toxicities of AuNPs in cell such as cell membrane disruption based on electrostatic interactions (18), triggered necrosis (19), mitochondrial damage, oxidative stress induction on cell lines (19, 20), intracellular distribution, entrapment within organelles (10, 21), and possible immunotoxicity (22,23). It is thus reasonable to presume that the behavior of AuNPs within biological systems depend on the nanoparticles' size, concentration and capping agents, all of which affect their interactions with cellular processes. Intracellular uptake of AuNPs was observed previously (21). However, detailed mechanisms of cellular function alteration by AuNPs are unknown. A few studies have focused on the toxicity of AuNPs at the enzyme level (e.g., human CYP inhibition) (24). However, the effects of AuNPs on enzyme activity and selectivity, and relevant mechanisms, are still poorly understood, hence our use of AuNPs and CYPs to elucidate such mechanisms on phase I biotransformation, an important enzymatic process.

Enantioselective analysis was employed for this research because it is a powerful tool to study the metabolism of xenobiotics in biological systems (25,26). Previous studies have demonstrated that chiral PCBs, a class of legacy POPs, could be biotransformed stereoselectively by rat CYP2B1 *in vitro* (27,28). Competition among different POPs and different interactions between chiral PCB congeners or atropisomers with rat CYP2B1 at the molecular level were the main factors affecting this stereoselective biotransformation process (28). However, the influence of other types of xenobiotics (e.g., nanoparticles) on this process is unknown. Accordingly, this study's objectives were to determine how AuNPs affect the stereoselective biotransformation of POPs by CYPs. Our probe compound, 2,2',3,5',6-pentachlorobiphenyl (PCB 95), was chosen because it is widely detected in organisms, can be stereoselectively biotransformed *in vitro* and *in vivo*, and is neurotoxic (27-30). To our knowledge, this is the first study to investigate the impacts of nanoparticles on biotransformation processes of chiral organic contaminants and relevant mechanisms.

3.2. Materials and Methods

3.2.1. Chemicals and Reagents

Racemic chiral PCB 95, recovery standards PCBs 30 and 204 and internal standard PCB 159 (all purities >99%) were purchased from Accustandard (West Haven, CT) and prepared in acetone. Rat CYP2B1 mixture (CYP2B1 itself+CPR+cytochrome b₅), insect cell control supersomes (CPR and cytochrome b₅) (stored at -80 °C until use) and NADPH regeneration system (solution A: 31 mM NADP⁺, 66 mM glucose-6-phosphate and 66 mM MgCl₂ in water; solution B: 40 U/ml glucose-6-phosphate dehydrogenase in 5 mM sodium citrate) (stored at -20 °C until use) were purchased from BD Biosciences (San Jose,

CA). Gold (III) chloride trihydrate ($\text{HAuCl}_4 \cdot 3\text{H}_2\text{O}$) and sodium citrate tribasic dihydrate ACS reagent 99.0% ($\text{Na}_3\text{C}_6\text{H}_5\text{O}_7 \cdot 2\text{H}_2\text{O}$), were purchased from Sigma-Aldrich and used as received. Dialysis tubing was purchased from Spectrum Laboratories, Inc. (Spectra/Por 6 Dialysis membrane, Lot Number 3244650), approximate molecular weight cut off (MWCO) is 8,000 Daltons (flat width is 50 mm and thickness is 0.0011 inches).

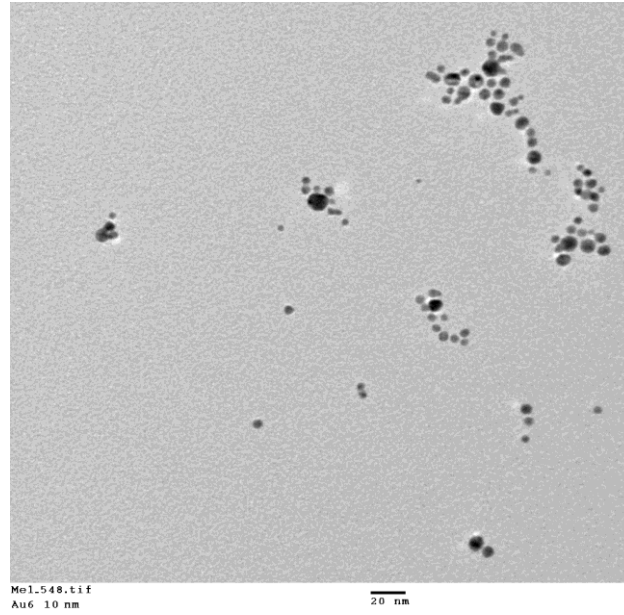
3.2.2. Synthesis of Citrate-capped AuNPs

The preparation was carried out using a modified procedure similar to that previously published (31). A stock solution of gold nanoparticles was prepared in aqueous solution via reduction of $\text{HAuCl}_4 \cdot 3\text{H}_2\text{O}$ (0.25 mM, 1 liter) upon addition of an aqueous NaBH_4 solution (0.015 g dissolved in 5 ml of distilled water containing 0.11 g sodium citrate tribasic salt) in one rapid addition. Particle growth was arrested by surface passivation with the sodium citrate tribasic salt of citrate (0.11 g) that was present in the initial $\text{HAuCl}_4 \cdot 3\text{H}_2\text{O}$ solution. The AuNPs were purified using dialysis. The 200 mL of the stock solution of choice was poured into a dialysis tube. The filled tubes were submerged in distilled water (4-liter capacity beaker) for 4 days (bath water was changed at regular 4-5 hour intervals).

3.2.3. Characterization of Citrate-capped AuNPs

Transmission electron microscopy (TEM) analysis of the citrate-capped AuNPs is shown in Figure 3.1. The particle diameters are approximately 7.5 nm as determined using TEM.

(a)



(b)

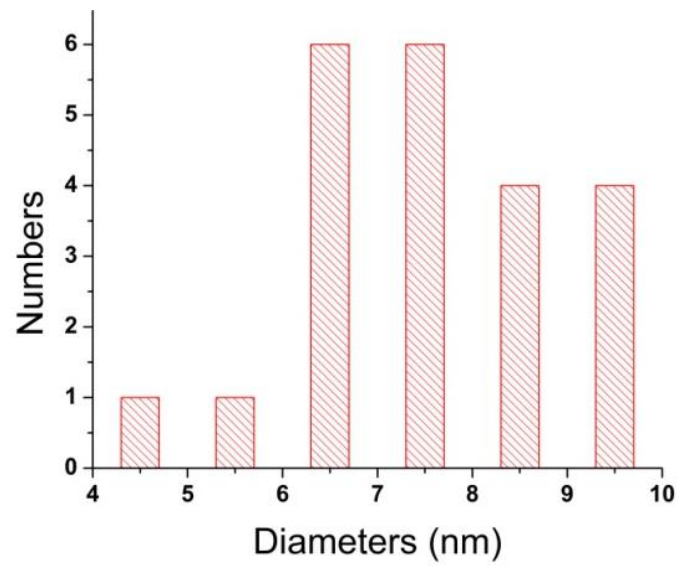


Figure 3.1 TEM image of citrate-capped AuNPs. (a) and statistical size distribution ($d = 7.5 \pm 3$ nm) (b).

3.2.4. *In Vitro* Biotransformation Experiments

Detailed incubation methods were previously published (27,28). Briefly, incubations were conducted in glass tubes containing 5 pmol of rat CYP2B1, 50 μ L of solution A, 10 μ L of solution B, 100 ng or 500 ng PCB 95, 10 nmol or 200 nmol AuNPs (sonicated for 5 minutes before use) and potassium phosphate buffer (110 mM, pH 7.4) in 1 mL total volume at 37°C. Incubations were terminated with 1 mL ice-cold methanol and immediately extracted. PCB 95 was used as positive control substrate for 30 minutes incubation instead of testosterone (28). PCB 95 was incubated with insect cell control supersomes for 30 minutes as negative control, instead of the rat CYP 2B1+CPR+cytochrome b₅ mixture.

3.2.5. Chemical Extraction and Clean-up

Briefly, after the incubations were terminated, PCBs 30 and 204 were added as recovery standards to the test tubes before extraction. The incubations were further denatured using HCl and 2-propanol, vortexed for 1 min and centrifuged for 10 min. The liquid supernatant was then washed with KCl and extracted with 6 mL of 1:1 (v/v) methyl-*t*-butyl ether/hexane. All extraction procedures were repeated three times for each sample. The organic fraction was purified using an acidified silica gel column (1 g anhydrous sodium sulfate on top, 3 g 22% H₂SO₄ coated silica gel at the bottom, *w/w*) and eluted with 20 mL of 15% (v/v) dichloromethane/hexane. PCB 159 was used as a volume corrector.

3.2.6. Instrumentation and Measurements

PCBs were quantified using an Agilent 5890 gas chromatograph with an electron capture detector and a Chirasil-Dex column (25 m \times 0.25 mm \times 0.25 μ m d_f, Varian, CA)

(27,28). Briefly, 1 μ L samples were injected in splitless mode at 250°C with helium as carrier gas and at a constant column head pressure of 10.6 psi. Initial oven temperature was held at 60 °C for 2 min, then ramped at 10 °C/min to 160 °C, ramped at 1 °C/min to 210 °C, held for 25 min. PCB 95 concentrations were recovery-corrected; recoveries of PCBs 30 and 204 were 77 \pm 9% and 79 \pm 6% (mean \pm σ), respectively. PeakFit v4.12 (Systat Software, San Jose, CA) was used to deconvolute chromatograms (32).

A ZetaPALS dynamic light scattering (DLS) analyzer (Brookhaven Instruments Corporation, Holtsville, NY, USA) was used to characterize size, zeta potential and conductance of particles in liquid samples. UV-Vis spectra were recorded using a Shimadzu UV-2501PC spectrophotometer with a Lauda temperature control system. Spectra were collected over ranges of 300-620 nm and 400-800 nm for NADPH and AuNPs, respectively.

3.2.7. Data Analyses

Enantiomer fractions (EFs) (33) (Equation 1.1) were used to describe atropisomer distributions. EF is defined as the concentration ratio of the first-eluting atropisomer and the total concentration of both atropisomers of PCB 95.

Prism 5 (GraphPad Software, La Jolla, CA) and Origin 6.0 (Microcal Software, Northampton, USA) were used for plotting and statistical analyses. The t-test was used for data analyses, with statistically significant levels at 0.05.

3.3. Results and Discussion

3.3.1. Stereoselective Biotransformation of PCB 95

Our hypothesis was that AuNPs affect the biotransformation activity and stereoselectivity of CYPs. To test this hypothesis, three biotransformation experiments

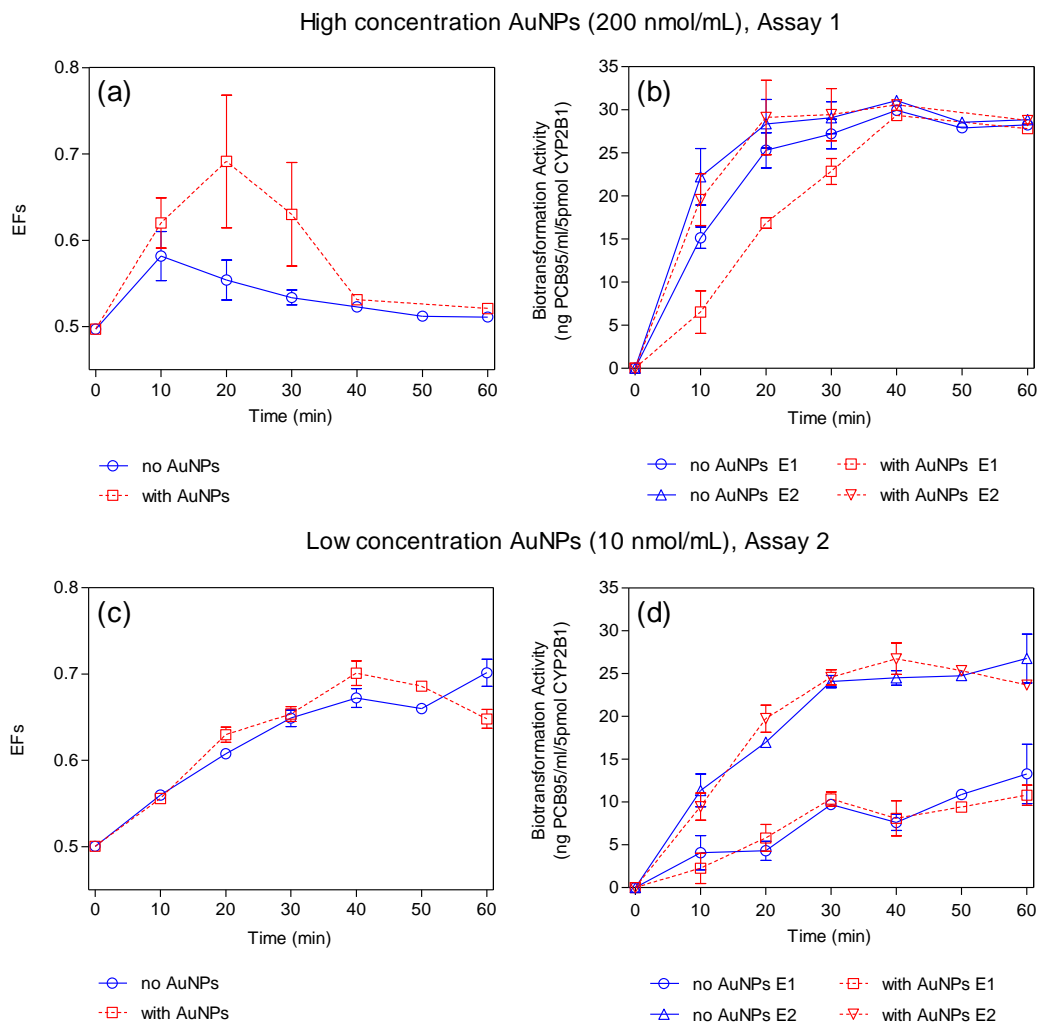


Figure 3.2 Biotransformation activity of PCB 95 by rat CYP2B1 isozyme and change of EFs. Data reported as mean \pm standard error with three replicates. The incubations without AuNPs (in blue) were control samples.

were conducted: incubations without AuNPs (as control), incubations with a high concentration of AuNPs, and incubations with a low concentration of AuNPs. The concentration of PCB 95 (100 ng/mL, about 1300 ng/g in lipid weight) we used in this

experiment was environmentally relevant, because high trophic level organisms contaminated with PCBs would have high levels from bioaccumulation. For example, the mean concentration of total PCBs in the Arctic narwhal (*Monodon monoceros*), beluga (*Delphinapterus leucas*) and Greenland shark (*Somniosus microcephalus*) were about 4080 (252-526 ng/g PCB 95), 2440 (53-500 ng/g PCB 95) and 5766 (40-1680 ng/g PCB 95) ng/g (lipid weight), respectively (34,35).

For incubations without AuNPs, the biotransformation rates of the second-eluting (E2) atropisomer of PCB 95 were faster than those of its antipode (Figure 3.2), depending on incubation conditions. Depletion of E1- and E2-PCB 95 was 30% and 45% of the initial concentrations, respectively, after 10 min of incubation, and reached 60% after 60 min for assay 1 (Figure 3.2b). Correspondingly, EFs increased from racemic (0.500) to 0.582 in 10 mins, then decreased to 0.511 after 60 min (Figure 3.2a). Assay 2 (Figure 3.2c and 2d) differed slightly for reasons discussed below, as E1- and E2-PCB 95 had about 20% and 50% depletion respectively within 60 min of incubation, that resulted in an increase of EFs from an initial racemic value of 0.500 to about 0.702. Preferential depletion of E2-PCB 95 is consistent with observations of similar non-racemic PCB 95 atropisomer compositions after incubations with rat CYP2B1 or phenobarbital-induced rat liver microsomes (CYP2B isozyme-enriched) *in vitro* (27,28,36), possibly because the two PCB 95 atropisomers could bind at different positions in the active site of rat CYP2B1 (28). *In vivo* enrichment of E1-PCB 95 (EF>0.5) was also found in tissues of rats injected with Aroclor 1254 or Chlorofen-contaminated soil extracts (37). These results all suggest that CYP2B1 should be responsible for much of the stereoselective metabolism of chiral PCBs in mammals.

We used different concentrations of AuNPs, since the effects of AuNPs on biological systems are concentration-dependent (10,38). As yet, there is no reliable measurement-based data on AuNP concentrations in the aquatic environment (39), and indeed on most NPs given the extreme difficulties in measuring NPs under environmentally relevant *in situ* conditions. However, previous studies used 0-5.6 mM of AuNPs for different toxicity tests *in vitro* (10). In addition, application of AuNPs in biomedical treatment and subsequent exposure in organisms can be at high levels. For example, AuNPs were used as cisplatin's carrier to improve the biodistribution of this anticarcinogen *in vivo* and about 50-60 $\mu\text{g/g}$ tissue "free" gold was detected in rat liver after 24 hour intraperitoneal injection of AuNP-cisplatin conjugates (40). Thus, the AuNPs used in the present study (10 and 200 μM) was comparable to that observed in previous literature and reasonable in terms of potential exposure (10,14).

Incubations with AuNPs altered biotransformation activities and EFs of PCB 95 (Figure 3.2). As expected, a high concentration of AuNPs appeared simply to lower the biotransformation of E1-PCB 95 (Figure 3.2b, 200 μM AuNPs, statistically significant at 20 min, paired *t*-test) thereby increasing EFs (Figure 3.2a). The activity decrease mainly occurred early on in the incubation, and waned with increasing incubation time.

Enzyme activity inhibition by nanoparticles might be due to various factors. First, the affinity between enzymes and the substrates may be reduced because both may be able to bind with nanoparticles (41). Given the polarity of the citrate-capped AuNPs, it is unlikely that hydrophobic PCB 95 will bind to them. Second, the stabilization and function of membrane-bounded enzymes may be affected by nanoparticles, resulting in membrane damage to the cell or its organelles. For example, CYP and CPR are anchored

in the endoplasmic reticulum of cells with CYP activity. The composition of such phospholipid membranes plays an important role in modulating the functions of membrane-bounded CYP and CPR (e.g., ligand binding and electron transfer) (42). AuNPs are believed to be able to fluidize and penetrate the phospholipid bilayer (18,24). Thus, AuNPs may be able to disrupt the structure and function of the membrane to which CYP and CPR are bound, thereby changing the biotransformation performance of these enzymes. However, given that our study focuses on *in vitro* biotransformation dynamics, evaluation of this hypothesis is beyond the scope of our current study. Third, the substrate binding or product release kinetics may be changed through effects of nanoparticles on the diffusion or mobility of enzymes and/or substrates. Fourth, nanoparticles may be able to disrupt the electron transfer chain (e.g., inhibition of the production rate of NADPH). This factor is further investigated in Sections 3.3.3-3.3.6 of the present study.

Incubations with a relatively low concentration of AuNPs (10 μ M) were hypothesized to have little to no inhibition of CYP activity. However, the results showed slight albeit not statistically significant enhancements of the biotransformation activity of E2-PCB 95 at 20 min and 40 min (Figure 3.2d). Correspondingly, EFs were also higher than in the control incubations without AuNPs (Figure 3.2c). There are some possible explanations for these observations. First, this AuNP concentration is still very high compared to the 5 pmol rat CYP2B1 present. Also, data on cation-AuNP interactions and buffer salinity-enzyme activity relationships indicated that AuNPs could affect the behavior of cations in buffer solution, and therefore must also influence CYPs and other enzymes involved in phase I biotransformation (details are discussed in Sections 3.3.3-3.3.6). In addition, after a long incubation time (i.e., 60 minutes), AuNPs exhibited

some inhibition of the biotransformation activity of both PCB 95 atropisomers, which could be because the influence of AuNPs on the substrate's binding kinetics with CYP2B1 became more important when the substrate concentration eventually dropped to a low enough level over time.

Furthermore, rat CYP2B1 had higher biotransformation activity in assay 1 (high concentration AuNP assay, Figure 3.2b) than in assay 2 (low concentration AuNP assay, Figure 3.2d). This might be due to different incubation conditions of the two assays (i.e., different amounts of AuNP solution or nanopure water were added in the incubations, consequently changing the ionic strength of the buffer system, which finally led to the observed changes in biotransformation activity and stereoselectivity). The influence of ionic strength on the biotransformation activity and stereoselectivity is further discussed in Section 3.3.6.

3.3.2. DLS Characterization of AuNPs and Enzyme Solutions

We hypothesized that the morphology of AuNPs in incubations could be changed, due to the high ionic strength of buffer solution, and that AuNPs may interact directly with enzymes in the incubation. We used DLS to test this hypothesis (Table 3.1). Aggregation of AuNPs in buffer solution was observed. DLS results indicated that the effective hydrodynamic diameter and zeta potential (both mean \pm standard error) of AuNPs in nanopure water was 40.5 ± 0.1 nm and -29.1 ± 0.9 mV, respectively (Table 3.1). After adding phosphate buffer, the effective diameter of AuNPs significantly increased with incubation time (Figure 3.3); the zeta potential dropped to -14.9 ± 0.8 mV (Table 3.1) and was stable during incubation. These results indicated that ionic strength increases could significantly reduce the stability of AuNPs and result in aggregation, consistent with

Table 3.1 Effective diameter and zeta potential of AuNPs and rat CYP2B1 mixture in incubations (37 °C). Each sample was measured 10 times over 60 min incubation and reported as mean \pm standard error.

Sample	Hydrodynamic diameter	Zeta potential
	(nm)	(mV)
AuNPs in water	40.5 \pm 0.1	-29.1 \pm 0.9
AuNPs (10 μ M) in buffer	continued increase (see Figure 3.3)	-14.9 \pm 0.8
AuNPs (10 μ M) in buffer with NADPH	81.3 \pm 0.3 (6-60 min)	-6.3 \pm 0.5
CYP2B1 control (denatured by heating)	1284 \pm 15	-14.5 \pm 0.7
CYP2B1 in buffer with NADPH	572 \pm 9	-10.6 \pm 0.6
CYP2B1 reacting with PCB 95	540 \pm 5	-10.1 \pm 0.4
CYP2B1 reacting with PCB 95 after addition of AuNPs (10 μ M)	458 \pm 3	-8.8 \pm 0.7

Derjaguin-Landau-Verwey-Overbeek (DLVO) theory. The presence of NADPH in incubations could slow down the aggregation rate of AuNPs (Figure 3.3). After NADPH addition, the AuNP effective diameter increased from 40.5 nm to about 80 nm within 3 min and was then stable with 10 μ M AuNPs, and increased to about 120 nm within 3 min and then slowly increased with 100 μ M AuNPs. However, the decrease of zeta potential (close to 0 mV; Table 3.1) was inconsistent with the slower aggregation rate of AuNPs according to DLVO theory, for reasons that remain unclear. Our preliminary results suggested that at least one of the components in solution A of the NADPH regenerating

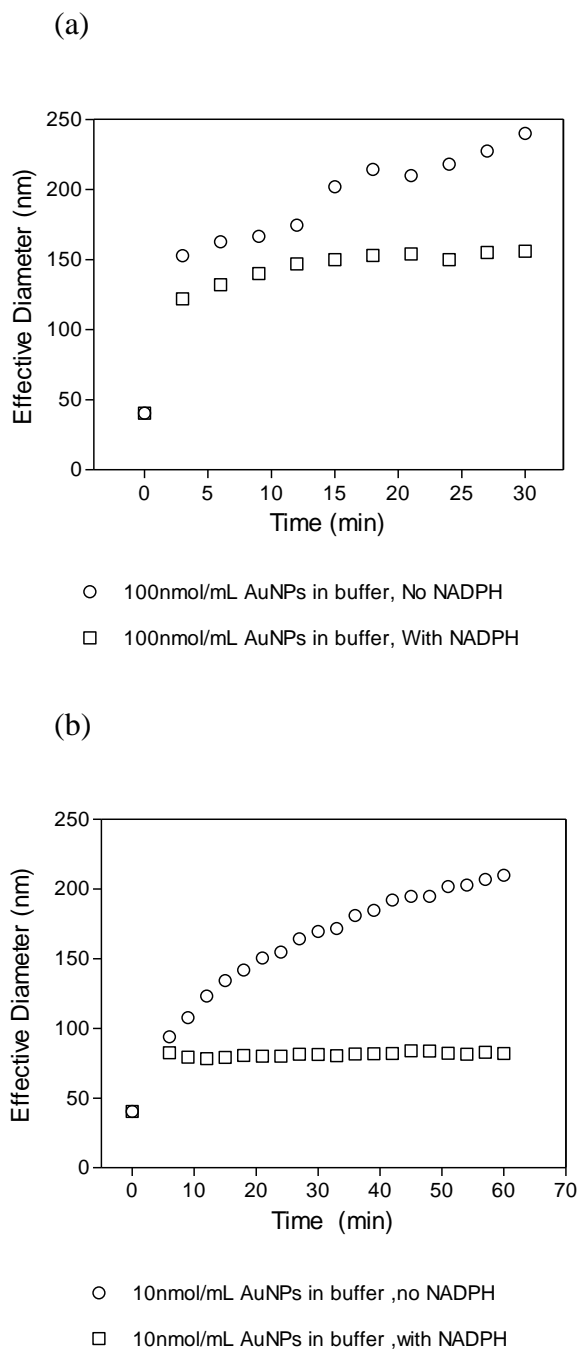


Figure 3.3 Effective diameter of AuNPs (a) 100 nmol/mL and (b) 10 nmol/mL in potassium phosphate buffer.

system could either affect the ionic strength or interact with AuNPs and consequently change the aggregation behavior of AuNPs.

The mean effective hydrodynamic size (not molecular size) and zeta potential of components in the rat CYP2B1 mixture (including rat CYP2B1, cytochrome b₅, and CPR) were stable in buffer solution (with NADPH) during incubations without AuNPs (Table 3.1). After PCB 95 substrate addition, the mean effective particle diameter in solution dropped significantly from 572 nm to 540 nm (paired *t*-test). When AuNPs (10 μM) were added, the mean effective size of the enzyme mixture was 458 nm, considerably smaller ($p < 0.0001$).

This decrease in mean effective size to 458 nm was only due to the addition of small AuNP particles decreasing the average number. To understand better the variation in the enzyme conformation, a bimodal particle size distribution in terms of light scattering intensity was plotted (Figure 3.4). By comparing the size distribution of the CYP2B1 mixture and the insect cell supersomes used as the CYP negative control (including cytochrome b₅ and CPR), we note that the largest distribution likely consists of CPR, while the medium component is CYP2B1 and the smallest is likely cytochrome b₅. This is supported by the known molecular weights of these components, which are 77 kDa, 52 kDa and 17 kDa for CPR, rat CYP2B1 and cytochrome b₅, respectively (43-45). The CPR component was not observed in CYP2B1 mixture samples (Figure 3.4a-3.4f), consistent with a 12-fold lower concentration of CPR in the CYP2B1 mixture than in the insect cell control supersomes. The effective size of the suspected CYP2B1 component in the enzyme mixture increased after PCB 95 was added (Figure 3.4a and 3.4c; 3.4b and 3.4d), but this increase was smaller in the presence of AuNPs (Figure 3.4e and 3.4f). For

the incubations without AuNPs, 60 min incubations resulted in a larger size distribution of the CYP2B1 component (Figure 3.4b and 3.4d) compared to that of 30 min incubations (Figure 3.4a and 3.4c). In contrast, 60 min incubations had a smaller size distribution of CYP2B1 components than 30 min incubations when AuNPs were present (Figure 3.4e and 3.4f), which is consistent with our hypothesis that the AuNPs were interfering with CYP2B1 conformation. This interference should increase over time, consistent with the changes in size distributions observed between 30 and 60 min incubations. Our observations were consistent with a conformation adjustment of rat CYP2B1 during the catalytic reaction. For example, the backbones of enzymes move during the catalytic process, and the heme catalytic center of CYPs do change, although the extent of this is not currently known for CYP2B1 in particular (2). This process may be disrupted by AuNPs, possibly because the isoelectric point of the rat CYP2B1 mixture was about 5.5, indicating that the enzymes' surfaces were negatively charged in phosphate buffer (pH 7.4). Thus, electrostatic repulsion might exist between rat CYP2B1 mixture components and the negatively-charged citrate-capped AuNPs, resulting in interference in the enzymes' performance. The presence of AuNPs might therefore be interrupting the function of rat CYP2B1 affecting its regular conformation change processes, resulting in biotransformation activity change as further discussed below. We note, however, that the exact nature of this likely disruption is beyond the scope of our study.

3.3.3. Impacts of AuNPs on Buffer Conductance

We also hypothesized that AuNPs may be able to change the microenvironment of biomolecules (e.g., CYPs) by affecting the ionic strength, thereby altering enzymatic

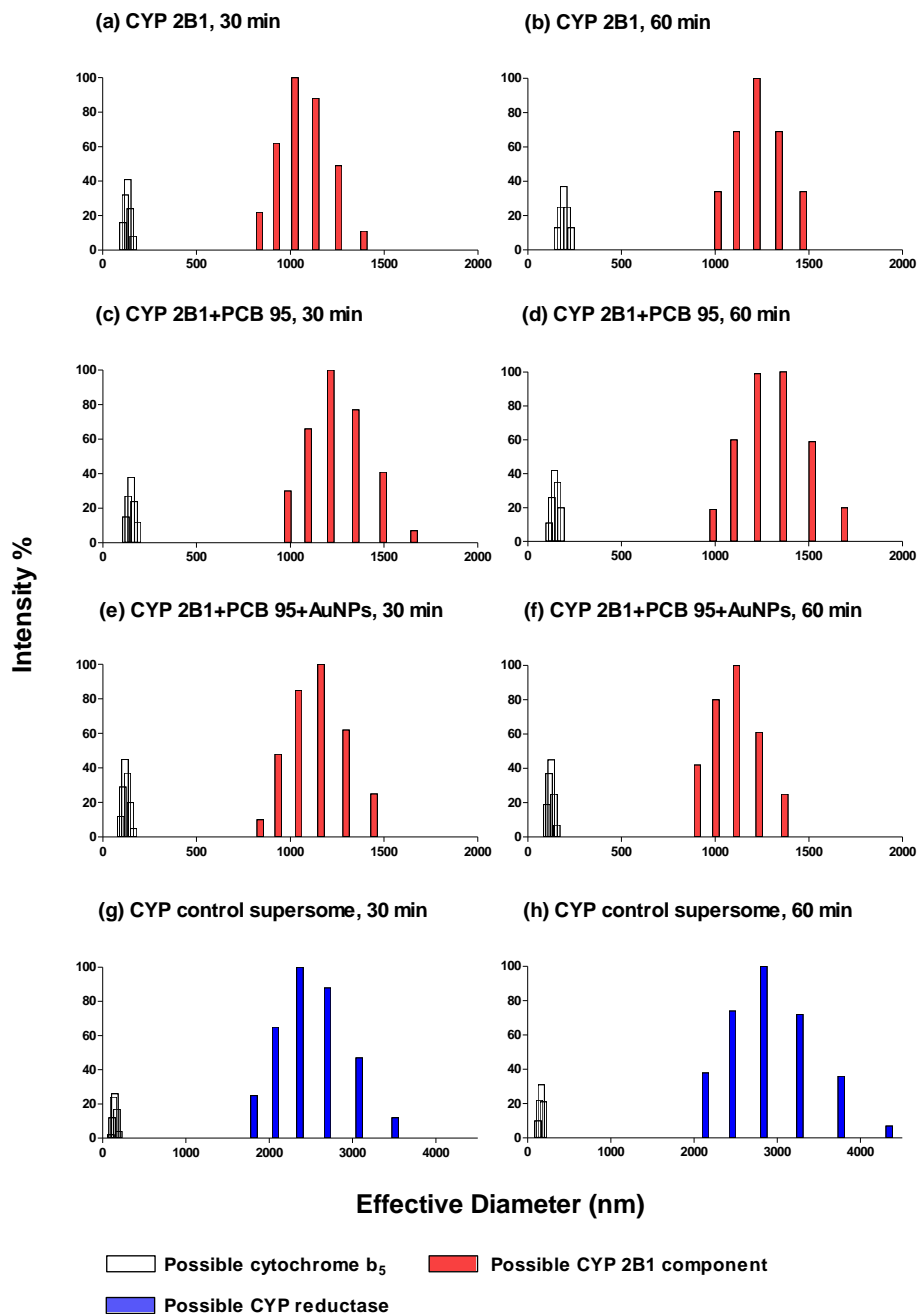


Figure 3.4 DLS-based particle distribution of different incubations after 30 and 60 minutes. (a) 30 min incubation of CYP2B1; (b) 60 min incubation of CYP2B1; (c) 30 min incubation of CYP2B1 with PCB 95; (d) 60 min incubation of CYP2B1 with PCB 95; (e) 30 min incubation of CYP 2B1 with PCB 95 and AuNPs; (f) 60 min incubation of

CYP 2B1 with PCB 95 and AuNPs; (g) 30 min incubation of CYP control supersomes; (h) 60 min incubation of insect cell control supersomes used as negative control. Please note that the particle size scale of (g) and (h) are different from others.

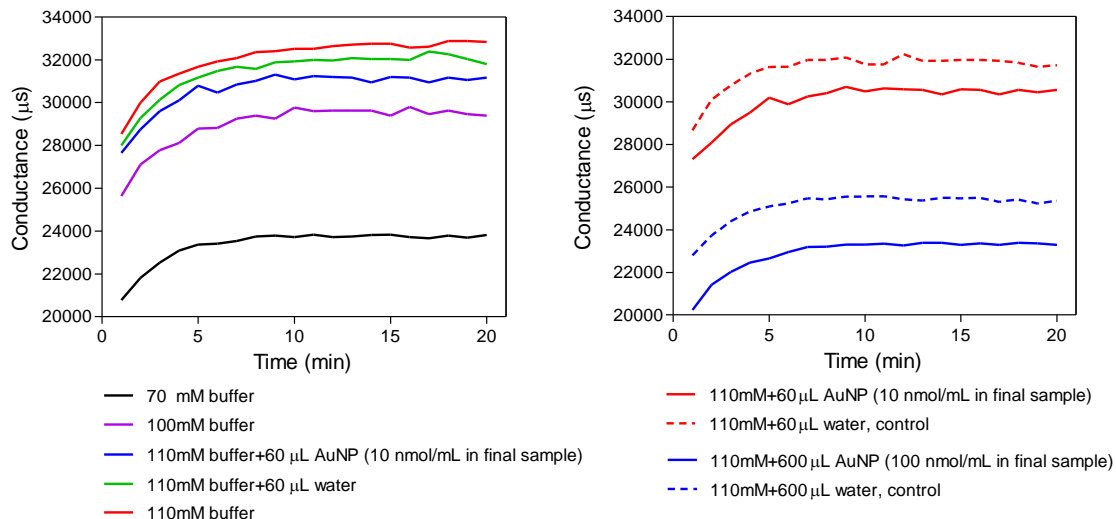


Figure 3.5 Influence of AuNPs on the conductance of phosphate buffer solution over 20 min incubation. Data were collected at one minute intervals at 37 °C. The increase of conductance over the first three minutes was due to sample temperature increase from 25 °C (room temperature) to 37 °C. The incubations without AuNPs were control samples.

function. Conductance can reflect the buffer's ionic strength (salinity), which is important for enzyme stability and activity (46-51). Thus, we measured the conductance of buffer solution with or without (as control) AuNPs to test this hypothesis.

The conductance of nanopure water and 10 µM AuNPs in nanopure water were 5 µS and 109 µS respectively, negligible compared with the 20,000-30,000 µS conductance contributed by electrolyte in the buffer. However, AuNPs could reduce the conductance

of the buffer, in an AuNP concentration-dependent manner (Figure 3.5). Higher concentrations of AuNPs resulted in greater conductance decreases. These observations were consistent with the ability of AuNPs to adsorb cations (i.e., K^+ or Mg^{2+} , with the latter neglected because of its relatively low concentration) in the buffer solution by electrostatic attraction either directly onto the citrate-capped surface, or associated strongly with the AuNP double layer (52-54). Either process would make these cations unavailable for conductance.

The conductance was measured by a Zeta PALS zeta potential analyzer (Brookhaven Instruments Corporation, Holtzville, NY, USA) at 37 °C. Data was collected at one minute intervals for 20 minutes total. The average conductance (9-20 min) was used for the linear regression. The speciation and concentration of K^+ were determined by MINEQL 4.6 software. The total concentration of K^+ in the original 110 mM potassium phosphate buffer was about 150 mM, as KOH was used to adjust the pH to 7.4. Therefore, the concentration of K^+ and $KHPO_4^-$ were about 110 mM and 40 mM respectively at 37 °C.

The conductance and K^+ concentration followed a linear relationship (Figure 3.6). From this equation, the K^+ concentrations of the samples with or without low concentration AuNPs (10 nmol/mL) were calculated to be 102 mM and 109 mM, respectively. Therefore, the AuNPs might “lock up” about 0.011 mmol K^+ in the system $[(109 \text{ mM} - 102 \text{ mM}) * 1.6 \text{ mL} = 0.011 \text{ mmol}]$; sample volume was 1.6 mL]. This was about 6% of the K^+ in the sample $(110 \text{ mM} * (1.6 \text{ mL} - 0.06 \text{ mL}) = 0.17 \text{ mmol})$, 0.06 mL AuNPs was added in the sample; $0.011 / 0.17 * 100\% = 6\%$). In addition, the K^+ concentration of the samples with or without high concentration AuNPs (100 nmol/mL) were about 68 mM

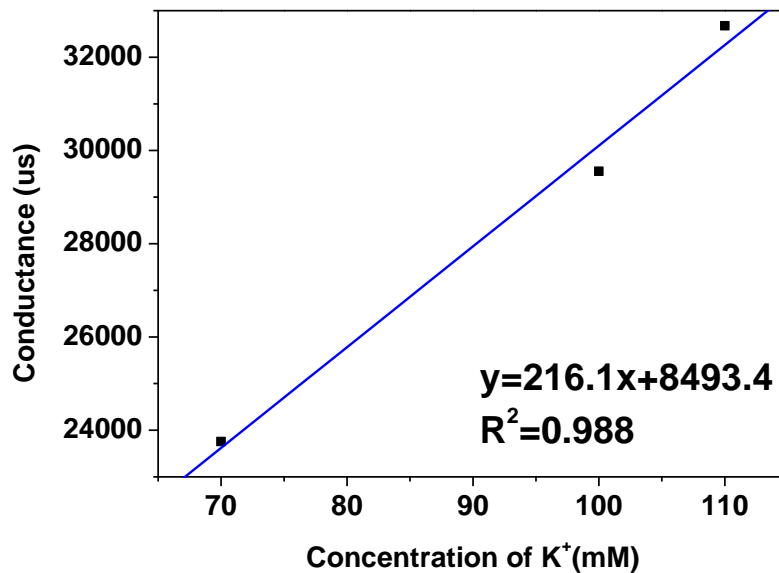


Figure 3.6 Relationship between average conductance and K⁺ concentration.

and 78 mM, respectively. Thus, the AuNPs might “lock up” about 0.016 mmol K⁺ in the system [(78 mM-68 mM)*1.6 mL=0.016 mmol; sample volume was 1.6 mL]. This was about 14% of the K⁺ in the sample (110 mM*(1.6 mL-0.6 mL) =0.11 mmol, 0.6 mL AuNPs was added in the sample; 0.016/0.11*100%=14%). Meanwhile, after the addition of low concentration or high concentration AuNPs, the decreases of sample conductance were about 5% and 9%, respectively.

Thus, from our calculations, the “lock up” of K⁺ by 10 μM or 100 μM AuNPs was 6% or 14% respectively, similar to the drop in conductance of 5% or 9% respectively. Different ions in buffer solution may be able to influence the enzyme hydration environment by modifying the water structure and by acting as substrates, co-substrates or co-factors that interact with the enzyme (48,50). Therefore, the surface charge distribution and structure of the enzyme may be changed by interaction with charged

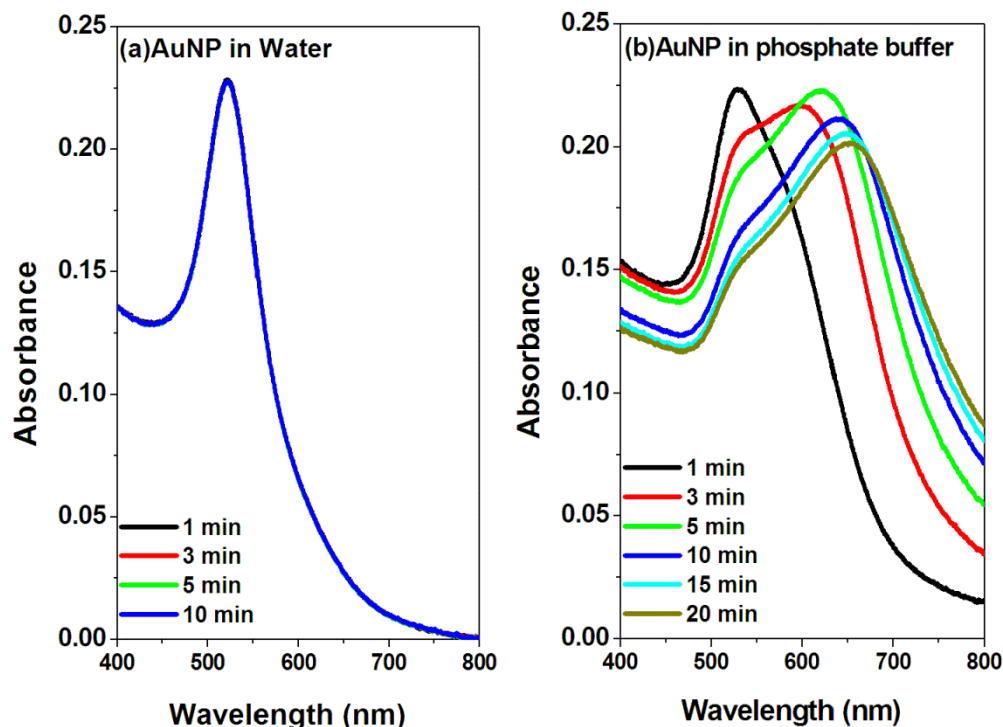


Figure 3.7 UV-Vis Spectra of AuNPs (200 μM) in water as control sample (a) and phosphate buffer (b) (pH 7.4 and 110mM) over 20 minutes. All absorbance spectra in Figure 3a overlap.

ions, leading to alteration of enzyme activity (50). The effects of salinity on enzyme activity depend on both salt concentration and ion type, and can be interpreted as noted above using Hofmeister series theory (48-50). Thus, AuNPs are a potential ionic strength disruptor in biological systems and might be able to affect the behavior of biomolecules and osmotic balance in this manner.

3.3.4. Interactions between AuNPs and K^+

We hypothesized that AuNP aggregation and cation sequestration by AuNPs were

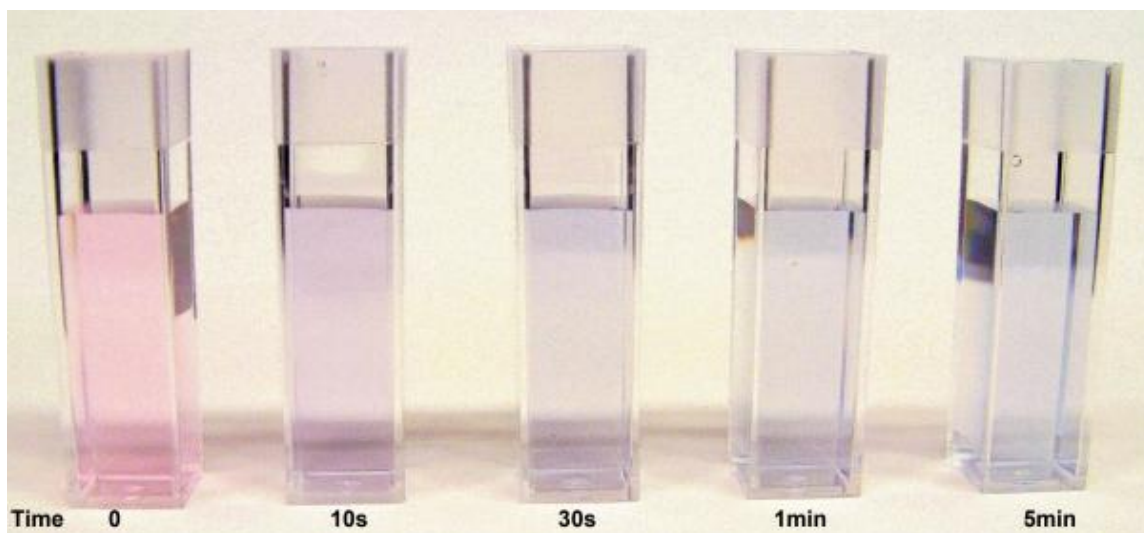


Figure 3.8 Color change of AuNPs (50 nmol/mL) in potassium phosphate buffer solution at room temperature, from red at 0 min to blue at 5 min.

responsible for observed ionic strength changes in the previous experiments. Thus, AuNP absorption spectra experiments were performed to understand better the interaction mechanisms between AuNPs and cations in buffer solution.

It is clear that the highest absorbance (λ_{\max}) of AuNPs in water (as control) occurred at 525 nm (Figure 3.7a), consistent with previous work (55,56). After adding buffer solution, significant color changes and red shifts with two plasmon bands were observed (Figure 3.7b and Figure 3.8). According to Mie's equation (57), these results indicated that the electron density of AuNPs decreased in the buffer solution. This reduction could be due to a particle size increase (i.e., from aggregation) and/or interactions between AuNPs and cations in buffer (52-57). A particle size increase during incubation was indeed observed (Figure 3.3 and Figure 3.9b), confirming that AuNPs were aggregating

without CYPs and NADPH. There are two relationships proposed to link quantitatively AuNP size of diameter <120 nm with absorbance wavelength in water (Figure 3.10) (55,56). However, our AuNP absorption wavelength data fit neither relationship very well. For example, for an increase in effective diameter from 40.5 nm (0 min) to 94.3 nm (1 min) and then to 107.6 nm (2 min) (from DLS) we would predict AuNP absorbance λ_{\max} of 526 nm, 562 nm and 579 nm (55), or of 525 nm, 562 nm and 573 nm (56), respectively. However, λ_{\max} actually shifted from 525 nm to 625 nm and to about 640 nm (no data for 2 min, estimated from 3 min data) in two minutes (Figure 3.9). In addition, although NADPH could slow down the aggregation rate of AuNPs in buffer as mentioned above, no effect of NADPH on the absorbance red shift of AuNPs was observed. These results suggest that there were processes other than size increases, i.e., cation-AuNP interactions as noted below, which decreased the electron density of AuNPs.

In addition to the red shifts, two plasmon bands were observed, suggesting a rod-like structure of aggregates consistent with previous literature (52,53). Those studies (52,53) demonstrated that cations could perform as “bridges” or “glue” linking citrate-capped AuNPs together to form web-like or string-like aggregates, depending on the ion concentration and charge. These findings are also consistent with our observations suggesting that some K^+ ions in our incubations were “locked up” in AuNP aggregates by electrostatic attraction forces. In addition, surface binding of cations on silver nanoparticles and on AuNPs were also observed previously (54,57). All these phenomena could also decrease the intensity of λ_{\max} at 525 nm and generate absorption around 640 nm. Thus, interactions between cations and AuNPs in buffer solution could also result in a change of AuNPs electron density and Localized Surface Plasmon Resonance (SLPR).

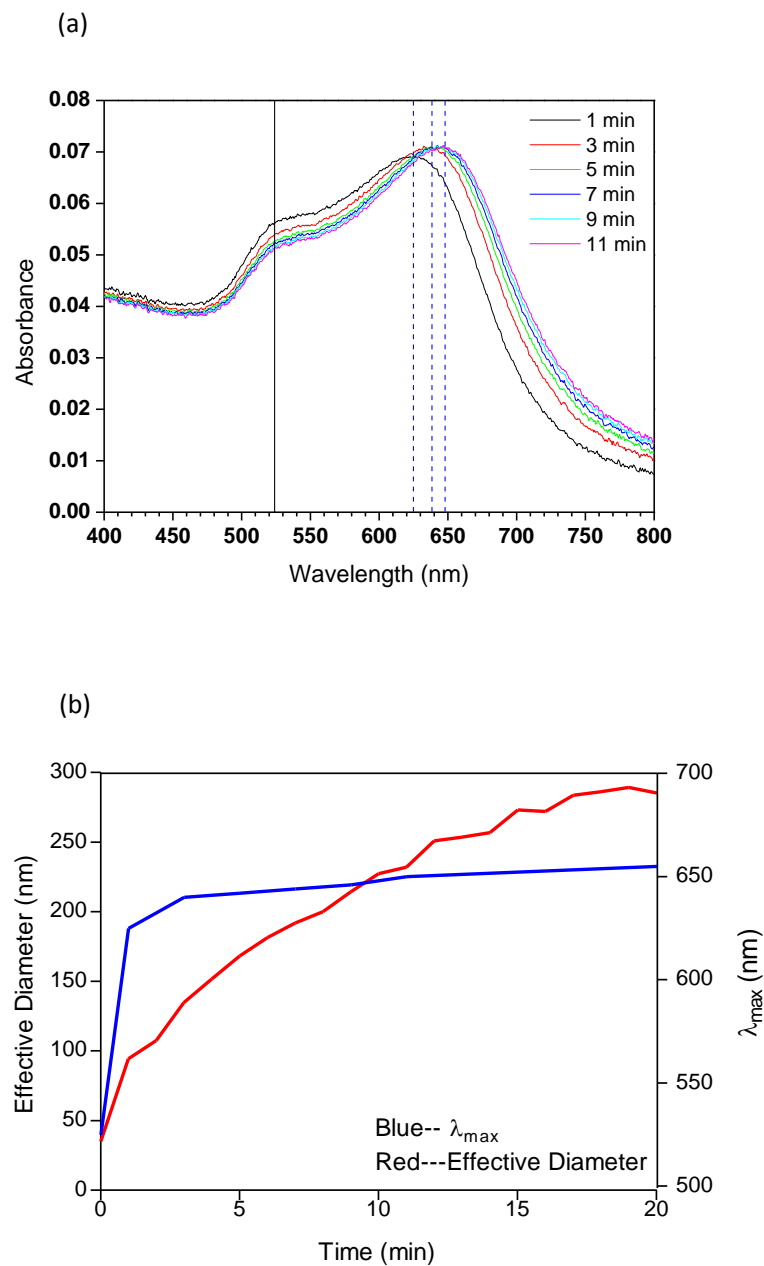


Figure 3.9 (a) UV-Vis Spectra of AuNPs (25 nmol/mL) in phosphate buffer in 20 minutes; (b) Effective diameter and UV-Vis adsorption λ_{max} change of AuNPs (25 nmol/mL) in phosphate buffer over 20 minutes.

However, we cannot confirm this point directly through environmental scanning electron

microscopy.

3.3.5. Influence of AuNPs on NADPH Production

NADPH is a necessary co-factor in phase I biotransformation of xenobiotics by CYPs (2). A common source of NADPH in an oxidase enzyme assay is an *in situ* enzymatic NADPH regenerating system. In our study, glucose-6-phosphate dehydrogenase in solution B was used to convert NADP^+ to NADPH in the presence of glucose-6-phosphate substrate in solution A. Subsequently, NADPH could convert back to NADP^+ and release electrons to activate the CYP biotransformation cycle (2). Thus,

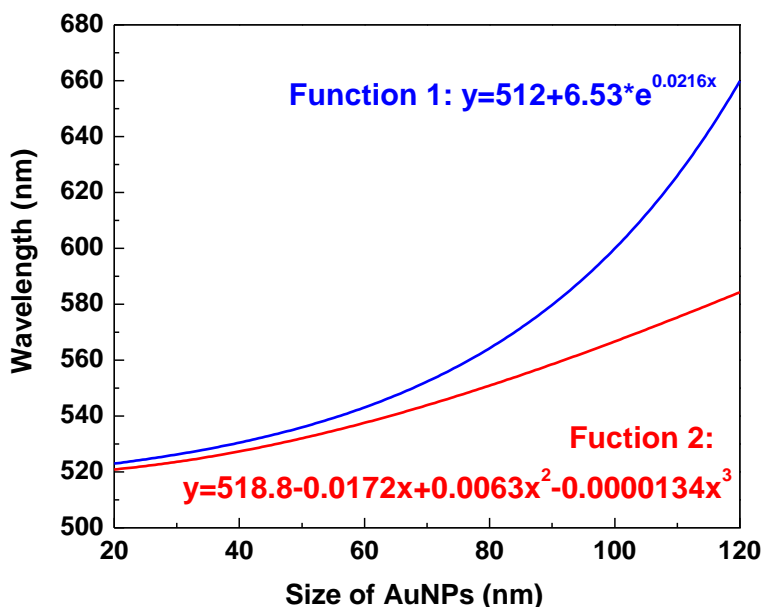


Figure 3.10 Theoretical position of the surface plasmon resonance peak (λ_{max}) as a function of the particle diameter for AuNPs in water. (Function 1: Haiss et al., 2007 (55); Function 2: Njoki et al., 2007 (56)).

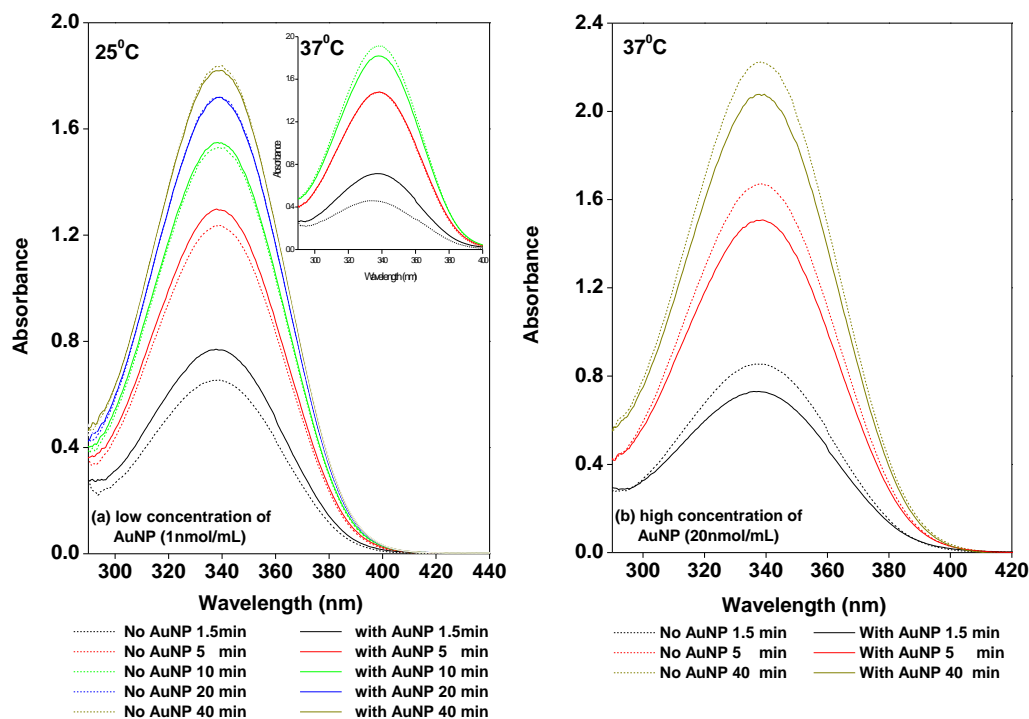


Figure 3.11 Selected UV-Vis spectra of NADPH formation activity by enzymatic reaction between solution A and solution B over 60 min. (3.5 times more dilute compared to biotransformation incubations (Figure 3.2), data from 50 to 60 min similar to that at 40 min and therefore not shown). Absorbance higher than 1 indicates the solution is too concentrated to follow Beer's law. All dash lines stand for control incubations without AuNPs.

the NADPH production rate will significantly affect the electron transfer efficiency in CYP-mediated reactions and thus change biotransformation performance. It is possible that AuNPs can affect this electron transfer process. To test this hypothesis, we measured the production of NADPH in the incubations with or without (as control) AuNPs.

We analyzed the influence of AuNPs on NADPH production by UV-Vis

spectrometry. NADPH had the highest absorbance at 340 nm, consistent with previous literature (58). For mixtures containing solution A and solution B, the NADPH concentration increased with incubation time and reached steady-state within 60 min. A low concentration of AuNPs (10 μ M) increased the production of NADPH (Figure 3.11a) at the beginning of incubation (0-10 min at 25°C; 0-1.5 min at 37°C). After that, the NADPH formation rate was similar to that of incubations without AuNPs (10-40 min at 25°C; 1.5-5 min at 37°C). Finally, the production of NADPH was slightly inhibited by AuNPs (40-60 min at 25°C; >10 min at 37°C). These changes in NADPH production with incubation time did not directly fit the rat CYP2B1 activity change at 37°C (Figure 3.2d and Figure 3.11a). This is because the consumption and regeneration of NADPH in CYP-mediated biotransformation is a complex dynamic process when substrate is present, which differs from the single NADPH generating process in these absorbance studies. However, it is clear that the co-factors of phase I biotransformation could be affected by AuNPs, that change CYP activity and selectivity. In contrast, high concentrations of AuNPs (200 μ M) could only inhibit NADPH generation (Figure 3.11b) over the entire incubation period, consistent with the observed inhibition of CYP2B1 activity (Figure 3.2a and Figure 3.2b).

In addition, we found that AuNPs could not directly transport electrons to CYPs to start biotransformation without NADPH. Furthermore, CYP2B1 (5 pmol/mL) could react with single solution A to generate NADPH in the incubation very slowly (about 10 times slower than regular reaction between solution A and solution B, containing 0.4 U/mL glucose-6-phosphate dehydrogenase) without glucose-6-phosphate dehydrogenase. A low concentration of AuNPs (10 μ M) could increase the production rate of this process by 7%

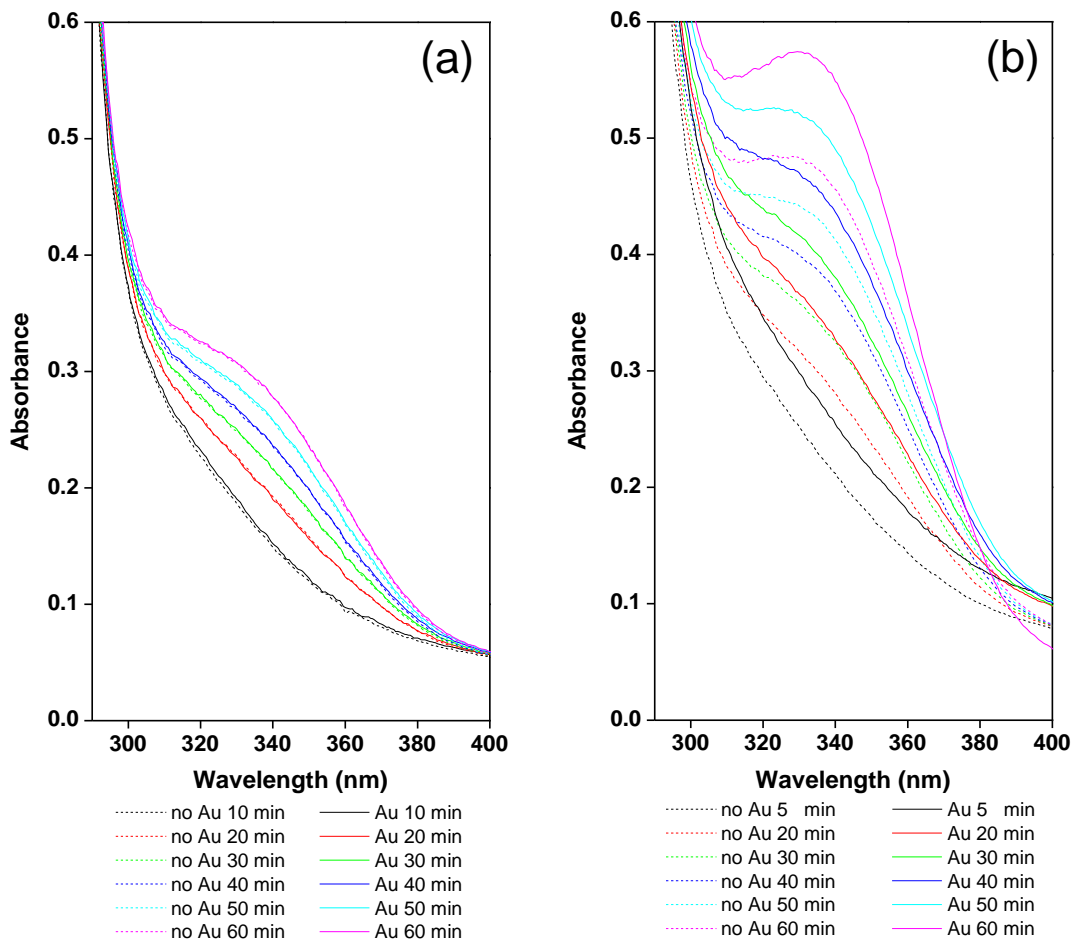


Figure 3.12 Selected UV-Vis spectra of NADPH formation activity by enzymatic reaction between (a) solution A (50 $\mu\text{L}/\text{mL}$) and cytochrome P-450 reductase (CPR) (5 pmol/mL) or (b) solution A (50 $\mu\text{L}/\text{mL}$) and rat CYP 2B1 (5 pmol/mL) over 60 mins of incubation. (The concentration of AuNPs was 10 nmol/mL; same volume of water was added in the control incubations without AuNPs.)

in 60 min compared with control samples without AuNPs (Figure 3.12b). CPR also exhibited a weak capacity to generate NADPH with only solution A present, however low concentrations of AuNPs (10 μM) could not affect this process (Figure 3.12a). The reasons for these observations are not clear. It is possible that a trace of the NADPH

regenerating co-factors were present in rat CYP2B1 and CPR products, or these enzymes could use glucose-6-phosphate as substrate.

There are two possible reasons for the disruption of NADPH production (between solution A and solution B) by AuNPs. First, the presence of AuNPs might be able to influence the diffusion or mobility of glucose-6-phosphate dehydrogenase, NADP^+ or glucose-6-phosphate in the incubation, thereby affecting the reaction kinetics. Second, as mentioned above, AuNPs could change the ionic strength of the buffer solution, which might be able to disrupt the enzymatic NADPH formation process. According to Hofmeister theory, kosmotropic anions and chaotropic cations can stabilize enzymes, whereas chaotropic anions and kosmotropic cations destabilize them (48-50). The kosmotropicity of ions can be quantified by their viscosity B-coefficients. Kosmotropes usually have positive B-coefficients and chaotropes have negative values (50). Phosphate anions in our incubations are kosmotropic (B-coefficient about 0.495), while K^+ is a chaotropic cation (B-coefficient about -0.009) (50). Thus, these ions could stabilize glucose-6-phosphate dehydrogenase in normal incubations without AuNPs (48,50). Therefore, any factors (e.g., variation of buffer salinity) that change the status of these ions in solution could affect glucose-6-phosphate dehydrogenase activity. Similarly, buffer concentration change may also be able to affect the activity and selectivity of CYPs. To confirm this hypothesis, we tested the NADPH production efficiency and CYP activity under different buffer concentrations (without AuNPs).

3.3.6. The Effects of Buffer Salinity on NADPH Production and CYP Activity

We found that glucose-6-phosphate dehydrogenase and CYPs had different activities in different concentrations (salinities) of buffers when no AuNPs were present. We

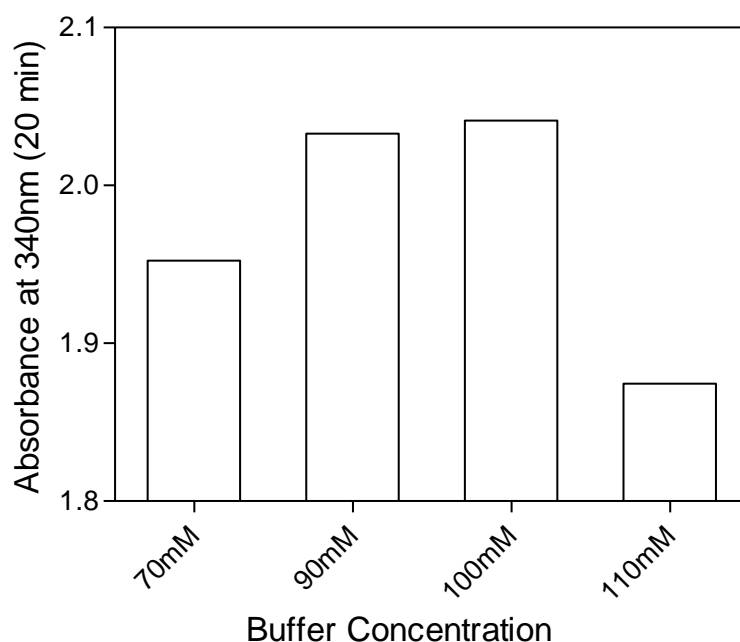


Figure 3.13 The influence of buffer salinity on NADPH production (3.5 times dilute compared to biotransformation incubations). Absorbance values higher than 1 indicates the solution is too concentrated to follow Beer's law. The incubation in 110 mM buffer was considered as the control sample.

usually used 110 mM buffer in CYP- mediated phase I biotransformation experiments to maintain consistency with previous studies (27). However, somewhat higher activities of glucose-6-phosphate dehydrogenase were found in 90 mM and 100 mM buffers, although these absorbances were too high (≈ 2) for NADPH quantitation based on Beer's law (Figure 3.13). This observation was similar with previous work suggesting that glucose-6-phosphate dehydrogenase had the highest activity in 100 mM NaCl incubations (51). The activity and stereoselectivity of CYPs were also affected by ionic strength, in a substrate concentration dependent manner (Figure 3.14, two substrate concentration

incubations were conducted). The biotransformation activity of both atropisomers of PCB 95 increased as ionic strength was lowered from 110 mM to 90 mM, and either leveled off or continued to increase depending on the atropisomer at lower ionic strengths (Figure 3.14), even though NADPH production was reduced at ionic strengths less than 90 mM (Figure 3.13). The net result was variation in EF values (Figure 3.14). These results were also consistent with the higher observed biotransformation activity by CYP2B1 in assay 1 compared to assay 2 (Figure 3.2), which may be due to differences in ionic strength as discussed above.

The above results revealed that ionic strength is an important factor affecting stereoselective biotransformation of chiral compounds. In addition, any factor that lowers the buffer salinity could disrupt the NADPH production rate and CYP activity. For example, low concentrations of AuNPs (e.g., 10 μ M) could “lock up” some cations (e.g., K^+), thereby decreasing the buffer conductance (salinity) to an optimal range (i.e., around 100 mM). As a consequence, the activity of glucose-6-phosphate dehydrogenase and CYPs increased, as did the NADPH formation rate and biotransformation rate of PCB 95.

High concentrations of AuNPs could change the salinity of buffer solution too much (e.g., <90 mM), leading to lower NADPH production rate and higher CYP biotransformation activity. In our normal experiments, a high level of NADPH was used in the incubations to optimize biotransformation. NADPH was not a limiting reagent in these reactions. This is supported by the increase of CYP activity when NADPH production decreased in lower buffer salinity incubations (Figure 3.14). If NADPH was a limiting reagent, the CYP activity should decrease with lower NADPH production rates. Thus, the decrease of biotransformation activity of E1-PCB95 in assay 1 (Figure 3.2) was

not due to ionic strength changes, but may have resulted from direct interactions between AuNPs and CYPs.

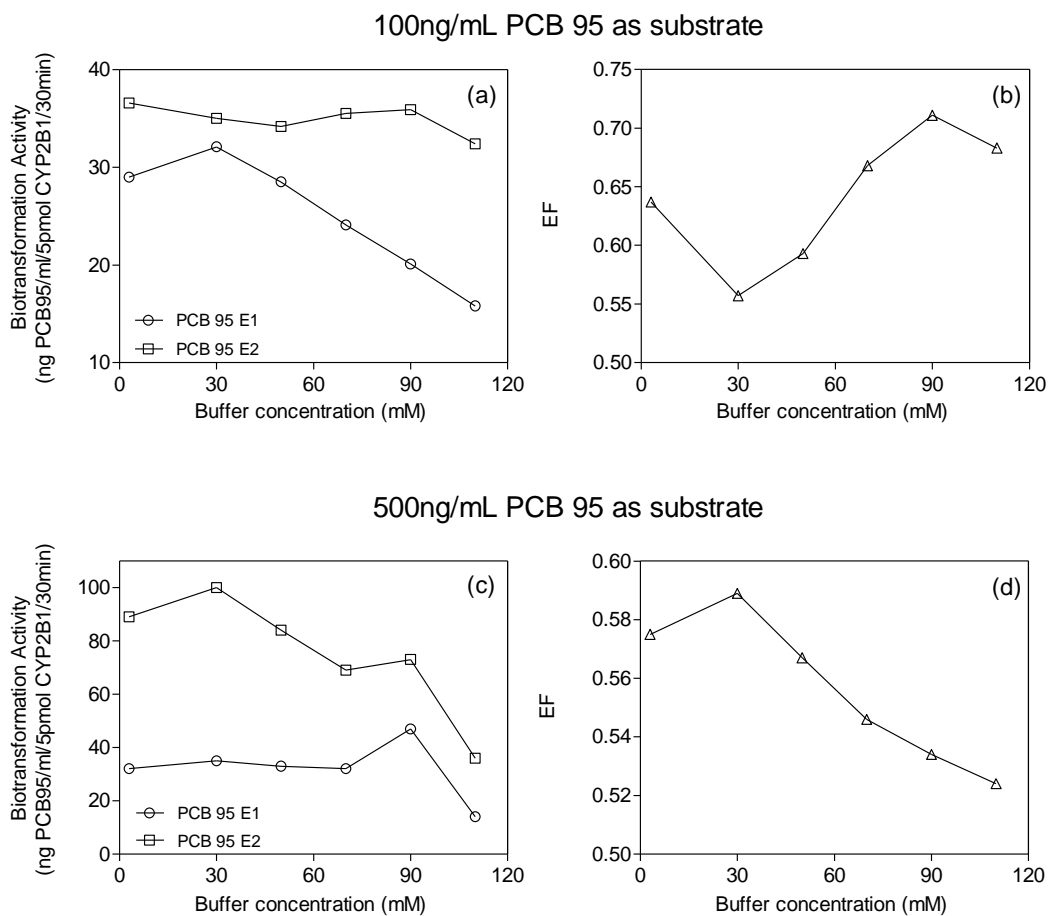


Figure 3.14 The influence of buffer salinity on CYP biotransformation activity and stereoselectivity of 100 ng/mL PCB 95 or 500 ng/mL PCB 95 for 30 min incubation. Two PCB 95 concentrations were used to test whether this process depend on substrate concentration. The incubations in 110 mM buffer were considered as control samples.

3.3.7. Proposed Mechanism

In summary, the influence of AuNPs on CYP-mediated biotransformation could be due to two factors. The direct factor, based on DLS data, is enzyme structure disruption due to AuNP interaction with CYPs and other phase I proteins. This factor is more obvious when a high concentration AuNPs was present. The indirect factor is modification by AuNPs of co-factor production necessary for phase I biotransformation, due to: (1) negatively-charged AuNPs “locking up” cations in solution via sorption from electrostatic attraction; (2) low concentrations of AuNPs reducing conductance of reaction solutions; (3) higher NADPH generation and CYP activity at lower conductance, particularly at low AuNP concentrations; (4) higher concentrations of AuNPs possibly reducing NADPH production and increasing CYP activity by overly affecting conductance when NADPH is not a limiting reagent, leading to direct interactions between enzymes and AuNPs that reduce CYP activity; (5) when NADPH is a limiting reagent, higher concentrations of AuNPs possibly reducing NADPH production and CYP activity by overly affecting conductance and direct electrostatic disruption. These indirect factors may affect not only glucose-6-phosphate dehydrogenase and CYPs, but any other enzymes, related to biotransformation or otherwise, that rely on cofactor production or otherwise have activities significantly affected by ionic strength. The influence of AuNPs on biological enzymatic processes is a combined effect of both factors. Such direct and indirect factors may be a possible explanation why conflicting behavior of nanoparticles (i.e., catalysis or inhibition) has been observed previously for nanoparticles (12).

Although it seems that the capping agent and surface charge of nanoparticles play predominant roles in our proposed mechanisms, it is not clear how other nanoparticles

with similar surface charge characteristics might behave, although if they adsorb ions they could behave analogously. This is because different metal-cores of charged nanoparticles can also directly interact with the surrounding components in different manners due to their own electron distribution properties, or indirectly affect the function of the capping agent (e.g., stability of capping agent), thereby changing the nanoparticle behavior (e.g., aggregation processes).

Although AuNPs are known to distribute into cells from previous *in vitro* work, it is difficult to translate our results to predict behavior and effects *in vivo* (as with any *in vitro* and *in vivo* comparison) because other factors (e.g., uptake, distribution, excretion) may alter how AuNPs may interact and the target enzymatic system. As well, interactions between AuNPs and other pieces of cellular machinery may also exist. Therefore, further studies are necessary. However, the proposed indirect factors are not limited within cells. It would be true for any nanoparticle that influences ionic strength in its microenvironment, and any enzymatic or other biochemical process that is influenced by ionic strength.

References

- (1) Tompkins, L.M. and Wallace, A.D. Mechanisms of cytochrome P450 induction. *J. Biochem. Mol. Toxicol.* **2007**, *21*, 176-181.
- (2) Meunier, B.; De Visser, S.P.; Shaik, S. Mechanism of oxidation reactions catalyzed by cytochrome P450 enzymes. *Chem. Rev.* **2004**, *104*, 3947-3980.
- (3) Laursen, T.; Jensen, K.; Møller, B.L. Conformational changes of the NADPH-dependent cytochrome P450 reductase in the course of electron transfer to cytochromes P450. *BBA-Proteins Proteom.* **2011**, *1814*, 132-138.
- (4) Pudney, C.R.; Khara, B.; Johannissen, L.O.; Scrutton, N.S. Coupled motions direct electrons along human microsomal P450 chains. *PLoS Biology* **2011**, *9*, e1001222.
- (5) Leferink, N.G.H.; Pudney, C.R.; Brenner, S.; Heyes, D.J.; Eady, R.R.; Samar Hasnain, S.; Hay, S.; Rigby, S.E.J.; Scrutton, N.S. Gating mechanisms for biological electron transfer: Integrating structure with biophysics reveals the nature of redox control in cytochrome P450 reductase and copper-dependent nitrite reductase. *FEBS Lett.* **2012**, *586*, 578-584.
- (6) Clark, R.J.; Veinot, J.G.C.; Wong, C.S. Nanomaterials in the environment: the good, the bad, and the ugly. In *Trace Analysis with Nanomaterials* (eds. D.T. Pierce and J.X. Zhao), Wiley-VCH, **2010**, 255-282.
- (7) Scown, T.M.; Goodhead, R.M.; Johnston, B.D.; Moger, J.; Baalousha, M.; Lead J.R.; Aerle, R.; Lguchi, T.; Tyler, C.R. Assessment of cultured fish hepatocytes for studying cellular uptake and (eco)toxicity of nanoparticles. *Environ. Chem.* **2010**, *7*, 36-49.
- (8) Nowack, B. and Bucheli, T.D. Occurrence, behavior and effects of nanoparticles in

- the environment. *Environ. Pollut.* **2007**, *150*, 5-22.
- (9) Petosa, A.R.; Jaisi, D.P.; Quevedo, I.R.; Elimelech, M.; Tufenkji, N. Aggregation and deposition of engineered nanomaterials in aquatic environments: Role of physicochemical interactions. *Environ. Sci. Technol.* **2010**, *44*, 6532-6549.
- (10) Alkilany, A.M. and Murphy, C.J. Toxicity and cellular uptake of gold nanoparticles: what we have learned so far? *J. Nanopart. Res.* **2010**, *12*, 2313-2333.
- (11) Fröhlich, E.; Kueznik, T.; Samberger, C.; Roblegg, E.; Wrighton, C.; Pieber, T.R. Size-dependent effects of nanoparticles on the activity of cytochrome P450 isoenzymes. *Toxicol. Appl. Pharmacol.* **2010**, *242*, 326-332.
- (12) Lynch, I. and Dawson, K.A. Protein-nanoparticle interactions. *Nano Today* **2008**, *3*, 40-47.
- (13) Giljohann, D.A.; Seferos, D.S.; Daniel, W.L.; Massich, M.D.; Patel, P.C.; Mirkin, C.A. Gold nanoparticles for biology and medicine. *Angew. Chem. Int. Edit.* **2010**, *49*, 3280-3294.
- (14) Judy, J.D.; Unrine, J.M.; Bertsch, P.M. Evidence for biomagnification of gold nanoparticles within a terrestrial food chain. *Environ. Sci. Technol.* **2011**, *45*, 776-781.
- (15) Schaeublin, N.M.; Braydich-Stolle, L.K.; Schrand, A.M.; Miller, J.M.; Hutchison, J.; Schlager, J.J.; Hussain, S.M. Surface charge of gold nanoparticles mediates mechanism of toxicity. *Nanoscale* **2011**, *3*, 410-420.
- (16) Connor, E.E.; Mwamuka, J.; Gole, A.; Murphy, C.J.; Wyatt, M.D. Gold nanoparticles are taken up by human cells but do not cause acute cytotoxicity. *Small* **2005**, *1*, 325-327.
- (17) Dobrovolskaia, M.A.; Patri, A.K.; Zheng, J.; Clogston, J.D.; Ayub, N.; Aggarwal, P.;

- Neun, B.W.; Hall, J.B.; McNeil, S.E. Interaction of colloidal gold nanoparticles with human blood: effects on particle size and analysis of plasma protein binding profiles. *Nanomed-Nanotechnol.* **2009**, *5*, 106-117.
- (18) Goodman, C.M.; McCusker, C.D.; Yilmaz, T.; Rotello, V.M. Toxicity of gold nanoparticles functionalized with cationic and anionic side chains. *Bioconjug. Chem.* **2004**, *15*, 897-900.
- (19) Pan, Y.; Leifert, A.; Ruau, D.; Neuss, S.; Bornemann, J.; Schmid, G.; Brandau, W.; Simon, U.; Jahnen-Dechent, W. Gold nanoparticles of diameter 1.4 nm trigger necrosis by oxidative stress and mitochondrial damage. *Small* **2009**, *5*, 2067-2076.
- (20) Li, J.J.; Zou, L.; Hartono, D.; Ong, C.N.; Bay, B.H.; Lanry Yung, L.Y. Gold nanoparticles induce oxidative damage in lung fibroblasts *in vitro*. *Adv. Mater.* **2008**, *20*, 138-142.
- (21) Chithrani, B.D.; Ghazani, A.A.; Chan, W.C.W. Determining the size and shape dependence of gold nanoparticle uptake into mammalian cells. *Nano Letters* **2006**, *6*, 662-668.
- (22) Dobrovolskaia, M.A. and McNeil, S.E. Immunological properties of engineered nanomaterials. *Nat. Nanotechnol.* **2007**, *2*, 469-478.
- (23) Bastús, N.G.; Sánchez-Tilló, E.; Pujals, S.; Farrera, C.; Kogan, M.J.; Giralt, E.; Celada, A.; Lloberas, J.; Puentes, V. Peptides conjugated to gold nanoparticles induce macrophage activation. *Mol. Immunol.* **2009**, *46*, 743-748.
- (24) Sereemasun, A.; Hongpiticharoen, P.; Rojanathanes, R.; Maneewattanapinyo, P.; Ekgasit, S.; Warisnoicharoen, W. Inhibition of human Cytochrome P450 enzymes by metallic nanoparticles: A preliminary to nanogenomics. *Int. J. Pharmacol.* **2008**, *4*,

- 492-495.
- (25) Lehmler, H.-J.; Harrad, S.J.; Hühnerfuss, H.; Kania-Korwel, I.; Lee, C.M.; Lu, Z.; Wong, C.S. Chiral Polychlorinated biphenyl transport, metabolism, and distribution: A review. *Environ. Sci. Technol.* **2010**, *44*, 2757-2766.
- (26) Wong, C.S. and Warner, N.A. Chirality as an Environmental Forensics Tool. In *Persistent Organic Pollutants*. (ed. SJ Harrad), Wiley, 2010, pp71-136.
- (27) Warner, N.A.; Martin, J.W.; Wong, C.S. Chiral polychlorinated biphenyls are biotransformed enantioselectively by mammalian cytochrome P-450 isozymes to form hydroxylated metabolites. *Environ. Sci. Technol.* **2009**, *43*, 114-121.
- (28) Lu, Z. and Wong, C.S. Factors affecting phase I stereoselective biotransformation of chiral polychlorinated biphenyls (PCBs) by rat Cytochrome P-450 2B1 isozyme. *Environ. Sci. Technol.* **2011**, *45*, 8298-8305.
- (29) Wayman, G. A.; Bose, D. D.; Yang, D.; Lesiak, A.; Bruun, D.; Impey, S.; Ledoux, V.; Pessah, I. N.; Lein, P. J. PCB-95 modulates the calcium-dependent signaling pathway responsible for activity-dependent dendritic growth. *Environ. Health Perspect.* **2012**, *120*, 1003-1009.
- (30) Wayman, G. A.; Yang, D.; Bose, D. D.; Lesiak, A.; Ledoux, V.; Bruun, D.; Pessah, I. N.; Lein, P. J. PCB-95 promotes dendritic growth via ryanodine receptor-dependent mechanisms. *Environ. Health Perspect.* **2012**, *120*, 997-1002.
- (31) Ji, X.-H.; Song, X.-N.; Li, J.; Bai, Y.-B.; Yang W.-S.; Peng, X.G. Size control of gold nanocrystals in citrate reduction: The third role of citrate. *J. Am. Chem. Soc.* **2007**, *129*, 13939-13948.
- (32) Asher, B.J.; D'Agostino, L.A.; Way, J.D.; Wong, C.S.; Harynuk, J.J. Comparison of

- peak integration methods for the determination of enantiomeric fraction in environmental samples. *Chemosphere* **2009**, *75*, 1042-1048.
- (33) Harner, T.; Wiberg, K.; Norstrom, R. Enantiomer fractions are preferred to enantiomer ratios for describing chiral signatures in environmental analysis. *Environ. Sci. Technol.* **2000**, *34*, 218-220.
- (34) McKinney, M.A.; McMeans, B.C.; Tomy, G.T.; Rosenberg, B.; Ferguson, S.H.; Morris, A.; Muir, D.C.G.; Fisk, A.T. Trophic transfer of contaminants in a changing Arctic marine food web: Cumberland Sound, Nunavut, Canada. *Environ. Sci. Technol.* **2012**, *46*, 9914-9922.
- (35) Molde, K.; Ciesielski, T.M.; Fisk, A.T.; Lydersen, C.; Kovacs, K.M.; Sørmo, E.G.; Jenssen, B.M. Associations between vitamins A and E and legacy POP levels in highly contaminated Greenland sharks (*Somniosus microcephalus*), *Sci. Total Environ.* **2013**, *442*, 445-454.
- (36) Kania-Korwel, I.; Duffel, M.W.; Lehmler, H.-J. Gas chromatographic analysis with chiral cyclodextrin phases reveals the enantioselective formation of hydroxylated polychlorinated biphenyls by rat liver microsomes. *Environ. Sci. Technol.* **2011**, *45*, 9590-9596.
- (37) Kania-Korwel, I.; Garrison, A.W.; Avants, J.K.; Hornbuckle, K.C.; Robertson, L.W.; Sulkowski, W.W.; Lehmler, H.-J. Distribution of chiral PCBs in selected tissues in the laboratory rat. *Environ. Sci. Technol.* **2006**, *40*, 3704-3710.
- (38) Vujačić, A.; Vodink, V.; Joksić, G.; Petrović, S.; Leskovac, A.; Nastasijević, B.; Vasić, V. Particle Size and Concentration Dependent Cytotoxicity of Citrate Capped Gold Nanoparticles. *Dig. J. Nanomater. Bios.* **2011**, *6*, 1367-1376.

- (39) Farré M.; Gajda-Schranz, K.; Kantiani, L.; Barceló, D. Ecotoxicity and analysis of nanomaterials in the aquatic environment. *Anal. Bioanal. Chem.* **2009**, *393*, 81-95.
- (40) Comenge, J.; Sotelo, C.; Romero, F.; Gallego, O.; Barnadas, A.; Parada, T.G.; Domínguez, F.; Puentes V.F. Detoxifying Antitumoral Drugs via Nanoconjugation: The Case of Gold Nanoparticles and Cisplatin. *PLoS One* **2012**, *7*, e47562.
- (41) Kumar, V.; Rock, D.A.; Warren, C.J.; Tracy, T.S.; Wahlstrom, J.L. Enzyme source effects on CYP2C9 kinetics and inhibition. *Drug Metab. Disposition* **2006**, *34*, 1903-1908.
- (42) Cojocaru, V.; Balali-Mood, K.; Sansom, M.S.P.; Wade, R.C. Structure and Dynamics of the Membrane-Bound Cytochrome P450 2C9. *PLoS Computational Biology* **2011**, *7*, e1002152.
- (43) Aoyama, T.; Nagata, K.; Yamazoe, Y.; Kato, R.; Matsunaga, E.; Gelboin, H.V.; Gonzalez, F.J. Cytochrome b₅ potentiation of cytochrome P-450 catalytic activity demonstrated by a vaccinia virus-mediated *in situ* reconstitution system. *Proc. Natl. Acad. Sci. U.S.A.* **1990**, *87*, 5425-5429.
- (44) Czekaj, P.; Wiaderkiewicz, A.; Florek, E.; Wiaderkiewicz, R. Expression of cytochrome CYP2B1/2 in nonpregnant, pregnant and fetal rats exposed to tobacco smoke. *Acta Biochim. Pol.* **2000**, *47*, 1115-1127.
- (45) Ramji, S.; Lee, C.; Inaba, T.; Patterson, A.V.; Riddick, D.S. Human NADPH-cytochrome P450 reductase overexpression does not enhance the aerobic cytotoxicity of doxorubicin in human breast cancer cell lines. *Cancer Res.* **2003**, *63*, 6914-6919.
- (46) Ponnampereuma, F.; Tianco, E.M.; Loy, T.A. Ionic strengths of the solutions of

- flooded soils and other natural aqueous solutions from specific conductance. *Soil Sci.* **1966**, *102*, 408-413.
- (47) Griffin, B. and Jurinak, J. Estimation of activity coefficients from the electrical conductivity of natural aquatic systems and soil extracts. *Soil Sci.* **1973**, *116*, 26-30.
- (48) Obón, J.M.; Manjón, A.; Iborra, J.L. Comparative thermostability of glucose dehydrogenase from *Haloferax mediterranei*. Effects of salts and polyols. *Enzyme Microb. Technol.* **1996**, *19*, 352-360.
- (49) Bauduin, P.; Renoncourt, A.; Touraud, D.; Kunz, W.; Ninham, B. Hofmeister effect on enzymatic catalysis and colloidal structures. *Curr. Opin. Colloid In.* **2004**, *9*, 43-47.
- (50) Zhao, H. Effect of ions and other compatible solutes on enzyme activity, and its implication for biocatalysis using ionic liquids. *J. Molec. Catal. B-Enzym.* **2005**, *37*, 16-25.
- (51) Liu, Y.; Wu, R.; Wan, Q.; Xie, G.; Bi, Y. Glucose-6-phosphate dehydrogenase plays a pivotal role in nitric oxide-involved defense against oxidative stress under salt stress in red kidney bean roots. *Plant Cell Physiol.* **2007**, *48*, 511-522.
- (52) Shipway, A.N.; Lahav, M.; Gabai, R.; Willner, I. Investigations into the electrostatically induced aggregation of Au nanoparticles. *Langmuir* **2000**, *16*, 8789-8795.
- (53) Yang, Y.; Matsubara, S.; Nogami, M.; Shi, J. Controlling the aggregation behavior of gold nanoparticles. *Mat. Sci. Eng. B* **2007**, *140*, 172-176.
- (54) Xu, B. Adsorption behavior of metal cations on gold nanoparticle surfaces studied by isothermal titration microcalorimetry. *J. Chin. Chem. Soc.* **2010**, *57*, 309-315.

- (55) Haiss, W.; Thanh, N.T.K.; Aveyard, J.; Fernig, D.G. Determination of size and concentration of gold nanoparticles from UV-vis spectra. *Anal. Chem.* **2007**, *79*, 4215-4221.
- (56) Njoki, P.N.; Lim, I.I.S.; Mott, D.; Park, H.Y.; Khan, B.; Mishra, S.; Sujakumar, R.; Luo, J.; Zhong, C.J. Size correlation of optical and spectroscopic properties for gold nanoparticles. *J. Phys. Chem. C* **2007**, *111*, 14664-14669.
- (57) Liu, Y.; Liu, C.; Chen, L.; Zhang, Z. Adsorption of cations onto the surfaces of silver nanoparticles. *J. Colloid Interf. Sci.* **2003**, *257*, 188-194.
- (58) Olive, C.; Geroch, M.E.; Levy, H.R. Glucose 6-phosphate dehydrogenase from *Leuconostoc mesenteroides*. *J. Biol. Chem.* **1971**, *246*, 2047-2057.

Chapter 4

Stereoselective Formation of Mono- and Di-Hydroxylated Polychlorinated Biphenyls by Rat Cytochrome P450 2B1

The author of this dissertation designed the experiment along with his supervisor, as well as collaborators Dr. Hans-Joachim Lehmler and Dr. Izabela Kania-Korwel of the University of Iowa. Dr. Hans-Joachim Lehmler and Dr. Izabela Kania-Korwel were responsible for OH- and diOH-PCB standards preparation and chiral analyses of OH- and diOH-PCBs. The author of this dissertation performed the incubation, chiral analyses of parent PCBs and achiral analyses of OH- and diOH-PCBs; interpreted data; and wrote the manuscript. This manuscript was accepted for publication in *Environmental Science & Technology* on September 23rd 2013 (DOI:10.1021/es402838f). Reprinted with permission.

4.1. Introduction

Non-racemic atropisomer distributions of chiral polychlorinated biphenyls (PCBs) have been detected in many biota, both in the wild and the laboratory (1,2). Differential accumulation of the individual atropisomers of chiral PCBs in biota (species-specific, organ-specific and congener-specific) indicates that they are subject to different stereoselective metabolic processes, toxicities and fate in the biosphere. For example, the activation of ryanodine receptors and other cellular targets, and consequent disruption of Ca^{2+} signaling by chiral PCBs, are stereoselective processes in organisms and thus different atropisomers may cause different neurotoxicities (3-6).

Stereoselective biotransformation by cytochrome P450 isozymes (CYPs) is a major mechanism for the atropisomer composition change of chiral PCBs in biota (7-9). PCBs are oxidized by CYPs to generate PCB arene oxide intermediates and/or OH-PCBs, the former of which can be converted to OH-PCBs by epoxide hydroxylase (10). However, the individual stereoisomers of a chiral chemical can bind to CYPs with different affinities and thus have different biotransformation kinetics, which can be affected by the presence of other xenobiotics or endogenous chemicals (9). Therefore, it is plausible that the two atropisomers of a chiral PCB could disrupt the enzymatic biotransformation processes of each other, as previously observed for (+)- and (-)-PCB 132 with rat CYP2B1 (9). However, unanswered questions still remain due to limitations of these earlier studies, including low purity and/or concentration of CYPs and enantiopure PCB atropisomers, short incubation times and lack of analysis of metabolites (9,11).

OH-PCBs have been found in many species *in vitro* or *in vivo* (12-19). These metabolites are also of environmental concern because they can result in dysfunction of

thyroid and estrogenic activities (10), disruption of the homeostasis of vitamin A (20), disorder in neuronal and brain development (21), cytotoxicity and oxidative stress in cells (22), and interference with the metabolism of xenobiotics in organisms (23). Atropisomer accumulation of OH-PCBs in biota may also result in stereoselective toxicities.

Previous studies (8,24,25) found that 5-OH-PCBs were formed stereoselectively as the major metabolites of chiral PCBs by rat liver microsomes and tissue slices. Atropisomer enrichment of OH-PCB 136 and the formation of diOH-PCBs in the livers of rats and mice were also observed *in vivo* (26,27). *In vitro*, rat CYP2B1 could biotransform chiral PCBs stereoselectively to form OH-PCB metabolites (7). However, specific metabolites could not be identified due to lack of standards (7), nor were the EFs of OH-PCBs determined. Thus, although it is reasonable to presume that CYPs are the major enzymes responsible for stereoselective formation of OH-PCBs in animals, specific pathways for stereoselective biotransformation of PCBs to form specific OH-PCBs remain unclear. In addition, diOH-PCBs were also detected in some organisms as metabolites of PCBs (28-30). These metabolites can be formed through hydroxylation of OH-PCBs (31) by CYP2B1 (32) in rat liver microsomes (31,33). However, the stereoselectivities of this hydroxylation of OH-PCBs and the formation of diOH-PCBs by purified CYPs are unknown.

In the present study, we address the questions raised above by the previous studies. Rat CYP2B1 was used in our experiment because it could stereoselectively biotransform chiral PCBs (7). We hypothesized that 5-OH-PCB was the major metabolite of chiral PCB by rat CYP2B1 biotransformation and the formation of OH-PCB was a stereoselective process; that 4-OH-PCB and diOH-PCB metabolites could also be formed

in this biotransformation process as minor products; and that chiral OH-PCBs could be stereoselectively biotransformed by rat CYP2B1 to produce non-racemic diOH-PCBs. In addition, we also hypothesized that an increase in concentration of one atropisomer will decrease the biotransformation activity of its antipode, and that disruption in biotransformation activity when both atropisomers are present to varying degrees, stereoselectively or otherwise, will affect the formation of hydroxylated metabolites. To our knowledge, this is the first time that purified CYP isozymes are shown to produce OH-PCBs stereoselectively, which in turn are stereoselectively metabolized to diOH-PCBs.

4.2. Materials and Methods

4.2.1. Chemicals and Regents

Racemic 2,2',3,4',6-pentachlorobiphenyl (PCB 91), 2,2',3,5',6-pentachlorobiphenyl (PCB 95), 2,2',3,3',4,6'-hexachlorobiphenyl (PCB 132), 2,2',3,3',6,6'-hexachlorobiphenyl (PCB 136), 2,2',3,4',5',6-hexachlorobiphenyl (PCB 149), surrogate standards 2,4,6-trichlorobiphenyl (PCB 30), 2,2',3,4,4',5,6,6'-octachlorobiphenyl (PCB 204) and 2',3,3',4',5,5'-hexachlorobiphenyl-4-ol (4-159), and internal standards 2,3,4',5,6-pentachlorobiphenyl (PCB 117) and 2,3,3',4,5,5'-hexachlorobiphenyl (PCB 159) (all purities >99%) were purchased from Accustandard (West Haven, CT) and stock solutions were prepared in acetone. Rat CYP2B1 (CYP2B1 itself+CYP reductase+cytochrome b₅), insect cell control supersomes (CYP reductase+cytochrome b₅) (stored at -80 °C until use) and NADPH regeneration system (solution A: 31 mM NADP⁺, 66 mM glucose-6-phosphate and 66 mM MgCl₂ in water; solution B: 40 U/ml

glucose-6-phosphate dehydrogenase in 5 mM sodium citrate) (stored at -20 °C until use) were purchased from BD Biosciences (San Jose, CA).

Individual PCB 136 atropisomers were isolated as earlier published (11). The following authentic PCB metabolite standards were synthesized as described previously (11,32): 3-methoxy-2,2',4,4',6-pentachlorobiphenyl (3-100, NIH-shift metabolite of PCB 91); 2,2',3,4',6-pentachlorobiphenyl-4-ol (4-91); 2,2',3,4',6-pentachlorobiphenyl-5-ol (5-91); 3,4-dimethoxy-2,2',4',5,6-pentachlorobiphenyl; 3-methoxy-2,2',4,5',6-pentachlorobiphenyl (3-103, NIH-shift metabolite of PCB 95); 2,2',3,5',6-pentachlorobiphenyl-4-ol (4-95); 4-methoxy-2,2',3',5,6'-pentachlorobiphenyl (4'-95); 2,2',3,5',6-pentachlorobiphenyl-5-ol (5-95); 3,4-dimethoxy-2,2',5,5',6-pentachlorobiphenyl; 3-methoxy-2,2',3',4,4',6-hexachlorobiphenyl (3'-140); 2,2',3,3',4',6-hexachlorobiphenyl-4-ol (4'-132); 2,2',3,3',4',6-hexachlorobiphenyl-5-ol (5'-132); 3,4-dimethoxy-2,2',3',4',5,6-hexachlorobiphenyl; 2,2',3',4,6,6'-hexachlorobiphenyl-3-ol (3'-150); 2,2',3,3',6,6'-hexachlorobiphenyl-4-ol (4-136); 2,2',3,3',6,6'-hexachlorobiphenyl-5-ol (5-136); 3,4-dimethoxy-2,2',3',5,6,6'-hexachlorobiphenyl; 3-methoxy-2,2',4,4',5',6-hexachlorobiphenyl (3'-154); 2,2',4',5,5',6-hexachlorobiphenyl-3-ol (5-149). Standard solutions were prepared in isooctane for methoxy-compounds and in methanol for hydroxy-compounds.

The following abbreviations are used for diOH-PCBs: 4,5-91, 4,5-95, 4'5'-132 and 4,5-136 for 3,4-dihydroxy-2,2',4',5,6-pentachlorobiphenyl, 3,4-dihydroxy-2,2',5,5',6-pentachlorobiphenyl, 3,4-dihydroxy-2,2',3',4',5,6-hexachlorobiphenyl and

3,4-dihydroxy -2,2',3',5,6,6'-hexachlorobiphenyl, respectively.

4.2.2. *In Vitro* Biotransformation Experiments

Details on incubation methods were previously published (7,9). Briefly, incubations were conducted in glass tubes containing 10 pmol of rat CYP2B1, 50 μ L of solution A, 10 μ L of solution B, 1000 ng PCB or OH-PCB, and potassium phosphate buffer (110 mM, pH 7.4) in 1 mL total volume at 37°C for 60 minutes. Incubations were intended to generate enough products for enantioselective analyses. Hence, relatively high concentrations (1000 ng/mL) of PCBs or OH-PCBs were used, and enzymatic biotransformation activities may not necessarily be linear over the entire period of the incubation as previously observed (9). Incubations were terminated with 1 mL ice-cold methanol and immediately extracted. PCB 95 was used as a positive control substrate for 60 minute incubations. Different chiral PCBs were incubated with CYP control supersomes instead of rat CYP2B1 for 60 minutes as negative controls. Incubations were done in triplicate except for the control samples.

To understand better how the stereoisomers of a chiral contaminant may interfere with their enzymatic biotransformation, individual atropisomers of PCB 136 were isolated and used in the biotransformation experiment. We added the same concentration (500 ng/mL) of one atropisomer of PCB 136, i.e., (+)-136 or (-)-136, in the incubations and then varied the concentration (0, 100, 250, or 500 ng/mL) of its antipode i.e., (-)-136 or (+)-136 in that incubation. Please see the Table 4.1 for more details.

4.2.3. Chemical Extraction and Clean-up

Extraction methods are also detailed elsewhere (7,9). Briefly, PCBs 30, 204 and 4-

Table 4.1 Initial substrate amounts for experiments to study interference between the two atropisomers of PCB 136.

Samples	(-)-PCB 136 (ng/mL)	(+)-PCB 136 (ng/mL)
Incubation 1	500	0 (Acetone was added)
Incubation 2	500	100
Incubation 3	500	250
Incubation 4	500	500
Incubation 5	0 (Acetone was added)	500
Incubation 6	100	250
Incubation 7	250	500
Incubation 8 (negative control)	500	500

159 were added as surrogate standards after the incubations were terminated to the test tubes. The incubations were further denatured using HCl and 2-propanol, vortexed for 1 min and centrifuged for 10 min. The liquid supernatant was then washed with KCl and extracted with 6 mL of 1:1 (v/v) methyl-*t*-butyl ether (MTBE)/hexane. The organic phase was collected and partitioned with 6 mL of 1:1 (v/v) 1 M KOH/ethanol to separate the OH-PCBs from the neutral organic phase. PCBs in the neutral organic fraction were purified using an acidified silica gel column (3 g, 22% H₂SO₄) and eluted with 20 mL of 15% (v/v) dichloromethane/hexane. PCB fractions were solvent-exchanged to hexane, and PCB 159 was added as an internal standard. OH-PCBs in the aqueous fraction were then acidified by H₂SO₄ and back-extracted into MTBE/hexane (1:1, v/v). The organic

phase containing OH-PCBs was derivatized with diazomethane into their respective methoxy-PCBs (MeO-PCBs). The MeO-PCB fraction was purified using a 5 g column of the acidified silica gel and eluted with 50 mL of 1:1 (v/v) dichloromethane/hexane. MeO-PCB fractions were solvent-exchanged to hexane and PCB 117 was added as an internal standard. Every extraction step was repeated three times for each sample.

The average and standard deviations of PCBs 30 and 204 recoveries were $91 \pm 17\%$ and $79 \pm 9\%$ respectively, and PCB concentrations were corrected based on the average recoveries of PCBs 30 and 204 in each sample. Likewise, the recovery of 4-159 was $82 \pm 22\%$. MeO-PCB concentrations were corrected by the recovery of 4-159 in each sample except for PCB 132 which had co-elution issues (27). PCB concentrations were determined using PeakFit v4.12 (Systat Software, San Jose, CA) to deconvolute chromatographic peaks and maintain consistency with previous studies (9,34). For the same reason, integration of MeO-PCB peaks was performed using the valley-drop method (8).

4.2.4. Instrumentation and Measurements

PCBs were quantified using an Agilent 5890 gas chromatograph with a ^{63}Ni - μ electron capture detector (ECD) and a Chirasil-Dex (CD) column (25 m \times 0.25 mm internal diameter (i.d.) \times 0.25 μm d_f , Agilent, Santa Clara, CA) (7,9). One μL samples were injected in the splitless mode at 250 $^{\circ}\text{C}$ with helium as carrier gas and at a constant column head pressure of 0.71 bar. Initial oven temperature was held at 60 $^{\circ}\text{C}$ for 2 min, then ramped at 10 $^{\circ}\text{C}/\text{min}$ to 160 $^{\circ}\text{C}$, ramped at 1 $^{\circ}\text{C}/\text{min}$ to 210 $^{\circ}\text{C}$, held for 25 min. The detector temperature was 320 $^{\circ}\text{C}$.

MeO-PCB congeners were quantified using an Agilent 7890A gas chromatograph

with a ^{63}Ni - μECD detector and SPB-1 or Equity-1 column (60 m \times 0.25 mm i.d. \times 0.25 μm d_f , respectively; Supelco, St. Louis, MO). The following temperature program was used: 150 $^{\circ}\text{C}$ for 2 min, then 30 $^{\circ}\text{C}/\text{min}$ to 200 $^{\circ}\text{C}$, 1 $^{\circ}\text{C}/\text{min}$ to 230 $^{\circ}\text{C}$, 10 $^{\circ}\text{C}/\text{min}$ to 300 $^{\circ}\text{C}$, hold for 15 min, with the constant helium flow of 2 mL/min. The injector and detector temperatures were 280 $^{\circ}\text{C}$ and 300 $^{\circ}\text{C}$, respectively (27).

The identity of hydroxylated metabolites, as their methoxylated derivatives, was confirmed on an Agilent 7890A gas chromatograph with a 5975C mass spectrometry detector and a HP-5 column (30 m \times 0.32 mm i.d. \times 0.25 μm d_f , Agilent, Santa Clara, CA). The following temperature program was used: 100 $^{\circ}\text{C}$ for 1 min, then 5 $^{\circ}\text{C}/\text{min}$ to 280 $^{\circ}\text{C}$ with the constant helium flow of 1.5 mL/min. The ions monitored were m/z 356 and 358 for mono-methoxylated pentachlorobiphenyls, m/z 384 and 386 for di-methoxylated pentachlorobiphenyls, m/z 390 and 392 for mono-methoxylated hexachlorobiphenyls, and m/z 420 for di-methoxylated hexachlorobiphenyls. The injector, source and quadrupole temperatures were 280 $^{\circ}\text{C}$, 230 $^{\circ}\text{C}$ and 180 $^{\circ}\text{C}$, respectively (27).

To facilitate the enantioselective analysis, EF determinations of MeO-PCBs were performed using an Agilent 7890A gas chromatograph equipped with two ^{63}Ni - μECD detectors, a CD column (30 m \times 0.25 mm i.d. \times 0.39 μm d_f) and a ChiralDex B-DM (BDM) column (30 m \times 0.25 mm i.d. \times 0.12 μm d_f ; Supelco, St. Louis, MO). Two columns were used to help confirm enantiomeric composition, both of which could resolve all MeO-PCB congeners studied. The following temperature program was used: 100 $^{\circ}\text{C}$ for 1 min, 10 $^{\circ}\text{C}/\text{min}$ to 140 $^{\circ}\text{C}$, hold for 460 min, 1 $^{\circ}\text{C}/\text{min}$ to 200 $^{\circ}\text{C}$, hold for 35 min with the constant helium flow of 3 mL/min. The injector and detector temperatures were held at 250 $^{\circ}\text{C}$. For incubation samples containing PCB 132 and its metabolites, the final

temperature was 160 °C to optimize isomer/atropisomer separation (8).

4.2.5. Data Analyses

The enantiomer fraction (EF) was defined as $EF = E(+)/(E(+) + E(-))$, where the elution order of (+) and (-) atropisomer is known (PCBs 132, 136 and 149) (35,36), or $EF = E1/(E1 + E2)$ where the elution order is unknown (Equation 1.1). Prism 5 (GraphPad Software, La Jolla, CA) was used for plotting and statistical analyses. The *t*-test and one way ANOVA were used for data analyses, with statistically significant levels at 0.05 (please see figure captions for details).

4.3. Results and Discussion

4.3.1. Stereoselective Biotransformation of Chiral PCBs

PCBs 91, 95, 132, 136 and 149 were chosen as substrates because they are widely detected in organisms as non-racemic residues (37,38) and are neurotoxic (3-6). Depletions of PCBs 91, 95, 132, 136 and 149 were 25%, 17%, 11%, 21% and 4% after 60 min incubation, respectively. PCBs 91 and 95 were biotransformed more rapidly than PCBs 132 and 149, but were similar with that of PCB 136 (Figure 4.1A1). It is well-established that the biotransformation rate of PCBs depends on the presence of unsubstituted vicinal *meta* and *para* positions (10), as well as substrate sizes (39), binding positions and affinities to enzymes (9). All these congeners, except for PCB 149, were stereoselectively biotransformed by rat CYP2B1 (Figure 4.1A1 and 4.1A2). The biotransformation activities of E1-91, E2-95, (-)-132 and (+)-136 were significantly higher than their respective antipodes (Figure 4.1A1). Accordingly, the EFs of PCBs 91, 95, 132 and 136 changed from the racemic value (i.e., 0.50) to 0.45 (not statistically

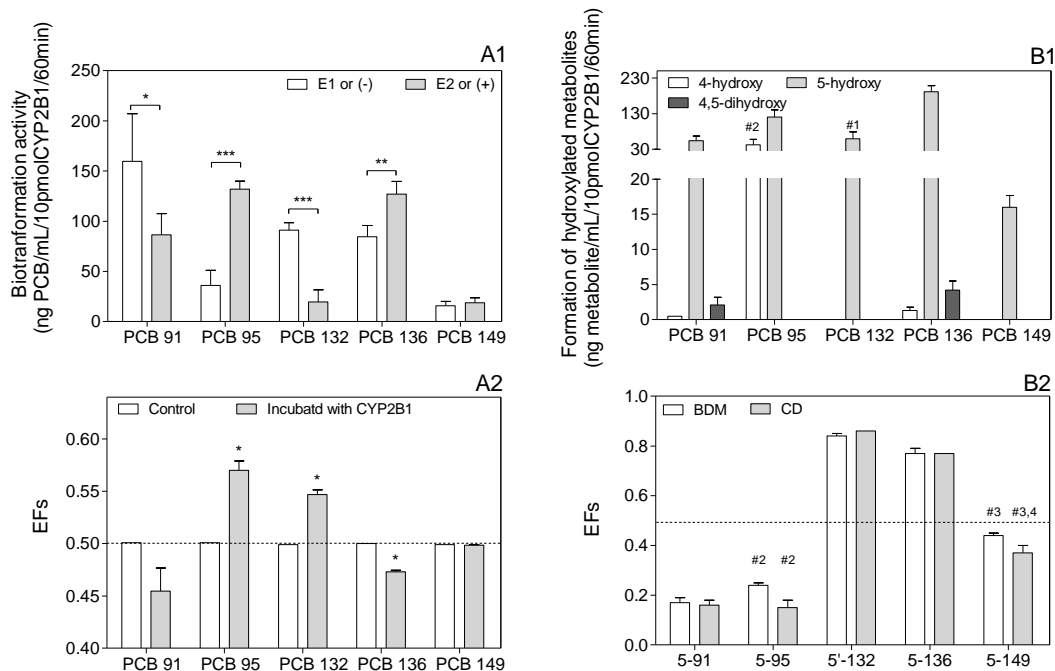


Figure 4.1 Stereoselective biotransformation of chiral PCBs and formation of hydroxylated metabolites by rat CYP2B1 over 60 min incubation time, under conditions to foster generation of metabolites. (A1) Biotransformation activities of chiral PCBs (asterisks indicate statistical difference between two atropisomers of a chiral PCB, unpaired t-test, one-tailed p value, * $p < 0.05$, ** $p < 0.01$, *** $p < 0.001$); (A2) Enantiomer fractions (EFs) of chiral PCBs after biotransformation (asterisks indicate statistical difference, one sample t-test, two-tailed p value, * $p < 0.05$, different from racemic i.e., 0.5); (B1) Formation activities of mono- and di-hydroxylated metabolites of PCBs; (B2) EFs of 5-hydroxy metabolites of chiral PCBs determined on two different enantioselective gas chromatography columns. All the EFs are statistically different from 0.5. CD: Chirasil-Dex column; BDM: ChiralDex B-DM column. All data reported as mean \pm standard deviation of three replicates (one sample for each negative control).

^{#1}Value not adjusted for recovery because the surrogate standard co-eluted with 4,5-132;
^{#2}Not detected by GC-MS; ^{#3}Imperfect agreement of EFs between BDM and CD column;
the atropisomers of various metabolites co-eluted on both columns, making the EF
determination difficult; ^{#4}The results were confirmed on CD column using a mass
selective detector, EF = 0.31 ± 0.03.

different), 0.57, 0.55 and 0.47, respectively. In contrast, PCB 149 was slightly
biotransformed by rat CYP2B1, but with no apparent stereoselectivity (Figure 4.1A1). All
atropisomer composition patterns observed in the present work were consistent with
previous rat CYP2B1-mediated *in vitro* experiments (7,9). One possible mechanism for
the stereoselective biotransformation at the molecular level is that the binding orientation
and affinities of two atropisomers with a specific enzyme are not exactly the same (9).
Consequently, these interaction differences could result in different biotransformation
kinetics of the two atropisomers of a congener.

Likewise, the atropisomer composition patterns of PCBs 91, 95, 132 and 136
observed in the present study (Figure 4.1A2) were consistent with previous rat liver
microsomal experiments. For example, the EFs of PCBs 91, 95, 132 and 136 after 30 min
microsomal incubations were 0.43, 0.64, 0.61 and 0.40 respectively (8,24), which were
similar to our observations (Figure 4.1A2). The slight differences in EFs observed
between the present study and previous literature might be due to differences in initial
substrate concentrations, rat CYP2B1 content, involvement of other CYPs in microsome
incubation, incubation time, and chromatographic integration methods (7,9,34). Taken
together, all these observations demonstrate that CYP2B1 is one of the enzymes

responsible for the stereoselective biotransformation of these chiral PCB congeners in rat liver. However, PCB 149 after 30 min biotransformation by rat liver microsomes was significantly non-racemic with an EF of 0.46 (8), in contrast to our observation of no significant atropisomer composition change in the present study. This difference in atropisomer composition pattern of PCB 149 suggests that CYPs other than CYP2B1 in the liver microsomes might have been involved. Phase II biotransformation was unlikely to affect stereoselectivity in that case, because cytosolic phase II enzymes and co-factors of cytosolic and microsomal phase II enzymes are removed during the preparation of microsomes by differential centrifugation.

Stereoselective biotransformation of chiral PCBs by different types of enzymes might be one of the major reasons for the tissue-, species- and congener-specific atropisomer accumulation observations *in vivo*. The atropisomer composition signatures of PCBs 95 and 132 measured in this study were consistent with the previous *in vivo* observations for rats (EFs>0.5) (40,41), suggesting that CYP2B1 mediated biotransformation might be one reason for the atropisomer composition change of these congeners in rats. Similar EFs of PCB 95 were also detected in thick-billed murre, ivory gull, ringed seal (37), and harbour porpoises (38), indicating that biotransformation mediated by CYP 2B1-like enzymes might be involved in these high tropic level species. However, different composition patterns of chiral PCBs were observed in some species. The EFs of PCBs 95 and 136 were about 0.3 and 0.7, respectively, in C57Bl/6 female mice tissues after oral administration (26,42). These results indicate that, besides CYP-mediated biotransformation, other processes (e.g. induction of CYP-enzymes by drugs or environmental contaminants (24,25), modulation of CYP activity by other

chemicals (e.g., gold nanoparticles) (43), phase II metabolism, or active transport processes) cannot be excluded as factors contributing to the atropisomer composition changes of PCBs *in vivo*.

4.3.2. Stereoselective Formation of Hydroxylated PCBs

Hydroxylated metabolites were detected in the incubations of parent PCB congeners, dominated by *meta*-substitution into the 2,3,6-trichlorinated ring to generate 5-OH-PCBs (or 5'-OH-PCB for PCB 132) (Figure 4.1B1 and Figure A3). The unsubstituted vicinal *meta* and *para* positions of 2,3,6-substituted PCBs make them amenable to oxidation by CYP2B isozymes (39). The yields, expressed as the percent of 5-OH-PCB over the initial PCB amount in the incubation, of 5-OH-PCBs were 5.4%, 12%, 5.9%, 19%, 1.6% for PCBs 91, 95, 132, 136 and 149, respectively. In addition, 4-OH-PCB metabolites were detected by GC-ECD analysis as minor products from incubations of PCBs 91, 95 and 136. The formation of these metabolites could not be confirmed by GC-MS due to the low levels of these metabolites in the incubations.

After 60 min, approximately 22%, 71%, 53%, 90%, and 46% of the depleted PCBs 91, 95, 132, 136, and 149 were converted to the corresponding 5-OH-PCBs metabolites, respectively. In contrast, relatively lower amounts of the observed depletion of PCBs 91 (less than 1%), 95 (about 25%) and 136 (less than 5%) were converted to their 4-hydroxylated and 4,5-dihydroxylated metabolites. This rough mass balance calculation suggests that the remaining fraction of the parent PCBs might have been biotransformed to currently unidentified metabolites, including other OH-PCB or arene oxide metabolites. Indeed, some unidentified peaks were observed in the chromatograms (e.g., metabolites of PCB 95, Figure A3.2), which was consistent with previous observations in rat liver

microsomes (8). We could not identify the arene oxide intermediates in the present study because the experiment was not designed for collecting these intermediates.

The formation of 5-OH-PCBs as major metabolites of PCBs by rat CYP2B1 in our experiments was consistent with previous work (32). Similar results were observed previously in the biotransformation of dichlorobiphenyls mediated by phenobarbital-induced (i.e., CYP2B enriched) CYPs in rat liver microsomes (33). Waller et al. (32) found that rat CYP2B1 generated 5-136 as the major metabolite of PCB 136. However, the yield rank order of 5-OH-PCB metabolites in previous rat liver microsomal studies (i.e., PCB 91 at 20% yield, PCB 95 at 8.8%, PCB 132 at 16%, PCB 136 at 22% and PCB 149 at 2.6%) (8,24) differed somewhat from that of the present work (i.e., PCB 91 at 5.4%, PCB 95 at 12%, PCB 132 at 5.9%, PCB 136 at 19% and PCB 149 at 1.6%). The obvious differences in the yields for 5-91 and 5'-132 suggests that other CYP isoforms, other than that mediated by CYP2B1, might be involved in the formation of these metabolites in liver microsomes. The formation of NIH-shift metabolites of chiral PCBs in the rat liver microsomes, not observed in the present study, confirmed the involvement of enzymes other than rat CYP2B1. Thus, different OH-PCBs may be formed by specific metabolic pathways. Certainly, differences in incubation conditions may also contribute to the noted differences in product formation. Similar comparisons can be made with previous *in vivo* work. For instance, 5-95, 5'-132 and 5-136 were identified as the major metabolites of the corresponding parent PCBs in rats (27,44,45). All these observations taken together indicate that CYP2B1 is a major contributor to the metabolism of chiral PCBs to 5-OH-PCBs in rats *in vivo* as well as *in vitro* regardless of the contribution of other CYP isoforms.

Atropisomer composition changes of 5-OH-PCBs were observed in the present study (Figure 4.1B2), confirming for the first time that CYP2B1 produces OH-PCBs stereoselectively. Similar EFs were measured on both enantioselective columns used (Figure 4.1B2). The average EFs of 5-91, 5-95, 5'-132, 5-136 and 5-149 were 0.17, 0.20, 0.85, 0.77 and 0.41, respectively. Although the biotransformation of PCB 149 by rat CYP2B1 was not a stereoselective process, atropisomer composition change of 5-149 was indeed observed. This might be due to the stereoselective depletion of 5-OH-PCBs to diOH-PCBs by CYP2B1, which will be discussed in next section. Alternatively, covalent binding of OH-PCBs with CYPs is another possible explanation (10,31). It was not possible to measure the EFs of 4-OH-PCBs in our study due to the low amounts of these metabolites; however, atropisomer composition change of 4-OH-PCB in rat CYP2B1 mediated biotransformation might exist as was observed in rat liver microsomes (27).

Comparison of our CYP-mediated OH-PCB atropisomer composition with that from liver microsomes (8,24) and slices (25), and *in vivo* (27) studies (Table 4.2) indicates that while CYP2B1 is likely a dominant isozyme for production of 5-OH-PCB metabolites, other enzymes are probably also involved. The EFs of 5-91, 5-95, 5'-132, 5-136 and 5-149 from incubations of their parent PCBs with rat liver microsomes were 0.54, 0.36, 0.30, 0.70 and 0.66, respectively (8,24). The EFs of 5-95 (EF=0.20) and 5-136 (EF=0.77) in our CYP2B1-mediated incubations are similar, indicating that CYP2B1 plays an important role in stereoselective formation of these OH-PCBs. However, accumulation of the antipodes of 5'-132 and 5-149 implies that other biotransformation processes (e.g., biotransformation of chiral PCBs or 5-OH-PCBs by other enzymes) might be involved in the stereoselective accumulation of these metabolites in rat liver microsomes. Little is

Table 4.2 Comparison of Enantiomer Fractions (EFs) of 5-OH-PCB metabolites from different studies.

5-OH-PCBs	Present study Rat CYP2B1	Rat liver microsomes ^{1,2}	Rat liver slices ³	Rat <i>in vivo</i> ⁴	Mice <i>in vivo</i> ⁵
5-91	0.17	0.54			
5-95	0.20	0.36			0.65
5'-132	0.85	0.30			
5-136	0.77	0.70	0.69~0.74	0.40	
5-149	0.41	0.66			

known about the atropisomer composition of OH-PCBs *in vivo*. Kania-Korwel et al.,(27) observed non-racemic 5-136 (EF≈0.4) (EFs were considered as statistically non-racemic if values deviated from racemic value beyond 0.032 (95% confidence interval)) in the livers of Sprague-Dawley rats after intraperitoneal injection of PCB 136, which contrasts with the atropisomer composition pattern of 5-136 observed in rat liver microsomes (EF=0.70) and our rat CYP2B1 incubation (EF=0.77). In female C57Bl/6 mice, the EFs of 4-95 and 5-95 in the liver were about 0.20 and 0.65 respectively (26). Thus, biotransformation by other CYP isoforms, sulfation, glucuronidation, the formation of methylsulfones via the mercapturic acid pathway, and other factors, such as exposure pathways (46), should be considered for fully understanding the atropisomer composition of OH-PCBs. The atropisomer compositions of OH-PCBs in wild animals are unknown and should be investigated in future studies.

4,5-DiOH-PCBs were formed as minor metabolites of PCBs 91 and 136 by rat

CYP2B1 in the present study (Figure 4.1B1). Enantioselective analyses of these diOH-PCBs were not performed because of their low concentrations. Similar diOH-PCB metabolites were observed previously in rat and mice (8,24). For instance, 4,5-136 and 4,5-91 were observed in rat liver microsomes as minor metabolites (8,24). 4,5-136 was also found in rat livers after intraperitoneal injection of PCB 136 (27). 4',5'-132 was detected in rat liver microsomes previously (8), which is different from our observation. Our study may not have produced enough 4',5'-132 to allow detection by our GC methods, or alternatively some other CYP isoforms might be responsible for generation of 4',5'-132 in the rat liver microsomes. 4,5-95 was found in the mice body after 39 days oral exposure (26). DiOH-PCBs were also found in other species such as laboratory-exposed Gunn rats (28) (i.e., 3',4'-dihydroxy-PCB 101) and fishes collected from Great Lakes (i.e., 4, 4'-dihydroxy-PCB 202) (29). Regardless, our study shows that hydroxylation of OH-PCBs by CYPs is a source of diOH-PCBs in biota, as noted below.

4.3.3. Stereoselective Biotransformation of OH-PCBs and Formation of DiOH-PCBs

To demonstrate that OH-PCBs can be stereoselectively biotransformed by CYPs and generate non-racemic diOH-PCBs, 4-95 and 5-95 were used as model compounds. Both OH-PCBs were biotransformed by rat CYP2B1 with 40% and 64% depletion after 60 min and with the 5-95 having a significantly greater biotransformation activity (Figure 4.2A1). Atropisomer composition change of both substrates was found, with EFs of 0.62 and 0.46 for 4-95 and 5-95, respectively. Thus, rat CYP2B1 could metabolize OH-PCBs stereoselectively. It also suggests that OH-PCBs are potential competitors for the biotransformation of parent PCBs since they were present in the biotransformation process at the same time and both of them can be metabolized by CYP2B1. The higher

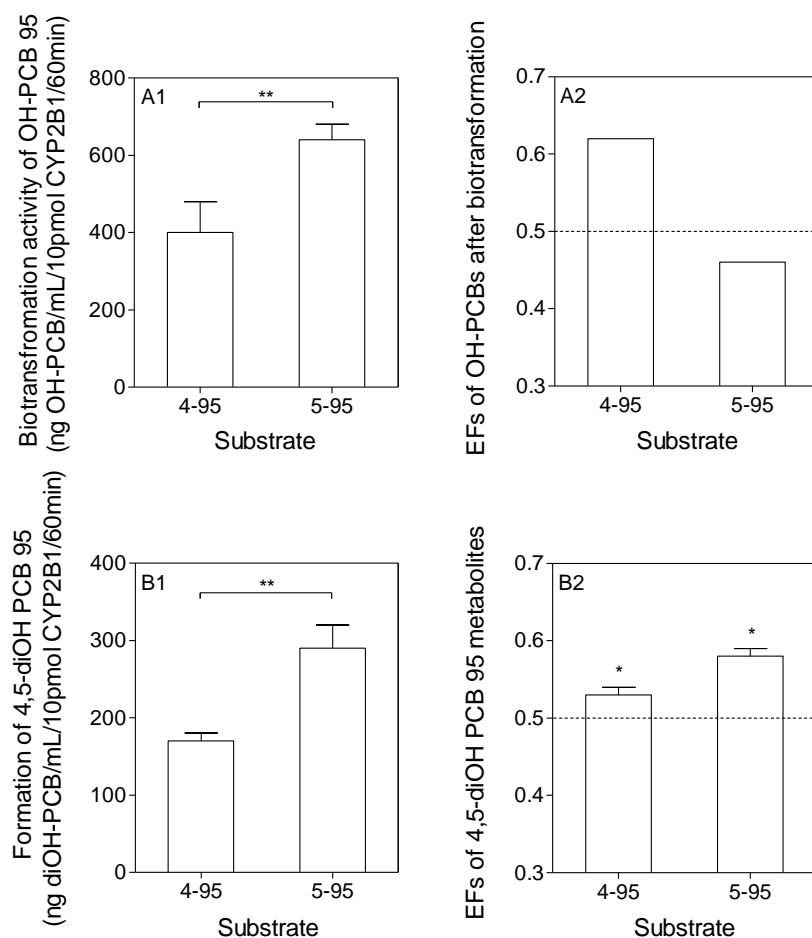


Figure 4.2 Stereoselective biotransformation of 4-95 and 5-95 and formation of 4,5-95 by rat CYP2B1, over 60 min incubation time. (A1) Biotransformation activities of 4-95 and 5-95 by rat CYP2B1 (asterisks indicate statistical difference, unpaired t-test, one-tailed p value, * $p<0.05$, ** $p<0.01$); (A2) EFs of 4-95 and 5-95 after biotransformation; (B1) Formation activities of 4,5-95 after biotransformation of 4-95 and 5-95 by rat CYP2B1 (asterisks indicate statistical difference, unpaired t-test, one-tailed p value, ** $p<0.01$); (B2) EFs of 4,5-95 as metabolite of OH-PCB 95 derivatives (asterisks indicate statistical difference from racemic, i.e., 0.5). Values are presented as mean \pm standard deviation of three replicates.

concentration of E2 5-95 in the incubation of PCB 95 with CYP2B1 (EF~0.20, Figure 4.1B2) was consistent with the incubation using 5-95 as substrate (EF~0.46, Figure 4.2A2). This means that both the stereoselective biotransformation of parent PCBs and OH-PCBs contribute to the atropisomer composition change of OH-PCBs observed in biological systems.

The metabolite observed was identified as 4,5-95 for 4-95 and 5-95 as substrates (Figure 4.2B1, Figure A3.8 and A3.9). The average yields of 4,5-95, expressed as the percent of 4,5-95 over the initial concentration of the appropriate OH-PCB, were 17% and 29% for 4-95 and 5-95, respectively. The incubation of 5-95 with rat CYP2B1 produced a significantly greater amount of 4,5-95 than the incubation of 4-95, consistent with the higher biotransformation rate of 5-95. Of the depleted OH-PCB congeners, 42% and 45% were biotransformed to 4,5-95 respectively. This result suggested that some unidentified metabolites or intermediates might have been produced. This was consistent with the unknown peaks detected in the chromatograms (Figure A3.8). The formation of 4,5-95 was also a stereoselective process, with measured EFs of 0.53 and 0.58 for 4-95 and 5-95 incubations, respectively. The atropisomer composition data of chiral diOH-PCBs in organisms are rare. Only one study demonstrated that non-racemic 4,5-95 was detected as the metabolite of PCB 95 in mice (26). Thus, future studies are necessary to identify the atropisomer enrichment of diOH-PCBs in wildlife.

4.3.4. Interference between the Two Atropisomers of PCB 136

To understand better the mutual interference between enantiomers of chiral contaminants, individual atropisomers of PCB 136 were isolated and used in the biotransformation experiment as a model. Previous achiral work (47) on PCB 136

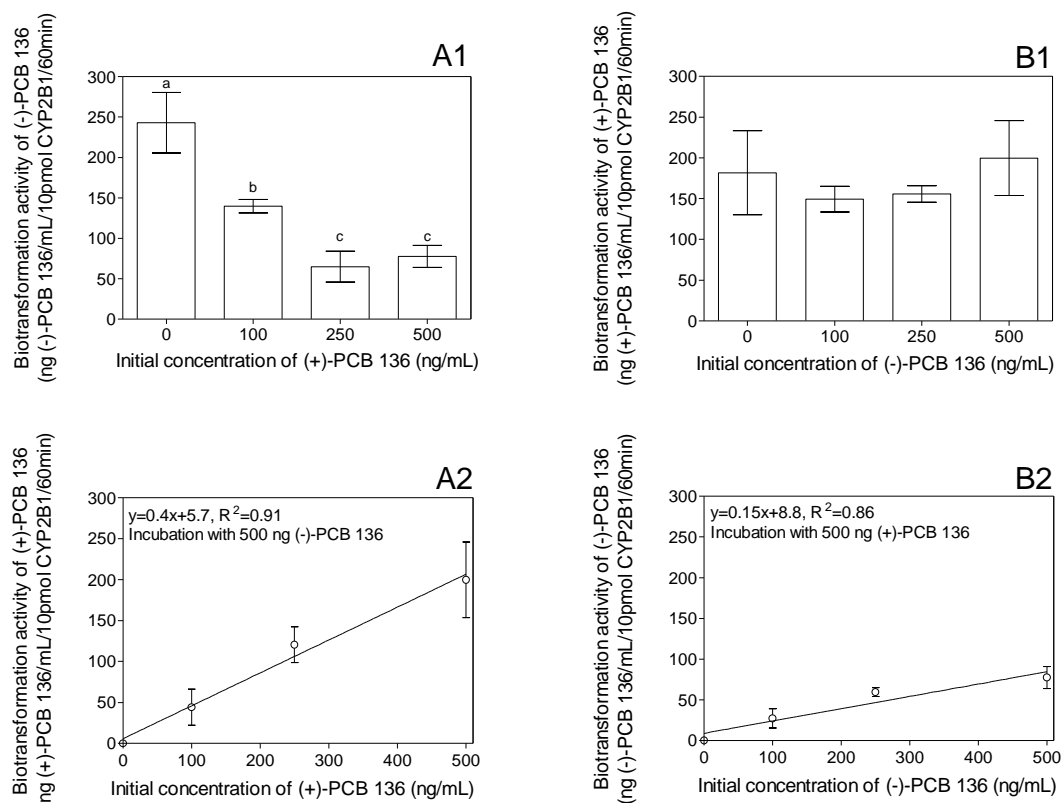


Figure 4.3 The two atropisomers of PCB 136 interfere with each other when biotransformed by rat CYP2B1. (A) Incubation of 500 ng (-)-PCB 136 with various initial concentrations of (+)-PCB 136: (A1) biotransformation activities of (-)-PCB 136, (A2) biotransformation activities of (+)-PCB 136; (B) Incubation of 500 ng (+)-PCB 136 with various initial concentrations of (-)-PCB 136: (B1) biotransformation activities of (+)-PCB 136, (A2) biotransformation activities of (-)-PCB 136. All data reported as mean \pm standard deviation of three replicates. Different letters in A1 and B1 indicate statistical difference in biotransformation activities, $p < 0.05$, one way ANOVA with post Tukey's multiple comparison test. All incubations over 60 min.

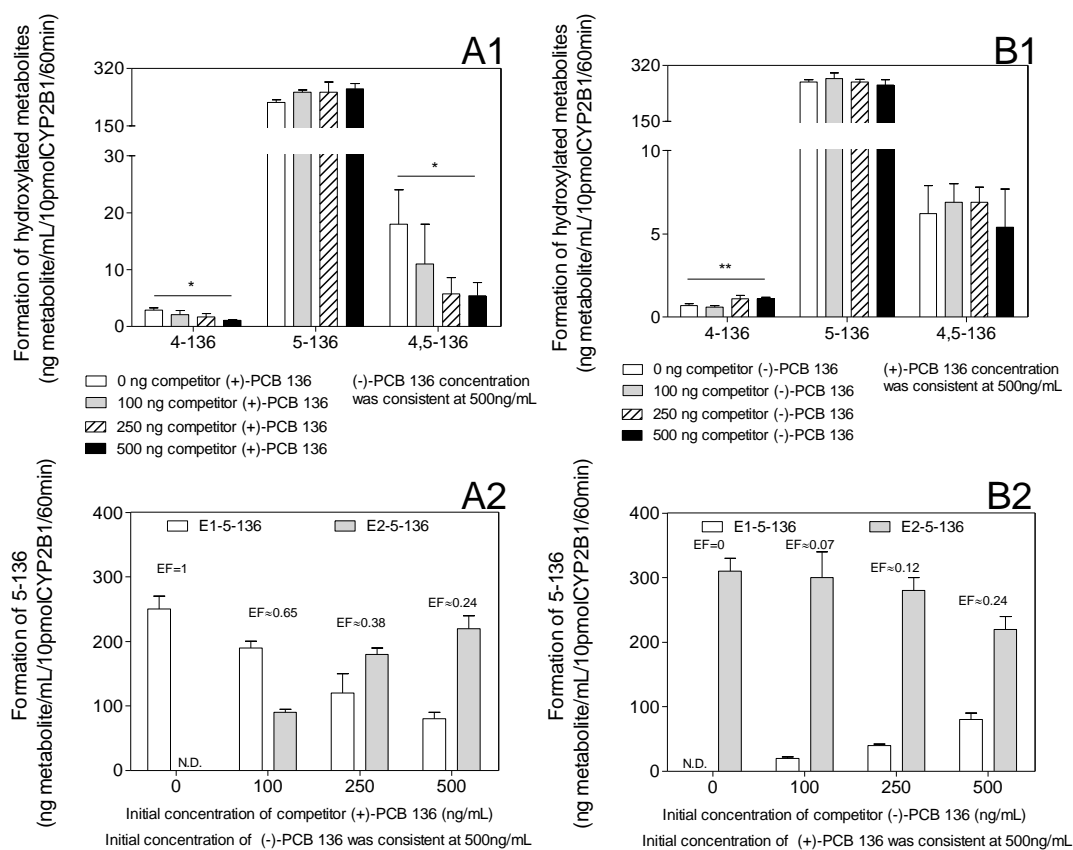


Figure 4.4 The two atropisomers of PCB 136 interfere with each other when producing hydroxylated metabolites in biotransformation by rat CYP2B1. (A) Incubation of 500 ng (-)-PCB 136 with various initial concentrations of (+)-PCB 136: (A1) formation activities of 4-136, 5-136 and 4,5-136, (A2) formation activity of the two atropisomers of 5-136; (B) Incubation of 500 ng (+)-PCB 136 with various initial concentrations of (-)-PCB 136: (B1) formation activities of 4-136, 5-136 and 4,5-136, (B2) formation activities of the two atropisomers of 5-136. All data reported as mean \pm standard deviation of three replicates. N.D. = not detected. Asterisks in A1 and B1 indicate statistical difference, * p <0.05, ** p <0.01, one way ANOVA with post Tukey's multiple comparison test. The chromatograms of the metabolites of pure (-)-or (+)-PCB 136 by rat CYP2B1 are shown

in SI (Figure A3.5 and A3.6). All incubations over 60 min.

biotransformation by human liver microsomes (280 pmole CYP/mg protein) suggested that the V_{\max} and K_m values were about 5 pmole PCB 136/mg protein/min (1.8 ng PCB 136/mg protein/min) and 8.8 μM (3200 ng/mL), respectively. In contrast, the highest substrate concentration and biotransformation activity in the present study (90 pmole CYP/mg protein) were about 3 μM (1000 ng/mL) and 96 pmole PCB 136/mg protein/min (35ng PCB136/mg protein/min), respectively. These results indicated that the biotransformation activity of chiral PCBs by rat CYP2B1 are faster than that mediated by human CYPs, which was consistent with previous observation (7). Certainly, different incubation conditions (47) were another possible factor contributing to the differences.

The biotransformation activity of the (-)-PCB 136 atropisomer significantly decreased with increases in initial (+)-PCB 136 concentration (Figure 4.3A1), indicating that the (+)-atropisomer disrupted the biotransformation rate of the (-)-atropisomer. Correspondingly, the formation of 4-136 and 4,5-136 metabolites were also significantly decreased with increases in the initial (+)-PCB 136 concentration, which suggested that (-)-PCB 136 was the major source of these two metabolites (Figure 4.4A1). While the formation of 5-136 was not influenced by adding more (+)-PCB 136 as competitor, the atropisomer composition of 5-136 was changed. In the pure (-)-PCB 136 incubations, E1-5-136 was the only metabolite (Figure 4.4A2). Increases in the initial (+)-PCB 136 concentration resulted in significant decreases in formation of E1-5-136 and increases in E2-5-136 (ANOVA, $p < 0.0001$), again consistent with the disruption of (-)-PCB 136 metabolism by (+)-PCB 136 (Figure 4.4A2).

Conversely, the biotransformation activity of (+)-PCB 136 was not significantly affected by the presence of (-)-PCB 136 (Figure 4.3B1). The concentration of 4-136 and 4,5-136 in these incubations were lower than the incubations which use (-)-PCB 136 as the major substrate (Figure 4.4A1 and 4.4B1). In addition, a significant increase in 4-136 formation with increases in initial (-)-PCB 136 concentration was observed (Figure 4.4B1). These results were consistent with the observations above, which suggested that (-)-PCB 136 was the major source of 4-136 and 4,5-136. A significant decrease in E2-5-136 formation was indeed observed (Figure 4.4B2) in these incubations. However, the decrease trend was not as significant as the decrease of E1-5-136 in Figure 4.4B1. These results suggest that disruption in product formation of (+)-PCB 136 metabolism by (-)-PCB 136 existed, but not as much as that of the disruption of (-)-PCB 136 by (+)-PCB 136.

Previously, Lu and Wong found that the two atropisomers of PCB 132 could disrupt the biotransformation process of each other *in vitro* (9). One possible mechanism was that (-)-PCB 132 could “inhibit” the metabolism of (+)-PCB 132 because of higher binding affinities of (-)-PCB 132 with rat CYP2B1. However, the “inhibition” of biotransformation activity of (-)-PCB 132 from (+)-PCB 132 could not be ruled out due to unavoidable impurities of the (-)-PCB 132 in that experiment (9). Similarly, two atropisomers of PCB 136 could bind with rat and mouse liver microsomal CYPs in a different manner (11). In the present study, we show that the accumulation of one atropisomer of chiral PCBs (e.g., (-)-PCB 136) in the biotransformation by CYPs was because its antipode (e.g., (+)-PCB 136), or by extension to other chemicals, were “better” substrates of the enzymes.

In addition, the biotransformation activity of the “competitor/inhibitor” increased to a different extent with increases in its initial concentration, compared to that of its antipode (Figure 4.3A2 and 4.3B2). It is possible that the reason why we did not see any further decreases in the biotransformation activity of (-)-PCB 136 above 250 ng/mL of (+)-PCB 136 (Figure 4.3A1) is because the enzyme was saturated, as suggested in Figure 4.3B2. Despite the good linear regression found, the activity may have leveled off between 250 and 500 ng/mL of (-)-PCB 136.

4.3.5. Environmental Implications

The present study demonstrated that CYP2B1-mediated biotransformation plays important roles in the atropisomer composition change of chiral PCBs and their hydroxylated metabolites in rats. The stereoselective metabolism of racemic OH-PCBs to non-racemic diOH-PCBs by rat CYP2B1 was confirmed as a mechanism for the atropisomer composition change of the chiral OH-PCBs. These findings indicated that the stereoselective biotransformation of chiral PCBs and OH-PCBs by CYPs are major sources of non-racemic PCBs, OH-PCBs and diOH-PCBs in the environment. The disruption of both biotransformation and the product formation of chiral compounds at the enantiomer level were confirmed by the present study. Our findings help explain the underlying processes for enantiomer composition change of chiral organic contaminants observed *in vivo* and *in vitro*. There were some unidentified metabolites in the biotransformation of chiral PCBs and OH-PCBs by rat CYP2B1, which may suggest potential exposure to these metabolites in the environment warranting further investigation.

References

- (1) Lehmler, H.-J.; Harrad, S. J.; Hühnerfuss, H.; Kania-Korwel, I.; Lee, C. M.; Lu, Z.; Wong, C. S. Chiral polychlorinated biphenyl transport, metabolism, and distribution: a review. *Environ. Sci. Technol.* **2010**, *44*, 2757-2766.
- (2) Zhai, G.; Hu, D.; Lehmler, H.-J.; Schnoor, J. L. Enantioselective biotransformation of chiral PCBs in whole poplar plants. *Environ. Sci. Technol.* **2011**, *45*, 2308-2316.
- (3) Wayman, G. A.; Bose, D. D.; Yang, D.; Lesiak, A.; Bruun, D.; Impey, S.; Ledoux, V.; Pessah, I. N.; Lein, P. J. PCB-95 modulates the calcium-dependent signaling pathway responsible for activity-dependent dendritic growth. *Environ. Health Perspect.* **2012**, *120*, 1003-1009.
- (4) Pessah, I. N.; Hansen, L. G.; Albertson, T. E.; Garner, C. E.; Ta, T. A.; Do, Z.; Kim, K. H.; Wong, P. W. Structure-activity relationship for noncoplanar polychlorinated biphenyl congeners toward the ryanodine receptor-Ca²⁺ channel complex type 1 (RyR1). *Chem. Res. Toxicol.* **2006**, *19*, 92-101.
- (5) Mariussen, E. and Fonnum, F., Neurochemical targets and behavioral effects of organohalogen compounds: An update. *Crit. Rev. Toxicol.* **2006**, *36*, 253-289.
- (6) Pessah, I. N.; Lehmler, H.-J.; Robertson, L. W.; Perez, C. F.; Cabrales, E.; Bose, D. D.; Feng, W. Enantiomeric specificity of (-)-2,2',3,3',6,6'-hexachlorobiphenyl toward Ryanodine receptor types 1 and 2. *Chem. Res. Toxicol.* **2009**, *22*, 201-207.
- (7) Warner, N. A.; Martin, J. W.; Wong, C. S. Chiral polychlorinated biphenyls are biotransformed enantioselectively by mammalian cytochrome P-450 isozymes to

- form hydroxylated metabolites. *Environ. Sci. Technol.* **2009**, *43*, 114-121.
- (8) Kania-Korwel, I.; Duffel, M. W.; Lehmler, H.-J. Gas chromatographic analysis with chiral cyclodextrin phases reveals the enantioselective formation of hydroxylated polychlorinated biphenyls by rat liver microsomes. *Environ. Sci. Technol.* **2011**, *45*, 9590-9596.
- (9) Lu, Z. and Wong, C. S. Factors affecting Phase I stereoselective biotransformation of chiral polychlorinated biphenyls by rat cytochrome P-450 2B1 isozyme. *Environ. Sci. Technol.* **2011**, *45*, 8298-8305.
- (10) Letcher, R.; Klasson-Wehler, E.; Bergman, Å. Methyl sulfone and hydroxylated metabolites of polychlorinated biphenyls. *Handbook of Environmental Chemistry*, **2000**, *3K*, 315-359.
- (11) Kania-Korwel, I.; Hrycay, E. G.; Bandiera, S. M.; Lehmler, H.-J. 2,2',3,3',6,6'-Hexachlorobiphenyl (PCB 136) atropisomers interact enantioselectively with hepatic microsomal cytochrome P450 enzymes. *Chem. Res. Toxicol.* **2008**, *21*, 1295-1303.
- (12) Buckman, A. H.; Wong, C. S.; Chow, E. A.; Brown, S. B.; Solomon, K. R.; Fisk, A. T. Biotransformation of polychlorinated biphenyls (PCBs) and bioformation of hydroxylated PCBs in fish. *Aquat. Toxicol.* **2006**, *78*, 176-185.
- (13) Richardson, K. L. and Schlenk, D. Biotransformation of 2,2',5,5'-tetrachlorobiphenyl (PCB 52) and 3,3',4,4'-tetrachlorobiphenyl (PCB 77) by liver microsomes from four species of sea turtles. *Chem. Res. Toxicol.* **2011**, *24*, 718-725.
- (14) Jörundsdóttir, H.; Ljöfstrand, K.; Svavarsson, J.; Bignert, A.; Bergman, Å.

- Organochlorine compounds and their metabolites in seven Icelandic seabird species - a comparative study. *Environ. Sci. Technol.* **2010**, *44*, 3252-3259.
- (15) Weijs, L.; Das, K.; Siebert, U.; van Elk, N.; Jauniaux, T.; Neels, H.; Blust, R.; Covaci, A. Concentrations of chlorinated and brominated contaminants and their metabolites in serum of harbour seals and harbour porpoises. *Environ. Int.* **2009**, *35*, 842–850.
- (16) McKinney, M. A.; De Guise, S.; Martineau, D.; Bédard, P.; Lebeuf, M.; Letcher, R. J. Organohalogen contaminants and metabolites in beluga whale (*Delphinapterus leucas*) liver from two Canadian populations. *Environ. Toxicol. Chem.* **2006**, *25*, 1246-1257.
- (17) Routti, H.; Letcher, R. J.; Arukwe, A.; van Bavel, B.; Yoccoz, N. G.; Chu, S.; Gabrielsen, G. W. Biotransformation of PCBs in relation to Phase I and II xenobiotic-metabolizing enzyme activities in Ringed Seals (*Phoca hispida*) from Svalbard and the Baltic Sea. *Environ. Sci. Technol.* **2008**, *42*, 8952-8958.
- (18) Sandala, G.M.; Sonne-Hansen, C.; Dietz, R.; Muir, D.C.G.; Valters, K.; Bennett, E.R.; Born, E.; Letcher, R.J. Hydroxylated and methyl sulfone PCB metabolites in adipose and whole blood of polar bear (*Ursus maritimus*) from East Greenland. *Sci. Total Environ.* **2004**, *331*, 125-141.
- (19) Gómara, B.; Athanasiadou, M.; Quintanilla-López, J. E.; González, M. J.; Bergman, Å. Polychlorinated biphenyls and their hydroxylated metabolites in placenta from Madrid mothers. *Environ. Sci. Pollut. Res.* **2012**, *19*, 139-147.
- (20) Berghe, M. V.; Weijs, L.; Habran, S.; Das, K.; Bugli, C.; Pillet, S.; Rees, J. F.; Pomeroy, P.; Covaci, A.; Debier, C. Effects of polychlorobiphenyls,

- polybromodiphenylethers, organochlorine pesticides and their metabolites on vitamin A status in lactating grey seals. *Environ. Res.* **2013**, 120, 18-26.
- (21) Kimura-Kuroda, J.; Nagata, I.; Kuroda, Y. Disrupting effects of hydroxy-polychlorinated biphenyl (PCB) congeners on neuronal development of cerebellar Purkinje cells: a possible causal factor for developmental brain disorders? *Chemosphere* **2007**, 67, S412-S420.
- (22) Dreiem, A.; Rykken, S.; Lehmler, H.-J.; Robertson, L. W.; Fonnum, F. Hydroxylated polychlorinated biphenyls increase reactive oxygen species formation and induce cell death in cultured cerebellar granule cells. *Toxicol. Appl. Pharm.* **2009**, 240, 306-313.
- (23) Mortensen, A. S.; Braathen, M.; Sandvik, M.; Arukwe, A. Effects of hydroxy-polychlorinated biphenyl (OH-PCB) congeners on the xenobiotic biotransformation gene expression patterns in primary culture of Atlantic salmon (*Salmo salar*) hepatocytes. *Ecotox. Environ. Safe.* **2007**, 68, 351-360.
- (24) Wu, X.; Pramanik, A.; Duffel, M. W.; Hrycak, E. G.; Bandiera, S. M.; Lehmler, H.-J.; Kania-Korwel, I. 2, 2', 3, 3', 6, 6'-Hexachlorobiphenyl (PCB 136) is enantioselectively oxidized to hydroxylated metabolites by rat liver microsomes. *Chem. Res. Toxicol.* **2011**, 24, 2249-2257.
- (25) Wu, X.; Kania-Korwel, I.; Chen, H.; Stamou, M.; Dammanahalli, K.J.; Duffel, M.; Lein, P.J.; Lehmler, H.-J. Metabolism of 2,2',3,3',6,6'-hexachlorobiphenyl (PCB 136) atropisomers in tissue slices from phenobarbital or dexamethasone-induced rats is sex-dependent. *Xenobiotica* **2013**, 43, 933-947.
- (26) Kania-Korwel, I.; Barnhart, C. D.; Stamou, M.; Truong, K. M.; El-Komy, M. H.;

- Lein, P. J.; Veng-Pedersen, P.; Lehmler, H.-J. 2,2',3,5',6-pentachlorobiphenyl (PCB 95) and its hydroxylated metabolites are enantiomerically enriched in female mice. *Environ. Sci. Technol.* **2012**, *46*, 11393-11401.
- (27) Kania-Korwel, I.; Vyas, S. M.; Song, Y.; Lehmler, H.-J. Gas chromatographic separation of methoxylated polychlorinated biphenyl atropisomers. *J. Chromatogr. A* **2008**, *1207*, 146-154.
- (28) Haraguchi, K.; Kato, Y.; Koga, N.; Degawa, M. Metabolism of polychlorinated biphenyls by Gunn Rats: Identification and serum retention of catechol metabolites. *Chem. Res. Toxicol.* **2004**, *17*, 1684-1691.
- (29) Campbell, L. M.; Muir, D. C. G.; Whittle, D. M.; Backus, S.; Norstrom, R. J.; Fisk, A. T. Hydroxylated PCBs and other chlorinated phenolic compounds in lake trout (*Salvelinus namaycush*) blood plasma from the Great Lakes region. *Environ. Sci. Technol.* **2003**, *37*, 1720-1725.
- (30) Nomiya, K.; Uchiyama, Y.; Horiuchi, S.; Eguchi, A.; Mizukawa, H.; Hirata, S. H.; Shinohara, R.; Tanabe, S. Organohalogen compounds and their metabolites in the blood of Japanese amberjack (*Seriola quinqueradiata*) and scalloped hammerhead shark (*Sphyrna lewini*) from Japanese coastal waters. *Chemosphere* **2011**, *85*, 315-321.
- (31) McLean, M. R.; Bauer, U.; Amaro, A. R.; Robertson, L. W. Identification of catechol and hydroquinone metabolites of 4-monochlorobiphenyl. *Chem. Res. Toxicol.* **1996**, *9*, 158-164.
- (32) Waller, S. C.; He, Y. A.; Harlow, G. R.; He, Y. Q.; Mash, E. A.; Halpert, J. R. 2,2',3,3',6,6'-hexachlorobiphenyl hydroxylation by active site mutants of

- cytochrome P450 2B1 and 2B11. *Chem. Res. Toxicol.* **1999**, *12*, 690-699.
- (33) Kaminsky, L. S.; Kennedy, M. W.; Adams, S. M.; Guengerich, F. P. Metabolism of dichlorobiphenyls by highly purified isozymes of rat liver cytochrome P-450. *Biochemistry* **1981**, *20*, 7379-7384.
- (34) Asher, B. J.; D'Agostino, L. A.; Way, J. D.; Wong, C. S.; Harynuk, J. J. Comparison of peak integration methods for the determination of enantiomeric fraction in environmental samples. *Chemosphere* **2009**, *75*, 1042-1048.
- (35) Haglund, P. and Wiberg, K. Determination of the gas chromatographic elution sequences of the (+)- and (-)-enantiomers of stable atropisomeric PCBs on Chirasil-Dex. *J. High Resolut. Chromatogr.* **1996**, *19*, 373-376.
- (36) Wong, C.S.; Hoekstra, P.F.; Karlsson, H.; Backus, S.M.; Mabury, S.A.; Muir, D.C.G. Enantiomer fractions of chiral organochlorine pesticides and polychlorinated biphenyls in Standard and Certified Reference Materials. *Chemosphere* **2002**, *49*, 1339-1347.
- (37) Warner, N. A.; Norstrom, R. J.; Wong, C. S.; Fisk, A. T. Enantiomeric fractions of chiral polychlorinated biphenyls provide insights on biotransformation capacity of arctic biota. *Environ. Toxicol. Chem.* **2005**, *24*, 2763-2767.
- (38) Chu, S.; Covaci, A.; Van de Vijver, K.; De Coen, W.; Blust, R.; Schepens, P. Enantiomeric signatures of chiral polychlorinated biphenyl atropisomers in livers of harbour porpoises (*Phocoena phocoena*) from the southern North Sea. *J. Environ. Monitor.* **2003**, *5*, 521-526.
- (39) Borlakoglu, J. T. and Wilkins, J. P. Correlations between the molecular structures of polyhalogenated biphenyls and their metabolism by hepatic

- microsomal monooxygenases. *Comp. Biochem. Physiol.* **1993**, *105C*, 113-117.
- (40) Kania-Korwel, I.; Garrison, A. W.; Avants, J. K.; Hornbuckle, K. C.; Robertson, L. W.; Sulkowski, W. W.; Lehmler, H.-J. Distribution of chiral PCBs in selected tissues in the laboratory Rat. *Environ. Sci. Technol.* **2006**, *40*, 3704-3710.
- (41) Norström, K.; Eriksson, J.; Haglund, J.; Silvani, V.; Bergman, Å. Enantioselective formation of methyl sulfone metabolites of 2,2',3,3',4,6'-hexachlorobiphenyl in rat. *Environ. Sci. Technol.* **2006**, *40*, 7649-7655.
- (42) Kania-Korwel, I.; Hornbuckle, K. C.; Robertson, L. W.; Lehmler, H.-J. Dose-dependent enantiomeric enrichment of 2,2',3,3',6,6'-hexachlorobiphenyl in female mice. *Environ. Toxicol. Chem.* **2008**, *27*, 299-305.
- (43) Lu, Z., Ma, G., Veinot, J.G.C., Wong, C.S. Disruption of biomolecule function by nanoparticles: How do gold nanoparticles affect phase I biotransformation of persistent organic pollutants? *Chemosphere* **2013**, *93*, 123-132.
- (44) Sundström, G. and Jansson, B. The metabolism of 2,2',3,5',6-pentachlorobiphenyl in rats, mice and quails. *Chemosphere* **1975**, *4*, 361-370.
- (45) Haraguchi, K.; Kato, Y.; Koga, N.; Degawa, M. Species differences in the tissue distribution of catechol and methylsulphonyl metabolites of 2,4,5,2',5'-penta- and 2,3,4,2',3',6'-hexachlorobiphenyls in rats, mice, hamsters and guinea pigs. *Xenobiotica* **2005**, *35*, 85-96.
- (46) Kania-Korwel, I.; Shaikh, N. S.; Hornbuckle, K. C.; Robertson, L. W.; Lehmler, H.-J. Enantioselective disposition of PCB 136 (2,2',3,3',6,6'-hexachlorobiphenyl)

in C57BL/6 mice after oral and intraperitoneal administration. *Chirality* **2007**, *66*, 56-66.

- (47) Schnellmann, R.; Putnam, C.; Sipes, I. Metabolism of 2, 2',3,3',6,6'-hexachlorobiphenyl and 2,2',4,4',5,5'-hexachlorobiphenyl by human hepatic microsomes. *Biochem. Pharmacol.* **1983**, *32*, 3233-3239.

Chapter 5

Temporal and Spatial Trends of Polychlorinated Biphenyl Chiral Signatures in the Greenland Shark (*Somniosus microcephalus*) and Its Arctic Food Web

This study was a collaboration with Dr. Aaron T. Fisk of the University of Windsor and Dr. Gregg T. Tomy, formerly of the Department of Fisheries and Oceans, Freshwater Institute and now of the Department of Chemistry at the University of Manitoba. Fisk and Tomy were responsible for sample collection and achiral analyses, with chiral analyses, data interpretation and manuscript writing by the author of this dissertation. This manuscript has been submitted on September 27th, 2013 to *Environmental Pollution* for peer review.

5.1. Introduction

Chiral molecules exist as non-superimposable mirror image forms with the same physical-chemical properties, except for optical rotation. Chirality is valuable for understanding the environmental effects and fates of persistent organic pollutants (POPs) because different enantiomers of a chiral compound usually have different biological impacts (1). For example, chiral polychlorinated biphenyls (PCBs) can stereoselectively disrupt Ca^{2+} ion signaling via sensitization of ryanodine receptors, thereby causing stereoselective neurotoxicity (2). Therefore, enantiomer-specific contaminant analysis is necessary to assess exposure and toxicity of compounds to organisms accurately (3). Chirality can also be exploited as a marker to trace biological weathering processes (3), because changes in the enantiomer distributions of chiral chemicals in the environment are generally due only to biological processes (e.g., interactions with biological molecules, microbial degradation, metabolism).

Although PCB production has been widely banned since the mid-1970s, PCBs are still ubiquitous in the environment. As with other legacy POPs, PCBs typically degrade very slowly. However, atropisomer analysis of the 19 environmentally stable chiral PCB congeners has demonstrated that atropisomer-, congener- and species-specific biochemical weathering processes occur for various PCBs in some aquatic food webs (4-7). The different environmental fates of chiral PCB atropisomers might be due to stereoselective biotransformation of chiral PCBs *in vivo* or uptake of non-racemic residues from prey or sediments.

Although marked declines in concentrations of legacy POPs, including PCBs, have been observed in arctic biota after these pollutants were banned by the Stockholm

Convention (8-10), it is unclear how the enantiomer signatures of POPs change through time and space in food webs, particularly in the Arctic. A constant chiral signature of POPs in organisms can result from an equilibrium between uptake and elimination processes (11). Therefore, changes in the enantiomer compositions of chiral POPs are good indicators for disruption of such equilibrium in organisms; and also perhaps indicators of disturbances in relevant ecosystem processes (11). Given the limited biotransformation capacity of some arctic species such as Greenland sharks (*Somniosus microcephalus*) towards POPs (12,13), any shifts in the chiral signatures of POP residues might indicate a change in POP uptake from prey (i.e., changes in dietary composition from prey with racemic signatures to those with non-racemic signatures). McKinney et al. (14) recently found that increasing numbers of transient/subarctic animals, potentially related to recent climate change, might alter the food web dynamics of organochlorine contaminants in Cumberland Sound, Nunavut, Canada by affecting consumption patterns and thus POP uptake. However, the influence of climate-change related distributional shifts of organisms on the bioaccumulation of POPs at the stereoisomer level is still unknown. If any temporal changes in the chiral PCB signatures of arctic biota have occurred, we hypothesize that they are due to changes in feeding strategies (i.e., diet choices).

Top trophic-feeding Greenland sharks collected from Cumberland Sound and Svalbard (Norway) were used to address these issues. The Greenland shark is a suitable organism for tracing spatial and temporal trends of POPs in arctic biota, because Greenland sharks are widely distributed in the Arctic, potentially have a long life span (>50 years) and are top predators (12,13,15). Concentrations and atropisomer

compositions of chiral PCBs were also determined in potential prey species of Greenland sharks within the Cumberland Sound food web to assess whether trophic transfer influences the EFs of PCBs in these sharks. Temporal trends in the stereoisomer composition of chlordanes and PCBs in air (16,17), PCBs in soil (17), hexachlorocyclohexanes in water (18) and hexabromocyclododecanes in biological samples (19,20) have been previously investigated. These studies provided important information about the source, behavior and fate of POPs in the environment. However, to our knowledge, the present study is the first study that compares temporal patterns (i.e., a decade apart) in EFs of chiral PCBs in an arctic species.

5.2. Materials and Methods

5.2.1. Sample Information

Biota samples were collected from Cumberland Sound (Figure 5.1) in 2007-2008, from different trophic levels of the area's food web: mixed zooplankton ($n=6$), scallop (*Chlamys islandica* $n=7$), herring (*Clupea harengus*, $n=1$), capelin (*Mallotus villosus*, $n=5$), Greenland halibut (*Reinhardtius hippoglossoides*, $n=8$), Arctic skate (*Amblyraja hyperborea*, $n=5$), sculpin (*Myoxocephalus scorpius*, $n=9$), Arctic char (*Salvelinus alpinus*, $n=5$), Greenland shark ($n=11$), ringed seal (*Pusa hispida*, $n=5$), harp seal (*Pagophilus groenlandicus*, $n=4$), narwhal (*Monodon monoceros*, $n=7$) and beluga whale (*Delphinapterus leucas*, $n=4$) (14). Greenland shark samples were also collected from Cumberland Sound from 1999 to 2000 and Svalbard (Figure 5.1) from 2008 to 2009 (12,15). Zooplankton, scallop, Greenland halibut, Arctic skate, sculpin, Arctic char, ringed seal and beluga whale were classified as resident species, while herring, capelin,



Figure 5.1 Location of sampling sites in Cumberland Sound, Nunavut, Canada and Svalbard, Norway.

harp seal, Greenland shark and narwhal were considered to be transient species (14).

Extraction, cleanup and achiral analyses methods have been published previously (12,14,21,22). Briefly, for the organisms collected in Cumberland from 2007-2008, samples were spiked with PCBs 30 and 204 as recovery standards and extracted by different methods. Marine mammal samples were extracted by vortexing and centrifugation with 5 mL of a dichloromethane/hexane/acetone mixture (45:45:10 by volume). Other samples were mixed with dry ice, hydromatrix (Agilent Technologies, Palo Alto, CA, USA) and Ottawa sand (Fisher Scientific, Ottawa, ON, Canada) and then extracted using a pressurized solvent extractor (Dionex, Sunnyvale, CA, USA) with dichloromethane/hexane (50:50) as solvent. Bulk lipids in extracts were removed by

automated gel permeation chromatography (GPC; OI Analytical, College Station, TX, USA). Then, about 100 mg of marine mammal lipid extracts or whole extracts for other samples were cleaned by Florisil column chromatography (8 g, 1.2% deactivated; Floridin, Berkeley Springs, West Virginia, USA) and analyzed on a Varian 3800 GC (Agilent Technologies) with an electron capture detector (ECD).

For the Greenland shark liver analysis, about 5 g of sample was mixed with Na_2SO_4 until a free-flowing mixture was obtained. Six $^{13}\text{C}_{12}$ -labeled PCB congeners were added in the samples as recovery standards. The mixtures were then packed in a glass column and extracted with 250 mL of dichloromethane/hexane (1:1) eluent. Lipids were then removed by GPC. The samples were then reduced to 1 mL and applied to a Florisil column (8 g 1.2% deactivated; Floridin, Berkeley Springs, West Virginia, USA). PCBs were eluted using 110 mL of dichloromethane/hexane (1:1). The Florisil column eluates were reduced to 500 μL after addition of 1 mL of isooctane to the eluates. Prior to analysis, $^{13}\text{C}_{12}$ -PCB 138 was added to all samples and standards as a volume corrector. PCBs were analyzed using a 5890 Series II GC (Agilent, Wilmington, Delaware, USA) equipped with a Hewlett Packard 5987B mass spectrometer under electron impact ionization. A 30 m \times 0.25 mm inner diameter DB5 column (J&W Scientific, Folsom, California, USA) was used for separation. 2 μL of sample was injected in splitless mode. All compounds were analyzed in single-ion-monitoring mode. PCBs were quantitated using an external standard containing equal amounts of Aroclors 1242, 1254, and 1260 (Accustandard, Brockville, Ontario, Canada). The level of detection varied with the compound and the amount of tissue extracted, but was about 0.1 pg/g. Concentrations were recovery-corrected, with recovery percentages of ^{13}C -PCB internal standards of 75

±1.4%.

Plasma samples of Greenland sharks (about 1 g) were weighed and homogenized with 15 g of activated Na₂SO₄, and wet packed into a 20 mL glass syringe containing 15 mL of dichloromethane (DCM): hexane (1:1). PCB-30 (AccuStandard, New Haven, CT, USA) was used as a recovery standard. Another 10 mL of DCM:hexane was used to rinse the mortar and pestle and added to the syringe. The manifold valves were closed and the sample was extracted in the solvent for 1 h, after which the valve was opened and the column was eluted by gravity. An additional 15 mL of DCM: hexane was added to the column while the solvent was being eluted. Vacuum suction was used to draw any remaining solvent from the syringes and bedding into the reservoirs. The extracts were concentrated using a rotary-evaporator to approximately 2 mL and then cleaned up by Florisil chromatography as described above. Subsequently, extracts were concentrated to 1 mL using a rotary evaporator and placed in gas chromatography vials. The samples were measured by GC-ECD.

Total PCB concentrations and trophic position data were taken from previous publications (12,14,21,22). PCBs were analyzed in the blubber of marine mammals and muscle of fishes, in the liver or plasma of Greenland shark samples, and in whole organism homogenates of other species. All data were normalized to lipid weight concentrations for comparison with lipid-normalized concentrations in the literature, unless otherwise indicated.

5.2.2. Atropisomer Analyses

Chiral PCBs were quantified using an Agilent 5890 gas chromatograph/5989 mass

spectrometer (GC/MS) under electron impact ionization (70 eV) as described in Wong et al. (23). A Chirasil-Dex column (25 m length \times 0.25 mm internal diameter \times 0.25 μ m film thickness, Varian, Palo Alto, CA) was used for atropisomer analysis. The Standard Reference Material SRM 1945 (organics in whale blubber) was used for quality control (23).

5.2.3. Data Analyses

EFs were used to describe atropisomer distributions, and are defined as the concentration ratio of the first-eluting atropisomer (E1) and the total concentration of both atropisomers (E1+E2) (PCBs 91 and 95) or as the concentration ratio of the (+)-atropisomer and total concentration for PCBs for which optical rotation is known (PCBs 136, 149, 174 and 176) (23-25) (Equation 1.1).

PCB concentrations were determined using PeakFit v4.12 (Systat Software, San Jose, CA) to deconvolute chromatograms (26). Prism 5 (GraphPad Software, La Jolla, CA) was used for statistical analyses (one way ANOVA with *post-hoc* Tukey's multiple comparison test), with statistical significance set at $\alpha=0.05$. Data are reported as mean \pm standard error unless otherwise indicated. Racemic standards had EF values that ranged from 0.496 ± 0.002 to 0.503 ± 0.004 . EFs were considered as statistically non-racemic if values deviated from racemic value beyond 0.032 (95% confidence interval) (5).

5.3. Results and Discussion

5.3.1. Spatial and Temporal Trends of PCBs

5.3.1.1. Cumberland Sound food web

PCB concentrations in organisms of the Cumberland Sound food web are illustrated in Figure 5.2, and generally fall into expected levels compared with other temperate and arctic ecosystems (Table 5.1). Penta- and hexa-chlorinated PCBs were the predominate congeners in all species. Σ PCBs in Cumberland Sound zooplankton (~5 ng/g wet wt.) were lower than values observed for zooplankton in temperate freshwater lakes (Lake Superior, ~370 ng/g wet wt., collected in 1998) (5), but higher than in zooplankton from the Bering-Beaufort-Chukchi Seas (collected in 1997-1998; (27)). Scallops contained lower concentrations of Σ PCBs than similar species collected from Spain (collected in 2010; (28)). Pelagic fishes in Cumberland Sound also had lower PCB contamination compared with that in the Western Baltic Sea and the Barents Sea (collected between 1994-2006; (29,30)). These comparisons must be interpreted with caution because these samples, and the PCB concentrations therein, were collected at different time points, and the number of congeners making up the sum of PCBs may also differ.

PCBs levels in Cumberland Sound sculpins were lower than in specimens from east Greenland, south Greenland and Saglek Bay (Canada) (collected between 1994-2000; (31-33)). Sixteen PCB congeners in skates (*Raja* spp.) from the Mediterranean Sea were 897 ng/g (collected in 2000; (34)), higher than concentrations in Arctic skate from Cumberland Sound (750 ng/g). Σ PCB concentrations in Greenland halibut increased from 58 ± 12 ng/g in 1999 (12) to 221 ± 15 ng/g in 2008 in Cumberland Sound for reasons that are unclear. Greenland halibut in both sampling periods were approximately the same size (report as mean \pm standard deviation): 59 ± 9 cm in 1999 and 64 ± 14 cm in 2008. The piscivorous Arctic char had lower PCB levels than the same species found in east

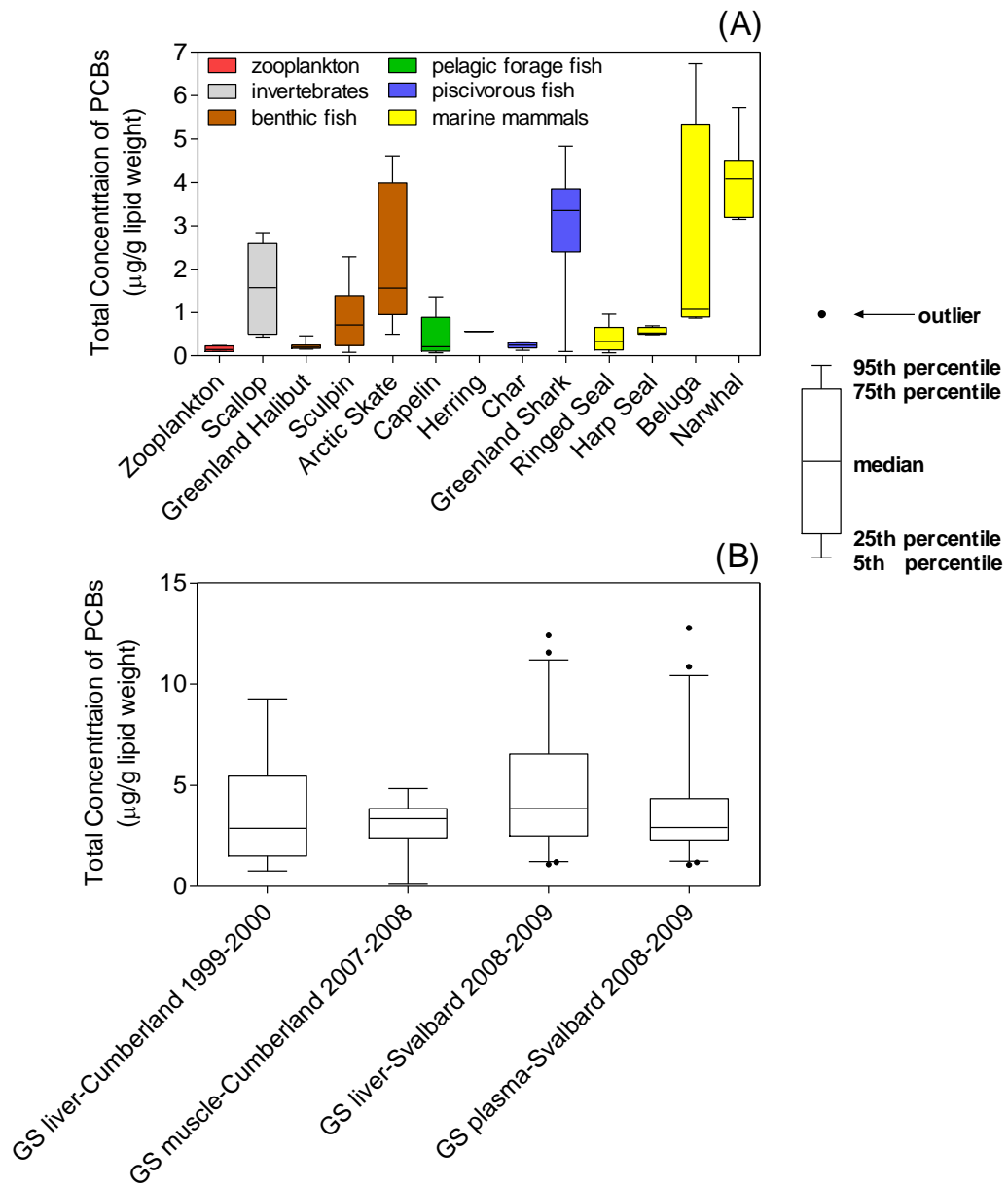


Figure 5.2 Total concentrations of PCBs in (A) organisms collected from the Cumberland Sound food web 2007-2008, and (B) Greenland sharks (GS) collected from Cumberland Sound and Svalbard at different time points.

Greenland in 2001 (35). These results indicated that high trophic level organisms in Cumberland Sound (e.g., Greenland sharks) were exposed to relatively lower concentrations of PCBs via their diets compared with conspecifics from other arctic areas. However, variation in PCB concentrations of some prey species (e.g., Greenland halibut) between 1999 and 2008 may influence contaminant levels in these predators (e.g., Greenland shark—see below).

PCB levels in Cumberland Sound marine mammals were generally lower than in specimens from other locales, and were lower than in samples collected from similar location at earlier time points. Average Σ PCBs in Cumberland Sound ringed seals in the present study were much lower than in conspecifics collected in 2001 in Outer Dvina Bay and Onega Bay deep in the White Sea of Russia (36); however, it must be noted that this Russian location is likely to be heavily polluted. Concentrations in Cumberland Sound ringed seals were also lower than in conspecifics from Hudson Strait (Canadian Arctic, collected between 1999-2003) (37) and East Greenland conspecifics (collected in 2004; (38)), but similar to ringed seals more proximately located in West Greenland (collected in 2006; (39)). In Cumberland Sound, Σ PCBs in ringed seals collected in 1993 (12) were about 1.8 times higher than in samples collected in 2007-2008. A similar temporal trend was observed previously of ringed seals from Svalbard (40). Subadult ringed seals sampled in 2004 in Svalbard had about three-fold lower concentrations of Σ PCBs compared to subadults collected in 1996 (40). Σ PCB concentrations in harp seals from the White Sea were about 2 times higher than those in harp seals in the present study (collected between 1998-2001; (36)). The Σ PCB concentrations in Cumberland Sound beluga were similar to those in Alaskan beluga (collected between 1989-2006; (41)) and

in female beluga from Hudson Strait (collected between 1998-2003; (37)), but were lower than those measured from Svalbard (collected between 1995-1997; (42)) or male beluga from Hudson Strait (collected between 1998-2003; (37)). Σ PCBs in Cumberland Sound narwhal was lower than that in narwhal from Svalbard in 2001 (43), but similar to levels measured in conspecifics in West Greenland (collected in 1993; (44)).

5.3.1.2. Greenland sharks

Σ PCBs in Greenland sharks from Cumberland Sound did not change between 1999 (3400 \pm 700 ng/g in liver) (12) and 2008 (3100 \pm 400 ng/g in muscle) (Figure 5.2B). The levels of Σ PCBs in the Svalbard Greenland sharks (4600 \pm 400 ng/g in liver, 3900 \pm 400 ng/g in plasma) in 2008 were higher than those of Greenland sharks from Cumberland Sound (Figure 5.2B), but not statistically significant. High organochlorine contaminant concentrations have been reported from Svalbard and East Greenland biota previously (45,46). The concentrations of 17 PCB congeners in Greenland sharks from Iceland in 2001-2003 were about 4100 (muscle)-4400 (liver) ng/g (47). This appears higher than in sharks from Cumberland Sound but similar to Svalbard.

Chiral PCB concentrations in Greenland sharks from Cumberland Sound were not different between 1999 and 2008 (Figure 5.3). However, higher levels of PCB 149 were measured in Svalbard sharks compared with Cumberland Sound sharks during similar sampling periods, indicating geographic differences in chiral PCB contamination (Figure 5.3). Data for other chiral PCBs are not available for Svalbard Greenland sharks. Thus, PCB levels in Greenland sharks from Cumberland Sound were similar in 1999 compared with 2008, and generally lower than those found in the European Arctic.

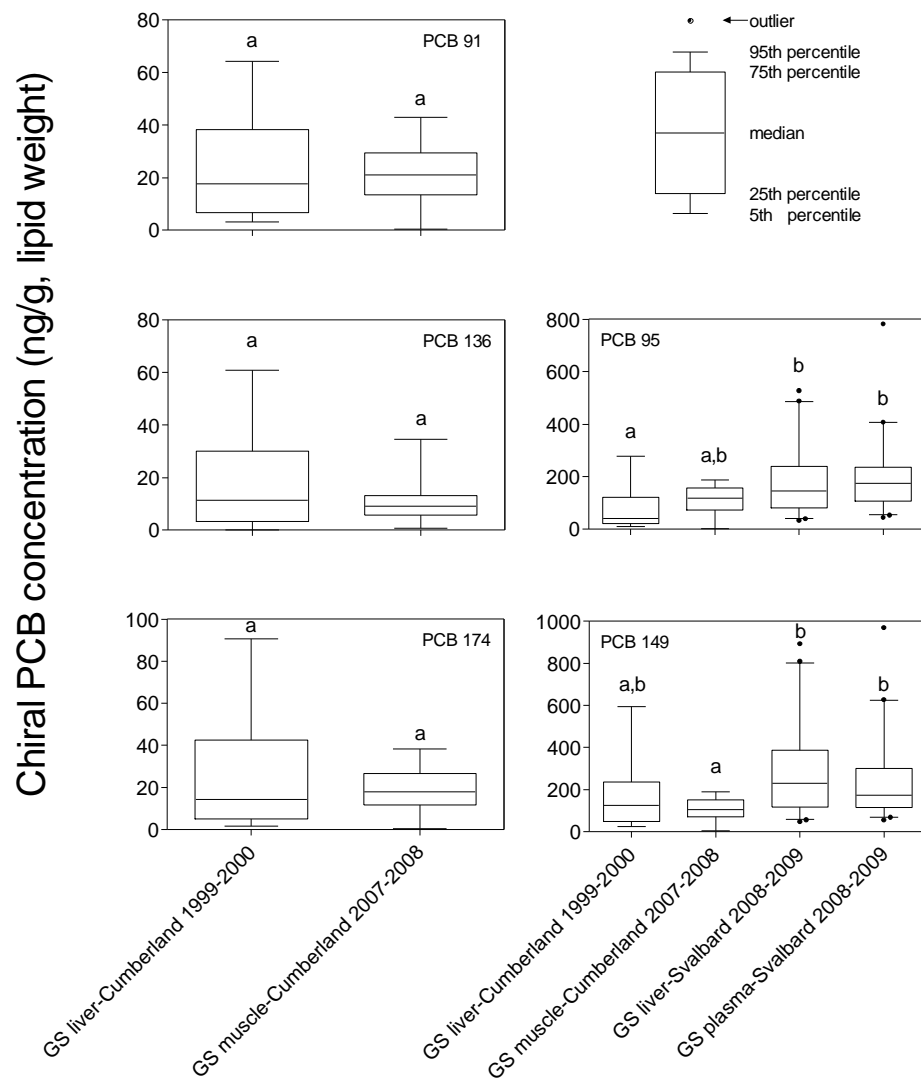


Figure 5.3 Temporal and spatial trends of chiral PCB concentrations in Greenland sharks (GS) collected from Cumberland Sound (1999-2000 and 2007-2008) and Svalbard (2008-2009). Different letters indicate statistically different concentrations, $p < 0.05$, one-way ANOVA with *post-hoc* Tukey's multiple comparison test.

5.3.2. Atropisomer Enrichment of Chiral PCBs in the Cumberland Sound Food

Web

PCBs 95 and 149 were the predominant chiral PCB congeners in Cumberland Sound organisms, while PCBs 91, 136, 174 and 176 were only detected in some high trophic level species (Figure 5.4), consistent with results from the Northwater Polynya (NOW) north of Cumberland Sound in 1998 (6). Transient species had higher chiral PCB concentrations than resident species, consistent with the higher occurrence of penta-, hexa- and hepta-chlorinated PCBs in transient species (14). In addition, species-specific EFs were observed in the Cumberland Sound food web, but no obvious differences in EF patterns were observed between the two groups (Figure 5.4). This result indicated that the atropisomer compositions of chiral PCBs in these organisms were not dependent on their initial concentrations (11), but more likely depended on biotransformation activities and prey sources (see below).

5.3.2.1. Zooplankton and benthic invertebrates

Mixed zooplankton had average racemic EF values of 0.500 ± 0.007 , 0.472 (single measurement) and 0.487 ± 0.008 for PCBs 95, 136 and 149, respectively, similar to those observed in plankton from Lake Superior in Canada (5) and the NOW (6). They are also consistent with racemic chiral signatures of other POPs in arctic zooplankton, indicating that these species likely have poor biotransformation capabilities and do not stereoselectively bioaccumulate POPs (48).

The EFs of PCBs 95 and 149 in Cumberland Sound scallops were 0.498 ± 0.015 and 0.504 ± 0.010 , respectively. Since scallops feed mainly on plankton, these racemic atropisomer compositions indicate that scallops do not stereoselectively accumulate nor

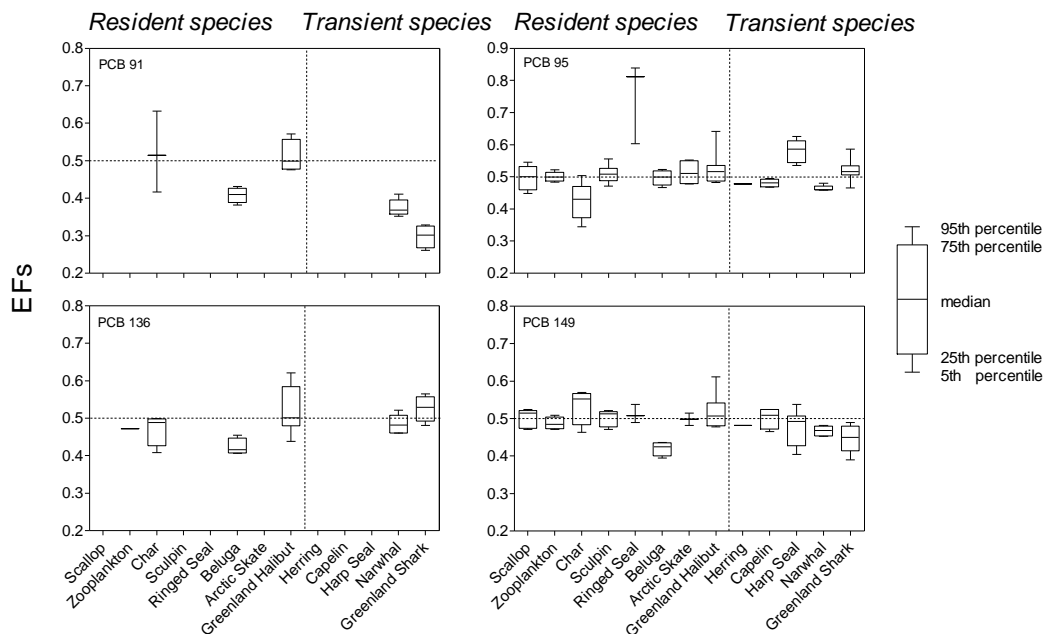


Figure 5.4 Enantiomer fractions (EFs) for PCBs 91, 95, 136 and 149 for the organisms collected from Cumberland Sound food web between 2007-2008. Dotted line represents racemic EFs of 0.5. Data not shown for PCBs 174 (Greenland shark: $n=3$; beluga: $n=2$; narwhal: $n=4$) and 176 (Arctic char: $n=1$; Greenland halibut: $n=5$; beluga: $n=1$) given limited numbers of data points (see Appendix 7 for details).

biotransform these PCBs. Similarly, near-racemic PCB 149 was observed in blue mussels (*Mytilus edulis*) in the German Bight (49), consistent with the generally poor capacities to biodegrade of PCBs shown by many invertebrate species.

5.3.2.2. Pelagic fishes

The racemic signatures for both herring and capelin (Figure 5.4) also suggest limited biotransformation abilities towards PCBs in these species and in their prey, although it is important to note that only a single measurement exists for herring. As with invertebrates, many freshwater pelagic fishes have more non-racemic PCB residues and higher

biotransformation capacities than similar marine species. For example, atropisomer enrichment of chiral PCBs in cisco (*Coregonus artedii*) was detected in Lake Superior (5); *in vivo* metabolism or uptake from prey were identified as two reasons responsible for the non-racemic signatures of PCBs in this species (5).

5.3.2.3. Benthic fishes

Short-homed sculpin, Greenland halibut and Arctic skate in Cumberland Sound did not exhibit atropisomer enrichment for most PCB congeners. The only exception was for PCB 176 in Greenland halibut ($EF=0.433 \pm 0.023$). However, significant atropisomer enrichments of PCBs 91, 95, 136 and 149 have previously been observed in freshwater sculpins (*Cottus cognatus*) compared to their food sources, indicating stereoselective biotransformation of these pollutants in that freshwater species (5). While congener-specific stereoselective biotransformation of PCB 176 or take up of non-racemic PCB 176 from scavenging on dead marine mammals that fall to the bottom (Jeremiah Young, personal observation) may explain the observed enrichment in Greenland halibut, these reasons do not fully explain the atropisomeric composition of other, more easily biodegradable congeners (e.g., PCBs 91 and 95).

5.3.2.4. Arctic char

Arctic char from Cumberland Sound showed significant PCB atropisomer enrichment, with EFs of PCBs 95 and 176 of 0.423 ± 0.026 and 0.459 (one measurement), respectively. Arctic char exposed intraperitoneally in the laboratory had racemic proportions of PCB 95, suggesting no stereoselective biotransformation capacity of this congener in this species (50). Thus, the non-racemic chiral PCBs in wild char likely come from stereoselective bioaccumulation from Cumberland Sound or freshwater prey

sources (during anadromous periods) or sediment, which were not measured in the present study. Alternatively, different exposure pathways (oral versus intraperitoneal injection) of chiral PCBs may result in different atropisomer signatures in organisms (51). Thus, comparison of chiral PCB EFs in wild char with previous laboratory exposures (50) must be considered cautiously, although similar atropisomer enrichment patterns were observed previously in lake trout (*Salvelinus namaycush*), a salmonid species which apparently does biotransform PCBs (5).

5.3.2.5. Marine mammals

Marine mammals in this study had species- and congener-specific PCB atropisomer signatures similar to those documented previously in many species (6,27,52). This is the first report of stereoselective PCB enrichment in harp seals, narwhals and beluga whales. The EFs of PCB 95 in harp seals and ringed seals were 0.581 ± 0.013 and 0.751 ± 0.076 , respectively. No significant atropisomer enrichment was observed for PCB 149 in these species. Atropisomer signatures of these two congeners in Cumberland Sound ringed seals were consistent with that measured in ringed seals (0.849 ± 0.072 for PCB 95, 0.478 ± 0.045 for PCB 149, mean \pm standard deviation) captured a decade ago in the NOW (6). The racemic atropisomer distributions of chiral PCBs in their potential prey such as herring, capelin (from the present study) and Arctic cod (6) indicated that biotransformation is likely the major reason for non-racemic chiral signatures in seals. Indeed, CYP2B-like enzymes, which biotransform chiral PCBs stereoselectively (53,54), were suggested to be involved in biotransformation processes of xenobiotics in harp and ringed seals (55,56).

The EFs of PCBs 91, 136, 149 and 174 in beluga whales were 0.409 ± 0.010 ,

0.423±0.011, 0.420±0.009 and 0.552±0.004, respectively, with no significant atropisomer enrichment observed for PCBs 95 (0.497±0.012) and 176 (0.486). In narwhals, significant non-racemic atropisomer distributions were detected for PCBs 91 (0.375±0.010), 95 (0.464±0.004) and 149 (0.467±0.006). Bowhead whales (*Balaena mysticetus*) in the Bering-Chukchi-Beaufort Sea showed similar EF patterns for PCBs 91 (0.456±0.021) in blubber compared with beluga whales and narwhals in the present study (27). However, no significant atropisomer enrichments were observed for PCBs 95, 136, 149 and 174 in those bowhead whales (27). This is consistent with the fact that bowhead whales are baleen whales that filter-feed on plankton, which usually contain racemic chiral PCBs. Therefore diet, combined with poor biotransformation activity, probably explain the EFs of bowhead whales (27). In contrast, belugas and narwhals are toothed whales and mainly feed on fish. Thus, different diet compositions and biotransformation abilities among these whales may explain the different EFs of chiral PCBs in their tissues.

The enrichment of (-)-PCB 149 in belugas and narwhals from Cumberland Sound was in agreement with values measured for dolphins and larger whales collected in the Mediterranean Sea (57). Although the expression of CYP2B-like activity is low in belugas (58), *in vitro* metabolism of certain PCBs (59) and formation of hydroxylated-PCB (OH-PCB) and methylsulfonyl-PCB (MeSO₂-PCB) metabolites have been observed in beluga liver subcellular fractions (60), indicating that stereoselective biotransformation could be the source of non-racemic chiral PCBs EFs observed in this species.

5.3.3. Temporal and Spatial Trends of PCB Chiral Signatures in Greenland Sharks

Non-racemic chiral signatures of PCBs were found in Greenland sharks, depending on sampling time, tissues and locations (Figure 5.5). A significant decrease was observed for PCB 91 in the Cumberland Sound Greenland sharks between 1999 and 2008, with EFs changing from 0.447 ± 0.024 to 0.298 ± 0.015 ($p=0.007$) (Figure 5.5A). In contrast, the EFs of PCB 91 were similar in the sharks sampled from Cumberland Sound and Svalbard in 2008 (Figure 5.5A). For PCB 95, no significant changes of EFs in Cumberland Sound Greenland sharks were observed between the two time periods (Figure 5.5B). However, a different enrichment pattern of PCB 95 was detected in the liver of Greenland sharks from Svalbard compared to the samples from Cumberland Sound (Figure 5.5B). There was no significant temporal or spatial shift in EFs of PCBs 136 and 149 in Greenland sharks (Figure 5.5C and 5.5D), suggesting as with Cumberland Sound ringed seals that the chiral signatures of some PCB congeners did not change significantly in Greenland sharks between 1998 and 2008 (11).

A review of contaminants in Greenland sharks suggested that they have very limited biotransformation capacities for organochlorine contaminants (13). Thus, chiral signatures of contaminants in Greenland sharks are likely driven by values in their prey. Greenland sharks are an apex predator in both pelagic and benthic food webs where they exist, as they opportunistically consume invertebrates, fish and marine mammals (13). Since invertebrates (Figure 5.4) and forage fishes (e.g., herring, capelin and Arctic cod) (6) in the Arctic usually contain racemic atropisomers, marine mammals are likely the major source of non-racemic chiral PCBs for Greenland sharks. Indeed, ringed seals and

whales (e.g., minke whale, *Balaenoptera acutorostrata*, beluga and narwhal) have been found in the stomachs and gastrointestinal tracks of Greenland sharks, indicating the

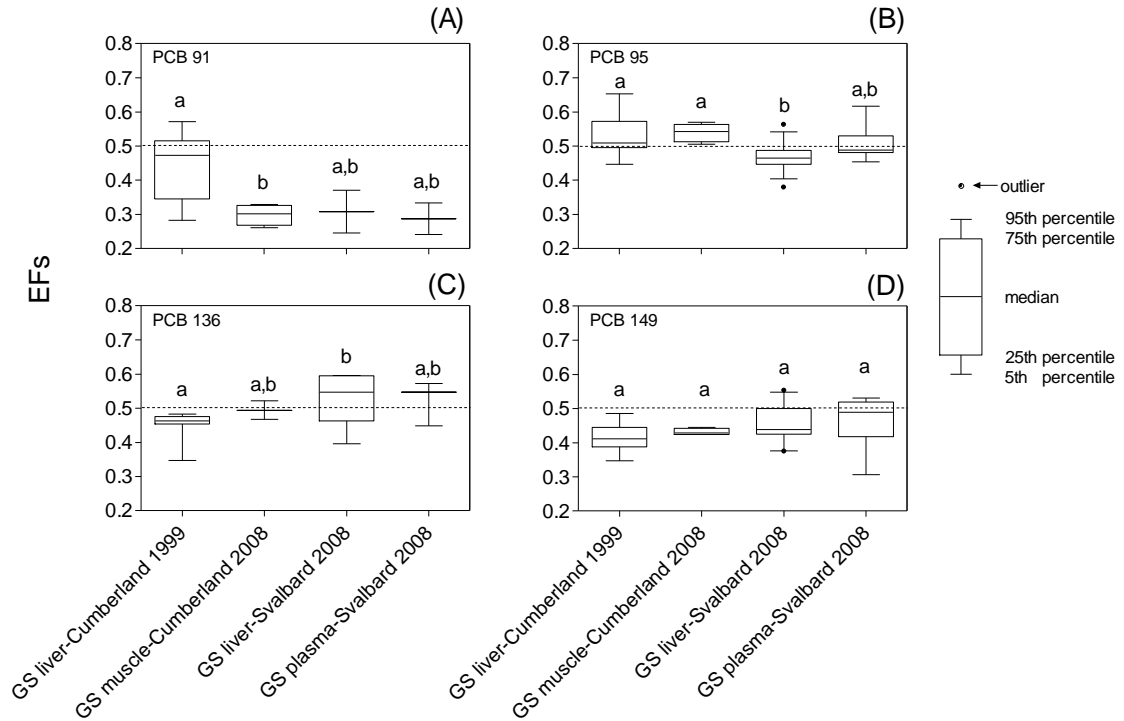


Figure 5.5 Temporal and spatial trends in the enantiomer fractions (EFs) of PCBs 91, 95, 136 and 149 in Greenland sharks (GS) collected from Cumberland Sound and Svalbard. Different letters indicate statistically different concentrations ($p < 0.05$) assessed by one-way ANOVA followed by *post-hoc* Tukey's multiple comparison test. Dotted lines represent racemic EFs of 0.5.

consumption of these mammals either by scavenging or active feeding (13,15,61). The chiral signatures of PCB 91 in Greenland shark were consistent with the patterns in ringed seal (6), beluga and narwhal (Figure 5.4), indicating the possible influence of atropisomer signatures of these prey on the shark signatures.

One possible explanation for chiral signature shifting in Greenland sharks might be related to changes in their feeding ecology towards consumption of more marine mammals, which could be related to climate change. The increased consumption of marine mammals could affect the sharks' overall contamination levels (14,22) and perhaps chiral signatures of some pollutants in Greenland sharks. Climate change-related temperature increases, sea ice declines and other concomitant habitat changes are having important impacts on arctic marine mammals (62). For example, decreases in sea ice reduce available habitat for lair construction by ringed seals, and therefore less protection against predators (62,63). Ice-associated whales, such as belugas and narwhals also use sea ice to avoid predators (e.g., killer whales *Orca orcinus* etc.) (62), though fish predators such as Greenland sharks are not likely to be detoured by ice cover. Bite wounds attributed to Greenland sharks have been observed recently, suggesting that sharks actively prey on live whales (13). Greenland shark feeding on dead narwhals has also been observed in the Canadian Arctic (13). Consumption of marine mammals by Greenland sharks is also supported by the observation that the percentage of marine mammal tissues in Cumberland Sound Greenland sharks' stomachs increased from 14% to 33% during 1999 to 2008 (12,64). The temporal shift of PCB 91 chiral signatures in Cumberland Sound Greenland sharks was consistent with this increased consumption of marine mammals.

The different atropisomer distribution of PCB 95 in Greenland sharks between Cumberland Sound and Svalbard may be due to different feeding regimes in these two areas (12,15,22,61,64). The chiral signature of PCB 95 in Cumberland Sound Greenland sharks was consistent with the signature in harp seals and ringed seals (Figure 5.4). The

atropisomer compositions of chiral PCBs in the marine mammals from Svalbard were not explored due to lack of samples. However, dietary composition differences of Greenland sharks from Cumberland Sound and Svalbard were observed previously. Greenland sharks from both Svalbard (42.3%, sampled in 2008, (15)) and Cumberland Sound (14%, sampled in 1999, (12); 33%, sampled in 2008, (64)) can have a high percentage of marine mammal tissues in their stomachs, although fatty acid data suggested a higher consumption of gadoids and seals by Greenland shark from Svalbard (sampled in June 2008, 2009) than sharks from Cumberland Sound (sampled in April 2008, (65)). It is not clear whether this difference is due only to spatial variation or different sampling times or both factors. Based on the high diversity of known prey items (12,15) and the opportunistic nature of Greenland shark feeding behavior (13), the precise makeup of this species' diet (e.g. extent of marine mammal consumption) is likely variable in space and time. The observation that PCB 95 was consistent through time (in Cumberland Sound) but different between habitats, while PCB 91 exhibited the opposite trend, further suggests that the diet composition of Greenland sharks, and its overlap with conspecifics, can vary with time and space. ^{13}C and ^{15}N data cannot easily be used to support this, because the stable isotope data were calculated based on different baselines in different locations and from different tissues.

Another factor that undoubtedly affects the feeding ecology of Greenland sharks is human activities. Greenland sharks scavenge floating minke whale blubber left as a by-product of whaling activities near Svalbard (61). According to the International Whaling Commission, the number of minke whales harvested for commercial purposes increased from 218 in 1995 to 639 in 2005 and now is now stable around 500-600 per

year (66). Marine mammal harvests also occur in Cumberland Sound, although on a subsistence scale, not a commercial scale. However, these hunts could also provide Greenland sharks with scavenging opportunities. Differences in opportunities to scavenge marine mammals could contribute to altered contaminant levels and chiral signatures in Greenland sharks among Arctic areas. Our results suggest that the enantiomer signatures of chiral contaminants might be a useful tool to trace the response of organisms to climate changes, such as changes in feeding ecology. More investigations are needed to fully test these hypotheses.

It is possible that EFs have changed in the food sources of Greenland sharks, resulting in the spatial and temporal EF patterns observed in the sharks. However, our current data do not support this explanation. For example, as a food source of Greenland sharks, ringed seals showed constant EFs in NOW and Cumberland Sound from 1999-2008 (see discussion above). However, we cannot distinguish among these potential reasons with the existing data.

Table 5.1 Comparison of PCB levels in different marine food webs.

Species	Location and time	Tissue	Concentration ^a	Reference
zooplankton	Cumberland Sound, 2007-2008	Whole	153±26 l.w.	Present study
	Bering-Beaufort-Chukchi Seas, 1997-1998	Whole	48±15 l.w.	(27)
Invertebrate				
scallop	Cumberland Sound, 2007-2008	Whole	1571±451 l.w. or 0.3-10 w.w.	Present study
	Galician Littoral, Spain, 2010	Whole	1.6-41 w.w.	(28)
Pelagic fishes				
herring	Cumberland Sound, 2007-2008	Muscle	561 l.w., 109 l.w. ^b	Present study
	Western Baltic Sea, 2006	Muscle	189-869 l.w. ^b	(29)
capelin	Cumberland Sound, 2007-2008	Muscle	438±236 l.w. or 1.5 w.w. ^b	Present study
	Barents Sea, 1994-2001	Muscle	3.1 w.w. ^b	(30)
Benthic fishes				
sculpin	Cumberland Sound, 2007-2008	Muscle	867±248 l.w. or 0.4-2.9 w.w.	Present study
	Eastern Greenland, 1994-1995	Liver	7.1-23 w.w. ^c	(31)
	Western Greenland, 1994-1995	Liver	54 w.w. ^c	(31)
	South Greenland, 2000	Liver	217-1717 l.w. ^d	(15)
	Saglek Bay, Labrador, Canada, 1997-1999	Whole (except liver)	4.8-13,070 w.w.	(33)
Arctic skate	Cumberland Sound, 2007-2008	Muscle	2285±744 l.w. or 750 ^e	Present study
	Mediterranean Sea, 2000 (similar species)	Liver	889 l.w. ^e	(34)
Greenland halibut	Cumberland Sound, 2007-2008	Muscle	221±15 l.w.	Present study
	Cumberland Sound, 1999-2000	Muscle	58±12 l.w.	(12)

Piscivorous fishes				
char	Cumberland Sound, 2007-2008	Muscle	238±33 l.w. or 122-322 l.w.	Present study
	Eastern Greenland, 2001	Muscle	700 l.w. or 76-4810 l.w.	(35)
Greenland shark	Cumberland Sound, 2007-2008	Muscle	3100±400 l.w.	Present study
	Cumberland Sound, 1999-2000	Liver	3400±700 l.w.	(12)
	Svalbard, 2008	Liver	4600±400 l.w.	(22) and present study
	Svalbard, 2008	Plasma	3900±400 l.w.	(22) and present study
	Iceland, 2001-2003	Muscle	4100 l.w.	(47)
	Iceland, 2001-2003	Liver	4400 l.w.	(47)
Marine mammals				
ringed seals	Cumberland Sound, 2007-2008	Blubber	382±152 l.w. or 234 l.w. ^c	Present work
	Cumberland Sound, 1993	Blubber	704 l.w.	(12)
	Outer Dvina Bay, White Sea, 1998	Blubber	1740±1060 l.w. ^f	(36)
	Onega Bay, White Sea, 2001	Blubber	999±304 l.w. in females ; 955±385 l.w. in males ^f	(36)
	Hudson Strait, Canadian Arctic, 1999-2003	Blubber	602 l.w.	(37)
	Eastern Greenland, 2004	Blubber	605±240 l.w. ^c	(38)
	Western Greenland, 2006	Blubber	200 l.w. ^c	(39)
harp seals	Cumberland Sound, 2007-2008	Blubber	555±93 l.w.	Present work
	White Sea, 1998-2001	Blubber	1070±504 l.w.	(36)
beluga	Cumberland Sound, 2007-2008	Blubber	2436±1433 l.w.	Present study
	Alaska, 1989-2006	Blubber	2276 l.w.	(41)
	Hudson Strait, Canadian Arctic, 1999-2003	Blubber	661 l.w. in females; 3690 l.w. in males;	(37)

	Svalbard, 1995-1997	Blubber	5103 ± 1874 l.w.	(42)
narwhal	Cumberland Sound, 2007-2008	Blubber	4082 ± 335 l.w. or 1406 l.w. ^c	Present work
	Svalbard, 2001	Blubber	9904 lw	(43)
	Western Greenland, 1993	Blubber	1222 l.w., in Avanersuaq; 1988 l.w., in Uummannaq ^c	(44)

^a Mean ± S.E. or concentration range (ng/g) of PCBs

1,3,4/10,7,6,8/5,19,18,17,24/27,16/32,26,25,31,28,33,22,

45,46,52,49,47,48,44,42,41/71,64,40,74,70/76,66,95,56/60,91,84/89,101,99,83,97,87,85,136,110,82,1

51,144/135,149,118,134,114,131,146,153,132,105,141,179,137,130/176,138,158,178/129,175,187,18

3,128,185,174,177,171/156,201/157,172/197,180,193,191,200,170,190,198,199,196/203,189,208,195,

207,194,205,206 and 209 for the present study. l.w.-lipid weight; w.w.-wet weight;

^b6 congeners: PCBs 28, 52, 101, 138, 153, 180;

^c10 congeners: PCBs 28, 31,52, 101, 105, 118, 138, 153, 156 and 180;

^d13 congeners: PCBs 28, 31,52, 101, 105, 118, 128, 138, 149, 153, 156, 170 and 180;

^e16 congeners: PCBs 20, 28, 35, 52,60,77,101,105,118,126,138,153,156,169,180 and 209;

^fMean ± S.D.; ng/g.

References

- (1) Wong, C.S. and Warner, N.A. Chirality as an environmental forensics tool, in Harrad, S. (Ed), Persistent Organic Pollutants. John Wiley & Sons, Ltd, Chichester, UK, **2009**, pp 71-136.
- (2) Pessah, I.N.; Lehmler, H.-J.; Robertson, L.W.; Perez, C.F.; Cabrales, E.; Bose, D.D.; Feng, W. Enantiomeric specificity of (-)-2,2',3,3',6,6'-hexachlorobiphenyl toward ryanodine receptor types 1 and 2. *Chem. Res. Toxicol.* **2009**, *22*, 201–207.
- (3) Lehmler, H.-J.; Harrad, S.J.; Hühnerfuss, H.; Kania-Korwel, I.; Lee, C.M.; Lu, Z.; Wong, C.S. Chiral polychlorinated biphenyl transport, metabolism, and distribution: a review. *Environ. Sci. Technol.* **2010**, *44*, 2757–2766.
- (4) Wong, C.S.; Garrison, A.W.; Smith, P.D.; Foreman, W.T. Enantiomeric composition of chiral polychlorinated biphenyl atropisomers in aquatic and riparian biota. *Environ. Sci. Technol.* **2001**, *35*, 2448–2454.
- (5) Wong, C.S.; Mabury, S.A.; Whittle, D.M.; Backus, S.M.; Teixeira, C.; DeVault, D.S.; Bronte, C.R.; Muir, D.C.G. Organochlorine compounds in Lake Superior: chiral polychlorinated biphenyls and biotransformation in the aquatic food web. *Environ. Sci. Technol.* **2004**, *38*, 84–92.
- (6) Warner, N.A.; Norstrom, R.J.; Wong, C.S.; Fisk, A.T. Enantiomeric fractions of chiral polychlorinated biphenyls provide insights on biotransformation capacity of arctic biota. *Environ. Toxicol. Chem.* **2005**, *24*, 2763–2767.
- (7) Dang, V.D.; Walters, D.M.; Lee, C.M. Transformation of chiral polychlorinated

- biphenyls (PCBs) in a stream food web. *Environ. Sci. Technol.* **2010**, *44*, 2836–2841.
- (8) Braune, B.M. Temporal trends of organochlorines and mercury in seabird eggs from the Canadian Arctic, 1975–2003. *Environ. Pollut.* **2007**, *148*, 599–613.
- (9) Rig á, F.; Bignert, A.; Braune, B.; Stow, J.; Wilson, S. Temporal trends of legacy POPs in Arctic biota, an update. *Sci. Total Environ.* **2010**, *408*, 2874–2884.
- (10) Vorkamp, K.; Rig á, F.F.; Bossi, R.; Dietz, R. Temporal trends of hexabromocyclododecane, polybrominated diphenyl ethers and polychlorinated biphenyls in ringed seals from east Greenland. *Environ. Sci. Technol.* **2011**, *45*, 1243–1249.
- (11) Vetter, W.; Smalling, K.L.; Maruya, K.A. Interpreting nonracemic ratios of chiral organochlorines using naturally contaminated fish. *Environ. Sci. Technol.* **2001**, *35*, 4444–4448.
- (12) Fisk, A.T.; Tittlemier, S.A.; Pranschke, J.L.; Norstrom, R.J. Using anthropogenic contaminants and stable isotopes to assess the feeding ecology of Greenland sharks. *Ecology* **2002**, *83*, 2162–2172.
- (13) MacNeil, M.A.; McMeans, B.C.; Hussey, N.E.; Vecsei, P.; Svavarsson, J.; Kovacs, K.M.; Lydersen, C.; Treble, M.A.; Skomal, G.B.; Ramsey, M.; Fisk, A.T. Biology of the Greenland shark *Somniosus microcephalus*. *J. Fish Biol.* **2012**, *80*, 991–1018.
- (14) McKinney, M.A.; McMeans, B.C.; Tomy, G.T.; Rosenberg, B.; Ferguson, S.H.; Morris, A.; Muir, D.C.G.; Fisk, A.T. Trophic transfer of contaminants in a changing

- Arctic marine food web: Cumberland Sound, Nunavut, Canada. *Environ. Sci. Technol.* **2012**, *46*, 9914-9922.
- (15) Leclerc, L-M.; Lydersen, C.; Haug, T.; Bachmann, L.; Fisk, A.T.; Kovacs, K.M. A missing piece in the Arctic food web puzzle? Stomach contents of Greenland sharks sampled in Svalbard, Norway. *Polar Biol.* **2012**, *35*, 1197–1208.
- (16) Bidleman, T.F.; Jantunen, L.M.M.; Helm, P.A.; Brorström-Lundén, E.; Juntto, S. Chlordane enantiomers and temporal trends of chlordane isomers in Arctic air. *Environ. Sci. Technol.* **2002**, *36*, 539–544.
- (17) Jamshidi, A.; Hunter, S.; Hazrati, S.; Harrad, S. Concentrations and chiral signatures of polychlorinated biphenyls in outdoor and indoor air and soil in a major U.K. conurbation. *Environ. Sci. Technol.* **2007**, *41*, 2153–2158.
- (18) Padma, T.V. and Dickhut, R.M. Spatial and temporal variation in hexachlorocyclohexane isomers in a temperate estuary. *Mar. Pollut. Bull.* **2002**, *44*, 1345–1353.
- (19) Peck, A.M.; Pugh, R.S.; Moors, A.; Ellisor, M.B.; Porter, B.J.; Becker, P.R.; Kucklick, J.R. Hexabromocyclododecane in white-sided dolphins: temporal trend and stereoisomer distribution in tissues. *Environ. Sci. Technol.* **2008**, *42*, 2650–2655.
- (20) Esslinger, S.; Becker, R.; Jung, C.; Schröter-Kermani, C.; Bremser, W.; Nehls, I. Temporal trend (1988-2008) of hexabromocyclododecane enantiomers in herring gull eggs from the German coastal region. *Chemosphere* **2011**, *83*, 161–167.

- (21) Fisk, A.T.; Hobson, K.A.; Norstrom, R.J. Influence of chemical and biological factors on trophic transfer of persistent organic pollutants in the Northwater Polynya marine food web. *Environ. Sci. Technol.* **2001**, *35*, 732–738.
- (22) Molde, K.; Ciesielski, T.M.; Fisk, A.T.; Lydersen, C.; Kovacs, K.M.; Sørmo, E.G.; Jenssen, B.M. Associations between vitamins A and E and legacy POP levels in highly contaminated Greenland sharks (*Somniosus microcephalus*). *Sci. Total Environ.* **2013**, *442*, 445–454.
- (23) Wong, C.S.; Hoekstra, P.F.; Karlsson, H.; Backus, S.M.; Mabury, S.A.; Muir, D.C.G. Enantiomer fractions of chiral organochlorine pesticides and polychlorinated biphenyls in Standard and Certified Reference Materials. *Chemosphere* **2002**, *49*, 1339–1347.
- (24) Harner, T.; Wiberg, K.; Norstrom, R. Enantiomer fractions are preferred to enantiomer ratios for describing chiral signatures in environmental analysis. *Environ. Sci. Technol.* **2000**, *34*, 218–220.
- (25) Haglund, P. and Wiberg, K. Determination of the gas chromatographic elution sequences of the (+)- and (-)-enantiomers of stable atropisomeric PCBs on Chirasil-dex. *J. High Resol. Chromatogr.* **1996**, *19*, 373–376.
- (26) Asher, B.J.; D'Agostino, L.A.; Way, J.D.; Wong, C.S.; Harynuk, J.J. Comparison of peak integration methods for the determination of enantiomeric fraction in environmental samples. *Chemosphere* **2009**, *75*, 1042–1048.
- (27) Hoekstra, P.F.; Wong, C.S.; O'Hara, T.M.; Solomon, K.R.; Mabury, S.A.; Muir,

- D.C.G. Enantiomer-specific accumulation of PCB atropisomers in the Bowhead Whale (*Balaena mysticetus*). *Environ. Sci. Technol.* **2002**, *36*, 1419–1425.
- (28) Carro, N., García, I., Ignacio, M., Mouteira, A. Distribution and spatial trends of PCBs in commercial scallops from Galician Littoral (NW, Spain). Possible influence of biometric parameters. *J. Food Sci.* **2012**, *77*, T89–T97.
- (29) Karl, H.; Bladt, A.; Rottler, H.; Ludwigs, R.; Mathar, W. Temporal trends of PCDD, PCDF and PCB levels in muscle meat of herring from different fishing grounds of the Baltic Sea and actual data of different fish species from the Western Baltic Sea. *Chemosphere* **2010**, *78*, 106–112.
- (30) Julshamn, K.; Lundebye, A.K.; Heggstad, K.; Berntssen, M.H.G.; Boe, B. Norwegian monitoring programme on the inorganic and organic contaminants in fish caught in the Barents Sea, Norwegian Sea and North Sea, 1994–2001. *Food Addit. Contam.* **2004**, *21*, 365–376.
- (31) Cleemann, M.; Riget, F.; Paulsen, G.B.; Boer, J.; Klungsøyr, J.; Aastrup, P. Organochlorines in Greenland lake sediments and landlocked Arctic char (*Salvelinus alpinus*). *Sci. Total Environ.* **2000**, *245*, 173–185.
- (32) Glasius, M.; Christensen, J.H.; Platz, J.; Vorkamp, K. Halogenated organic contaminants in marine fish and mussels from southern Greenland-pilot study on relations to trophic levels and local sources. *J. Environ. Monit.* **2005**, *7*, 127–131.
- (33) Brown, T.M.; Kuzyk, Z.Z.A.; Stow, J.P.; Burgess, N.M.; Solomon, S.M.; Sheldon, T.A.; Reimer, K.J. Effects-based marine ecological risk assessment at a

- polychlorinated biphenyl-contaminated site in Saglek, Labrador, Canada. *Environ. Toxicol. Chem.* **2013**, *32*, 453–467.
- (34) Storelli, M.M.; Storelli, A.; D'Addabbo, R.; Barone, G.; Marcotrigiano, G.O. Polychlorinated biphenyl residues in deep-sea fish from Mediterranean Sea. *Environ. Int.* **2004**, *30*, 343–349.
- (35) Vorkamp, K.; Christensen, J.H.; Riget, F. Polybrominated diphenyl ethers and organochlorine compounds in biota from the marine environment of East Greenland. *Sci. Total Environ.* **2004**, *331*, 143–155.
- (36) Muir, D.C.G.; Savinova, T.; Savinov, V.; Alexeeva, L.; Potelov, V.; Svetochov, V. Bioaccumulation of PCBs and chlorinated pesticides in seals, fishes and invertebrates from the White Sea, Russia. *Sci Total Environ.* **2003**, *306*, 111–131.
- (37) Kelly, B.C.; Ikonomou, M.G.; Blair, J.D.; Gobas, F.A.P.C. Hydroxylated and methoxylated polybrominated diphenyl ethers in a Canadian Arctic marine food web. *Environ. Sci. Technol.* **2008**, *42*, 7069–7077.
- (38) Rig , F.; Vorkamp, K.; Dietz, R.; Rastogi, S.C. Temporal trend studies on polybrominated diphenyl ethers (PBDEs) and polychlorinated biphenyls (PCBs) in ringed seals from east Greenland. *J. Environ. Monitor.* **2006**, *8*, 1000-1005.
- (39) Vorkamp, K.; Rig , F.F.; Glasius, M.; Muir, D.C.G.; Dietz, R. Levels and trends of persistent organic pollutants in ringed seals (*Phoca hispida*) from central west Greenland, with particular focus on polybrominated diphenyl ethers (PBDEs). *Environ. Int.* **2008**, *34*, 499–508.

- (40) Wolkers, H., Krafft, B. A., Bavel, B. Van, Helgason, L. B., Lydersen, C., Kovacs, K. M. Biomarker responses and decreasing contaminant levels in ringed seals (*Pusa hispida*) from Svalbard, Norway. *J. Toxicol. Environ. Hea. A* **2008**, *71*, 1009-1018.
- (41) Hoguet, J.; Keller, J.M.; Reiner, J.L.; Kucklick, J.R.; Bryan, C.E.; Moors, A.J.; Pugh, R.S.; Beker, P.R. Spatial and temporal trends of persistent organic pollutants and mercury in beluga whales (*Delphinapterus leucas*) from Alaska. *Sci.Total Environ.* **2013**, *449*, 285–294.
- (42) Andersen, G.; Kovacs, K.M.; Lydersen, C.; Skaare, J.U.; Gjertz, I.; Jenssen, B.M. Concentrations and patterns of organochlorine contaminants in white whales (*Delphinapterus leucas*) from Svalbard, Norway. *Sci. Total Environ.* **2001**, *264*, 267–281.
- (43) Wolkers, H.; Lydersen, C.; Kovacs, K.M.; Burkow, I.; Bavel, B. Accumulation, metabolism, and food-chain transfer of chlorinated and brominated contaminants in subadult white whales (*Delphinapterus leucas*) and narwhals (*Monodon monoceros*) from Svalbard, Norway. *Arch. Environ. Contam. Toxicol.* **2005**, *50*, 69–78.
- (44) Dietz, R.; Rig , F.; Hobson, K.A.; Rgensen, M.P.H.-J.; M ller, P.; Cleemann, M.; Boer, J.; Glasius, M. Regional and inter annual patterns of heavy metals, organochlorines and stable isotopes in narwhals (*Monodon monoceros*) from West Greenland. *Sci. Total Environ.* **2004**, *331*, 23–23.
- (45) Letcher, R.J.; Bustnes, J.O.; Di z, R.; Jenssen, B.M.; J rgensen, E.H.; Sonne, C.; Verreault, J.; Vijayan, M.M.; Gabrielsen, G.W. Exposure and effects assessment of persistent organohalogen contaminants in arctic wildlife and fish. *Sci.Total Environ.*

- 2010**, 408, 2995–3043.
- (46) Sonne, C. Health effects from long-range transported contaminants in Arctic top predators: An integrated review based on studies of polar bears and relevant model species. *Environ. Int.* **2010**, 36, 461–491.
- (47) Strid, A.; Jürundsóttir, H.; Päpke, O.; Svavarsson, J.; Bergman, Å. Dioxins and PCBs in Greenland shark (*Somniosus microcephalus*) from the North-East Atlantic. *Mar. Pollut. Bull.* **2007**, 54, 1514–1522.
- (48) Hoekstra, P.F.; Hara, T.M.; Karlsson, H.; Solomon, K.R.; Muir, D.C. Enantiomer-specific biomagnification of α -hexachlorocyclohexane and selected chiral chlordane-related compounds within an arctic marine food web. *Environ. Toxicol. Chem.* **2003**, 22, 2482–2491.
- (49) Hühnerfuss, H.; Pfaffenberger, B.; Gehrcke, B.; Karbe, L.; König, W.; Landgraff, O. Stereochemical effects of PCBs in the marine environment: seasonal variation of coplanar and atropisomeric PCBs in blue mussels (*Mytilus edulis* L.) of the german bight. *Mar. Pollut. Bull.* **1995**, 30, 332–340.
- (50) Wiberg, K.; Andersson, P.L.; Berg, H.; Olsson, P-E.; Haglund, P. The fate of chiral organochlorine compounds and selected metabolites in intraperitoneally exposed arctic char (*Salvelinus alpinus*). *Environ. Toxicol. Chem.* **2006**, 25, 1465-1473.
- (51) Kania-Korwel, I.; Shaikh, N.S.; Hornbuckle, K.C.; Robertson, L.W.; Lehmler, H.-J. Enantioselective disposition of PCB 136 (2,2',3,3',6,6'-hexachlorobiphenyl) in C57BL/6 mice after oral and intraperitoneal administration. *Chirality* **2006**, 19,

56–66.

- (52) Ross, M.S.; Pulster, E.L.; Ejsmont, M.B.; Chow, E.A.; Hessel, C.M.; Maruya, K.A.; Wong, C.S. Enantioselectivity of polychlorinated biphenyl atropisomers in sediment and biota from the Turtle/Brunswick River estuary, Georgia, USA. *Mar. Pollut. Bull.* **2011**, *63*, 548–555.
- (53) Warner, N.A.; Martin, J.W.; Wong, C.S. Chiral polychlorinated biphenyls are biotransformed enantioselectively by mammalian Cytochrome P-450 isozymes to form hydroxylated metabolites. *Environ. Sci. Technol.* **2009**, *43*, 114–121.
- (54) Lu, Z. and Wong, C.S. Factors affecting phase I stereoselective biotransformation of chiral polychlorinated biphenyls by rat cytochrome P-450 2B1 isozyme. *Environ. Sci. Technol.* **2011**, *45*, 8298–8305.
- (55) Wolkers, J.; Witkamp, R.; Nijmeijer, S.; Burkow, I.; De Groene, E.M.; Lydersen, C.; Dahle, S.; Monshouwer, M. Phase I and phase II enzyme activities in Ringed seals (*Phoca hispida*): characterization of hepatic cytochrome P450 by activity patterns, inhibition studies, mRNA analyses, and western blotting. *Aquat. Toxicol.* **1998**, *44*, 103–115.
- (56) Wolkers, J.; Burkow, I.; Monshouwer, M.; Lydersen, C.; Dahle, S.; Witkamp, R. Cytochrome P450-mediated enzyme activities and polychlorinated biphenyl accumulation in harp seal (*Phoca groenlandica*). *Mar. Environ. Res.* **1999**, *48*, 59–72.
- (57) Reich, S.; Jimenez, B.; Marsili, L.; Hernández, L.M.; Schurig, V.; González, M.J. Congener specific determination and enantiomeric ratios of chiral polychlorinated

- biphenyls in striped dolphins (*Stenella coeruleoalba*) from the Mediterranean Sea. *Environ. Sci. Technol.* **1999**, *33*, 1787–1793.
- (58) McKinney, M.A.; Arukwe, A.; De Guise, S.; Martineau, D.; Bédand, P.; Dallaire, A.; Lair, S.; Lebeuf, M.; Letcher, R.J. Characterization and profiling of hepatic cytochromes P450 and phase II xenobiotic-metabolizing enzymes in beluga whales (*Delphinapterus leucas*) from the St. Lawrence River estuary and the Canadian Arctic. *Aquat. Toxicol.* **2004**, *69*, 35–49.
- (59) McKinney, M.A.; De Guise, S.; Martineau, D.; Bédand, P.; Arukwe, A.; Letcher, R.J. Biotransformation of polybrominated diphenyl ethers and polychlorinated biphenyls in beluga whale (*Delphinapterus leucas*) and rat mammalian model using an *in vitro* hepatic microsomal assay. *Aquat. Toxicol.* **2006a**, *77*, 87–97.
- (60) McKinney, M.A.; De Guise, S.; Martineau, D.; Bédand, P.; Lebeuf, M.; Letcher, R.J. Organohalogen contaminants and metabolites in beluga whale (*Delphinapterus leucas*) liver from two Canadian populations. *Environ. Toxicol. Chem.* **2006b**, *25*, 1246–1257.
- (61) Leclerc, L.-M.; Lydersen, C.; Haug, T.; Glover, K.A.; Fisk, A.T.; Kovacs, K.M. Greenland sharks (*Somniosus microcephalus*) scavenge offal from minke (*Balaenoptera acutorostrata*) whaling operations in Svalbard (Norway). *Polar Res.* **2011**, *30*, 7342, DOI: 10.3402/polar.v30i0.7342.
- (62) Kovacs, K.M. and Lydersen, C. Climate change impacts on seals and whales in the North Atlantic Arctic and adjacent shelf seas. *Sci. Prog.* **2008**, *91*, 117–150.

- (63) Kovacs, K.M.; Lydersen, C.; Overland, J. E.; Moore, S.E. Impacts of changing sea-ice conditions on Arctic marine mammals. *Mar. Biodiv.* **2011**, *41*, 181–194.
- (64) McMeans, B.C., Arts, M.T., Fisk, A.T. Similarity between predator and prey fatty acid profiles is tissue dependent in Greenland sharks (*Somniosus microcephalus*): Implications for diet reconstruction. *J.Exp.Mar. Biol.Ecol.* **2012**, *429*, 55-63.
- (65) McMeans, B. C.; Arts, M. T.; Lydersen, C.; Kovacs, K.M.; Hop,H.; Falk-Petersen, S.; Fisk, A.T. The role of Greenland sharks (*Somniosus microcephalus*) in an Arctic ecosystem: assessed via stable isotopes and fatty acids. *Mar. Biol.* **2013**, *160*, 1223-1238.
- (66) International Whaling Commission. Catches taken: under objection or under reservation. **2013**. http://iwc.int/table_objection, accessed August 9th 2013.

Chapter 6

Conclusions and Future Directions

6.1. Conclusions

Chirality can be exploited to gain insight into stereoselective fate processes that may otherwise remain undetected, because only biological, but not physical and chemical transport and transformation processes in an achiral environment will generally change enantiomer compositions. As with other chiral compounds, individual PCB atropisomers may interact stereoselectively with chiral macromolecules, such as CYP enzymes or ryanodine receptors, leading to differences in their toxicological effects and in stereoselective biotransformation products. Species- and congener-specific atropisomer enrichment has been demonstrated in wildlife and humans, likely due to a complex combination of stereoselective biotransformation processes and uptake of the non-racemic mixture via the diet. Other factors such as influence of emerging pollutants (e.g., nanoparticles) and changes in environmental condition may also play important roles in determining the atropisomer enrichment of chiral PCBs. However, detailed mechanisms were previously understood poorly. This dissertation provides an in-depth understanding of the application of chirality to studying the environmental fate of chiral PCB atropisomers at both the enzymatic and food web levels.

At the enzyme level, rat CYP2B1 preferentially biotransformed the second-eluting atropisomers of PCBs 45 and 95 at low substrate concentration ranges ($\leq 15 \mu\text{M}$). Biotransformation competition by different congeners was also observed, with increasing competition at higher chlorination. Competition decreased the biotransformation rates of each congener stereoselectively, affecting atropisomeric composition. Significant differences in biotransformation kinetics were observed in individual atropisomer incubations of PCB 132, indicating that (+)-PCB 132 and (-)-PCB 132 were

competitively biotransformed. Homology modeling and docking studies suggested that each atropisomer had different interactions with rat CYP2B1, and could dock with the isozyme at different locations. This is one possible explanation for stereoselective biotransformation and competition of chiral PCBs at the molecular level. Our results suggest that the lack of predictive capability for stereoselectivity of PCBs and other chiral pollutants in biota may be due to competitive and/or inhibitory activities of different substrates, including individual enantiomers of the same compound.

AuNPs affected the biotransformation activity of rat CYP2B1 and changed the atropisomeric composition of PCB 95, depending on the incubation time and the AuNP concentration. Electrostatic repulsion between citrate-coated AuNPs and rat CYP2B1 may influence the active conformation of the isozyme and consequently affect its activity and stereoselectivity. In addition, the effects of AuNPs on rat CYP2B1 activity also appeared to be through interference with the CYP catalytic cycle's electron transfer chain. Incubations with AuNPs had a decline in buffer conductance and an absorbance band red shift of AuNPs, from electrostatic interactions of K^+ with negatively-charged AuNP aggregates. These ionic strength changes affected the formation rate of nicotinamide adenine dinucleotide phosphate, which provides electrons for the oxidative reaction cycle, and the biotransformation activity and stereoselectivity of CYP.

From this study, we found that nanoparticles may be able to alter the biological functions by directly interacting with biomolecules and/or indirectly affecting the microenvironment of biomolecules through changes in ionic strength. Organisms may be exposed to different concentrations of AuNPs due to multiple applications of AuNPs (e.g., exposure to medical treatment). Different exposure doses of AuNPs may lead to different

fates of this contaminant in organisms, with potential differences in toxic mechanisms. Moreover, the occurrence and aggregation of charged nanoparticles in biological systems may interfere with both the functional structure of enzymes, and with the co-factors involved in biotransformation. Consequently, these nanoparticles can either catalyze or inhibit enzymatic biotransformation activity, depending on reaction conditions. These processes could potentially influence regular metabolism in organisms, which include the biotransformation of organic pollutants. For those chiral contaminants which have stereoselective toxicity and fate, such as PCBs and some chiral pesticides, the two atropisomers may be affected by nanoparticles in different manner through disruption of relevant biomolecules' functions, be they CYPs or other enzymes. It is clear that these nanoparticle behaviors are important in understanding and predicting the environmental fate of both nanoparticles and POPs.

Rat CYP2B1 could stereoselectively biotransform chiral PCBs to generate 5-OH-PCBs as the major metabolites after 60 min incubations. The present study demonstrated that CYP2B1-mediated biotransformation plays an important role in the atropisomer enrichment of chiral PCBs and their hydroxylated metabolites in rats. The stereoselective metabolism of racemic OH-PCBs to non-racemic diOH-PCBs by rat CYP2B1 was confirmed as a mechanism for the atropisomer enrichment of the chiral OH-PCBs. These findings indicated that the stereoselective biotransformation of chiral PCBs and OH-PCBs by CYPs are major sources of non-racemic PCBs, OH-PCBs and diOH-PCBs in the environment. The disruption of both biotransformation and the product formation of chiral compounds at the enantiomer level were confirmed by the present study. Our findings help explain the underlying processes for enantiomer enrichment of

chiral organic contaminants observed in wildlife, laboratory exposure organisms and *in vitro* studies. There were some unidentified metabolites in the biotransformation of chiral PCBs and OH-PCBs by rat CYP2B1, which may suggest unidentified exposure risk in the environment warranting further investigation.

In the arctic food web, levels of PCBs contamination in Cumberland Sound organisms was generally lower than in similar species from other locations in the Arctic. Racemic compositions of chiral PCBs were detected in mixed zooplankton, invertebrates, benthic fishes and pelagic forage fishes, indicating low biotransformation capacities towards PCBs by these organisms (and in their prey). Non-racemic atropisomer enrichment of PCBs in Arctic char might suggest stereoselective bioaccumulation of chiral PCBs in piscivorous fishes. Marine mammals showed species-specific EFs, likely due to a combination of *in vivo* biotransformation and trophic transfer. The chiral signatures of PCBs 136 and 149 in Greenland sharks did not vary temporally over the period of a decade at one location or spatially across the North Atlantic Arctic. In contrast, the atropisomer signature shifts of PCBs 91 and 95 might indicate changes in the feeding ecology of Greenland sharks with time and in different areas. The observed patterns warrant further investigation.

6.2. Future Research Directions

6.2.1. Distribution of POPs in the Environment

Although many of the legacy POPs have been banned or are restricted in use, it is still necessary to investigate their environmental behavior and fate because of the continued presence of POPs in the environment, as well as the release of POPs from old products and subsequent exposure risk to wildlife and humans. Temporal and spatial

trends of POPs in different environmental compartments should continue to be monitored in future work to trace the fate of these contaminants. These investigations could help us to evaluate the contamination situation of POPs, to avoid the exposure of pollutants and to predict the fate of other emerging contaminants. This is especially important for those populations have high exposure risk to POPs (e.g., Inuit people in the Arctic).

6.2.2. Chiral Organic Pollutants

6.2.2.1. Interactions between chiral molecules

Molecular structure determines chemical function. For chiral POPs, such as chiral PCBs, efforts at understanding enantiomer-specific chemical function would be facilitated by determination of absolute configurations. The key amino acids in rat CYP2B1 or other enzymes, which are responsible for the stereoselective biotransformation of chiral PCBs, should be identified. This would help us to understand the nature of interaction processes (e.g., interaction energy calculations) of different atropisomers with biomolecules at the molecular level. The understanding of stereoselective processes of chiral pollutants with biomolecules at the molecular level could provide us useful information for new chemical design and use, and help to avoid the stereoselective toxicities.

Development of novel chiral stationary phases with improved lifetimes and better resolution of chiral PCBs and their metabolite atropisomers are necessary. More studies should focus on the mechanisms of how chiral stationary phases interact with chiral compounds at the molecular structure level. In addition, we need to determine the absolute elution order of different atropisomers of chiral PCBs and their metabolites based on their optical rotations or absolute structures. All these efforts on the chiral

analysis are helpful for the scientific research of chiral organic pollutants.

6.2.2.2. Stereospecific toxicities of chiral pollutants

In-depth understanding of stereoselective metabolism and toxicities of chiral PCBs is needed. This is because the detailed adverse effects of the two atropisomers and mechanisms are different and poorly understood. Phase I enzyme induction by chiral PCBs is a stereoselective process and congener-dependent. The stereoselectivity of phase I enzyme induction of those more environmentally relevant chiral PCB congeners such as PCBs 95, 132 and 136 is poorly understood. Phase II enzyme induction and/or conjugation stereoselectivity of chiral PCBs' metabolites is unknown. More work should focus on the stereospecific toxicities of chiral PCBs. These issues are important for accurate accessing of toxicities at the stereotypic isomer level.

In addition, our results in Chapter 4 indicated that some phase I enzymes and processes other than rat CYP2B1 are responsible for the stereoselective biotransformation of chiral PCBs. It is necessary to identify these enzymes and processes in order to understand the biotransformation processes of chiral PCBs. This information is also necessary for predicting the distribution and metabolism for chiral pollutants in organisms. The unknown metabolites in phase I reactions should be identified in future research to clarify the potential exposure risk of these metabolites. Moreover, it would be of interest to know if rat CYP2B1 can biotransform other chiral organic contaminants. This could help understanding of the common interactions between chiral chemicals with enzymes.

6.2.2.3. Development of research material

To provide insight into metabolism and toxicology, commercial standards of mono-

and di-OH-PCB need development. Much research on the biotransformation of chiral PCBs was limited by the lack of commercial standards. Furthermore, it is important to know the stereoselectivity of phase II biotransformation of chiral PCBs metabolites.

6.2.2.4. Use of chirality as a forensics tool to detect environment change

Additional work is needed to understand how stereoselectivity operates within food webs to use chiral PCBs effectively as probes for contaminant transfer and ecological processes. For example, as discussed in Chapter 5, it is interesting to use chiral signatures of POPs to trace the feeding ecology change of Arctic marine mammals during climate change. Moreover, building an improved database of chiral signatures, including water and human blood, will expand the use of chiral chemistry.

All of the future research directions discussed above are not limited to chiral PCBs, but also true for other chiral organic pollutants.

Appendix 1

Chiral Polychlorinated Biphenyl Transport, Metabolism, and Distribution: A Review

A version of this chapter has been previously published as Lehmler, H.-J., Harrad, S. J., Hühnerfuss, H., Kania-Korwel, I., Lee, C. M., Lu, Z., Wong, C. S. Chiral polychlorinated biphenyl transport, metabolism, and distribution: a review. *Environmental Science & Technology*. 2010, 44, 2757-2766. (DOI: 10.1021/es902208u). Copyright 2010 © American Chemical Society. Reprinted with permission.

The author of this dissertation is a coauthor of the published and peer-reviewed manuscript, and was responsible for writing the introduction and section A1.4, plotting Figure A1.1, editing the overall manuscript and arranging the references. This review has been updated since the time in which it was published with more recent literature.

A1.1. Introduction

Chirality is a growing aspect of environmental research. About 25% of agrochemicals are chiral (*1*), as are a similar proportion of other environmental contaminants. Chirality is significant for several reasons. The enantiomers of a chiral compound rotate polarized light in opposite directions, but otherwise exhibit identical physical and chemical properties. Consequently, environmental physical and chemical processes generally affect both enantiomers identically. However, individual enantiomers may interact differentially with other chiral molecules, such as enzymes or biological receptors, leading to different biological and toxicological effects (*2*). Hence, determining effects of chiral compounds is confounded by differing concentrations of enantiomers, which may arise from enantioselective biotransformation (e.g., by cytochrome P-450 enzymes or CYPs), exerting differing biological activities. Therefore, chirality must be considered for accurate pollutant exposure and effects assessment (*3, 4*). Moreover, chirality can be exploited to gain insight into enantioselective fate processes that may otherwise remain undetected, because physical and chemical transport and transformation processes will not generally change enantiomer compositions, but biological processes may.

Polychlorinated biphenyls (PCBs) are a well-known class of pollutants. Given their inherent stability, PCBs are difficult to eliminate from environmental matrices, and distinguishing elimination processes in the uncontrolled open environment from a plethora of other fate processes is nontrivial. Because 19 PCB congeners are axially chiral and stable under environmental and instrumental analytical conditions (*5*), stereoisomer analysis is a useful tool for characterizing biochemical processes affecting

PCBs. The atropisomers (stereoisomers of axially chiral chemicals) of PCBs also show differential toxicity (6-10), thus understanding atropisomer specific PCB toxicity is of importance.

This review highlights the state of knowledge about chiral PCBs in the environment, with two major foci. First, we show how the atropisomer compositions of PCBs and their chiral metabolites (e.g., methylsulfonyl PCBs or MeSO₂-PCBs) in both controlled laboratory experiments and field studies provides deepened insight into their sources, fate, and effects, in matrices as varied as soils and sediments (microbial degradation), aquatic organisms, and mammals, such as rats, mice, and humans. Second, we highlight atropisomer-specific effects of PCBs. These studies demonstrate stereoisomer analysis reveals new features of the fate, transport, and effects of even heavily studied chemicals like PCBs. Throughout, we express atropisomer composition as enantiomer fraction or enantiomeric fraction (EF) (11):

$$EF = \frac{A}{A + B} \quad \text{Equation A1.1}$$

where A and B are the (+)- and (-)-atropisomers, respectively, if optical rotation is known, or are the first-eluting and second eluting atropisomer on a specified enantioselective chromatographic column otherwise.

A1.2. Stereoselective Biodegradation of Chiral PCBs in Sediments and Soils

Although many studies have investigated microbial transformation of PCBs in soils and sediments under both anaerobic and aerobic conditions (12), relatively few studies have considered stereoselective biodegradation, particularly under controlled laboratory conditions. The use of chiral PCBs to understand microbial transformation pathways holds promise for design of bioremediation schemes for dredged sediment removed from

sites, such as the Hudson River, and stored in secure landfills. *In situ* bioremediation of PCBs has faced a major roadblock, because completely mineralizing mixtures of PCBs containing highly chlorinated congeners requires sequential anaerobic-aerobic processes.

Significantly non-racemic chiral PCB signatures have been observed in sediments from several locations (13-15). Measurements of surface sediments collected from the Hudson River estuary (15) showed non-racemic EFs for PCBs 95 and 149. Non-racemic PCB compositions existed (13) in several surface sediments from rivers in the eastern (Hudson River, NY; Housatonic River, MA) and midwestern United States (White River, IN; Fox River, WI) and in sediments from Lake Hartwell, SC, a reservoir and Superfund site heavily contaminated with PCBs. Changes in EF with depth in cores from Lake Hartwell suggested a relationship with concentration and the likelihood of more than one microbial community responsible for dechlorination (14). Racemic EFs have also been measured in samples with low concentrations (ng/g) of total PCBs such as sediment cores from Lake Ontario (14) and surface sediment from the Mohawk River, NY (13).

Evidence of stereoselective microbial transformation in soils is sparser. Non-racemic EFs of PCBs 95, 136, and 149 were observed in UK top soils and grass (16-18) and in Canadian soils (19). Microbial transformation may have occurred in soils from one site at surprisingly low concentrations of PCBs 95, 136, and 149 at 51, 13, and 107 pg/g, respectively (16), as measured EF values were statistically significantly but not dramatically different from racemic. But as Jamshidi et al. (18) indicated, a stereoselective process clearly occurred. Soils from the Chemical, Metals, and Pesticide (CMP) pits at the Savannah River Site had non-racemic EFs for PCBs 84, 91, 95, and 149 at concentrations of 2 $\mu\text{g/g}$ or less total PCBs, implying individual congeners were at

concentrations of 1-175 ng/g (20, 21). Non-racemic EFs for PCBs 95 and 136 were found in soils from the area in Toronto, Canada (19), suggesting stereoselective microbial transformation at quite low concentrations (sum of PCBs 95, 136, and 149 was 7 ng/g). EFs of PCB 95 in Toronto soils favored degradation of the same atropisomer as observed in soil from two UK locations (16); however, EFs of PCB 136 in Toronto and UK soils displayed opposite preferences. To date the only atropisomer-specific aerobic PCB microcosm study is by Singer et al. (22), who tested one tetra-chlorinated congener (PCB 45) and three penta-chlorinated congeners (PCBs 84, 91, and 95) with five strains of PCB degrading bacteria. Three co-substrates--biphenyl, cymene, and (*S*)-carvones--were used with combinations of bacterial strains and PCB congeners. One hexa- (PCB 132) and two hepta-chlorinated congeners (PCBs 171 and 183) were also tested, but transformation was negligible, as expected (12) under aerobic conditions. Hydroxylated metabolites (OH-PCBs) of the penta-chlorinated congeners, but not PCB 45, were observed, with no reports of metabolite atropisomer composition (22).

Singer et al. (22) reported the stereoselectivity of the various strains for the chiral congeners with a “selectivity factor” rather than an EF, rendering comparisons with other studies difficult. The congeners were biotransformed by all strains tested in the order PCB 45>84>95>91. Selectivity among the congeners-strain-cosubstrate combinations varied significantly, suggesting a variety of biotransformation pathways were represented by the combinations. However, it was clear that gram-negative strains formed similar non-racemic PCB residues, while gram-positive strains formed different stereoselective residues (22). On the other hand, a gram-positive strain with dioxygenase genes similar to gram-negative strains exhibited the gram-negative residue pattern (22). This suggests two

different sets of dioxygenases existed, each with its own atropisomer preference. Only one published anaerobic microcosm study that considered biotransformation of chiral PCBs exists (23). The anaerobic microcosms differed from the aerobic cultures used by Singer et al. (22) in several aspects. Sediment from Lake Hartwell served as the inoculum, consisting of a mixed culture. Rather than a congener mixture, single congeners (PCBs 132 and 149) were spiked into the anaerobic microcosms. These were selected because the first byproduct of reductive dechlorination for each, PCBs 91 and 95, respectively, is also chiral. The two spiked compounds, PCBs 132 and 149, showed no changes in their racemic EFs as they were dechlorinated, in contrast to results with the aerobic microcosms (22). However, for both products, PCBs 91 and 95, significantly non-racemic EFs were measured as they appeared and were subsequently removed (23). The observation of non-stereoselective dechlorination of the initial congener followed by stereoselective dechlorination of the product generated the hypothesis that two different enzymatic pathways might be responsible. At a later time, enrichment of Hartwell sediment cultures that dechlorinated PCB 132 allowed tentative identification of at least two different strains of *Dehalococcoides* (24), supporting the hypothesis.

The implications of the above include confirmation that there are a wide variety of enzymatic processes capable of transforming PCBs under both anaerobic and aerobic conditions in sediments and soils and that there is potential for microbial transformation, in particular at very low PCB concentrations. The growing database of atropisomer-specific data offers potential for modeling approaches to explore the relationship between concentration and biotransformation and the roles of specific enzymes and microorganisms. Chiral PCB congeners thus offer insight into microbial transformation

pathways for a notoriously recalcitrant class of contaminants.

A1.3. Exploiting Enantiomer Signatures for Source Apportionment

Stereoselective weathering of PCBs has been used not only to gain insights on microbial degradation in sediments and soils, but also to delineate and quantify sources and transport of contaminants necessary for mitigating human and ecosystem exposure. Conventional approaches to apportionment of PCB sources to a given compartment such as the atmosphere have relied on indirect methods and mathematical modeling (25-27). More recently, researchers have utilized chiral properties of organochlorine pesticides such as (α)-hexachlorocyclohexane ((α)-HCH), heptachlor, and chlordane to distinguish directly between such sources (28, 29). Commercial formulations of chiral organochlorines are racemic. As discussed above, stereoselective differences in degradative processes cause EFs in soils to deviate from racemic (16, 19, 30). Such signatures are preserved on volatilization (31), and once in the atmosphere are unaltered by abiotic chemical and physical removal processes (32).

These facts have been incorporated into a two-source apportionment model quantifying the relative contribution of two sources of a chiral contaminant to an environmental compartment (11):

$$FC_{S1} = (EF_{RC} - EF_{S2}) / (EF_{S1} - EF_{S2}) \quad \text{Equation A1.2}$$

where FC_{S1} is the fractional contribution of source matrix 1 to the receiving compartment; EF_{RC} is the receiving compartment EF; and EF_{S1} and EF_{S2} are the EFs in source matrices 1 and 2, respectively.

This principle was exploited by Asher et al. (15), who observed racemic PCBs in air overlying the Hudson River Estuary at New York City, consistent with an unweathered

local urban source to the local atmosphere. In contrast, estuary waters displayed non-racemic PCB 95 residues similar to those in Hudson River sediment (13), and correlated to the Hudson River's water discharge. Using the two-source apportionment model, 85% of PCB 95, and by implication other medium-molecular-weight PCBs, in the estuary was concluded to originate from the Upper Hudson River.

Chirality was also applied for source apportionment by comparing EFs of PCBs 95, 136, and 149 in topsoil and outdoor air over a 12-month period at one urban and one rural site in Birmingham, UK (16). In contrast to the conventional view that contemporary concentrations of PCBs in outdoor air were driven by volatile emissions from topsoil (25); EFs in soil and air at both sites differed significantly, implying volatile emissions from soil exerted negligible influence on outdoor air. Furthermore, the racemic or near-racemic signatures observed in all outdoor air samples indicated the source(s) to be racemic. Subsequent work extended the comparison of EFs in outdoor air and soil to a further ten UK locations (18). These findings were similar to those of their earlier study (16). Additionally, EFs of the target PCBs in indoor air from buildings in the same city were racemic. These data, combined with concentrations of PCBs in indoor air that substantially exceed those in outdoor air (33, 34), are consistent with emissions from the built environment driving contemporary outdoor air concentrations. Similarly, chiral analysis suggested that the PCBs in the atmosphere around the Swan Hills Treatment Centre in Canada were from the facility, rather than from local soil emission (80).

A significant caveat to the above is that PCBs do volatilize from soil, but that at the comparatively low soil concentrations (0.36-13.3 ng Σ PCB/g) detected in the above studies (16, 18). Such volatilization exerts an impact on atropisomer signatures only in air

very close to the soil surface. For example, the concentration and chiral signature data indicated that emission of PCBs from soil to the airborne decreased with altitude, and emissions from built environments increased in Birmingham, U.K. (81). This was also reported for chiral signatures of (α)-HCH (31), and for concentrations of Σ PCB (35), where concentrations in soil were far higher (42 ng (α)-HCH/g, and between 1.1 and 635 μ g Σ PCB/g). The implication, thus, is that volatilization from soil was a far more important source to the atmosphere in the past, and continues to influence the contemporary atmosphere, albeit at most locations only at heights immediately above the soil-air interface.

This latter observation provides a potential explanation for the findings of a study that found atropisomer signatures of PCBs 95 and 149 in herbage very similar to those in soil, particularly during warmer sampling periods (81). One wholly unexpected implication is that the PCBs in vegetation arise principally via vapor phase foliar uptake of PCBs that have volatilized from soil (17, 81). The examples cited above have considerable policy relevance. In particular, the exploitation of the stereospecific properties of some PCBs has been crucial in establishing the causal link between the PCB burden in the contemporary built environment and outdoor contamination. This is consistent with the absence of significant decline in concentrations of Σ PCBs in UK indoor air between 1997-1998 and 2003-2004, which remain on average 30-40 times higher than those outdoors (34); and the lack of temporal decline in UK dietary exposure to Σ PCBs measured in 1992, 1997, and 2001 (36). Should these UK data be reflected elsewhere (and there is no reason to suspect otherwise), this suggests future efforts worldwide must focus on reducing the PCB burden in the built environment in

applications such as capacitors, transformers, acoustic ceiling tiles, and permanently elastic construction sealants. This will not only reduce exposure directly via inhalation of indoor air (34) and ingestion of indoor dust (37), but indirectly via dietary exposure following reductions in releases to the outdoor environment (38).

A 1.4. Chiral PCBs as a Marker of Biochemical Weathering in Aquatic Food Webs

The distribution of chiral PCBs is atropisomer-specific and species-specific in aquatic organisms (39-49). These results are caused by *in vivo* biotransformation and/or uptake from prey or the organisms' surroundings. Because PCBs were released into the environment as racemates, the finding of non-racemic residues in aquatic organisms suggests biotransformation of PCBs in the aquatic food web. This conclusion is significant, as aquatic organisms, such as fish and invertebrates, have much lower abundances and activities of CYPs, lower rates of electron transport, and less active monooxygenases than higher organisms (e.g., mammals and birds), and thereby much less capacity to detoxify and biotransform xenobiotic chemicals such as PCBs (50). Thus, chirality is useful as a tool to detect and to gain insight into the biotransformation of PCBs in various aquatic species, ranging from phytoplankton and invertebrates, to fish, to birds, and to aquatic mammals such as cetaceans, seals, and polar bears.

PCB atropisomers were almost racemic in phytoplankton and zooplankton collected from Lake Superior (Figure A1.1) (39), suggesting that these biota at the bottom of the food web have essentially no capability to biotransform PCBs. Similarly, omnivorous copepods (*Calanus hyperboreus*) collected from the Northwater Polynya in the Canadian Arctic (40) had racemic EF values of PCBs 91, 95, and 149. However, EFs for PCB 149 of 0.50-0.55 were observed in blue mussels (*Mytilus edulis*) of the German Bight (41).

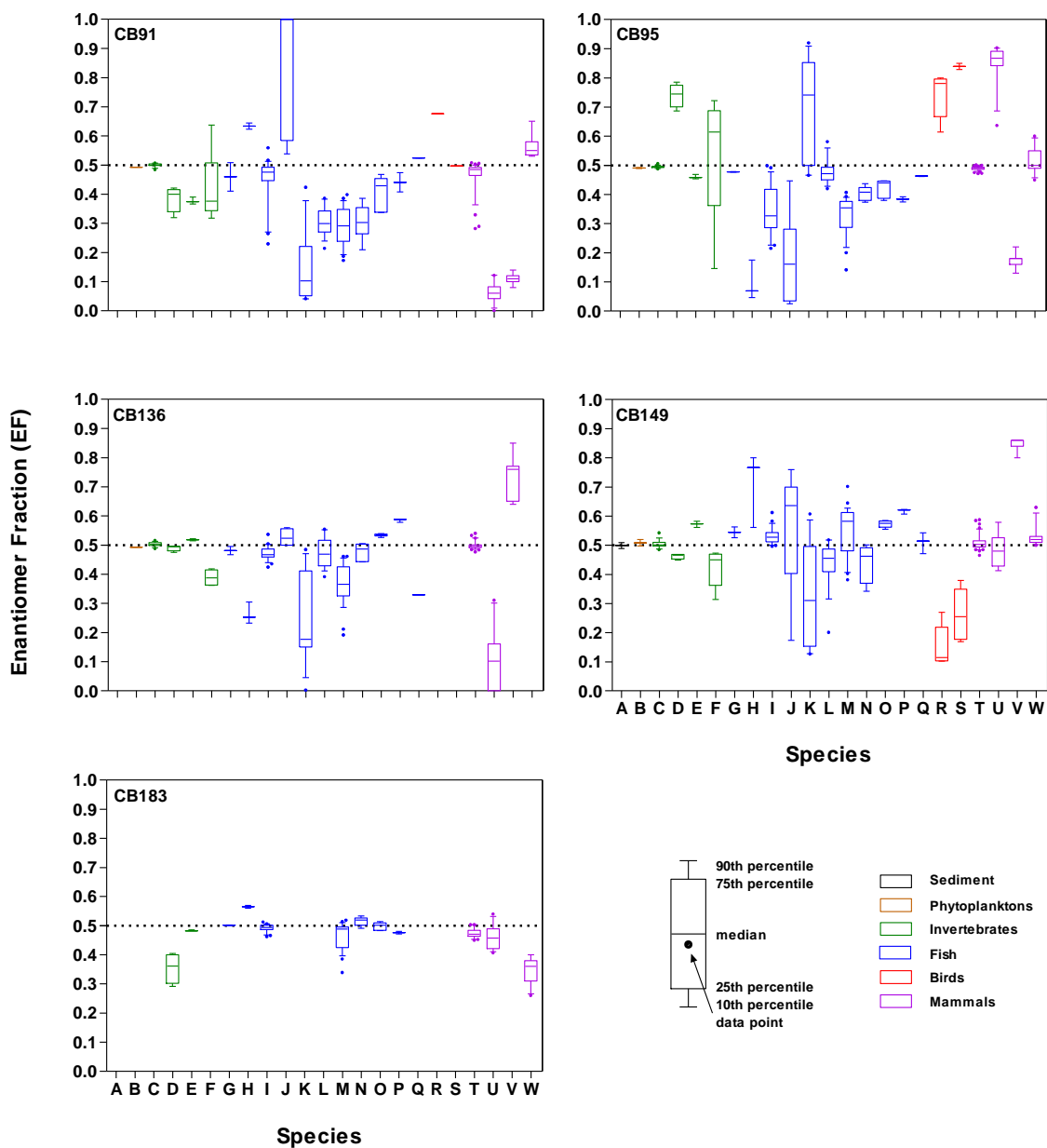


Figure A1.1 Box plots of EFs of some chiral PCBs in biota. Horizontal line across each panel indicates racemic EF of 0.5. Species and location: A, sediment (Northwater Polynya) (40); B, phytoplankton (Lake Superior) (39); C, zooplankton (Bering-Chukchi-Beaufort Sea) (44); D, bivalves (*Corbicula* sp., U.S. rivers) (42); E, mysids (*Mysis relicta*, Lake Superior) (39); F, crayfish (*Procambarus* sp., Lake Hartwell, SC) (42); G, carp (*Cyprinus carpio*, U.S. rivers) (42); H, sculpins (*Cottus* sp., U.S. rivers)

(42); I, white sucker (*Catostomus commersoni*, U.S. rivers) (42); G, watersnake (*Nerodea sipedon*, Lake Hartwell) (42); K, bluegill sunfish (*Lepomis macrochirus*, Lake Hartwell) (42); L, bass (*Micropterus salmoides*, Lake Hartwell) (42); M, lake trout (*Salvelinus namaycush*, Lake Superior) (39); N, lake herring (*Coregonus artedii*, Lake Superior) (39); O, rainbow smelt (*Osmerus mordax*, Lake Superior) (39); P, amphipods (*Diporeia hoyi*, Lake Superior) (39); Q, Arctic cod (*Boreogadus saida*, Northwater Polynya) (40); R, thick-billed murre (*Uria lomvia*, Northwater Polynya) (40); S, ivory gull (*Pagophila eburnea*, Northwater Polynya) (40); T, bowhead whale blubber (*Balaena mysticetus*, Bering-Chukchi-Beaufort Sea) (44); U, ringed seal (*Phoca hispida*, Northwater Polynya) (40); V, female mouse liver (65); W, human breast milk (58).

Non-racemic residues (EFs from 0.35-0.75) of PCBs 91, 95, 132, and 183 were also observed in freshwater bivalves (*Corbicula* sp.) in United States rivers (42). Although EFs of PCBs in phytoplankton, the food source for filter-feeders such as bivalves, were not measured in those studies (41, 42), it is likely they were racemic (39). If so, then *in vivo* stereoselective biotransformation processes in bivalves likely produced the observed residues. Bivalves could not accumulate non-racemic PCBs from their food source, nor was there evidence that the ambient waters and sediment of those sites had non-racemic PCBs. Crayfish (*Procambarus* sp.) in Lake Hartwell (42) also had non-racemic PCBs, but their source might be sediment, which as noted previously had non-racemic PCBs from microbial reductive dechlorination. Opossum shrimp (*Mysis relicta*) and amphipods (*Diporeia hoyi*) had significantly non-racemic residues of PCBs 91, 95, 136, 149, 174, 176, and 183 in Lake Superior (39), some of which was attributed to *in vivo*

biotransformation. The capability of mysids to eliminate stereoselectively PCBs 91, 95, and to a much lesser extent PCB 149 was later confirmed experimentally (46). In summary, enantioselective analyses showed that phytoplankton and zooplankton are unlikely to biotransform PCBs in the aquatic environment. However, larger invertebrates have some PCB biotransformation potential. It should be noted that unlike other chiral organochlorine pollutants (32), atropisomer compositions of dissolved phase PCBs have not been reported with one exception, a heavily contaminated urban site (15). Thus, it must be assumed that no EF changes occurred when phytoplankton bioconcentrated PCBs from the water column.

Prior non-stereoselective analysis has concluded that fish have limited biotransformation ability toward PCBs (50). However, atropisomer-specific and species-specific biotransformation differences of PCBs have also been found in fish, likely from a combination of *in vivo* biotransformation and uptake from prey. Furthermore, freshwater fish had more non-racemic PCB residues than marine fish. PCBs 95, 132, 136, 149, and 174 were racemic or near racemic in the livers of groupers from the northwest African Atlantic Ocean (43). PCBs 91 and 149 were also racemic in Arctic cod (*Boreogadus saida*) from the Canadian Arctic (40); however, a significant EF of 0.463 ± 0.001 (σ) for PCB 95 in that species suggested possible biotransformation capacity for that congener, although this conclusion is tentative given low sample size ($n=3$). Highly non-racemic compositions of PCBs 91, 95, 136, and 149 were found in largemouth bass (*Micropterus salmoides*) and bluegill sunfish (*Lepomis macrochirus*) in Lake Hartwell (42). Moreover, species-specific differences were found in these two species (Figure A1.1), despite sample variation in some matrices and some congeners

which likely arise from differences in accumulation, distribution, metabolism, and elimination. Lake trout in Lake Superior (39) had similar non-racemic residues of PCBs 91, 95, 149, and 174 as its major prey, lake herring (*Coregonus artedii*) and rainbow smelt (*Osmerus mordax*). This result suggested that these congeners in lake trout mainly accumulated from trophic transfer. In contrast, significant differences in the EFs of PCB 136 between lake trout and its prey suggested *in vivo* stereoselective biotransformation of this congener occurred. The capacity of salmonids to eliminate PCBs stereoselectively was later shown experimentally (46-49), and was affected by chemical (e.g., congener structure) and physiological (e.g., temperature, organism size) factors. Atropisomer enrichment of chiral PCBs was also observed in yellow shiners (*Notropis lutipinnis*) from Twelvemile Creek (USA), which might be due to both *in vivo* biotransformation and uptake from of non-racemic residues from food sources (82). Pseudo-first-order rate constants could be determined in both field studies (39) and laboratory based experiments (46-48) based on differences in EFs between predator and prey, and estimations of the timescale over which biotransformation may have occurred (e.g., organism lifespan). Such rates in field studies would be difficult if not impossible to ascertain without enantioselective analysis.

The higher abundances and activities of CYP isozymes in seabirds and aquatic mammals may enable them to detoxify PCBs more easily than lower trophic level biota. In addition, CYPs are more likely to be induced by higher concentrations of PCBs in high trophic level organisms due to greater biomagnification. Seabirds had higher capabilities for stereoselective biochemical weathering of PCBs than aquatic organisms, as seven species (40) collected from Northwater Polynya had significantly non-racemic

atropisomeric compositions of PCBs 91, 95, and 149 that were considerably different from the racemic residues in their arctic cod and zooplankton prey. In contrast, near racemic EFs were observed in barn swallows (*Hirundo rustica*) at Lake Hartwell (42). Bowhead whales (*Balaena mysticetus*) (44) in arctic waters had non-racemic EFs of PCBs in liver and blubber that differed from zooplankton. Moreover, EFs of PCBs 95 and 149 were correlated with specimen length for both males and females, while EFs of PCB 91 were correlated with length for males only. This observation suggests that stereoselective accumulation of these three congeners was affected by concentration, age, and an uncharacterized sex-related factor, factors also observed in the stereoselective accumulation of other chlorinated pollutants (51). Likewise, highly non-racemic EFs in ringed seals (*Phoca hispida*) (40) of the Northwater Polynya that differed from their prey suggested *in vivo* stereoselective biotransformation. This hypothesis was supported by the observation of non-racemic amounts of the metabolite 3-MeSO₂-PCB 149 (see (52) for the present nomenclature and (53) for an alternative nomenclature) in ringed seals (54). In contrast, harbor seals (*Phoca vitulina*) and gray seals (*Halichoerus grypus*) (45) had non-racemic EF values of PCB 149 (EF=0.58-0.71 and 0.60-0.70, respectively), which also demonstrated species-specific biochemical biotransformation in aquatic mammals.

A1.5. Chiral PCBs in Human Tissues, Milk, and Feces

Although PCBs are routinely measured in human blood, atropisomeric compositions have not been reported so far. Nonetheless, a few studies have investigated EF values of PCBs 95, 132, and 149 in a small number of human tissue samples (55,83). PCBs 95, 132, and 149 were near racemic in Belgian muscle, brain, and kidney samples. However, a significant enrichment of these three congeners was observed in liver. Racemic or near

racemic EFs of PCBs 95 and 132 were observed in human hair collected from an electronic waste recycling area in southern China (83). EFs have also been reported in human milk (Figure A1.1) from Germany (56, 57), Spain (58), and Switzerland (59). In these studies, (+)-PCB 132 was enriched in most samples, with EF values ranging from 0.53 to 0.82. In contrast, PCB 149 was near racemic (EF=0.49-0.63). PCB 95 was near racemic in breast milk from Germany and Spain (EF=0.45-0.60), but showed some atropisomeric enrichment in breast milk from Switzerland (EF=0.64-0.76). Several other PCBs also showed some atropisomeric enrichment in breast milk from Spain (58).

The extent of atropisomeric enrichment has been employed to investigate excretion of PCBs 95 and 149 in healthy volunteers from the UK (17). PCBs 95 and 149 in the diet and PCB 95 in the feces of the volunteers were near racemic, while PCB 149 was only detected in two feces samples with slight atropisomeric enrichment. These results are consistent with the near racemic compositions observed in human tissues (Figure A1.1).

A1.6. Mammalian Toxicokinetics of Chiral PCBs

Understanding the behavior of chiral pollutants in mammals is significant for several reasons. First, mammals have higher CYP levels and activities than aquatic organisms, as previously noted, making biotransformation much easier. In addition, the large body of literature on mammalian toxicokinetics and pharmacokinetics eases interpretation of atropisomer-specific data. Finally, of course, mammalian studies have relevance in terms of addressing human exposure and toxicity.

A1.6.1. Mice

Atropisomer enrichment and atropisomer dependent toxicokinetics of chiral PCBs 95, 132, 136, 149 and 176 have been observed in C57Bl/6 female mice by oral exposure

(89,90). The dose and tissue depended stereoselective formation of OH-PCBs in mice were also observed previously (90). Several recent studies investigated different chiral PCB congeners (60), route of administration (61), gender (61), dose (62), dietary fat content (63), induction of CYPs (64), and multidrug resistance transporters (65) as factors influencing the extent of the atropisomeric enrichment in female C57Bl/6 mice. Both PCBs 84 and 136 underwent atropisomeric enrichment in C57Bl/6 mice, with (+)-PCB 84 and (+)-PCB 136 enriched in all tissues and excreta (60-64). Intraperitoneal injection of PCB 136 produced significantly higher PCB concentrations in blood and tissues ($p < 0.05$), especially liver and brain, than oral administration (Figure A1.2A) (61). (+)-PCB 136 was significantly enriched in most organs, independent of the route of administration; however, more non-racemic PCB 136 were found in the oral compared to intraperitoneal treatment groups (Figure A1.2B). The same study did not show any gender-specific difference in PCB 136 concentrations or EF values (61).

A study investigating the dose dependence of the atropisomeric enrichment of PCB 136 after oral PCB administration showed that liver concentrations increased with increasing dose after oral PCB administration (Figure A1.2C), whereas the extent of (+)-PCB 136 enrichment decreased with increasing dose (Figure A1.2D) (62). The same trends were observed in other tissues, blood, and feces. These observations indicate a saturation of the processes responsible for atropisomeric enrichment at higher PCB doses, and also suggest that the less pronounced atropisomeric enrichment in animals receiving PCB 136 intraperitoneally may be due to higher PCB tissue concentrations. The drastic difference between fecal EF values in mice and humans, discussed previously, suggests

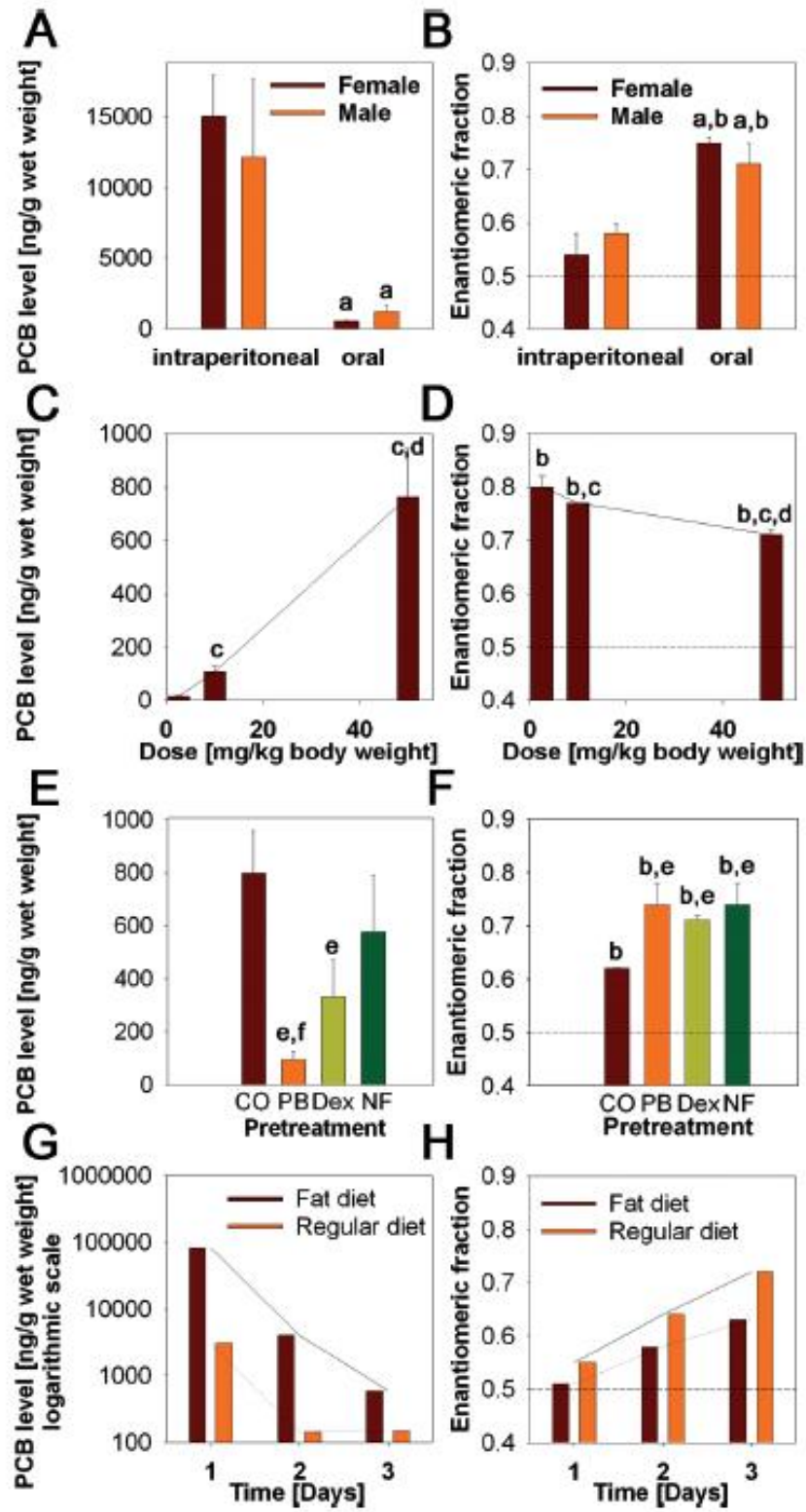


Figure A1.2 Effect of route of administration, dose, and fat content in diet on levels and enantiomeric fraction of PCB 136 in mice after oral administration of (\pm)-PCB 136. (A) Levels and (B) enantiomeric fraction in the liver of male and female mice exposed orally or intraperitoneally (61). Dose-dependence of (C) levels and (D) enantiomeric fraction in the liver of female mice (62). (E) Levels and (F) enantiomeric fraction in the liver of mice pretreated with CYP1A (β -naphthoflavone; NF), CYP2B (Phenobarbital; PB), and CYP3A (dexamethasone; DEX) inducers compared to corn oil (vehicle; CO) pretreated animals (64). Time-dependent changes of (G) levels and (H) enantiomeric fraction in the feces of mice fed a regular (10% fat) or high-fat (37% fat) diet (63). Notes: ^a different from intraperitoneally exposed mice, $p < 0.05$; ^b different from racemic (EF=0.05), $p < 0.05$; ^c different from lowest dose (2.5 mg/kg body weight), $p < 0.05$; ^d different from medium dose (10.0 mg/kg body weight), $p < 0.05$; ^e different from corn oil-treated animals, $p < 0.05$; ^f different from β -naphthoflavone-treated animals, $p < 0.05$.

differences in biotransformation and/or excretion of PCB atropisomers, an observation with potential human health implications given developmental neurotoxicity of PCBs with multiple *ortho* substituents (66).

Induction of different CYP enzymes by pretreatment with corn oil alone, β -naphthoflavone (CYP1As), Phenobarbital (CYP2Bs), or dexamethasone (CYP2Bs and CYP3As), followed by oral PCB administration, resulted in lower PCB 136 concentrations in phenobarbital- and, to a lesser extent, dexamethasone-pretreated animals (Figure A1.2E) (64), presumably due to the induction of PCB 136 metabolizing enzymes. Although (+)-PCB 136 was enriched in all tissues (Figure A1.2F), only EFs in liver of phenobarbital-, dexamethasone- and β -naphthoflavone-pretreated animals was

significantly different from animals treated with corn oil vehicle alone. These observations do not suggest a particular CYP subfamily as the cause of the enrichment of (+)-PCB 136. Instead, non-specific induction of hepatic enzymes in general seems to be correlated with increased atropisomeric enrichment.

In laboratory studies, PCBs are typically administered with a vehicle containing a comparatively high fat content (e.g., corn oil). To investigate the potential role of the dietary fat content on the disposition of PCBs, PCB 136 was administered orally to female mice fed an unrefined (10% fat) or high fat (37% fat) diet (63). As found previously, (+)-PCB 136 was enriched in all organs and in feces. The tissue EF values and PCB concentrations were independent of the dietary fat content. In contrast, PCB 136 levels and EF values in feces differed between the unrefined diet and high fat diet groups (Figure A1.2G and H) due to differences in the residual fecal fat content. The most intriguing finding of this study was the increase in fecal EF values with time. This suggests that non-absorbed, racemic PCB 136 was excreted within the first 24 h, whereas absorbed PCB 136 was excreted into the feces after undergoing atropisomeric enrichment *in vivo*. Thus, differences in atropisomeric enrichment can be used to gain further insight into the disposition of PCBs.

A1.6.2. Rats

A few studies have reported an atropisomeric enrichment of PCBs in rats after intraperitoneal administration. While (+)-PCB 139 was enriched in the liver of PCB 139-treated rats (9), near racemic PCB 136 (EF~0.49) was observed in PCB 136-treated male and female rats (67). Similarly, intraperitoneal administration of complex PCB mixtures to rats resulted in at most a slight atropisomeric enrichment (68). Similar to

mice (61), the comparatively low atropisomeric enrichment in rats is probably due to the intraperitoneal route of administration.

A1.7. Binding and Metabolism of PCB Atropisomers by CYPs

PCBs are metabolized *in vivo* to hydroxy- and sulfur containing metabolites (2, 69), i.e., CYP enzymes convert these lipophilic compounds to metabolites more easily eliminated from the body, thus preventing the cells from PCB intoxication. However, the PCB metabolites that CYPs produce are often more toxic than the parent molecule itself. Recent studies have shown that CYP enzymes stereoselectively bind and metabolize PCB congeners to hydroxylated metabolites. These processes are thought to cause the atropisomeric enrichment of PCBs observed *in vivo*.

A spectral binding study investigated binding of pure PCB 136 atropisomers to P-450 enzymes (70). Microsomes were obtained from mice or rats treated with prototypical inducers of CYPs. Depending on pretreatment, these microsomes contain predominantly CYP1A (β -naphthoflavone-treated mice and 3-methylcholanthrene-treated rats), CYP2B (phenobarbital-treated animals), and CYP2B/3A enzymes levels (dexamethasone-treated animals), respectively. In addition, high CYP2B enzyme levels were measured in hepatic microsomes from dexamethasone-treated mice. These microsomes were used to determine the binding of pure PCB 136 atropisomers to microsomal CYP enzymes. Binding of racemic PCB 136 and its atropisomers to CYP enzymes was greatest in microsomes from phenobarbital treated animals, and decreased in the order phenobarbital>dexamethasone> β -naphthoflavone/3-methylcholanthrene

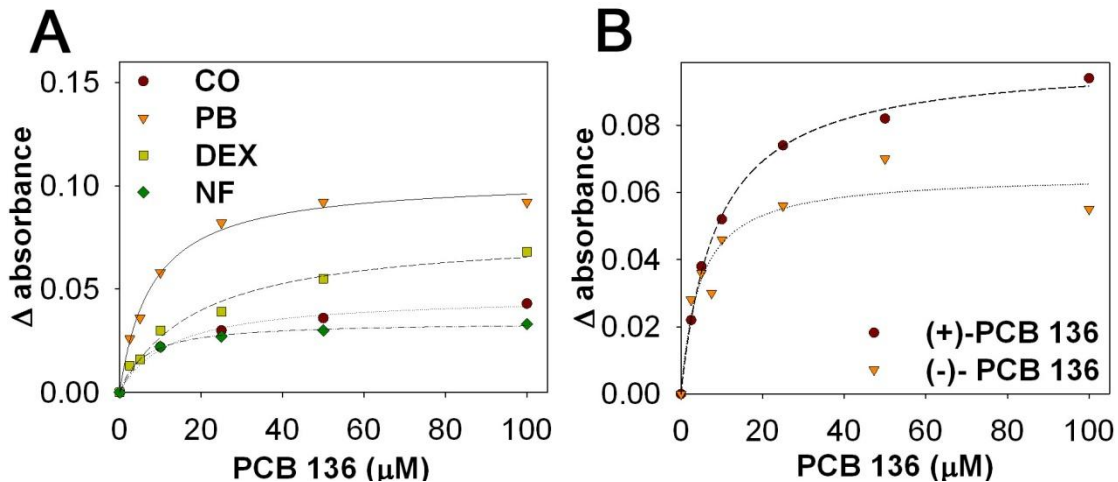


Figure A1.3 Absorbance changes elicited by increasing concentrations of PCB 136 in murine liver microsomes (70). (A) Effect of the (±)-PCB 136 concentration on the absorbance of microsomes from corn oil, phenobarbital, dexamethasone, and β -naphthoflavone-treated mice. (B) Effect of the concentration of (+)- or (-)-PCB 136 on the absorbance of microsomes from phenobarbital-treated mice. For each measurement, (±)-, (+)-, or (-)-PCB 136 in DMSO were added to 1 mL sample cuvettes containing 4 nmol P450/mL. Adapted with permission from (70). Copyright 2008 American Chemical Society.

≈corn oil (Figure A1.3A). A significantly larger absorbance change was observed with (+)-PCB 136 than with (-)-PCB 136 with all four hepatic microsomal preparations in mice and rats, indicating (+)-PCB 136 interacted with microsomal CYP enzymes to a greater degree than (-)-PCB 136 (Figure A1.3B). Finally, binding of PCB 136 was inhibited by CYP2B and CYP3A antibodies, indicating involvement of CYP2B. Together these results suggest preferential binding of (+)-PCB 136 to CYP enzymes, such as

CYP2B and CYP3A, in hepatic microsomes.

In vitro CYP-mediated biotransformation of chiral PCBs has been reported recently (71). Human CYP2B6 eliminated PCB 45 stereoselectively (EF=0.44) but not PCB 91 (EF=0.49). In contrast, rat CYP2B1 degraded PCBs 45, 84, 91, 95, 136, and 136 stereoselectively, with species-specific, opposite atropisomer preference for PCB 45 (EF=0.82). Each single-congener incubation with rat CYP2B1 produced one OH-PCB metabolite except for PCB 95, for which two OH-PCBs were formed. Although metabolites were not identified conclusively, they were likely chiral (see next section). Preferential elimination of (+)-PCB 136 (71) contrasted rat microsomal binding experiments (70) and *in vivo* experiments (67), in which stronger binding of (+)-PCB 136 to CYPs and near-racemic PCB 136 EFs were observed, respectively. However, it should be noted that single purified CYPs were used in the former experiment (71), compared to mixtures in microsomes and *in vivo*.

A1.8. Chiral PCB Metabolites

MeSO₂-PCBs and OH-PCBs were detected in fish, birds, and mammals, including humans (reviewed in (52)). More recently, some of the MeSO₂-PCBs in biota have also been observed to be selectively and strongly retained in liver tissue of mammals, including humans (52). However, the selectivity mechanism is still unknown, although reversible protein binding plays a major role for their retention in liver (72). The most important MeSO₂-PCBs bound in mammalian liver are 3-MeSO₂-2,2',3',4',5,6-hexachlorobiphenyl (abbreviated 3-MeSO₂-PCB 132; see (52)), 3-MeSO₂-2,2',4',5,5',6-hexachlorobiphenyl (3-MeSO₂-PCB 149), and 4-MeSO₂-2,2',4',5,5',6-hexachlorobiphenyl (4-MeSO₂-PCB 149). The MeSO₂-PCBs

formed are persistent and only slightly less hydrophobic than their parent compounds, making them long-lasting environmental contaminants. From a toxicological point, several of the *meta*-MeSO₂-PCBs strongly induce CYPs, such as CYP2B1, CYP2B2, CYP3A2, and CYP2C6 (73, 74). Thus, part of the toxicity of PCBs in the environment may be due to the presence of these metabolites. Furthermore, the main metabolites mentioned above are chiral and, accordingly, stereoselective transformation as well as toxic impacts cannot be excluded. Moreover, congener-specific atropisomer enrichment of MeSO₂-PCBs was observed in fish samples from a pond near an electronic waste recycling site in South China (84).

To gain deepened insight into the stereoselective transformation of atropisomeric PCBs, the research groups of Bergman and Hühnerfuss (52, 75) performed a systematic study, which included stereoselective separation of eight MeSO₂-PCB standards (4-MeSO₂-PCB 91, 4-MeSO₂-PCB 95, 3- and 4-MeSO₂-PCB 149, 3- and 4-MeSO₂-PCB 132, and 3- and 4-MeSO₂-PCB 174) by GC; atropisomer-specific measurement of MeSO₂-PCBs in extracts of rat and human liver as well as rat lung and adipose tissue; atropisomer separation of larger amounts of 3-MeSO₂-PCB 132, 3-MeSO₂-PCB 149, and 4-MeSO₂-PCB 149 and their parent PCBs by stereoselective preparative HPLC for determination of absolute structures; and investigation of stereoselective toxicity of MeSO₂-PCB atropisomers.

As a first step, 18-25 mg of each atropisomer of chiral methylsulfonyl- (3- and 4-MeSO₂-PCB 149), methylsulfyl (3- and 4-MeS-PCB 149), and methoxy-PCBs (4-MeO-PCB 149) were isolated, with atropisomeric purities of 95.0-99.9%, by stereoselective HPLC using semi-preparative β -cyclodextrin based HPLC columns.

Thereafter, their absolute structures were determined by electronic circular dichroism and vibrational circular dichroism in combination with quantum chemical calculations (69, 76). Rotational angles and absolute configurations were also determined. This study established a sound method for future preparation and absolute structure determination of compounds of the same chemical class, and identified enantioselective GC peaks of environmental sample extracts unequivocally.

Thus far, eight of the ten atropisomeric MeSO₂-PCBs found previously in environmental samples were separated into their atropisomers using a column coated with a 1:1 (w:w) mixture of OV 1701 and heptakis(6-*O*-*tert*-butyldimethylsilyl-2,3-di-*O*-methyl)- β -cyclodextrin (52). 3-MeSO₂-PCB 91 was separated using other columns (54), while 3-MeSO₂-PCB 95 was not studied because no standard was available. In general, MeSO₂-PCBs exert strong interactions with chiral cyclodextrin phases. Because of low maximum temperatures for stereoselective GC columns (468-498 K), retention times were long for all columns studied (52, 54, 77) e.g., from 50-130 min even for a 10 m column (52), with corresponding peak widths at half-height of 30-110 s. Although baseline separation was observed for most atropisomers and constitutional isomers (52), improving atropisomeric separation of MeSO₂-PCBs would be useful. Based on this preparatory work, systematic enzymatic transformation processes were investigated using human livers from two women and three men who had died from heart failure or accidents. Only (*R*)-3-MeSO₂-PCB 149 and the second-eluting atropisomer of 3-MeSO₂-PCB 132 were encountered in all liver extracts (52). Thus, not only was a high congener selectivity found as previously observed, but also a highly stereoselective liver retention of these

MeSO₂-PCBs. None of the MeSO₂-PCBs investigated (52) were detected in the two human lung samples also analyzed.

Furthermore, the presence of MeSO₂-PCB atropisomers was determined in liver, lung and adipose tissues of rats exposed to the technical PCB product Clophen A50 (75). In all tissues analyzed, especially lung, *para*-MeSO₂-PCBs were more abundant than *meta*-derivatives. An excess and dominance of (*R*)-3-MeSO₂-PCB 149 atropisomer in lung extracts was observed. Small amounts of (*S*)-3-MeSO₂-PCB 149 atropisomer were present in lung and adipose tissues but not liver. No significant changes in the atropisomeric excess of 4-MeSO₂-PCB 91, 3-MeSO₂-PCB 132, 4-MeSO₂-PCB 132, 3-MeSO₂-PCB 149, and 4-MeSO₂-PCB 149 atropisomers were found in lung, liver, or adipose tissues. The results suggest stereoselective formations occurred for both *meta*- and *para*-MeSO₂-PCBs. Rat hepatocytes transformed both PCB 149 atropisomers with comparable velocities, thus yielding a nearly racemic metabolite 3-MeSO₂-PCB 149, while subsequent transformation of the 3-MeSO₂-PCB149 atropisomers by rat hepatocytes led to a drastic transformation of the (*S*)-atropisomer. The (*R*)-atropisomer remained nearly unaffected, consistent with the above atropisomeric excesses in rat liver extracts. Thus, the dramatic atropisomeric excess of (*R*)-3-MeSO₂-PCB 149 was caused by enantioselective transformation of this metabolite, not production by the parent PCB 149.

Field measurements of chiral MeSO₂-PCBs have been performed on extracts of gray seal blubber (78) and pelican muscle tissues (79); ringed seals and polar bears (*Ursus maritimus*) in the Arctic (54); and livers of harbor porpoises (*Phocoena phocoena*) (77). As with humans, highly stereoselective residues of MeSO₂-PCBs were observed in

non-human mammalian tissues (54,77), indicating similar mechanisms for stereoselective binding and/or enrichment of MeSO₂-PCBs are shared among mammals, at least for those species studied. An enantioselective heart-cut column-switching liquid chromatography-atmospheric pressure photoionization-tandem mass spectrometry method has been developed recently for the analysis of MeSO₂-PCBs and non-racemic 4-MeSO₂-PCB 91 and 4'-MeSO₂-PCB 132 were detected in Greenland sledge dog (*Canis familiaris*) adipose tissues (85). The atropisomers of MeSO₂-PCBs were successfully separated in fish oil and cow liver samples by using a heart-cut multidimensional gas chromatographic system equipped with a BGB-176SE capillary column (91).

Compared to MeSO₂-PCBs, little work has been carried out on chiral OH-PCBs given lack of commercially available standards. However, OH-PCB metabolites of PCBs 45, 84, 91, 95, 132, 136, and 149 were synthesized, and atropisomers of several methylated derivatives separated by enantioselective GC (67) albeit with long retention times as with MeSO₂-PCBs. Male and female rats dosed with racemic PCB 136 produced four OH-PCBs with 3-OH-PCB 150 and 3-OH-PCB 136 formed stereoselectively, whereas parent PCB residues remained racemic (67). The stereoselective formation of 5-hydroxylated metabolites of PCBs 91, 95, 132, 136 and 149 by rat liver microsomes have been observed *in vitro* (86, 87). Understanding toxicokinetics of pollutant metabolite stereoisomers, as well as parent compounds, will greatly increase our understanding of their environmental fate and effects.

A1.9. Toxicity of Chiral PCBs

Chiral PCBs are expected to display stereoselective or even specific biological effects due to differences in pharmacokinetics and interaction with target receptors.

Indeed, atropisomers of PCBs 88, 139, and 197 had different enzyme inducing properties in chick embryo hepatocytes (10) and immature male Sprague-Dawley rats (8, 9). For example, (+)-PCB 197 induced total CYP to a larger extent than (-)-PCB 197 in cultured chick embryo hepatocytes, whereas the atropisomers of PCBs 88 and 139 had equal potencies (10). In contrast, the (+)-atropisomers of these three congeners were more potent at inducing ethoxyresorufin-*O*-deethylase activity in immature male Sprague-Dawley rats, but only PCB 197 atropisomers differed in their potency to induce total CYP, with (+)-PCB 197 being more potent (9).

PCB atropisomers can also interfere stereoselectively with intracellular signaling processes and calcium homeostasis, critical processes for normal nervous system function and growth (66). PCB 84 atropisomers increased [³H]-phorbol ester binding, a measure of protein kinase C (PKC) translocation from cytosol to the cell membrane, and altered Ca²⁺-sequestration, as determined by ⁴⁵Ca²⁺-uptake by microsomes isolated from adult rat cerebellum, in a concentration-dependent manner (6). However, only the effect on PKC translocation was stereoselective, with lowest observable effect levels of 30 and 50 μM for (+)-PCB 84 and (-)-PCB 84, respectively. PCB 136 atropisomers stereospecifically enhanced binding of [³H]-ryanodine to high affinity sites on ryanodine receptors (RyR) (7), a broadly expressed family of microsomal Ca²⁺ channels. While (-)-PCB 136 enhanced [³H]-ryanodine to RyR type 1 and type 2 with EC50s~0.95 μM, (+)-PCB 136 was inactive at ≤10 μM. Furthermore, (-)-PCB 136 induced rapid release of Ca²⁺ from microsomal vesicles by selective sensitization of RyRs, an effect not antagonized by (+)-PCB 136, and enhanced the open probability of reconstituted RyR1 channels 3-fold by stabilizing open and destabilizing closed conformational states. The stereospecific

effect of (-)-PCB 136 was also observable in intact HEK 293 cells expressing RyR1, where (-)-PCB 136 but not (+)-PCB 136, sensitized responses to caffeine. Neurotoxicity was also observed for PCB 95 (87, 88). However, the stereoselectivity and relevant mechanisms is still not clear. Together with the observation that a plethora of congener- and species-specific stereoselective biotransformation can result in non-racemic PCB signatures, the stereospecificity of PCB 136 atropisomers toward RyRs represents a significant health concern for wild life and human populations exposed to PCBs.

References

- (1) Williams, A. Opportunities for chiral agrochemicals. *Pestic. Sci.* **1996**, *46*, 3–9.
- (2) Kallenborn, R. and Hühnerfuss, H. *Chiral Environmental Pollutants*; Springer Verlag: New York, **2001**.
- (3) Magrans, J. O.; Alonso-Prados, J. L.; Garc ía-Baud ín, J. M. Importance of considering pesticide stereoisomerism-Proposal of a scheme to apply Directive 91/414/EEC framework to pesticide active substances manufactured as isomeric mixtures. *Chemosphere* **2002**, *49*, 461–469.
- (4) Stanley, J. K.; Brooks, B. W. Perspectives on ecological risk assessment of chiral compounds. *Integr. Environ. Assess. Manage.* **2009**, *5*, 364–373.
- (5) Kaiser, K. On the optical activity of polychlorinated biphenyls. *Environ. Pollut.* **1974**, *7*, 93–101.
- (6) Lehmler, H.-J.; Robertson, L. W.; Garrison, A. W.; Kodavanti, P. R. S. Effects of PCB 84 enantiomers on [³H]-phorbol ester binding in rat cerebellar granule cells and ⁴⁵Ca²⁺-uptake in rat cerebellum. *Toxicol. Lett.* **2005**, *156*, 391–400.
- (7) Pessah, I. N.; Lehmler, H. J.; Robertson, L. W.; Perez, C. F.; Cabrales, E.; Bose, D. D.; Feng, W. Enantiomeric specificity of (-)-2,2',3,3',6,6'-hexachlorobiphenyl toward ryanodine receptor types 1 and 2. *Chem. Res. Toxicol.* **2009**, *22*, 201–207.
- (8) Püttmann, M.; Arand, M.; Oesch, F.; Mannschreck, A.; Robertson, L. W., Chirality and the induction of xenobiotic-metabolizing enzymes: Effects of the atropisomers of the polychlorinated biphenyl 2,2',3,4,4',6-hexachlorobiphenyl. In *Chirality and Biological Activity*; Frank, H., Holmstedt, B., Testa, B., Eds.; Alan R. Liss, Inc.: New York, **1990**; pp 177-184.

- (9) Püttmann, M.; Mannschreck, A.; Oesch, F.; Robertson, L. Chiral effects in the induction of drug-metabolizing enzymes using synthetic atropisomers of polychlorinated biphenyls (PCBs). *Biochem. Pharmacol.* **1989**, *38*, 1345–1352.
- (10) Rodman, L. E.; Shedlofsky, S. I.; Mannschreck, A.; Püttmann, M.; Swim, A. T.; Robertson, L. W. Differential potency of atropisomers of polychlorinated biphenyls on cytochrome P450 induction and uroporphyrin accumulation in the chick embryo hepatocyte culture. *Biochem. Pharmacol.* **1991**, *41*, 915–922.
- (11) Harner, T.; Wiberg, K.; Norstrom, R. Enantiomer fractions are preferred to enantiomer ratios for describing chiral signatures in environmental analysis. *Environ. Sci. Technol.* **2000**, *34*, 218–220.
- (12) Abramowicz, D. A. Aerobic and anaerobic biodegradation of PCBs: A review. *Crit. Rev. Biotechnol.* **1990**, *10*, 241–251.
- (13) Wong, C. S.; Garrison, A. W.; Foreman, W. T. Enantiomeric composition of chiral polychlorinated biphenyl atropisomers in aquatic bed sediment. *Environ. Sci. Technol.* **2001**, *35*, 33–39.
- (14) Wong, C. S.; Pakdeesusuk, U.; Morrissey, J. A.; Lee, C. M.; Coates, J. T.; Garrison, A. W.; Mabury, S. A.; Marvin, C. H.; Muir, D. C. G. Enantiomeric composition of chiral polychlorinated biphenyl atropisomers in dated sediment cores. *Environ. Toxicol. Chem.* **2007**, *26*, 254–263.
- (15) Asher, B. J.; Wong, C. S.; Rodenburg, L. A. Chiral source apportionment of polychlorinated biphenyls to the Hudson River estuary atmosphere and food web. *Environ. Sci. Technol.* **2007**, *41*, 6163–6169.
- (16) Robson, M.; Harrad, S. Chiral PCB signatures in air and soil: Implications for

- atmospheric source apportionment. *Environ.Sci. Technol.* **2004**, *38*, 1662–1666.
- (17)Harrad, S.; Ren, J.; Hazrati, S.; Robson, M. Chiral signatures of PCBs 95 and 149 in indoor air, grass, duplicate diets and human faeces. *Chemosphere* **2006**, *63*, 1368–1376.
- (18)Jamshidi, A.; Hunter, S.; Hazrati, S.; Harrad, S. Concentrations and chiral signatures of polychlorinated biphenyls in indoor and outdoor air and soil in a major UK conurbation. *Environ.Sci. Technol.* **2007**, *41*, 2153–2158.
- (19)Wong, F.; Robson, M.; Diamond, M.; Harrad, S.; Truong, J. Concentrations and chiral signatures of POPs in soil and sediments: A comparative urban versus rural study in Canada and UK. *Chemosphere* **2009**, *74*, 404–411.
- (20)Hall, A. A. Application of chiral analytical method to determine enantiomeric fractions of polychlorinated biphenyls in composted PCB-contaminated soil. M.S. Thesis, Clemson University, Clemson, SC, **2004**.
- (21)Pressley, H. An evaluation of composting to treat soils contaminated with polychlorinated biphenyls at the Savannah River Site, Chemicals, Metals and Pesticide Pits. M.S. Thesis, Clemson University, Clemson, SC, **2004**.
- (22)Singer, A. C.; Wong, C. S.; Crowley, D. E. Differential enantioselective transformation of atropisomeric polychlorinated biphenyls by multiple bacterial strains with different inducing compounds. *Appl. Environ. Microbiol.* **2002**, *68*, 5756–5759.
- (23)Pakdeesusuk, U.; Jones, W. J.; Lee, C. M.; Garrison, A. W.; O’Niell, W. L.; Freedman, D. L.; Coates, J. T.; Wong, C. S. Changes in enantiomeric fractions (EF) during microbial reductive dechlorination of PCB 132, PCB 149, and Aroclor 1254 in

- Lake Hartwell sediment microcosms. *Environ. Sci. Technol.* **2003**, *37*, 1100–1107.
- (24)Brotherson, T.; Lee, C. M.; Freedman, D. L. Development and characterization of a nearly sediment-free polychlorinated biphenyl dechlorinating enrichment culture from a freshwater environment; 27th Annual Meeting of the Society of Environmental Toxicology and Chemistry, Montreal, Canada, November 5-9, **2006**.
- (25)Harrad, S. J.; Sewart, A. P.; Alcock, R.; Boumphrey, R.; Burnett, V.; Duarte-Davidson, R.; Halsall, C.; Sanders, G.; Waterhouse, K.; Wild, S. R.; Jones, K. C. Polychlorinated biphenyls (PCBs) in the British environment: Sinks, sources and temporal trends. *Environ. Pollut.* **1994**, *85*, 131–146.
- (26)Currado, G. M.; Harrad, S. Factors influencing atmospheric concentrations of polychlorinated biphenyls in Birmingham, UK. *Environ. Sci. Technol.* **2000**, *34*, 78–82.
- (27)Halsall, C. J.; Lee, R. G. M.; Coleman, P. J.; Burnett, V.; Harding-Jones, P.; Jones, K. C. PCBs in UK urban air. *Environ. Sci. Technol.* **1995**, *29*, 2368–2376.
- (28)Bidleman, T. F.; Falconer, R. F. Using enantiomers to trace pesticide emissions. *Environ. Sci. Technol.* **1999**, *33*, 206A–209A.
- (29)Bidleman, T. F.; Jantunen, L. M. M.; Wiberg, K.; Harner, T.; Brice, K. A.; Su, K.; Falconer, R. L.; Leone, A. D.; Aigner, E. J.; Parkhurst, W. J. Soil as a source of atmospheric heptachlor epoxide. *Environ. Sci. Technol.* **1998**, *32*, 1546–1548.
- (30)Aigner, E. J.; Leone, A. D.; Falconer, R. L. Concentrations and enantiomeric ratios of organochlorine pesticides in soils from the U.S. Corn Belt. *Environ. Sci. Technol.* **1998**, *32*, 1162–1168.
- (31)Finizio, A.; Bidleman, T. F.; Szeto, S. Y. Emission of chiral pesticides from an

- agricultural soil in the Fraser Valley, British Columbia. *Chemosphere* **1998**, *36*, 345–355.
- (32) Bidleman, T. F.; Jantunen, L. M.; Harner, T.; Wiberg, K.; Wideman, J. L.; Brice, K.; Su, K.; Falconer, R. L.; Aigner, E. J.; Leone, A. D.; Ridal, J. J.; Kerman, B.; Finizio, A.; Alegria, H.; Parkhurst, W. J.; Szeto, S. Y. Chiral pesticides as tracers of airwater exchange. *Environ. Pollut.* **1998**, *102*, 43–49.
- (33) Currado, G. M.; Harrad, S. A comparison of polychlorinated biphenyl concentrations in indoor and outdoor air and the potential significance of inhalation as a human exposure pathway. *Environ. Sci. Technol.* **1998**, *32*, 3043–3047.
- (34) Harrad, S.; Hazrati, S.; Ibarra, C. Concentrations of polychlorinated biphenyls in indoor air and polybrominated diphenyl ethers in indoor air and dust in Birmingham, United Kingdom: Implications for human exposure. *Environ. Sci. Technol.* **2006**, *40*, 4633–4638.
- (35) Krauss, M.; Moering, J.; Amelung, W. Does the soil-air-plant pathway contribute to the PCB contamination of apples from allotment gardens? *Organohalogen Compd.* **2004**, *66*, 2345–2351.
- (36) DEFRA (Department of Environment, Food and Rural Affairs). *2007 National Implementation Plan for the Stockholm Convention on Persistent Organic Pollutants, United Kingdom of Great Britain and Northern Ireland*; <http://www.defra.gov.uk/environment/chemicals/pdf/pop-nationalplan.pdf>; accessed April 1, 2009.
- (37) Harrad, S.; Ibarra, C.; Robson, M.; Melymuk, L.; Diamond, M.; Douwes, J. Polychlorinated biphenyls in indoor dust from Canada, New Zealand, United

- Kingdom and United States: Implications for human exposure. *Chemosphere* **2009**, *76*, 232–238.
- (38)Harrad, S.; Diamond, M. Exposure to polybrominated diphenyl ethers (PBDEs) and polychlorinated biphenyls (PCBs): Current and future scenarios. *Atmos. Environ.* **2006**, *40*, 1187–1188.
- (39)Wong, C. S.; Mabury, S. A.; Whittle, D. M.; Backus, S. M.; Teixeira, C.; DeVault, D. S.; Bronte, C. R.; Muir, D. C. G. Organochlorine compounds in Lake Superior: Chiral polychlorinated biphenyls and biotransformation in the aquatic food web. *Environ. Sci. Technol.* **2004**, *38*, 84–92.
- (40)Warner, N. A.; Norstrom, R. J.; Wong, C. S.; Fisk, A. T. Enantiomeric fractions of chiral polychlorinated biphenyls provide insights on biotransformation capacity of Arctic biota. *Environ. Toxicol. Chem.* **2005**, *24*, 2763–2767.
- (41)Hühnerfuss, H.; Pfaffenberger, B.; Gehrecke, B.; Karbe, L.; König, W. A.; Landgraff, O. Stereochemical effects of PCBs in the marine environment: seasonal variation of coplanar and atropisomeric PCBs in blue mussels (*Mytilus edulis* L.) of the German Bight. *Mar. Pollut. Bull.* **1995**, *30*, 332–340.
- (42)Wong, C. S.; Garrison, A. W.; Smith, P. D.; Foreman, W. T. Enantiomeric composition of chiral polychlorinated biphenyl atropisomers in aquatic and riparian biota. *Environ. Sci. Technol.* **2001**, *35*, 2448–2454.
- (43)Serrano, R.; Fernandez, M.; Rabanal, R.; Hernandez, L. M.; Gozales, M. J. Congener-specific determination of polychlorinated biphenyls in shark and grouper livers from Northwest African Atlantic Ocean. *Arch. Environ. Contam. Toxicol.* **2000**, *38*, 217–224.

- (44)Hoekstra, P. F.; Wong, C. S.; O'Hara, T. M.; Solomon, K. R.; Mabury, S. A.; Muir, D. C. G. Enantiomer-specific accumulation of PCB atropisomers in the bowhead whale (*Balaena mysticetus*). *Environ. Sci. Technol.* **2002**, *36*, 1419–1425.
- (45)Klobes, U.; Vetter, W.; Luckas, B.; Skirnisson, K.; Plotz, J. Levels and enantiomeric ratios of α -HCH, oxychlordan, and PCB 149 in blubber of harbour seals (*Phoca vitulina*) and grey seals (*Halichoerus grypus*) from Iceland and further species. *Chemosphere* **1998**, *37*, 2501–2512.
- (46)Warner, N. A.; Wong, C. S. The freshwater invertebrate *Mysis relicta* can eliminate chiral organochlorine compounds enantioselectively. *Environ. Sci. Technol.* **2006**, *40*, 4158–4164.
- (47)Wong, C. S.; Lau, F.; Clark, M.; Mabury, S. A.; Muir, D. C. G. Rainbow trout (*Oncorhynchus mykiss*) can eliminate chiral organochlorine compounds enantioselectively. *Environ. Sci. Technol.* **2002**, *36*, 1257–1262.
- (48)Buckman, A. H.; Wong, C. S.; Chow, E. A.; Brown, S. B.; Solomon, K. R.; Fisk, A. T. Biotransformation of polychlorinated biphenyls (PCBs) and bioformation of hydroxylated PCBs in fish. *Aquat. Toxicol.* **2006**, *78*, 176–185.
- (49)Wiberg, K.; Andersson, P. L.; Berg, H.; Olsson, P.-E.; Haglund, P. The fate of chiral organochlorine compounds and selected metabolites in intraperitoneally exposed Arctic char (*Salvelinus alpinus*). *Environ. Toxicol. Chem.* **2006**, *25*, 1465–1473.
- (50)Stegeman, J. J.; Klopper-Sams, P. J. Cytochrome P-450 isozymes and monooxygenase activity in aquatic animals. *Environ. Health Perspect.* **1987**, *71*, 87–95.
- (51)Karlsson, H.; Oehme, M.; Skopp, S.; Burkow, I. C. Enantiomer ratios of chlordan

- congeners are gender specific in cod (*Gadus morhua*) from the Barents Sea. *Environ. Sci. Technol.* **2000**, *34*, 2126–2130.
- (52) Ellerichmann, T.; Bergman, A.; Franke, S.; Hühnerfuss, H.; Jakobsson, E.; König, W. A.; Larsson, C. Gas chromatographic enantiomer separations of chiral PCB methyl sulfons and identification of selectively retained enantiomers in human liver. *Fresenius Environ. Bull.* **1998**, *7*, 244–257.
- (53) Maervoet, J.; Covaci, A.; Schepens, P.; Sandau, C. D.; Letcher, R. A reassessment of the nomenclature of polychlorinated biphenyl (PCB) metabolites. *Environ. Health Perspect.* **2004**, *112*, 291–294.
- (54) Wiberg, K.; Letcher, R.; Sandau, C. D.; Duffe, J.; Norstrom, R.; Haglund, P.; Bidleman, T. F. Enantioselective gas chromatography/mass spectrometry of methylsulfonyl PCBs with application of arctic marine mammals. *Anal. Chem.* **1998**, *70*, 3845–3852.
- (55) Chu, S.; Covaci, A.; Schepens, P. Levels and chiral signatures of persistent organochlorine pollutants in human tissues from Belgium. *Environ. Res.* **2003**, *93*, 167–176.
- (56) Glausch, A.; Hahn, J.; Schurig, V. Enantioselective determination of chiral 2,2',3,3',4,6'-hexachlorobiphenyl (PCB 132) in human milk samples by multidimensional gas chromatography/electron capture detection and by mass spectrometry. *Chemosphere* **1995**, *30*, 2079–2085.
- (57) Blanch, G. P.; Glausch, A.; Schurig, V. Determination of the enantiomeric ratios of chiral PCB 95 and 149 in human milk samples by multidimensional gas chromatography with ECD and MS(SIM) detection. *Eur. Food Res. Technol.* **1999**,

- 209, 294–296.
- (58)Bordajandi, L. R.; Abad, E.; Gonzales, M. J. Occurrence of PCBs, PCDD/Fs, PBDEs and DDTs in Spanish breast milk: Enantiomeric fraction of chiral PCBs. *Chemosphere* **2008**, *70*, 567–575.
- (59)Bucheli, T. D.; Brandli, R. C. Two-dimensional gas chromatography coupled to triple quadrupole mass spectrometry for the unambiguous determination of atropisomeric polychlorinated biphenyls in environmental samples. *J. Chromatogr. A* **2006**, *1110*, 156–164.
- (60)Lehmler, H.-J.; Price, D. J.; Garrison, A. W.; Birge, W. J.; Robertson, L. W. Distribution of PCB 84 enantiomers in C57Bl/6 mice. *Fresenius Environ. Bull.* **2003**, *12*, 254–260.
- (61)Kania-Korwel, I.; Shaikh, N.; Hornbuckle, K. C.; Robertson, L. W.; Lehmler, H.-J. Enantioselective disposition of PCB 136 (2,2',3,3',6,6'-hexachlorobiphenyl) in C57BL/6 mice after oral and intraperitoneal administration. *Chirality* **2007**, *19*, 56–66.
- (62)Kania-Korwel, I.; Hornbuckle, K. C.; Robertson, L. W.; Lehmler, H.-J. Dose-dependent enantiomeric enrichment of 2,2',3,3',6,6'-hexachlorobiphenyl in female mice. *Environ. Toxicol. Chem.* **2007**, *27*, 299–305.
- (63)Kania-Korwel, I.; Hornbuckle, K. C.; Robertson, L. W.; Lehmler, H.-J. Influence of dietary fat on the enantioselective disposition of 2,2',3,3',6,6'-hexachlorobiphenyl (PCB 136) in female mice. *Food Chem. Toxicol.* **2008**, *46*, 637–644.
- (64)Kania-Korwel, I.; Xie, W.; Hornbuckle, K. C.; Robertson, L. W.; Lehmler, H.-J. Enantiomeric enrichment of 2,2',3,3',6,6'-hexachlorobiphenyl (PCB 136) in mice

- after induction of CYP enzymes. *Arch. Environ. Contam. Toxicol.* **2008**, *55*, 510–517.
- (65) Milanowski, B.; Lulek, J.; Lehmler, H.-J.; Kania-Korwel, I. Assessment of disposition of chiral polychlorinated biphenyls in female mdr 1a/b knockout versus wild-type mice using multivariate analyses. *Environ. Int.* **2010**, *36*, 884–892.
- (66) Kodavanti, P. R. S., Intracellular signaling and developmental neurotoxicity. In *Molecular Neurotoxicology: Environmental Agents and Transcription-Transduction Coupling*; Zawia, N. H., Ed.; CRC Press: Boca Raton, FL, **2004**; pp 151–182.
- (67) Kania-Korwel, I.; Vyas, S.; Song, Y.; Lehmler, H. J. Gas chromatographic separation of methoxylated polychlorinated biphenyl atropisomers. *J. Chromatogr. A* **2008**, *1207*, 146–154.
- (68) Kania-Korwel, I.; Garrison, A. W.; Avants, J. K.; Hornbuckle, K. C.; Robertson, L. W.; Sulkowski, W. W.; Lehmler, H.-J. Distribution of chiral PCBs in selected tissues in the laboratory rat. *Environ. Sci. Technol.* **2006**, *40*, 3704–3710.
- (69) Pham-Tuan, H.; Larsson, C.; Hoffmann, F.; Bergman, A.; Fröba, M.; Hühnerfuss, H. Enantioselective semipreparative HPLC separation of PCB metabolites and their absolute structure elucidation using electronic and vibrational circular dichroism. *Chirality* **2005**, *17*, 266–280.
- (70) Kania-Korwel, I.; Hrycay, E. G.; Bandiera, S.; Lehmler, H.-J. 2,2',3,3',6,6'-hexachlorobiphenyl (PCB 136) atropisomers interact enantioselectively with hepatic microsomal cytochrome P450 enzymes. *Chem. Res. Toxicol.* **2008**, *21*, 1295–1303.
- (71) Warner, N. A.; Martin, J. W.; Wong, C. S. Chiral polychlorinated biphenyls are biotransformed enantioselectively by mammalian cytochrome P-450 isozymes to form

- hydroxylated metabolites. *Environ. Sci. Technol.* **2009**, *43*, 114–121.
- (72)Letcher, R. J.; Klasson-Wehler, E.; Bergman, A. Methyl sulfone and hydroxylated metabolite of polychlorinated biphenyls. In *The Handbook of Environmental Chemistry - New Types of Persistent Halogenated Compounds*; Passivirta, J., Ed.; Springer-Verlag: Berlin-Heidelberg, **2000**; Vol. 3K, pp 315-359.
- (73)Kato, Y.; Haraguchi, K.; Kawashima, M.; Yamada, S.; Isogai, M.; Masuda, Y.; Kimura, R. Characterization of hepatic microsomal cytochrome P-450 from rats treated with methylsulfonyl metabolites of polychlorinated biphenyl congeners. *Chem. Biol. Interact.* **1995**, *95*, 269–278.
- (74)Kato, Y.; Haraguchi, K.; Tomiyasu, K.; Saito, H.; Isogai, M.; Masuda, Y.; Kimura, R. Structure-dependent induction of CYP2B1/2 by 3-methylsulfonyl metabolites of polychlorinated biphenyl congeners in rats. *Environ. Toxicol. Pharmacol.* **1997**, *3*, 137–144.
- (75)Larsson, C.; Ellerichmann, T.; Hühnerfuss, H.; Bergman, A. Chiral PCB methyl sulfones in rat tissues after exposure to technical PCBs. *Environ. Sci. Technol.* **2002**, *36*, 2833–2838.
- (76)Döbler, J.; Peters, N.; Larsson, C.; Bergman, Å.; Geidel, E.; Hühnerfuss, H. The absolute structures of separated PCB methylsulfone enantiomers determined by vibrational circular dichroism and quantum chemical calculations. *J. Mol. Struct.* **2002**, *586*, 159–166.
- (77)Chu, S.; Covaci, A.; Haraguchi, K.; Voorspoels, S.; van de Vijver, K.; Das, K.; Bouquegneau, J.-M.; de Coen, W.; Blust, R.; Schepens, P. Levels and enantiomeric signatures of methyl sulfonyl PCB and DDE metabolites in livers of harbor porpoises

- (*Phocoena phocoena*) from the Southern North Sea. *Environ. Sci. Technol.* **2003**, *37*, 4573–4578.
- (78)Larsson, C.; Norström, K.; Athanansidais, I.; Bignert, A.; König, W. A.; Bergman, A. Enantiomeric specificity of methylsulfonyl-PCBs and distribution of bis(4-chlorophenyl) sulfone, PCB and DDE methyl sulfones in grey seal tissues. *Environ. Sci. Technol.* **2004**, *38*, 4950–4955.
- (79)Karasek, L.; Hajslova, J.; Rosmus, J.; Hühnerfuss, H. Methylsulfonyl PCB and DDE metabolites and their enantioselective gas chromatographic separation in human adipose tissues, seal blubber and pelican muscle. *Chemosphere* **2007**, *67*, S22–S27.
- (80)Asher, B.J.; Ross, M.S.; Wong, C.S. Tracking chiral polychlorinated biphenyl sources near a hazardous waste incinerator: fresh emissions or weathered revolatilization? *Environ. Toxicol. Chem.* **2012**, *31*, 1453-1460.
- (81)Desborough, J. and Harrad, S. Chiral signatures show volatilization from soil contributes to polychlorinated biphenyls in grass. *Environ. Sci. Technol.* **2011**, *45*, 7354–7357.
- (82)Dang, V.D.; Walters, D.M.; Lee, C.M. Transformation of chiral polychlorinated biphenyls (PCBs) in a stream food web. *Environ Sci Technol.* **2010**, *44*, 2836-2841.
- (83)Zheng, J.; Yan, X.; Chen, S.J.; Peng, X.W.; Hu, G.C.; Chen, K.H.; Luo, X.J.; Mai, B.X.; Yang, Z.Y. Polychlorinated biphenyls in human hair at an e-waste site in China: composition profiles and chiral signatures in comparison to dust. *Environ Int.* **2013**, *54*, 128-133.
- (84)Zhang, Y.; Wu, J.P.; Luo, X.J.; She, Y.Z.; Mo, L.; Mai, B.X. Methylsulfonyl polychlorinated biphenyls in fish from an electronic waste-recycling site

- in South China: levels, congener profiles, and chiral signatures. *Environ. Toxicol. Chem.* **2012**, 31, 2507-2512.
- (85)Cooper,V.I.; Letcher,R.J.; Dietz,R.; Sonne,C.; Wong,C.S. Quantification of achiral and chiral methylsulfonyl polychlorinated biphenyl metabolites by column-switching liquid chromatography-atmospheric pressure photoionization-tandem mass spectrometry. *J. Chromatogr. A.* **2012**, 1268, 64-73.
- (86)Kania-Korwel, I.; Duffel, M.W.; Lehmler, H.-J. Gas chromatographic analysis with chiral cyclodextrin phases reveals the enantioselective formation of hydroxylated polychlorinated biphenyls by rat liver microsomes. *Environ. Sci. Technol.* **2011**, 45, 9590-9596.
- (87)Wayman, G. A.; Bose, D. D.; Yang, D.; Lesiak, A.; Bruun, D.; Impey, S.; Ledoux, V.; Pessah, I. N.; Lein, P. J. PCB-95 modulates the calcium-dependent signaling pathway responsible for activity-dependent dendritic growth. *Environ. Health Perspect.* **2012**, 120, 1003-1009.
- (88)Wayman, G. A.; Yang, D.; Bose, D. D.; Lesiak, A.; Ledoux, V.; Bruun, D.; Pessah, I. N.; Lein, P. J. PCB-95 promotes dendritic growth via ryanodine receptor-dependent mechanisms. *Environ. Health Perspect.* **2012**, 120, 997-1002.
- (89)Kania-Korwel, I.; El-Komy, M.H.;Veng-Pedersen, P.; Lehmler, H.-J. Clearance of polychlorinated biphenyl atropisomers is enantioselective in female C57Bl/6 mice. *Environ Sci Technol.* **2010**, 44, 2828-2835.
- (90)Kania-Korwel, I.; Barnhart C.D.; Stamou M.; Truong K.M.; El-Komy, M.H.; Lein, P.J.; Veng-Pedersen, P.; Lehmler, H.-J. 2,2',3,5',6-Pentachlorobiphenyl (PCB 95) and its hydroxylated metabolites are enantiomerically enriched in female mice. *Environ.*

Sci. Technol. **2012**, *46*, 11393-11401.

(91) Pérez-Fernández, V.; Castro-Puyana, M.; González, M.J.; Marina, M.L.; García, M.Á.; Gómara, B. Simultaneous enantioselective separation of polychlorinated biphenyls and their methyl sulfone metabolites by heart-cut MDGC: determination of enantiomeric fractions in fish oils and cow liver samples. *Chirality* **2012**, *24*, 577-583.

Appendix 2

Operation Procedures for Size and Zeta-potential Measurements of Nanoparticles by Dynamic Light Scattering

Particle Size Distribution Analysis procedures of the ZetaPALS dynamic light scattering (DLS) analyzer (Brookhaven Instruments Corporation, Holtsville, NY, USA)

These procedures were initially written by Jennifer E. Low and modified by Zhe Lu.

1. Turn on the DLS and open “BIC particle sizing software”. Allow the laser to warm up for 25 minutes. Fill in the log book.
2. Do a validation run:
 - a. Put 1 drop of the “Nanosphere Size Standard - 90 nm” (BI-LTX92 from Brookhaven Instruments Corporation) in 20 mL of 1 mM KNO₃ (prepared with HPLC grade water), test results should give a diameter of 92 ± 3 nm.
3. Prepare sample:
 - a. The stock solution of samples (e.g., gold nanoparticles) should be sonicated for 15 minutes before use.
 - b. The stock solution should be filtered by appropriate filters (e.g., 0.2 μm).
 - c. Sonicate the filtered sample for 5 minutes in a sonicator bath.
 - d. Dilution is determined through trial and error. Start low, gold samples were 1:10-1:20 by volume.
 - e. Cuvette choice: quartz for solvents or aqueous solutions, plastic for aqueous only. More plastic cuvettes can be purchased through Brookhaven Instruments Corporation, “Cuvettes, Square, 10 mm, 2.5 mL, polystyrene, four sided, clear, 100 per box, BI-SCP”.
4. Load sample:
 - a. Rinse cuvette with appropriate grade water twice.
 - b. Sonicate the sample again for 5 min before adding it to a cuvette.

- c. Rinse cuvette with sample.
 - d. Load cuvette with sample (+2 mL) and cap the cuvette.
 - e. Clean cuvette well with lens paper (available at Henry's: #120-1580 Kenaston Blvd, Winnipeg, MB R3P 0Y4 - (204) 477-0000, or from VWR, product codes: 52845-009 or 52846-001). DO NOT use Kimwipes as they leave small particles behind that will interfere with results! Keep moisture away from cuvette holder in instrument. This is an expensive repair NOT covered under service warranty.
 - f. Check cuvette for scratches. If any, make sure laser does not impact that side of the cuvette.
 - g. Place cuvette in holder (remember the laser runs from right to left).
 - h. Place black cover on top of cuvette and close the door.
5. Create area to save file on the built-in acquisition computer:
- a. File→Database.
 - b. Create folder or open folder of choice (yymmdd).
 - c. Exit (with the folder of choice open).
6. Set parameters
- a. Click on the parameters button (bottom of screen).
 - b. Fill in:
 - i. Sample ID.
 - ii. Operator (initials).
 - iii. Notes (if required).
 - iv. Runs (will be determined through trial and error).

- v. Temperature (25 °C, if at room temp; 37 °C for enzyme incubations, DLS needs about 10 minutes to increase temperature).
- vi. Liquid (use the drop down menu, if your sample is not available please use 'unspecified' and fill in viscosity and refractive index manually).
- vii. Angle (90.00).
- viii. Dust cutoff (well below sample particle size, 30 nm for the standard, however this is sample-dependent).
- ix. Auto Save Results (Selected).

7. Begin run

- a. Press start.
- b. Allow error box to adjust machine as necessary (do not bypass).

8. Review results:

- a. Information:
 - i. Effective diameter – average size of the particles in the sample.
 - ii. Polydispersity – measure of the non-uniformity within the particle size distribution.
 - iii. Average count rate (Desired range 50-500).
 - iv. Sample Quality/Baseline Index, Baseline Index should be above 8.0.
 - v. Time remaining.
- b. To remove a run from calculation, double click on it (Turns from red to gray).

- c. To re-instate a run for calculation, double click on it again (Turns from gray to red).
- d. Graphs:
 - i. Use the “Zoom” Button to see a larger version. You can also show single runs or combined data by using the appropriate button on the bottom right side).
 - ii. Lognormal, uses the effective diameter and polydispersity to generate a log normal distribution of the particles (diameter vs. intensity).
 - iii. MSD will show diameter vs. intensity and show the user where the size distribution lays (description of size distribution).
 - iv. Corr. Funct (Shows the autocorrelation function).
- e. You can copy this information to the clipboard or spreadsheet as desired.
 - i. To “Copy to spreadsheet”, open Notepad and paste... your values will appear separated by a colon and you can paste this information into an Excel document.
 - ii. You can also access this data at a later time using this software.

9. Clean Up

- a. Solvents should be placed in solvent waste beakers and aqueous solutions may be disposed of down the sink with plenty of water.
- b. Please dispose of plastic cuvettes in the garbage.
- c. Any glassware, should be placed in the glass disposal.
- d. Make sure the cuvette holder is empty and computer is shut off.

e. Clean up your work area.

Zeta potential measurement procedures for the ZetaPALS dynamic light scattering (DLS) analyzer (Brookhaven Instruments Corporation, Holtsville, NY, USA)

These procedures were initially written by Jennifer E. Low and modified by Zhe Lu.

1. Turn on the DLS, and open “BIC Zeta Potential Analyzer”. Allow the laser to warm up for 25 minutes. Fill in the log book.
2. Do a validation run:
 - a. Run BI-ZR3 (BI-ZR3 reference material from Brookhaven Instruments Corporation), in 1 mM KCl (prepared with HPLC grade water). The test solution is prepared in one of three ways: after adding 100 mg of the dry powder to 20 mL of 1 mM KCl, then add 1 mL of this solution to 400 mL of 1mM KCl; or do two sequential 1/20 dilutions to get a 1:400; or measure ~500 μg of BI-ZR3, and dissolve in ~20 mL of 1 mM KCl. Sample conductance should read 320 $\mu\text{S} \pm 10\%$; Zeta Potential should be -49 mV to -57 mV in a single run with the average of many runs -53 ± 4 mV.
3. Prepare sample:
 - a. The stock solution of samples (e.g., gold nanoparticles) should be sonicated for 15 minutes before use.
 - b. The stock solution should be filtered by filters (e.g., 0.2 μm).
 - c. Sonicate the filtered sample for 5 minutes.
 - d. Dilution (dilute the sample properly).
 - e. Cuvette Choice (quartz for solvents or aqueous solutions, plastic for aqueous only. More can be purchased through Brookhaven Instruments

Corporation, “Cuvettes, Square, 10 mm, 2.5 mL, polystyrene, four sided, clear, 100 per box, BI-SCP”)

4. Prepare the electrode (SR-455): The electrode is fragile and can be easily destroyed from carelessness. A replacement will cost \$1,500 and several weeks of time to fill the order. Make sure you are aware of how to use it!
 - a. **Protect the electronics area** of the electrode by placing a paper towel over the electronics area (part that looks like a phone jack). **THE ELECTRONICS CAN BE DESTROYED BY WATER.**
 - b. **Rinse the electrode** (point the electrode down so you avoid water near the electronics and clean the electrode with appropriate grade (or nano pure) water. Use the electrode-cleaning wand (metal wand with red handle and gray Teflon pad) to clean the electrodes. GENTLY place the wand between the electrodes (i.e., in the gap at the bottom) and use the TEFLON-side of the wand to gently wipe off (barely touch) the electrode to remove any build up. **DO NOT TOUCH THE NON-TEFLON SIDE OF THE WAND TO THE ELECTRODE SURFACE** to avoid scratching it.
 - c. Rinse the electrode again with appropriate grade water (no need to use the Teflon wand this time).
 - d. Dry the electrode using lens paper including the space between the two electrodes.
5. Load sample:
 - a. Rinse the cuvette with appropriate grade water twice.
 - b. Sonicate your sample for 5 min before use.

- c. Rinse the cuvette with your sample solution.
 - d. Load the cuvette with 1.5 ml of sample and cap with the electrode, be VERY CAREFUL, do not put the electrode completely into the cuvette. Allow a small space between the top of the cuvette and the electrode to easy disassembly.
 - e. There should be no air bubbles in the sample and the sample should completely cover the electrodes. Gently tap the cuvette to get rid of air bubbles.
 - f. Clean cuvette well with lens paper (available at Henry's: #120-1580 Kenaston Blvd, Winnipeg, MB R3P 0Y4 - (204) 477-0000, or from VWR, product codes: 52845-009 or 52846-001). DO NOT use Kimwipes as they leave small particles behind that will interfere with results! Keep moisture away from cuvette holder in instrument... this is an expensive repair NOT covered under service warranty.
 - g. Place sample in cuvette holder with electronics facing the right and plug in the electrode (remember the laser runs from right to left). Check cuvettes for scratches along pathway of laser.
6. Create area to save file:
 - a. File→Database.
 - b. Create folder or open folder of choice (yymmdd).
 - c. Exit (with the folder of choice open).
 7. Set parameters
 - a. Click on the parameters button (bottom of screen)

- b. Fill in:
 - i. Sample ID.
 - ii. Operator (initials).
 - iii. Notes (if required).
 - iv. pH (if known).
 - v. Concentration (if known).
 - vi. Particle size (if known).
 - vii. Temperature (25 °C, if at room temp; 37 °C for enzyme incubations, DLS needs about 10 minutes to increase temperature).
 - viii. Liquid (use the drop down menu, if your sample is not available please use 'unspecified' and fill in viscosity and refractive index manually).
 - ix. User 1 and User 2 are for you to put any notes you deem necessary
 - x. Auto Save Results (Selected)

8. Begin run

- a. Press start.
- b. Allow error box to adjust machine as necessary (i.e. do not bypass).

9. Review results:

- a. Information:
 - i. Stabilizing Signal-Cycle: (tells you which cycle you are on).
 - ii. Stable readings.
 - iii. Combined Signal.
 - iv. Zeta potential, half width and data retention (in the chart on your

left).

v. Measurement Parameters.

1. Conductance.
2. Current.
3. Electric Field.
4. Sample Count Rate.
5. Ref. Count Rate.
6. Uncorrected Temp. (What you entered).

10. Graphs:

- i. Use the “Zoom” Button to see a larger version. You can also show single runs or combined data by using the appropriate button on the bottom right side.
 - ii. Zeta Potential.
 - iii. Mobility.
 - iv. Frequency Shift.
 - v. Frequency.
- b. You can copy this information to the clipboard or spreadsheet as desired.
- i. To “Copy to spreadsheet”, open notepad and paste... your values will appear separated by a colon and you can paste this information into an excel document.

11. Copy Data to USB key.

12. Clean Up

- a. Clean electrode and place back in box.

- b. Solvents should be placed in the solvent waste beakers and aqueous solutions may be disposed of down the sink with plenty of water.
- c. Please dispose of plastic cuvettes in the garbage.
- d. Any disposable glassware should be placed in glass disposal waste.
- e. Make sure the cuvette holder is empty and computer is shut off.
- f. Clean up your work area.

Appendix 3

GC-MS Chromatogram of Mono- and Di- Hydroxylated Metabolites

(Shown as their Methoxylated Derivatives)

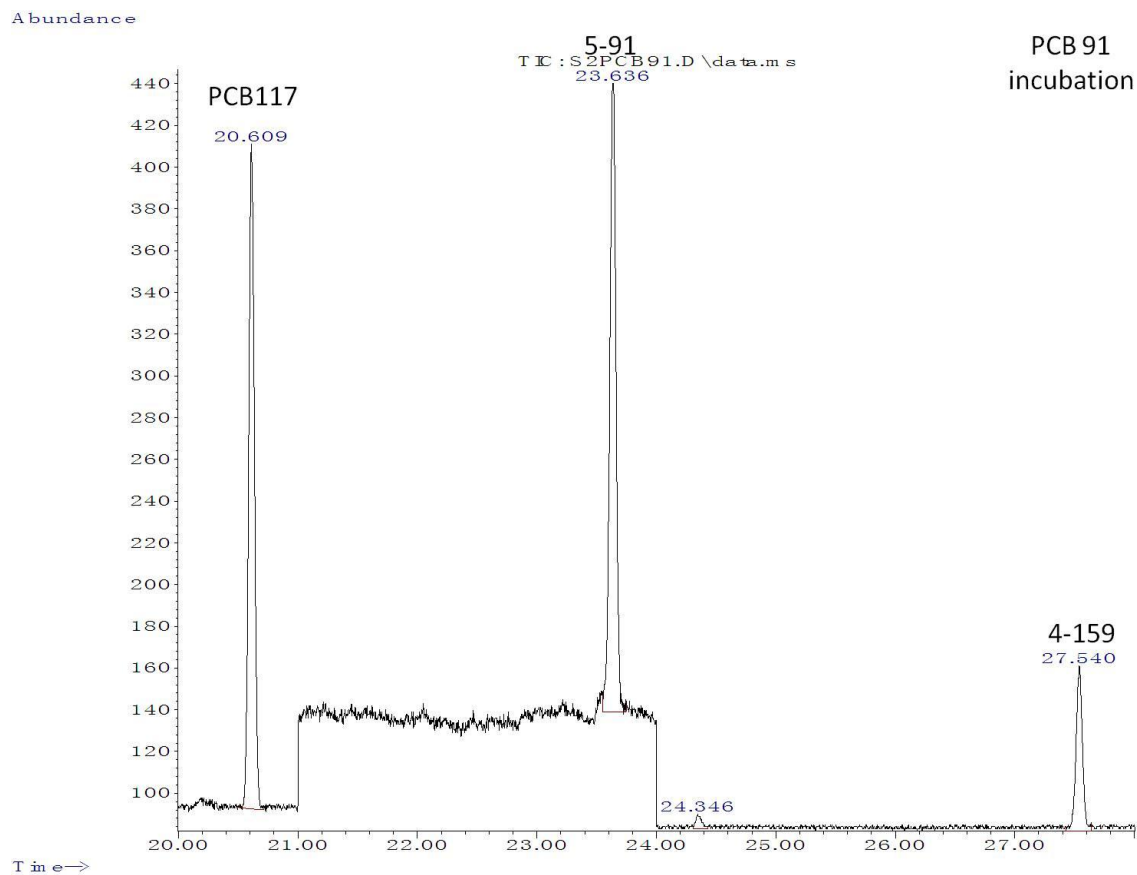


Figure A3.1 Metabolites of PCB 91 formed by rat CYP2B1. GC-MS chromatogram of a PCB 91 incubation sample recorded in SIM mode.

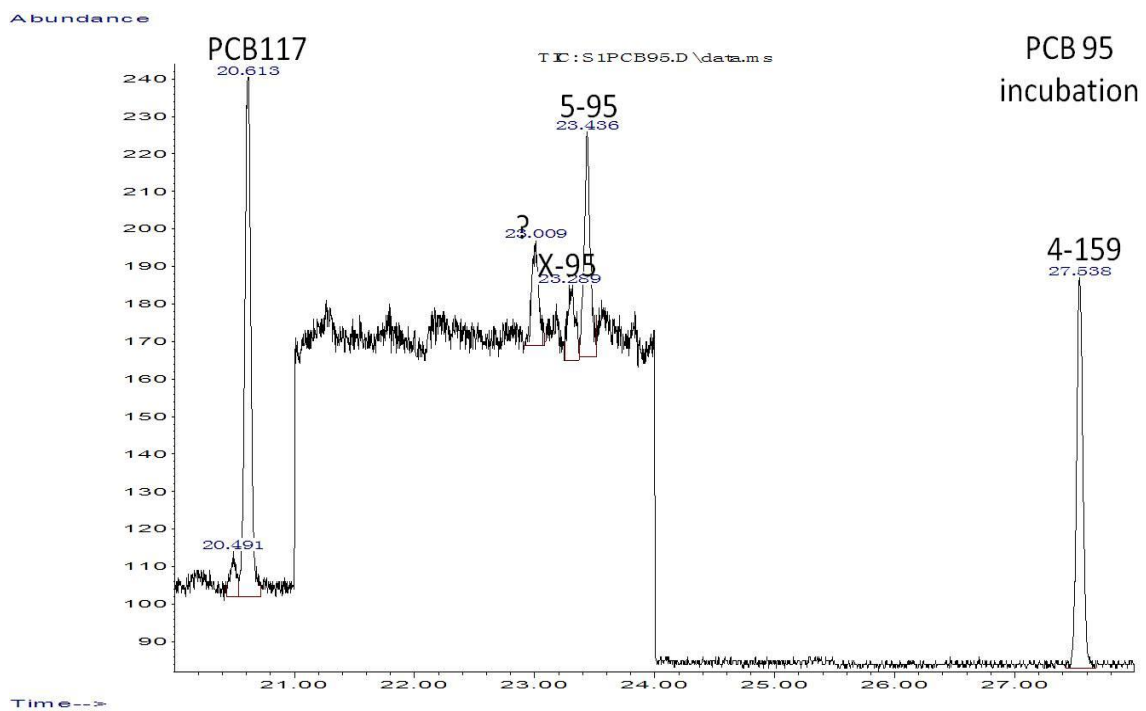


Figure A3.2 Metabolites of PCB 95 formed by rat CYP2B1. GC-MS chromatogram of a PCB 95 incubation sample recorded in SIM mode. Peaks at 23.009 and 23.289 min are currently unidentified mono-hydroxylated metabolites of PCB 95. The peak at 23.289 min (X-95) was previously observed in incubations with rat liver microsomes*.

*Kania-Korwel, I.; Duffel, M. W.; Lehmler, H.-J. Gas chromatographic analysis with chiral cyclodextrin phases reveals the enantioselective formation of hydroxylated polychlorinated biphenyls by rat liver microsomes. *Environ. Sci. Technol.* **2011**, *45*, 9590–9596.

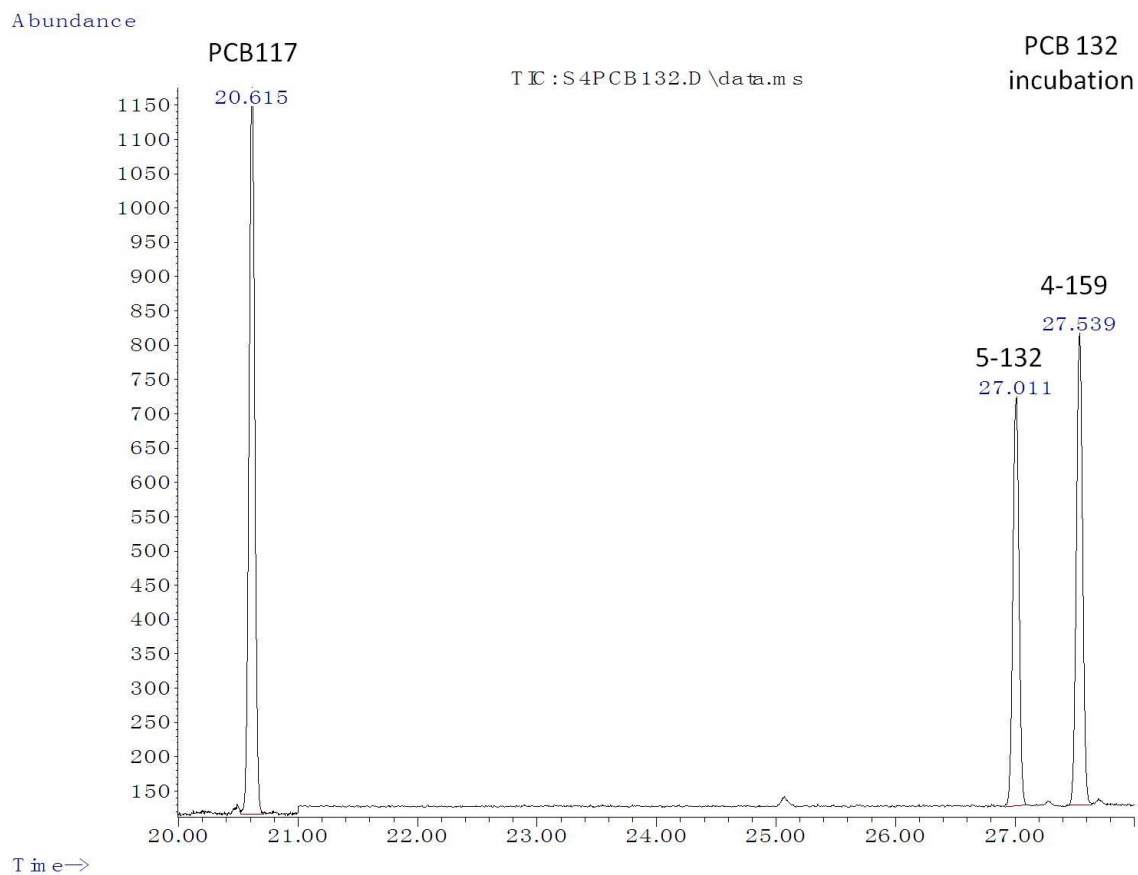


Figure A3.3 Metabolites of PCB 132 formed by rat CYP2B1. GC-MS chromatogram of a PCB 132 incubation sample recorded in SIM mode.

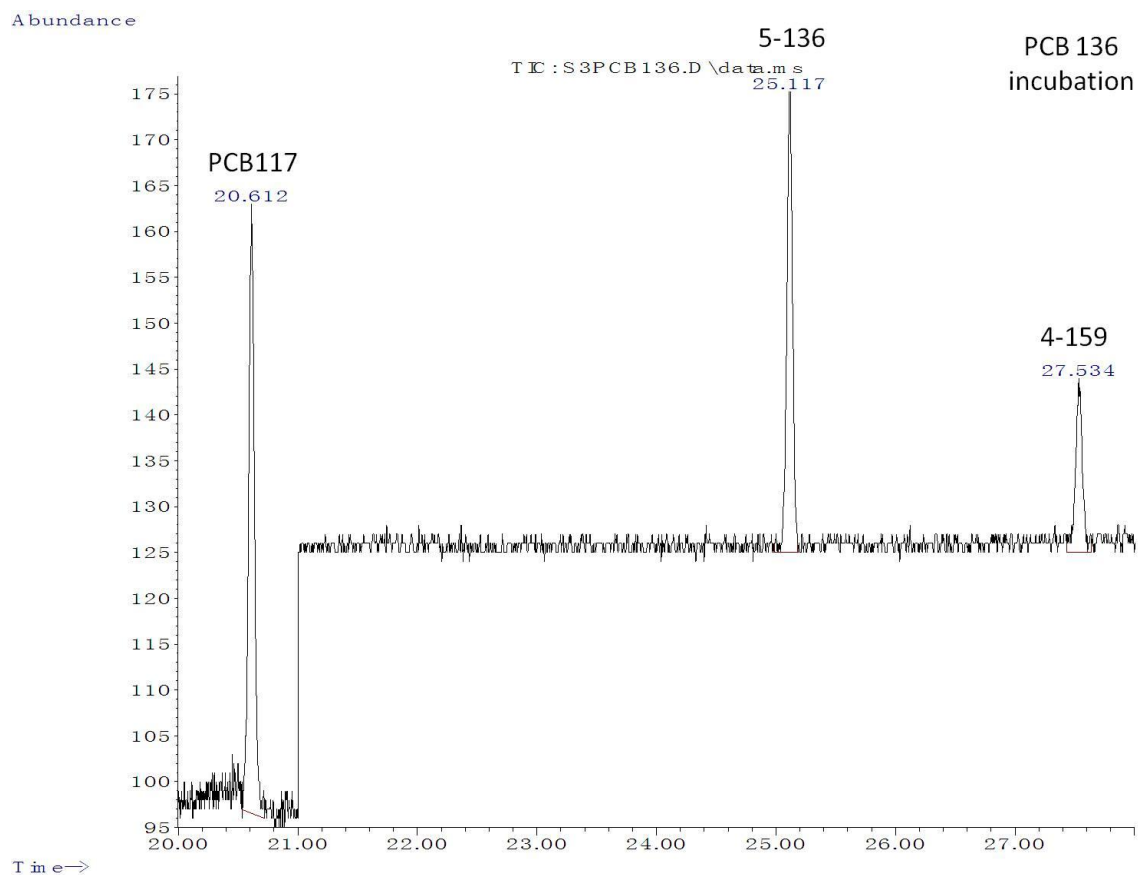


Figure A3.4 Metabolites of PCB 136 formed by rat CYP2B1. GC-MS chromatogram of a PCB 136 incubation sample were recorded in SIM mode.

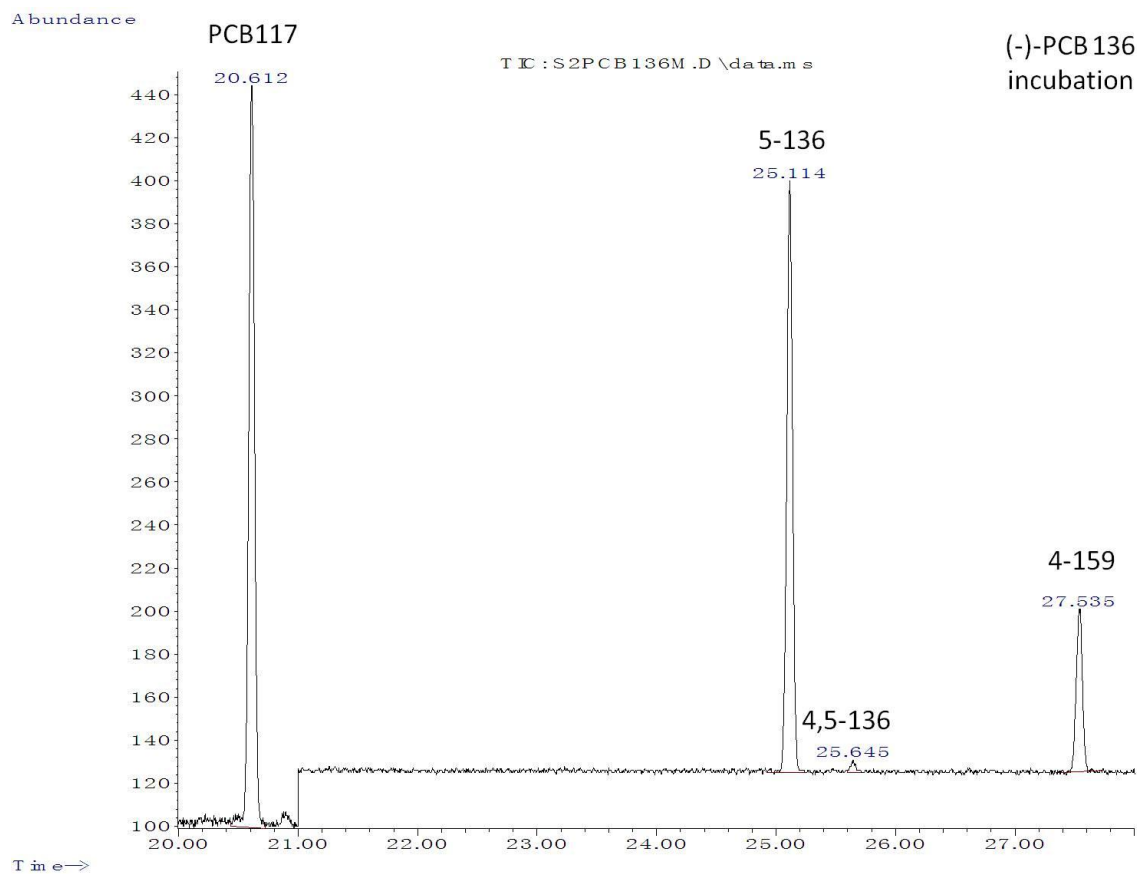


Figure A3.5 Metabolites of (-)-PCB 136 formed by rat CYP2B1. GC-MS chromatogram of a (-)-PCB 136 incubation sample recorded in SIM mode.

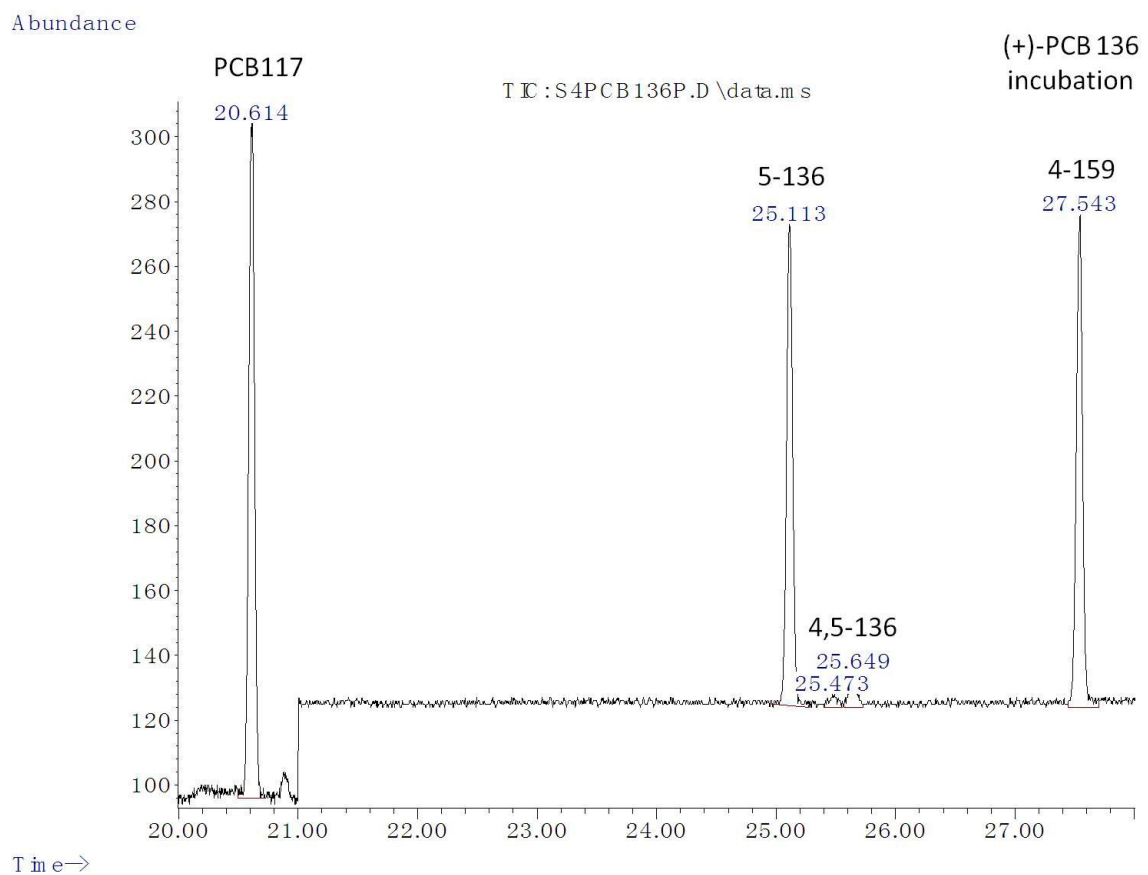


Figure A3.6 Metabolites of (+)-PCB 136 formed by rat CYP2B1. GC-MS chromatogram of a (+)-PCB 136 incubation sample recorded in SIM mode.

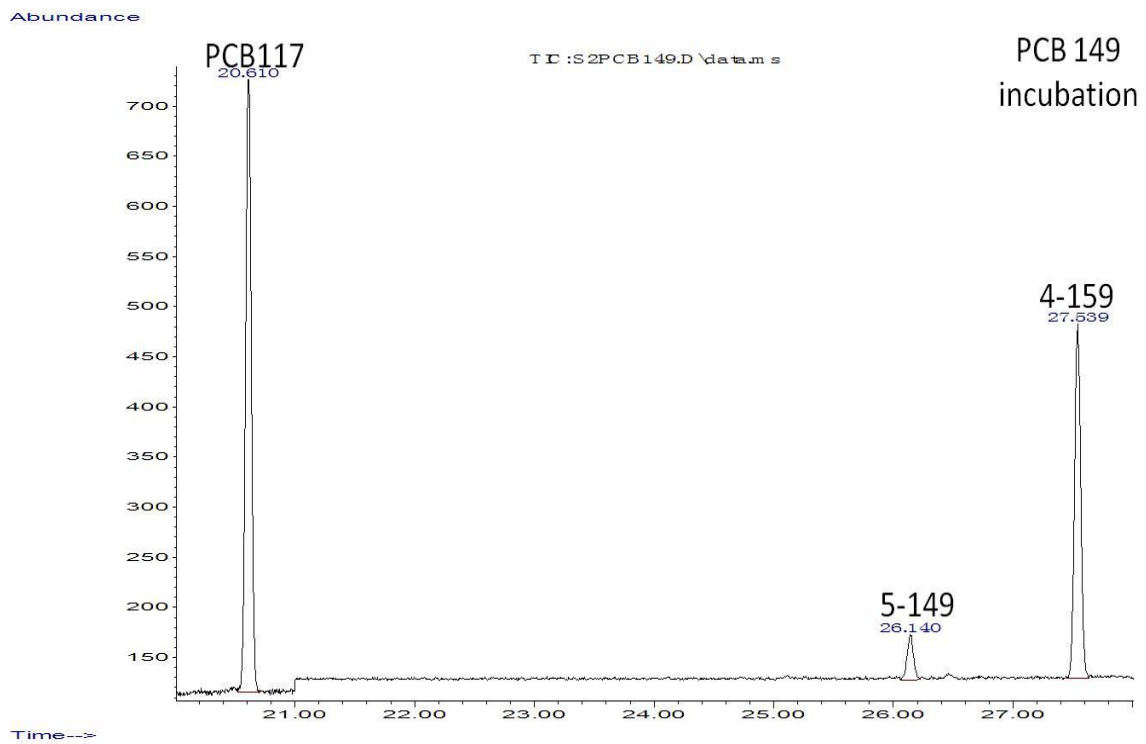


Figure A3.7 Metabolites of PCB 149 formed by rat CYP2B1. GC-MS chromatogram of a PCB 149 incubation sample recorded in SIM mode.

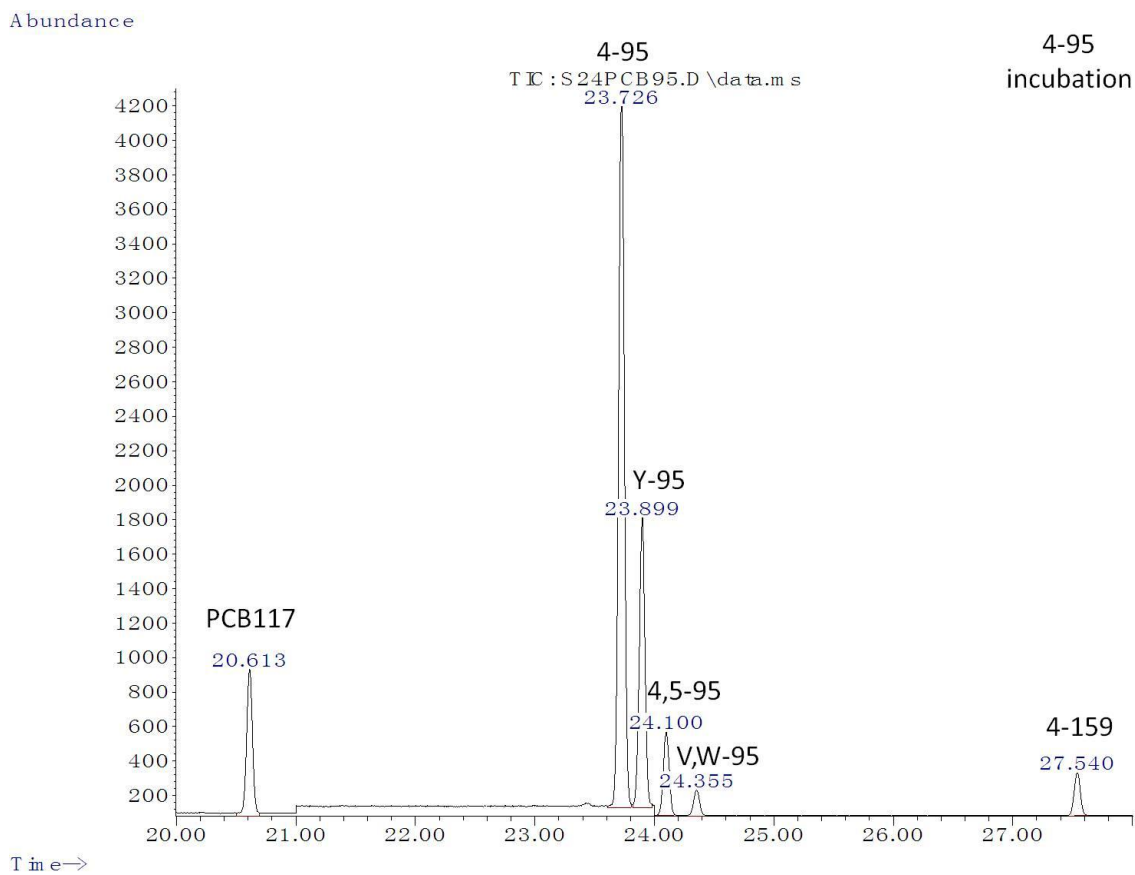


Figure A3.8: Metabolites of 4-95 formed by rat CYP2B1. GC-MS chromatogram of a 4-95 incubation sample recorded in SIM mode. The peak at 23.899 min (Y-95) is a currently unidentified mono-hydroxylated metabolite. The peak at 24.355 min (V,W-95) is a unknown dihydroxylated metabolite.

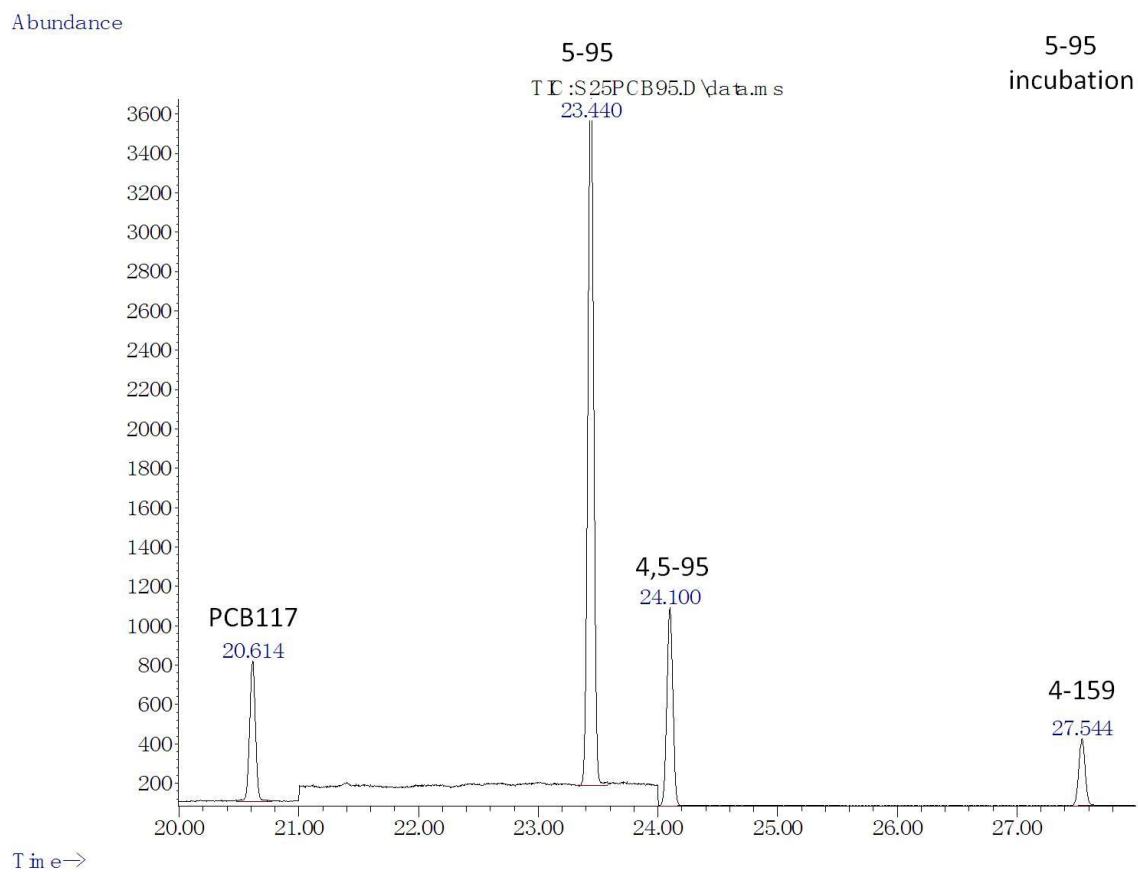


Figure A3.9 Metabolites of 5-95 formed by rat CYP2B1. GC-MS chromatogram of a 5-PCB 95 incubation sample recorded in SIM mode.

Appendix 4

PCB Concentrations and Trophic Levels of Cumberland Sound (Canada) Organisms Collected from 2007-2008

Appendix 4. Concentration and trophic level data was analyzed and provided by Dr. Aaron T. Fisk. and Dr. Gregg T. Tomy. N.D. = not detected. TL is the abbreviation of trophic level. PCB congeners are presented as **bold** numbers.

Capelin		Recovery %	Recovery %	PCB concentrations (ng/g) wet weight			
Samples	Lipid %	PCB 30	PCB 204	1	3	4/10	7
CA 14	2.14	8.54×10^1	7.00×10^1	N.D.	N.D.	1.43×10^{-2}	7.07×10^{-3}
CA 17	2.65	1.10×10^2	1.04×10^2	N.D.	N.D.	N.D.	1.52×10^{-1}
CA 18	1.31	1.33×10^2	1.04×10^2	N.D.	N.D.	4.84×10^{-2}	7.77×10^{-1}
CA 22	5.10	9.35×10^1	8.31×10^1	N.D.	N.D.	N.D.	3.73×10^{-2}
CA 23	2.10	1.46×10^2	1.06×10^2	N.D.	N.D.	N.D.	N.D.
	6	8/5	19	18	17	24/27	16/32
CA 14	1.72×10^{-1}	N.D.	N.D.	2.12×10^{-2}	1.17×10^{-2}	N.D.	1.75×10^{-2}
CA 17	N.D.	1.65×10^{-1}	N.D.	1.30×10^{-1}	4.34×10^{-2}	N.D.	3.72×10^{-3}
CA 18	3.99×10^{-1}	N.D.	N.D.	1.25×10^{-1}	3.75×10^{-2}	N.D.	1.07×10^{-1}
CA 22	N.D.	N.D.	N.D.	1.75×10^{-2}	N.D.	N.D.	1.64×10^{-2}
CA 23	2.84×10^{-1}	N.D.	N.D.	7.04×10^{-1}	6.27×10^{-1}	N.D.	3.17×10^{-1}

	26	25	31	28	33	22	45
CA 14	2.16×10^{-2}	8.42×10^{-2}	2.31×10^{-1}	4.52×10^{-2}	8.29×10^{-2}	N.D.	N.D.
CA 17	7.62×10^{-2}	1.72×10^{-1}	7.37×10^{-1}	1.05×10^{-1}	1.82×10^{-1}	1.83×10^{-1}	N.D.
CA 18	1.28×10^{-1}	2.18×10^{-1}	5.15×10^{-1}	4.70×10^{-2}	1.51×10^{-1}	N.D.	9.71×10^{-2}
CA 22	N.D.	N.D.	4.29×10^{-2}	4.58×10^{-2}	N.D.	N.D.	5.91×10^{-2}
CA 23	1.36	2.31	1.09	2.66×10^{-1}	1.52	2.27×10^{-1}	5.05×10^{-1}
	46	52	49	47	48	44	42
CA 14	N.D.	5.82×10^{-2}	3.51×10^{-2}	2.56×10^{-2}	N.D.	6.13×10^{-2}	2.93×10^{-2}
CA 17	5.00×10^{-2}	7.12×10^{-2}	1.05×10^{-1}	7.19×10^{-2}	N.D.	1.04×10^{-1}	3.40×10^{-2}
CA 18	1.57×10^{-2}	4.56×10^{-2}	1.17×10^{-1}	1.28×10^{-1}	N.D.	7.10×10^{-2}	2.90×10^{-2}
CA 22	5.28×10^{-2}	9.61×10^{-2}	3.97×10^{-2}	2.51×10^{-2}	N.D.	7.49×10^{-2}	5.17×10^{-2}
CA 23	N.D.	6.24×10^{-1}	6.06×10^{-1}	4.95×10^{-1}	N.D.	3.78×10^{-1}	N.D.
	41/71	64	40	74	70/76	66	95

CA 14	3.76×10^{-2}	8.61×10^{-2}	7.21×10^{-3}	6.08×10^{-2}	1.23×10^{-1}	N.D.	2.63×10^{-1}
CA 17	N.D.	1.77×10^{-1}	N.D.	8.72×10^{-2}	2.19×10^{-1}	N.D.	3.84×10^{-1}
CA 18	6.69×10^{-2}	7.61×10^{-2}	N.D.	1.14×10^{-1}	8.37×10^{-2}	N.D.	1.61×10^{-1}
CA 22	N.D.	8.97×10^{-2}	N.D.	6.24×10^{-2}	6.10×10^{-2}	N.D.	1.84×10^{-1}
CA 23	N.D.	3.00×10^{-1}	N.D.	2.11×10^{-1}	1.82×10^{-1}	N.D.	1.40
	56/60	91	84/89	101	99	83	97
CA 14	1.39×10^{-1}	1.38×10^{-2}	7.60×10^{-2}	8.66×10^{-2}	5.55×10^{-2}	1.58×10^{-2}	2.22×10^{-3}
CA 17	N.D.	1.58×10^{-2}	N.D.	8.57×10^{-2}	5.22×10^{-2}	5.33×10^{-2}	4.50×10^{-2}
CA 18	4.54×10^{-3}	N.D.	N.D.	6.82×10^{-2}	3.67×10^{-2}	4.38×10^{-2}	3.52×10^{-2}
CA 22	8.30×10^{-2}	3.01×10^{-2}	2.09×10^{-1}	8.68×10^{-2}	8.58×10^{-2}	3.98×10^{-2}	3.08×10^{-2}
CA 23	N.D.	5.05×10^{-1}	2.96×10^{-1}	3.60×10^{-1}	3.40×10^{-1}	N.D.	2.54×10^{-1}
	87	85	136	110	82	151	144/135
CA 14	7.37×10^{-2}	3.94×10^{-2}	6.51×10^{-2}	1.54×10^{-1}	1.79×10^{-2}	2.25×10^{-2}	1.06×10^{-2}

CA 17	9.79×10^{-2}	4.03×10^{-2}	N.D.	1.94×10^{-1}	N.D.	2.21×10^{-2}	N.D.
CA 18	1.43×10^{-1}	2.18×10^{-2}	N.D.	1.80×10^{-1}	N.D.	4.25×10^{-2}	N.D.
CA 22	1.61×10^{-1}	4.51×10^{-2}	N.D.	7.49×10^{-2}	N.D.	1.88×10^{-2}	4.77×10^{-2}
CA 23	6.18×10^{-1}	1.39×10^{-1}	N.D.	1.30	N.D.	3.39×10^{-2}	4.42×10^{-2}
	149	118	134	114	131	146	153
CA 14	3.60×10^{-2}	2.30×10^{-1}	N.D.	1.15×10^{-2}	N.D.	1.17×10^{-2}	7.67×10^{-2}
CA 17	9.62×10^{-2}	7.07×10^{-1}	N.D.	1.67×10^{-1}	N.D.	N.D.	1.48×10^{-1}
CA 18	1.04×10^{-1}	4.89×10^{-1}	N.D.	2.43×10^{-2}	N.D.	2.43×10^{-2}	1.40×10^{-1}
CA 22	5.31×10^{-2}	9.57×10^{-1}	N.D.	1.79×10^{-2}	1.43×10^{-2}	2.29×10^{-2}	8.74×10^{-2}
CA 23	6.14×10^{-1}	1.97	N.D.	N.D.	N.D.	1.72×10^{-1}	1.44
	132	105	141	179	137	130/176	138
CA 14	2.36×10^{-2}	2.97×10^{-2}	1.74×10^{-2}	N.D.	N.D.	5.02×10^{-2}	1.26×10^{-1}
CA 17	3.45×10^{-2}	3.35×10^{-2}	4.20×10^{-2}	1.49×10^{-2}	N.D.	N.D.	1.74×10^{-1}

CA 18	4.58×10^{-2}	3.90×10^{-2}	3.15×10^{-2}	1.39×10^{-2}	6.98×10^{-3}	N.D.	2.18×10^{-1}
CA 22	2.27×10^{-2}	N.D.	1.85×10^{-2}	N.D.	3.86×10^{-2}	1.48×10^{-1}	1.78×10^{-1}
CA 23	4.53×10^{-1}	7.07×10^{-1}	8.35×10^{-1}	1.07×10^{-1}	N.D.	3.54×10^{-1}	2.85
	158	178/129	175	187	183	128	185
CA 14	1.19×10^{-2}	N.D.	2.95×10^{-3}	2.04×10^{-2}	1.13×10^{-2}	1.01×10^{-2}	N.D.
CA 17	N.D.	N.D.	N.D.	2.56×10^{-2}	N.D.	9.45×10^{-3}	N.D.
CA 18	1.44×10^{-2}	N.D.	N.D.	3.27×10^{-2}	1.37×10^{-2}	1.53×10^{-2}	N.D.
CA 22	N.D.	1.90×10^{-2}	N.D.	2.61×10^{-2}	N.D.	N.D.	N.D.
CA 23	4.17×10^{-1}	2.15×10^{-1}	N.D.	1.54×10^{-1}	6.00×10^{-2}	1.55×10^{-1}	N.D.
	174	177	171/156	201/157	172/197	180	193
CA 14	1.84×10^{-2}	1.56×10^{-2}	3.09×10^{-4}	N.D.	5.13×10^{-2}	1.91×10^{-2}	N.D.
CA 17	4.43×10^{-2}	1.47×10^{-1}	N.D.	N.D.	N.D.	2.21×10^{-2}	N.D.
CA 18	1.82×10^{-2}	5.75×10^{-2}	N.D.	N.D.	N.D.	9.82×10^{-3}	N.D.

CA 22	N.D.	N.D.	N.D.	N.D.	N.D.	N.D.	N.D.
CA 23	2.52×10^{-1}	1.55×10^{-1}	7.78×10^{-2}	N.D.	N.D.	1.27×10^{-1}	1.21×10^{-2}
	191	200	170	190	198	199	196/203
CA 14	N.D.	N.D.	5.09×10^{-3}	N.D.	N.D.	N.D.	N.D.
CA 17	N.D.	N.D.	N.D.	N.D.	N.D.	N.D.	N.D.
CA 18	N.D.	N.D.	N.D.	N.D.	N.D.	N.D.	N.D.
CA 22	N.D.	N.D.	N.D.	N.D.	N.D.	N.D.	N.D.
CA 23	N.D.	N.D.	3.66×10^{-2}	N.D.	N.D.	N.D.	N.D.
	189	208	195	207	194	205	206
CA 14	N.D.	N.D.	N.D.	N.D.	N.D.	N.D.	N.D.
CA 17	N.D.	N.D.	N.D.	N.D.	N.D.	N.D.	N.D.
CA 18	N.D.	N.D.	N.D.	N.D.	N.D.	N.D.	N.D.
CA 22	N.D.	N.D.	N.D.	N.D.	N.D.	N.D.	N.D.

CA 23	N.D.	N.D.	N.D.	N.D.	N.D.	N.D.	N.D.
	209	TL					
CA 14	N.D.	2.74					
CA 17	N.D.	2.71					
CA 18	N.D.	2.70					
CA 22	N.D.	2.75					
CA 23	N.D.	2.72					

Herring		Recovery %	Recovery %	PCB concentrations (ng/g) wet weight			
Samples	Lipid %	PCB 30	PCB 204	1	3	4/10	7
HE 1	2.15	1.04×10^2	5.70×10^1	N.D.	N.D.	4.61×10^{-2}	N.D.
	6	8/5	19	18	17	24/27	16/32
HE 1	N.D.	N.D.	N.D.	N.D.	N.D.	N.D.	N.D.
	26	25	31	28	33	22	45
HE 1	9.55×10^{-3}	9.02×10^{-2}	1.15	7.71×10^{-2}	N.D.	2.26×10^{-1}	2.61×10^{-1}
	46	52	49	47	48	44	42
HE 1	N.D.	3.23×10^{-1}	1.16×10^{-1}	8.70×10^{-2}	N.D.	1.40×10^{-1}	5.30×10^{-2}
	41/71	64	40	74	70/76	66	95
HE 1	N.D.	2.57×10^{-1}	3.99×10^{-2}	1.82×10^{-1}	4.01×10^{-1}	N.D.	8.03×10^{-1}
	56/60	91	84/89	101	99	83	97
HE 1	2.38×10^{-1}	5.57×10^{-2}	2.84×10^{-1}	4.47×10^{-1}	1.88×10^{-1}	1.61×10^{-1}	1.01×10^{-1}

	87	85	136	110	82	151	144/135
HE 1	1.98×10^{-1}	2.63×10^{-1}	5.32×10^{-2}	7.26×10^{-1}	3.23×10^{-2}	1.39×10^{-1}	1.10×10^{-1}
	149	118	134	114	131	146	153
HE 1	2.74×10^{-1}	1.69	N.D.	1.91×10^{-1}	N.D.	5.69×10^{-2}	6.66×10^{-1}
	132	105	141	179	137	130/176	138
HE 1	1.28×10^{-1}	8.08×10^{-2}	8.15×10^{-2}	1.20×10^{-2}	N.D.	4.02×10^{-1}	6.80×10^{-1}
	158	178/129	175	187	183	128	185
HE 1	N.D.	3.39×10^{-2}	N.D.	1.21×10^{-1}	4.83×10^{-2}	2.27×10^{-2}	N.D.
	174	177	171/156	201/157	172/197	180	193
HE 1	8.46×10^{-2}	1.12×10^{-1}	N.D.	N.D.	N.D.	1.38×10^{-1}	N.D.
	191	200	170	1.90×10^2	198	199	196/203
HE 1	N.D.	N.D.	N.D.	N.D.	N.D.	N.D.	N.D.
	189	208	195	207	194	205	206

HE 1	N.D.	N.D.	N.D.	N.D.	N.D.	N.D.	N.D.
	209	TL					
HE 1	N.D.	2.65					

Scallop		Recovery %	Recovery %	PCB concentrations (ng/g) wet weight			
Samples	Lipid %	PCB 30	PCB 204	1	3	4/10	7
SCA 1	5.80×10^{-2}	9.06×10^1	1.20×10^2	N.D.	N.D.	N.D.	N.D.
SCA 2	1.01×10^{-1}	8.20×10^1	8.13×10^1	N.D.	N.D.	N.D.	2.76×10^{-2}
SCA 3	1.11×10^{-1}	6.93×10^1	7.15×10^1	N.D.	N.D.	N.D.	N.D.
SCA 4	1.67×10^{-1}	7.09×10^1	6.90×10^1	N.D.	N.D.	N.D.	N.D.
SCA 6	3.58×10^{-1}	7.28×10^1	5.81×10^1	N.D.	N.D.	N.D.	N.D.
SCA 7	9.68×10^{-2}	9.79×10^1	6.92×10^1	N.D.	N.D.	N.D.	N.D.
SCA 8	no measureable lipid	1.49×10^2	5.75×10^1	N.D.	N.D.	N.D.	N.D.
	6	8/5	19	18	17	24/27	16/32
SCA 1	N.D.	N.D.	N.D.	1.09×10^{-2}	N.D.	N.D.	2.39×10^{-3}
SCA 2	N.D.	N.D.	N.D.	1.06×10^{-2}	N.D.	N.D.	4.35×10^{-3}
SCA 3	N.D.	N.D.	N.D.	N.D.	N.D.	N.D.	N.D.

SCA 4	N.D.	N.D.	N.D.	N.D.	N.D.	N.D.	N.D.
SCA 6	N.D.	N.D.	N.D.	N.D.	N.D.	N.D.	8.79×10^{-2}
SCA 7	N.D.	N.D.	N.D.	2.10×10^{-1}	N.D.	N.D.	9.35×10^{-2}
SCA 8	1.23×10^{-1}	N.D.	N.D.	5.71×10^{-1}	1.06×10^{-1}	2.25×10^{-2}	3.04×10^{-1}
	26	25	31	28	33	22	45
SCA 1	N.D.	9.89×10^{-3}	N.D.	4.35×10^{-3}	N.D.	N.D.	N.D.
SCA 2	N.D.	5.63×10^{-3}	5.87×10^{-3}	5.16×10^{-3}	6.16×10^{-3}	5.79×10^{-3}	N.D.
SCA 3	N.D.	2.98×10^{-2}	5.95×10^{-2}	8.53×10^{-2}	N.D.	4.06×10^{-2}	N.D.
SCA 4	N.D.	N.D.	N.D.	3.89×10^{-2}	N.D.	N.D.	N.D.
SCA 6	N.D.	5.45×10^{-2}	2.57×10^{-1}	N.D.	N.D.	N.D.	N.D.
SCA 7	3.79×10^{-2}	3.07×10^{-2}	3.91×10^{-2}	3.69×10^{-2}	N.D.	N.D.	N.D.
SCA 8	2.14×10^{-1}	3.85×10^{-1}	1.46×10^{-1}	3.73×10^{-2}	2.28×10^{-1}	N.D.	1.24×10^{-1}
	46	52	49	47	48	44	42

SCA 1	N.D.	2.52×10^{-2}	6.22×10^{-3}	8.11×10^{-3}	N.D.	1.01×10^{-2}	3.87×10^{-3}
SCA 2	N.D.	1.39×10^{-2}	4.34×10^{-3}	6.36×10^{-3}	N.D.	9.56×10^{-3}	4.38×10^{-3}
SCA 3	N.D.	1.74×10^{-2}	4.86×10^{-4}	5.88×10^{-2}	N.D.	3.10×10^{-2}	3.06×10^{-2}
SCA 4	N.D.	2.46×10^{-2}	6.17×10^{-3}	N.D.	1.76×10^{-2}	3.83×10^{-2}	2.78×10^{-2}
SCA 6	N.D.	6.90×10^{-2}	1.42×10^{-2}	N.D.	N.D.	1.46×10^{-1}	1.45×10^{-1}
SCA 7	N.D.	4.86×10^{-3}	2.90×10^{-3}	N.D.	7.83×10^{-2}	N.D.	N.D.
SCA 8	N.D.	4.50×10^{-2}	2.13×10^{-1}	2.25×10^{-1}	1.25×10^{-1}	3.91×10^{-2}	N.D.
	41/71	64	40	74	70/76	66	95
SCA 1	N.D.	1.35×10^{-2}	N.D.	1.48×10^{-2}	2.72×10^{-2}	N.D.	2.18×10^{-2}
SCA 2	4.71×10^{-3}	1.08×10^{-2}	3.53×10^{-3}	1.91×10^{-2}	3.66×10^{-2}	N.D.	3.56×10^{-2}
SCA 3	N.D.	1.53×10^{-2}	N.D.	4.42×10^{-2}	7.95×10^{-2}	N.D.	1.24×10^{-1}
SCA 4	N.D.	2.54×10^{-1}	N.D.	N.D.	6.48×10^{-2}	N.D.	7.54×10^{-2}
SCA 6	N.D.	1.44	N.D.	1.82×10^{-1}	4.03×10^{-1}	N.D.	3.19×10^{-1}

SCA 7	N.D.	N.D.	N.D.	N.D.	5.17×10^{-2}	N.D.	8.23×10^{-2}
SCA 8	N.D.	1.59×10^{-2}	N.D.	N.D.	N.D.	7.29×10^{-2}	N.D.
	56/60	91	84/89	101	99	83	97
SCA 1	2.03×10^{-2}	N.D.	1.08×10^{-2}	1.02×10^{-2}	1.18×10^{-2}	N.D.	4.58×10^{-3}
SCA 2	2.84×10^{-2}	3.63×10^{-3}	5.00×10^{-3}	9.84×10^{-3}	1.43×10^{-2}	4.71×10^{-3}	6.58×10^{-3}
SCA 3	7.92×10^{-2}	N.D.	N.D.	5.24×10^{-2}	3.39×10^{-2}	N.D.	2.94×10^{-2}
SCA 4	9.42×10^{-2}	N.D.	N.D.	3.15×10^{-2}	1.83×10^{-2}	N.D.	N.D.
SCA 6	1.70×10^{-1}	N.D.	N.D.	1.80×10^{-1}	1.50×10^{-1}	N.D.	9.31×10^{-2}
SCA 7	N.D.	N.D.	N.D.	6.84×10^{-2}	4.80×10^{-2}	N.D.	N.D.
SCA 8	4.92×10^{-2}	N.D.	N.D.	5.32×10^{-2}	2.70×10^{-2}	1.79×10^{-1}	1.48×10^{-1}
	87	85	136	110	82	151	144/135
SCA 1	9.22×10^{-3}	5.74×10^{-3}	N.D.	1.96×10^{-2}	2.42×10^{-3}	2.28×10^{-3}	N.D.
SCA 2	1.34×10^{-2}	4.81×10^{-3}	3.79×10^{-3}	2.54×10^{-2}	1.56×10^{-3}	1.86×10^{-3}	1.79×10^{-3}

SCA 3	6.19×10^{-2}	N.D.	N.D.	1.40×10^{-1}	2.41×10^{-2}	2.94×10^{-2}	1.73×10^{-2}
SCA 4	3.02×10^{-2}	N.D.	N.D.	8.70×10^{-2}	N.D.	1.75×10^{-2}	N.D.
SCA 6	2.81×10^{-1}	1.21×10^{-1}	N.D.	7.78×10^{-1}	N.D.	4.47×10^{-2}	5.47×10^{-2}
SCA 7	9.69×10^{-2}	N.D.	N.D.	2.08×10^{-1}	N.D.	1.53×10^{-2}	N.D.
SCA 8	1.50×10^{-1}	N.D.	N.D.	8.64×10^{-2}	N.D.	4.24×10^{-2}	N.D.
	149	118	134	114	131	146	153
SCA 1	5.89×10^{-3}	7.82×10^{-3}	N.D.	N.D.	N.D.	N.D.	6.23×10^{-3}
SCA 2	1.01×10^{-2}	1.53×10^{-2}	N.D.	1.72×10^{-3}	N.D.	1.36×10^{-3}	1.27×10^{-2}
SCA 3	1.00×10^{-1}	1.32×10^{-1}	N.D.	3.28×10^{-2}	N.D.	2.11×10^{-2}	1.61×10^{-1}
SCA 4	6.92×10^{-2}	5.91×10^{-2}	N.D.	N.D.	N.D.	N.D.	8.34×10^{-2}
SCA 6	3.61×10^{-1}	8.20×10^{-1}	N.D.	1.56×10^{-1}	N.D.	1.81×10^{-1}	5.99×10^{-1}
SCA 7	1.28×10^{-1}	2.22×10^{-1}	N.D.	2.71×10^{-2}	N.D.	2.75×10^{-2}	2.30×10^{-1}
SCA 8	8.99×10^{-2}	7.63×10^{-2}	N.D.	N.D.	N.D.	N.D.	7.53×10^{-2}

	132	105	141	179	137	130/176	138
SCA 1	N.D.	5.48×10^{-3}	1.19×10^{-3}	N.D.	N.D.	N.D.	1.17×10^{-2}
SCA 2	4.00×10^{-3}	6.41×10^{-3}	4.31×10^{-3}	1.32×10^{-3}	N.D.	N.D.	1.73×10^{-2}
SCA 3	5.99×10^{-2}	1.24×10^{-1}	5.09×10^{-2}	1.84×10^{-2}	N.D.	8.78×10^{-2}	3.36×10^{-1}
SCA 4	N.D.	3.32×10^{-2}	1.98×10^{-2}	N.D.	1.37×10^{-2}	N.D.	9.17×10^{-2}
SCA 6	2.83×10^{-1}	4.16×10^{-1}	1.50×10^{-1}	N.D.	2.54×10^{-1}	1.48×10^{-1}	1.27
SCA 7	7.93×10^{-2}	1.13×10^{-1}	4.05×10^{-2}	N.D.	N.D.	N.D.	3.25×10^{-1}
SCA 8	N.D.	N.D.	1.26×10^{-2}	N.D.	N.D.	N.D.	8.10×10^{-2}
	158	178/129	175	187	183	128	185
SCA 1	N.D.	N.D.	N.D.	1.75×10^{-3}	N.D.	N.D.	N.D.
SCA 2	1.89×10^{-3}	N.D.	N.D.	2.19×10^{-3}	1.01×10^{-3}	N.D.	N.D.
SCA 3	5.17×10^{-2}	4.05×10^{-2}	N.D.	2.98×10^{-2}	1.96×10^{-2}	5.15×10^{-2}	4.42×10^{-3}
SCA 4	N.D.	N.D.	N.D.	1.50×10^{-2}	N.D.	6.83×10^{-2}	N.D.

SCA 6	1.29×10^{-1}	N.D.	N.D.	7.83×10^{-2}	3.68×10^{-2}	7.22×10^{-2}	N.D.
SCA 7	2.07×10^{-2}	N.D.	N.D.	3.62×10^{-2}	N.D.	N.D.	N.D.
SCA 8	N.D.	N.D.	N.D.	1.83×10^{-2}	N.D.	N.D.	N.D.
	174	177	171/156	201/157	172/197	180	193
SCA 1	3.02×10^{-3}	N.D.	N.D.	N.D.	N.D.	1.24×10^{-3}	N.D.
SCA 2	2.10×10^{-3}	N.D.	1.49×10^{-3}	N.D.	N.D.	2.66×10^{-3}	2.65×10^{-4}
SCA 3	4.58×10^{-2}	2.76×10^{-2}	1.38×10^{-2}	N.D.	N.D.	3.95×10^{-2}	3.70×10^{-3}
SCA 4	2.37×10^{-2}	N.D.	N.D.	N.D.	N.D.	1.13×10^{-2}	N.D.
SCA 6	1.04×10^{-1}	7.07×10^{-2}	N.D.	N.D.	N.D.	4.12×10^{-2}	N.D.
SCA 7	2.54×10^{-2}	2.58×10^{-2}	N.D.	N.D.	N.D.	2.58×10^{-2}	N.D.
SCA 8	N.D.	N.D.	N.D.	N.D.	N.D.	1.32×10^{-2}	7.02×10^{-3}
	191	200	170	190	198	199	196/203
SCA 1	N.D.	N.D.	N.D.	N.D.	N.D.	N.D.	N.D.

SCA 2	N.D.	N.D.	N.D.	N.D.	N.D.	N.D.	N.D.
SCA 3	7.54×10^{-3}	N.D.	2.52×10^{-2}	1.17×10^{-2}	N.D.	N.D.	1.58×10^{-2}
SCA 4	N.D.	N.D.	1.01×10^{-2}	N.D.	N.D.	N.D.	N.D.
SCA 6	N.D.	N.D.	N.D.	N.D.	N.D.	N.D.	N.D.
SCA 7	N.D.	N.D.	N.D.	N.D.	N.D.	N.D.	N.D.
SCA 8	N.D.	N.D.	N.D.	N.D.	N.D.	N.D.	N.D.
	189	208	195	207	194	205	206
SCA 1	N.D.	N.D.	N.D.	N.D.	N.D.	N.D.	N.D.
SCA 2	N.D.	N.D.	N.D.	N.D.	N.D.	N.D.	N.D.
SCA 3	N.D.	N.D.	N.D.	N.D.	N.D.	N.D.	N.D.
SCA 4	N.D.	N.D.	N.D.	N.D.	N.D.	N.D.	N.D.
SCA 6	N.D.	N.D.	N.D.	N.D.	N.D.	N.D.	N.D.
SCA 7	N.D.	N.D.	N.D.	N.D.	N.D.	N.D.	N.D.

SCA 8	N.D.	N.D.	N.D.	N.D.	N.D.	N.D.	N.D.
	209	TL					
SCA 1	N.D.	1.65					
SCA 2	N.D.	1.69					
SCA 3	N.D.	1.66					
SCA 4	N.D.	1.63					
SCA 6	N.D.	1.71					
SCA 7	N.D.	1.62					
SCA 8	N.D.	N.D.					

Sculpin		Recovery %	Recovery %	PCB concentrations (ng/g) wet weight			
Samples	Lipid %	PCB30	PCB 204	1	3	4/10	7
SS 6	2.19×10^{-1}	1.14×10^2	1.16×10^2	N.D.	N.D.	N.D.	N.D.
SS 8	9.23×10^{-2}	1.30×10^2	1.11×10^2	N.D.	N.D.	N.D.	N.D.
SS 9	2.89×10^{-1}	1.30×10^2	1.11×10^2	N.D.	N.D.	N.D.	N.D.
SS 11	3.00×10^{-1}	7.42×10^1	8.78×10^1	N.D.	N.D.	N.D.	N.D.
SS 12	4.93×10^{-1}	1.02×10^2	1.08×10^2	N.D.	N.D.	N.D.	N.D.
SS 17	5.07×10^{-1}	9.01×10^1	7.66×10^1	N.D.	N.D.	N.D.	5.38×10^{-3}
SS 20	1.57×10^{-1}	7.08×10^1	6.92×10^1	N.D.	N.D.	N.D.	N.D.
SS 21	1.81×10^{-1}	1.15×10^2	1.23×10^2	N.D.	N.D.	N.D.	N.D.
SS 3	1.54×10^{-1}	6.46×10^1	9.52×10^1	N.D.	N.D.	N.D.	N.D.
	6	8/5	19	18	17	24/27	16/32
SS 6	N.D.	N.D.	N.D.	N.D.	N.D.	N.D.	N.D.

SS 8	N.D.	N.D.	N.D.	N.D.	N.D.	N.D.	N.D.
SS 9	N.D.	N.D.	N.D.	N.D.	N.D.	N.D.	N.D.
SS 11	N.D.	N.D.	N.D.	N.D.	N.D.	N.D.	N.D.
SS 12	N.D.	N.D.	N.D.	1.70×10^{-3}	1.43×10^{-3}	N.D.	4.02×10^{-3}
SS 17	1.27×10^{-2}	3.10×10^{-2}	5.99×10^{-3}	7.48×10^{-3}	6.66×10^{-3}	N.D.	2.60×10^{-3}
SS 20	N.D.	N.D.	N.D.	8.20×10^{-3}	1.18×10^{-2}	N.D.	8.60×10^{-3}
SS 21	N.D.	N.D.	N.D.	8.64×10^{-3}	9.54×10^{-3}	N.D.	N.D.
SS 3	N.D.	N.D.	N.D.	2.41×10^{-2}	N.D.	N.D.	N.D.
	26	25	31	28	33	22	45
SS 6	N.D.	3.42×10^{-2}	N.D.	2.99×10^{-2}	N.D.	N.D.	N.D.
SS 8	N.D.	N.D.	2.32×10^{-2}	2.63×10^{-2}	N.D.	N.D.	N.D.
SS 9	N.D.	N.D.	2.26×10^{-2}	1.65×10^{-2}	1.32×10^{-2}	N.D.	N.D.
SS 11	N.D.	1.30×10^{-2}	2.47×10^{-2}	1.61×10^{-2}	2.01×10^{-2}	1.95×10^{-2}	1.08×10^{-2}

SS 12	N.D.	N.D.	1.57×10^{-2}	5.69×10^{-3}	N.D.	N.D.	2.89×10^{-3}
SS 17	N.D.	5.44×10^{-3}	3.03×10^{-2}	9.23×10^{-3}	3.63×10^{-3}	N.D.	N.D.
SS 20	N.D.	1.35×10^{-2}	3.31×10^{-2}	3.55×10^{-2}	2.25×10^{-2}	2.38×10^{-2}	N.D.
SS 21	N.D.	N.D.	3.46×10^{-2}	2.29×10^{-2}	N.D.	N.D.	N.D.
SS 3	N.D.	N.D.	N.D.	N.D.	N.D.	N.D.	3.79×10^{-2}
	46	52	49	47	48	44	42
SS 6	N.D.	4.54×10^{-2}	3.81×10^{-2}	1.22×10^{-2}	N.D.	8.33×10^{-2}	2.97×10^{-2}
SS 8	N.D.	2.85×10^{-2}	2.37×10^{-2}	2.07×10^{-2}	N.D.	6.98×10^{-2}	2.88×10^{-2}
SS 9	N.D.	1.29×10^{-2}	1.12×10^{-2}	7.11×10^{-3}	N.D.	4.71×10^{-2}	1.54×10^{-2}
SS 11	N.D.	3.23×10^{-2}	1.33×10^{-2}	1.41×10^{-2}	N.D.	4.02×10^{-2}	1.65×10^{-2}
SS 12	3.93×10^{-3}	7.81×10^{-3}	4.38×10^{-3}	6.11×10^{-3}	N.D.	1.24×10^{-2}	5.00×10^{-3}
SS 17	3.83×10^{-3}	1.55×10^{-2}	8.26×10^{-3}	5.41×10^{-3}	N.D.	2.75×10^{-2}	1.09×10^{-2}
SS 20	N.D.	6.26×10^{-2}	2.68×10^{-2}	1.01×10^{-2}	N.D.	7.09×10^{-2}	2.69×10^{-2}

SS 21	N.D.	2.49×10^{-2}	2.16×10^{-2}	2.16×10^{-2}	N.D.	4.46×10^{-2}	2.23×10^{-2}
SS 3	N.D.	1.06×10^{-1}	5.10×10^{-2}	N.D.	N.D.	6.82×10^{-2}	2.34×10^{-2}
	41/71	64	40	74	70/76	66	95
SS 6	4.40×10^{-2}	1.43×10^{-1}	2.05×10^{-2}	1.33×10^{-1}	2.77×10^{-1}	N.D.	2.28×10^{-1}
SS 8	3.70×10^{-2}	1.31×10^{-1}	N.D.	1.27×10^{-1}	2.73×10^{-1}	N.D.	2.06×10^{-1}
SS 9	1.23×10^{-2}	5.10×10^{-2}	N.D.	4.59×10^{-2}	8.18×10^{-2}	N.D.	7.73×10^{-2}
SS 11	1.76×10^{-2}	6.30×10^{-2}	N.D.	4.86×10^{-2}	1.07×10^{-1}	N.D.	9.30×10^{-2}
SS 12	3.14×10^{-3}	1.43×10^{-2}	N.D.	1.31×10^{-2}	3.27×10^{-2}	N.D.	2.74×10^{-2}
SS 17	1.09×10^{-2}	3.92×10^{-2}	3.73×10^{-3}	3.41×10^{-2}	7.83×10^{-2}	N.D.	6.32×10^{-2}
SS 20	3.74×10^{-2}	1.18×10^{-1}	1.65×10^{-2}	8.22×10^{-2}	1.10×10^{-1}	N.D.	1.59×10^{-1}
SS 21	N.D.	6.69×10^{-2}	3.71×10^{-2}	8.90×10^{-2}	1.79×10^{-1}	N.D.	1.47×10^{-1}
SS 3	N.D.	6.27×10^{-2}	N.D.	N.D.	2.76×10^{-2}	N.D.	9.39×10^{-2}
	56/60	91	84/89	101	99	83	97

SS 6	2.35×10^{-1}	3.57×10^{-2}	8.48×10^{-2}	1.16×10^{-1}	1.24×10^{-1}	N.D.	5.20×10^{-2}
SS 8	2.07×10^{-1}	2.92×10^{-2}	4.99×10^{-2}	6.94×10^{-2}	8.64×10^{-2}	N.D.	3.90×10^{-2}
SS 9	5.92×10^{-2}	N.D.	N.D.	2.59×10^{-2}	2.58×10^{-2}	N.D.	1.54×10^{-2}
SS 11	8.74×10^{-2}	9.66×10^{-3}	2.89×10^{-2}	3.31×10^{-2}	3.30×10^{-2}	1.74×10^{-3}	1.59×10^{-2}
SS 12	2.06×10^{-2}	2.05×10^{-3}	N.D.	1.27×10^{-2}	1.24×10^{-2}	N.D.	6.57×10^{-3}
SS 17	4.89×10^{-2}	4.94×10^{-3}	2.17×10^{-3}	1.96×10^{-2}	1.96×10^{-2}	N.D.	1.33×10^{-2}
SS 20	1.47×10^{-1}	1.25×10^{-2}	5.16×10^{-2}	6.76×10^{-2}	6.09×10^{-2}	N.D.	3.78×10^{-2}
SS 21	1.44×10^{-1}	N.D.	N.D.	9.15×10^{-2}	8.72×10^{-2}	N.D.	5.82×10^{-2}
SS 3	2.98×10^{-2}	N.D.	6.35×10^{-2}	N.D.	2.21×10^{-2}	N.D.	3.99×10^{-2}
	87	85	136	110	82	151	144/135
SS 6	7.84×10^{-2}	3.66×10^{-2}	N.D.	1.56×10^{-1}	2.16×10^{-2}	1.74×10^{-2}	N.D.
SS 8	6.06×10^{-2}	3.00×10^{-2}	N.D.	1.42×10^{-1}	1.62×10^{-2}	1.18×10^{-2}	N.D.
SS 9	1.67×10^{-2}	2.18×10^{-2}	1.70×10^{-2}	4.22×10^{-2}	N.D.	5.15×10^{-3}	N.D.

SS 11	3.17×10^{-2}	2.43×10^{-2}	6.61×10^{-3}	5.86×10^{-2}	2.75×10^{-3}	6.22×10^{-3}	N.D.
SS 12	8.53×10^{-3}	7.63×10^{-3}	N.D.	1.82×10^{-2}	N.D.	1.28×10^{-3}	N.D.
SS 17	1.94×10^{-2}	1.48×10^{-2}	N.D.	3.60×10^{-2}	4.01×10^{-3}	3.37×10^{-3}	N.D.
SS 20	6.22×10^{-2}	2.26×10^{-2}	1.01×10^{-2}	1.11×10^{-1}	1.10×10^{-2}	1.62×10^{-2}	4.73×10^{-3}
SS 21	8.76×10^{-2}	6.52×10^{-2}	N.D.	2.35×10^{-1}	2.32×10^{-2}	1.80×10^{-2}	N.D.
SS 3	3.84×10^{-2}	N.D.	N.D.	1.05×10^{-1}	N.D.	N.D.	N.D.
	149	118	134	114	131	146	153
SS 6	4.49×10^{-2}	7.09×10^{-2}	N.D.	N.D.	N.D.	N.D.	7.14×10^{-2}
SS 8	3.49×10^{-2}	6.83×10^{-2}	N.D.	N.D.	N.D.	5.48×10^{-3}	5.75×10^{-2}
SS 9	2.38×10^{-2}	4.19×10^{-2}	N.D.	5.00×10^{-3}	N.D.	1.93×10^{-3}	9.20×10^{-2}
SS 11	1.46×10^{-2}	4.01×10^{-2}	N.D.	5.03×10^{-3}	8.93×10^{-3}	8.67×10^{-3}	3.46×10^{-2}
SS 12	7.28×10^{-3}	2.41×10^{-2}	N.D.	1.71×10^{-3}	N.D.	3.24×10^{-3}	1.94×10^{-2}
SS 17	1.22×10^{-2}	4.14×10^{-2}	N.D.	2.23×10^{-3}	N.D.	3.52×10^{-3}	2.07×10^{-2}

SS 20	4.29×10^{-2}	6.53×10^{-2}	N.D.	6.55×10^{-3}	N.D.	3.14×10^{-3}	4.17×10^{-2}
SS 21	9.10×10^{-2}	2.20×10^{-1}	5.16×10^{-3}	3.37×10^{-2}	N.D.	2.63×10^{-2}	2.02×10^{-1}
SS 3	3.13×10^{-2}	N.D.	N.D.	N.D.	N.D.	N.D.	7.52×10^{-2}
	132	105	141	179	137	130/176	138
SS 6	2.54×10^{-2}	3.56×10^{-2}	5.40×10^{-3}	N.D.	N.D.	N.D.	8.55×10^{-2}
SS 8	1.76×10^{-2}	3.70×10^{-2}	9.68×10^{-3}	N.D.	1.51×10^{-2}	N.D.	8.24×10^{-2}
SS 9	N.D.	1.11×10^{-2}	3.92×10^{-3}	N.D.	N.D.	N.D.	6.38×10^{-2}
SS 11	1.10×10^{-2}	2.17×10^{-2}	6.63×10^{-3}	4.10×10^{-3}	N.D.	N.D.	4.28×10^{-2}
SS 12	2.23×10^{-3}	5.20×10^{-3}	1.79×10^{-3}	N.D.	N.D.	N.D.	1.94×10^{-2}
SS 17	4.40×10^{-3}	6.85×10^{-3}	2.66×10^{-3}	N.D.	N.D.	N.D.	2.72×10^{-2}
SS 20	2.03×10^{-2}	2.82×10^{-2}	9.03×10^{-3}	8.95×10^{-3}	N.D.	N.D.	5.29×10^{-2}
SS 21	5.46×10^{-2}	1.23×10^{-1}	3.79×10^{-2}	N.D.	1.16×10^{-2}	6.68×10^{-2}	3.30×10^{-1}
SS 3	N.D.	N.D.	7.77×10^{-3}	N.D.	N.D.	N.D.	1.00×10^{-1}

	158	178/129	175	187	183	128	185
SS 6	N.D.	N.D.	N.D.	1.61×10^{-2}	N.D.	N.D.	N.D.
SS 8	N.D.	N.D.	N.D.	1.38×10^{-2}	N.D.	3.54×10^{-3}	N.D.
SS 9	N.D.	N.D.	N.D.	6.93×10^{-3}	3.85×10^{-3}	N.D.	N.D.
SS 11	N.D.	N.D.	N.D.	2.47×10^{-3}	3.17×10^{-3}	1.33×10^{-3}	N.D.
SS 12	N.D.	N.D.	N.D.	3.53×10^{-3}	1.44×10^{-3}	6.40×10^{-4}	N.D.
SS 17	N.D.	N.D.	N.D.	4.39×10^{-3}	1.35×10^{-3}	6.29×10^{-4}	N.D.
SS 20	2.08×10^{-3}	N.D.	N.D.	1.09×10^{-2}	2.77×10^{-3}	1.41×10^{-4}	N.D.
SS 21	N.D.	3.15×10^{-2}	N.D.	2.93×10^{-2}	1.20×10^{-2}	2.44×10^{-2}	N.D.
SS 3	N.D.	N.D.	N.D.	2.35×10^{-2}	1.45×10^{-2}	N.D.	N.D.
	174	177	171/156	201/157	172/197	180	193
SS 6	N.D.	N.D.	N.D.	N.D.	N.D.	9.35×10^{-3}	N.D.
SS 8	1.12×10^{-2}	N.D.	N.D.	N.D.	N.D.	1.28×10^{-2}	N.D.

SS 9	4.93×10^{-3}	N.D.	N.D.	N.D.	N.D.	1.94×10^{-2}	1.93×10^{-3}
SS 11	6.49×10^{-3}	2.37×10^{-2}	N.D.	N.D.	N.D.	7.20×10^{-3}	7.17×10^{-4}
SS 12	1.47×10^{-3}	N.D.	N.D.	N.D.	N.D.	4.41×10^{-3}	4.40×10^{-4}
SS 17	2.48×10^{-3}	N.D.	N.D.	N.D.	N.D.	3.10×10^{-3}	2.84×10^{-4}
SS 20	1.23×10^{-2}	N.D.	N.D.	N.D.	N.D.	5.34×10^{-3}	5.34×10^{-4}
SS 21	2.98×10^{-2}	2.01×10^{-2}	N.D.	N.D.	N.D.	2.85×10^{-2}	2.86×10^{-3}
SS 3	2.53×10^{-2}	N.D.	N.D.	N.D.	N.D.	2.00×10^{-2}	N.D.
	191	200	170	190	198	199	196/203
SS 6	N.D.	N.D.	N.D.	N.D.	N.D.	N.D.	N.D.
SS 8	N.D.	N.D.	N.D.	N.D.	N.D.	N.D.	N.D.
SS 9	N.D.	N.D.	N.D.	N.D.	N.D.	N.D.	N.D.
SS 11	N.D.	N.D.	2.17×10^{-2}	N.D.	8.85×10^{-3}	N.D.	6.80×10^{-3}
SS 12	N.D.	N.D.	8.12×10^{-4}	N.D.	N.D.	N.D.	N.D.

SS 17	N.D.	N.D.	6.80×10^{-4}	N.D.	N.D.	N.D.	N.D.
SS 20	N.D.	N.D.	N.D.	N.D.	N.D.	N.D.	N.D.
SS 21	N.D.	N.D.	N.D.	N.D.	N.D.	N.D.	N.D.
SS 3	N.D.	N.D.	N.D.	N.D.	N.D.	N.D.	N.D.
	189	208	195	207	194	205	206
SS 6	N.D.	N.D.	N.D.	N.D.	N.D.	N.D.	N.D.
SS 8	N.D.	N.D.	N.D.	N.D.	N.D.	N.D.	N.D.
SS 9	N.D.	N.D.	N.D.	N.D.	N.D.	N.D.	N.D.
SS 11	N.D.	N.D.	N.D.	N.D.	N.D.	N.D.	N.D.
SS 12	N.D.	N.D.	N.D.	N.D.	N.D.	N.D.	N.D.
SS 17	N.D.	N.D.	N.D.	N.D.	N.D.	N.D.	N.D.
SS 20	N.D.	N.D.	N.D.	N.D.	N.D.	N.D.	N.D.
SS 21	N.D.	N.D.	N.D.	N.D.	N.D.	N.D.	N.D.

SS 3	N.D.	N.D.	N.D.	N.D.	N.D.	N.D.	N.D.
	209	TL					
SS 6	N.D.	3.36					
SS 8	N.D.	3.68					
SS 9	N.D.	3.25					
SS 11	N.D.	2.91					
SS 12	N.D.	3.23					
SS 17	N.D.	3.11					
SS 20	N.D.	3.23					
SS 21	N.D.	3.43					
SS 3	N.D.	3.11					

Skate		Recovery %	Recovery %	PCB concentrations (ng/g) wet weight			
Samples	Lipid %	PCB 30	PCB 204	1	3	4/10	7
TS 1	5.67×10^{-2}	9.77×10^1	7.62×10^1	N.D.	N.D.	N.D.	N.D.
TS 2	1.19×10^{-1}	1.11×10^2	1.13×10^2	N.D.	N.D.	N.D.	N.D.
TS 4	1.22×10^{-1}	6.67×10^1	1.05×10^2	N.D.	N.D.	N.D.	N.D.
TS 5	1.02×10^{-1}	1.11×10^2	8.09×10^1	N.D.	N.D.	N.D.	N.D.
TS 6	1.01×10^{-1}	1.12×10^2	9.99×10^1	N.D.	N.D.	N.D.	N.D.
	6	8/5	19	18	17	24/27	16/32
TS 1	N.D.	N.D.	1.50×10^{-2}	1.48×10^{-2}	2.06×10^{-2}	N.D.	2.27×10^{-2}
TS 2	N.D.	N.D.	N.D.	3.32×10^{-2}	8.02×10^{-2}	N.D.	4.32×10^{-2}
TS 4	N.D.	N.D.	N.D.	N.D.	N.D.	N.D.	N.D.
TS 5	N.D.	N.D.	N.D.	1.32×10^{-2}	N.D.	N.D.	1.69×10^{-2}
TS 6	N.D.	N.D.	N.D.	N.D.	4.02×10^{-2}	N.D.	3.52×10^{-2}

	26	25	31	28	33	22	45
TS 1	5.82×10^{-3}	8.81×10^{-3}	4.37×10^{-2}	3.71×10^{-2}	2.64×10^{-2}	1.61×10^{-2}	8.69×10^{-3}
TS 2	N.D.	6.34×10^{-2}	1.45×10^{-1}	2.06×10^{-1}	8.53×10^{-2}	5.71×10^{-2}	5.98×10^{-2}
TS 4	9.39×10^{-2}	7.97×10^{-2}	N.D.	4.32×10^{-2}	N.D.	N.D.	N.D.
TS 5	N.D.	4.74×10^{-2}	3.38×10^{-2}	1.89×10^{-2}	N.D.	4.77×10^{-2}	N.D.
TS 6	1.56×10^{-1}	2.49×10^{-1}	2.04×10^{-1}	1.77×10^{-1}	1.43×10^{-1}	8.42×10^{-2}	N.D.
	46	52	49	47	48	44	42
TS 1	1.44×10^{-2}	2.35×10^{-2}	1.32×10^{-2}	1.52×10^{-2}	N.D.	2.33×10^{-2}	1.51×10^{-2}
TS 2	3.21×10^{-2}	1.57×10^{-1}	5.96×10^{-2}	7.39×10^{-2}	2.41×10^{-2}	1.46×10^{-1}	5.10×10^{-2}
TS 4	N.D.	N.D.	N.D.	N.D.	N.D.	2.32×10^{-2}	7.48×10^{-3}
TS 5	N.D.	9.91×10^{-3}	5.08×10^{-3}	2.18×10^{-2}	N.D.	2.05×10^{-2}	5.27×10^{-3}
TS 6	N.D.	6.81×10^{-2}	1.20×10^{-1}	1.76×10^{-1}	N.D.	2.01×10^{-2}	1.64×10^{-1}
	41/71	64	40	74	70/76	66	95

TS 1	8.08×10^{-2}	1.35×10^{-2}	2.62×10^{-3}	1.74×10^{-2}	3.11×10^{-2}	N.D.	4.69×10^{-2}
TS 2	8.62×10^{-3}	5.38×10^{-2}	N.D.	9.68×10^{-2}	1.73×10^{-1}	N.D.	2.78×10^{-1}
TS 4	N.D.	N.D.	N.D.	2.20×10^{-2}	1.05×10^{-2}	N.D.	8.16×10^{-3}
TS 5	N.D.	4.22×10^{-4}	N.D.	1.79×10^{-2}	3.87×10^{-2}	N.D.	9.62×10^{-2}
TS 6	N.D.	3.91×10^{-2}	N.D.	4.43×10^{-2}	6.93×10^{-2}	N.D.	2.86×10^{-1}
	56/60	91	84/89	101	99	83	97
TS 1	1.49×10^{-2}	2.05×10^{-4}	7.67×10^{-3}	3.14×10^{-2}	1.48×10^{-2}	2.73×10^{-4}	1.18×10^{-2}
TS 2	1.46×10^{-2}	2.84×10^{-2}	2.46×10^{-2}	2.03×10^{-1}	2.02×10^{-1}	N.D.	8.01×10^{-2}
TS 4	N.D.	N.D.	2.41×10^{-2}	3.90×10^{-2}	3.67×10^{-2}	1.31×10^{-3}	1.78×10^{-2}
TS 5	N.D.	N.D.	2.31×10^{-2}	4.33×10^{-2}	3.34×10^{-2}	N.D.	2.23×10^{-2}
TS 6	N.D.	N.D.	N.D.	9.37×10^{-2}	6.79×10^{-2}	N.D.	N.D.
	87	85	136	110	82	151	144/135
TS 1	1.70×10^{-2}	4.78×10^{-3}	N.D.	3.92×10^{-2}	N.D.	4.93×10^{-3}	N.D.

TS 2	1.11×10^{-1}	7.53×10^{-2}	3.54×10^{-2}	4.01×10^{-1}	N.D.	6.35×10^{-2}	2.09×10^{-2}
TS 4	3.19×10^{-2}	1.13×10^{-2}	N.D.	4.54×10^{-2}	N.D.	N.D.	N.D.
TS 5	5.13×10^{-2}	1.54×10^{-2}	2.42×10^{-2}	1.21×10^{-1}	N.D.	1.20×10^{-2}	1.61×10^{-3}
TS 6	9.98×10^{-2}	N.D.	N.D.	1.84×10^{-1}	N.D.	1.91×10^{-2}	1.43×10^{-3}
	149	118	134	114	131	146	153
TS 1	1.86×10^{-2}	4.39×10^{-2}	N.D.	6.57×10^{-3}	N.D.	4.23×10^{-3}	2.73×10^{-2}
TS 2	2.51×10^{-1}	3.31×10^{-1}	N.D.	3.65×10^{-2}	N.D.	5.08×10^{-2}	3.03×10^{-1}
TS 4	1.36×10^{-2}	1.61×10^{-2}	N.D.	1.32×10^{-3}	N.D.	N.D.	4.11×10^{-2}
TS 5	5.89×10^{-2}	1.10×10^{-1}	N.D.	3.00×10^{-2}	N.D.	8.25×10^{-3}	8.15×10^{-2}
TS 6	9.90×10^{-2}	1.99×10^{-1}	N.D.	N.D.	N.D.	N.D.	1.05×10^{-1}
	132	105	141	179	137	130/176	138
TS 1	1.22×10^{-2}	1.81×10^{-2}	5.63×10^{-3}	4.40×10^{-3}	N.D.	4.54×10^{-3}	4.67×10^{-2}
TS 2	1.72×10^{-1}	1.42×10^{-1}	7.23×10^{-2}	2.81×10^{-2}	1.60×10^{-2}	6.01×10^{-2}	5.03×10^{-1}

TS 4	9.16×10^{-3}	1.12×10^{-2}	8.02×10^{-3}	N.D.	N.D.	N.D.	1.56×10^{-2}
TS 5	4.41×10^{-2}	5.44×10^{-2}	1.99×10^{-2}	7.07×10^{-3}	N.D.	2.90×10^{-2}	1.40×10^{-1}
TS 6	N.D.	8.71×10^{-2}	1.33×10^{-2}	N.D.	N.D.	N.D.	2.14×10^{-1}
	158	178/129	175	187	183	128	185
TS 1	1.90×10^{-3}	2.40×10^{-4}	N.D.	7.01×10^{-3}	2.05×10^{-3}	2.31×10^{-3}	N.D.
TS 2	1.65×10^{-2}	3.77×10^{-2}	N.D.	6.57×10^{-2}	2.27×10^{-2}	1.18×10^{-2}	N.D.
TS 4	N.D.	N.D.	N.D.	N.D.	N.D.	N.D.	N.D.
TS 5	1.21×10^{-2}	N.D.	N.D.	1.43×10^{-2}	4.35×10^{-3}	2.26×10^{-2}	N.D.
TS 6	7.38×10^{-3}	N.D.	N.D.	3.06×10^{-2}	9.38×10^{-3}	N.D.	N.D.
	174	177	171/156	201/157	172/197	180	193
TS 1	5.42×10^{-3}	3.13×10^{-3}	N.D.	N.D.	N.D.	5.01×10^{-3}	4.54×10^{-4}
TS 2	5.35×10^{-2}	5.84×10^{-2}	1.31×10^{-2}	N.D.	N.D.	4.25×10^{-2}	4.16×10^{-3}
TS 4	N.D.	N.D.	N.D.	N.D.	N.D.	N.D.	N.D.

TS 5	2.05×10^{-2}	8.71×10^{-3}	N.D.	N.D.	N.D.	4.31×10^{-3}	N.D.
TS 6	5.53×10^{-2}	N.D.	N.D.	N.D.	N.D.	1.19×10^{-2}	N.D.
	191	200	170	190	198	199	196/203
TS 1	N.D.	N.D.	N.D.	N.D.	N.D.	N.D.	2.34×10^{-4}
TS 2	N.D.	N.D.	N.D.	N.D.	N.D.	2.86×10^{-3}	N.D.
TS 4	N.D.	N.D.	N.D.	N.D.	N.D.	N.D.	N.D.
TS 5	N.D.	N.D.	1.29×10^{-2}	N.D.	N.D.	N.D.	N.D.
TS 6	N.D.	N.D.	N.D.	N.D.	N.D.	N.D.	N.D.
	189	208	195	207	194	205	206
TS 1	N.D.	N.D.	N.D.	N.D.	N.D.	N.D.	N.D.
TS 2	N.D.	N.D.	N.D.	N.D.	N.D.	N.D.	N.D.
TS 4	N.D.	N.D.	N.D.	N.D.	N.D.	N.D.	N.D.
TS 5	N.D.	N.D.	N.D.	N.D.	N.D.	N.D.	N.D.

TS 6	N.D.	N.D.	N.D.	N.D.	N.D.	N.D.	N.D.
	209	TL					
TS 1	N.D.	3.54					
TS 2	N.D.	3.60					
TS 4	N.D.	3.32					
TS 5	N.D.	3.27					
TS 6	N.D.	3.74					

Zooplankton		Recovery %	Recovery %	PCB concentrations (ng/g) wet weight			
Samples	Lipid %	PCB 30	PCB 204	1	3	4/10	7
ZOO 1	1.49	8.00×10 ¹	7.50×10 ¹	N.D.	N.D.	3.10×10 ⁻²	N.D.
ZOO 2	1.90	1.21×10 ²	8.58×10 ¹	N.D.	N.D.	7.91×10 ⁻²	N.D.
ZOO 3	1.29	1.06×10 ²	8.58×10 ¹	N.D.	N.D.	3.76×10 ⁻²	N.D.
ZOO 4	1.04	1.23×10 ²	1.08×10 ²	N.D.	N.D.	N.D.	N.D.
ZOO 5	1.43	7.39×10 ¹	6.14×10 ¹	N.D.	N.D.	N.D.	N.D.
ZOO 6	1.55×10 ¹	9.30×10 ¹	8.32×10 ¹	N.D.	N.D.	N.D.	N.D.
	6	8/5	19	18	17	24/27	16/32
ZOO 1	N.D.	N.D.	N.D.	2.91×10 ⁻²	1.39×10 ⁻²	N.D.	3.85×10 ⁻³
ZOO 2	N.D.	N.D.	N.D.	3.02×10 ⁻²	4.39×10 ⁻²	N.D.	N.D.
ZOO 3	N.D.	N.D.	3.43×10 ⁻²	N.D.	N.D.	N.D.	7.47×10 ⁻³
ZOO 4	N.D.	N.D.	N.D.	8.36×10 ⁻³	1.11×10 ⁻²	N.D.	N.D.

ZOO 5	N.D.	N.D.	N.D.	N.D.	N.D.	N.D.	N.D.
ZOO 6	N.D.	N.D.	N.D.	1.38×10^{-1}	1.93×10^{-1}	N.D.	N.D.
	26	25	31	28	33	22	45
ZOO 1	1.47×10^{-3}	1.07×10^{-1}	3.71×10^{-1}	2.41×10^{-2}	1.85×10^{-2}	1.74×10^{-2}	2.58×10^{-2}
ZOO 2	3.81×10^{-3}	3.47×10^{-2}	5.18×10^{-1}	5.82×10^{-2}	1.13×10^{-1}	2.22×10^{-2}	2.99×10^{-2}
ZOO 3	6.97×10^{-2}	1.41×10^{-2}	3.88×10^{-1}	4.26×10^{-2}	5.51×10^{-2}	1.58×10^{-2}	5.85×10^{-4}
ZOO 4	7.62×10^{-3}	N.D.	1.46×10^{-1}	2.57×10^{-2}	5.39×10^{-2}	1.29×10^{-2}	N.D.
ZOO 5	7.94×10^{-2}	2.84×10^{-2}	1.73×10^{-1}	2.51×10^{-2}	8.54×10^{-2}	2.07×10^{-2}	N.D.
ZOO 6	1.17×10^{-1}	2.17×10^{-1}	2.14	4.04×10^{-1}	9.31×10^{-1}	1.94×10^{-1}	9.55×10^{-2}
	46	52	49	47	48	44	42
ZOO 1	3.34×10^{-2}	4.22×10^{-2}	3.07×10^{-2}	2.57×10^{-2}	1.02×10^{-3}	3.27×10^{-2}	2.29×10^{-2}
ZOO 2	3.30×10^{-2}	6.78×10^{-2}	5.55×10^{-2}	2.96×10^{-2}	N.D.	2.34×10^{-1}	5.47×10^{-2}
ZOO 3	4.78×10^{-2}	4.43×10^{-2}	4.30×10^{-2}	2.32×10^{-2}	N.D.	5.61×10^{-2}	2.92×10^{-2}

ZOO 4	N.D.	N.D.	N.D.	N.D.	N.D.	1.08×10^{-2}	9.93×10^{-3}
ZOO 5	2.71×10^{-2}	4.46×10^{-2}	2.97×10^{-2}	N.D.	1.22×10^{-2}	3.74×10^{-2}	7.67×10^{-3}
ZOO 6	N.D.	5.32×10^{-1}	4.32×10^{-1}	2.92×10^{-1}	N.D.	3.08×10^{-1}	1.28×10^{-1}
	41/71	64	40	74	70/76	66	95
ZOO 1	2.20×10^{-2}	3.60×10^{-2}	N.D.	3.27×10^{-2}	5.27×10^{-2}	N.D.	9.54×10^{-2}
ZOO 2	3.68×10^{-2}	1.32×10^{-1}	5.12×10^{-3}	8.70×10^{-2}	2.39×10^{-1}	N.D.	2.09×10^{-1}
ZOO 3	2.37×10^{-2}	6.90×10^{-2}	N.D.	4.81×10^{-2}	7.55×10^{-2}	N.D.	1.21×10^{-1}
ZOO 4	N.D.	1.21×10^{-3}	N.D.	N.D.	4.72×10^{-2}	N.D.	7.85×10^{-2}
ZOO 5	N.D.	2.19×10^{-2}	N.D.	N.D.	7.10×10^{-2}	N.D.	7.77×10^{-2}
ZOO 6	N.D.	2.84×10^{-1}	N.D.	N.D.	7.03×10^{-1}	N.D.	8.84×10^{-1}
	56/60	91	84/89	101	99	83	97
ZOO 1	4.37×10^{-3}	2.00×10^{-2}	2.97×10^{-2}	5.15×10^{-2}	5.05×10^{-2}	1.10×10^{-2}	2.63×10^{-2}
ZOO 2	1.57×10^{-1}	2.79×10^{-2}	8.98×10^{-2}	1.18×10^{-1}	1.05×10^{-1}	1.16×10^{-2}	5.30×10^{-2}

ZOO 3	2.10×10^{-2}	1.10×10^{-2}	2.87×10^{-2}	6.86×10^{-2}	8.59×10^{-2}	N.D.	2.98×10^{-2}
ZOO 4	3.55×10^{-2}	1.29×10^{-2}	2.15×10^{-2}	2.30×10^{-2}	6.25×10^{-3}	4.76×10^{-4}	1.30×10^{-2}
ZOO 5	2.58×10^{-2}	N.D.	5.04×10^{-3}	2.69×10^{-2}	2.67×10^{-2}	N.D.	N.D.
ZOO 6	2.70×10^{-1}	N.D.	1.99×10^{-1}	4.47×10^{-1}	3.53×10^{-1}	N.D.	2.91×10^{-1}
	87	85	136	110	82	151	144/135
ZOO 1	4.55×10^{-2}	1.79×10^{-2}	7.61×10^{-3}	6.26×10^{-2}	2.54×10^{-3}	2.50×10^{-2}	2.73×10^{-2}
ZOO 2	1.16×10^{-1}	3.66×10^{-2}	2.30×10^{-2}	1.51×10^{-1}	7.61×10^{-3}	3.85×10^{-2}	2.97×10^{-2}
ZOO 3	6.24×10^{-2}	2.61×10^{-2}	6.54×10^{-3}	8.99×10^{-2}	N.D.	2.11×10^{-2}	1.78×10^{-2}
ZOO 4	3.06×10^{-2}	1.07×10^{-2}	N.D.	3.58×10^{-2}	3.72×10^{-3}	1.04×10^{-2}	6.19×10^{-3}
ZOO 5	3.58×10^{-2}	1.01×10^{-2}	N.D.	4.78×10^{-2}	N.D.	1.15×10^{-2}	N.D.
ZOO 6	3.50×10^{-1}	1.78×10^{-1}	N.D.	7.80×10^{-1}	N.D.	2.57×10^{-1}	N.D.
	149	118	134	114	131	146	153
ZOO 1	4.56×10^{-2}	5.16×10^{-1}	N.D.	3.47×10^{-2}	8.82×10^{-3}	7.06×10^{-3}	6.16×10^{-2}

ZOO 2	7.48×10^{-2}	7.08×10^{-1}	N.D.	4.26×10^{-2}	1.12×10^{-2}	9.47×10^{-3}	8.77×10^{-2}
ZOO 3	5.53×10^{-2}	4.13×10^{-1}	N.D.	2.41×10^{-2}	6.28×10^{-3}	9.02×10^{-3}	6.89×10^{-2}
ZOO 4	1.33×10^{-2}	1.53×10^{-1}	N.D.	6.62×10^{-3}	N.D.	3.56×10^{-3}	3.34×10^{-2}
ZOO 5	2.53×10^{-2}	1.34×10^{-1}	N.D.	N.D.	N.D.	1.42×10^{-2}	3.55×10^{-2}
ZOO 6	5.16×10^{-1}	1.72	N.D.	1.89×10^{-1}	9.51×10^{-2}	6.36×10^{-2}	8.24×10^{-1}
	132	105	141	179	137	130/176	138
ZOO 1	1.50×10^{-2}	6.60×10^{-3}	1.20×10^{-2}	8.01×10^{-3}	1.46×10^{-2}	7.75×10^{-2}	1.07×10^{-1}
ZOO 2	2.73×10^{-2}	N.D.	1.78×10^{-2}	9.65×10^{-3}	1.88×10^{-2}	8.93×10^{-2}	1.50×10^{-1}
ZOO 3	2.01×10^{-2}	N.D.	1.79×10^{-2}	7.34×10^{-3}	N.D.	6.49×10^{-2}	1.42×10^{-1}
ZOO 4	9.12×10^{-3}	N.D.	7.86×10^{-3}	6.08×10^{-3}	N.D.	1.70×10^{-2}	5.01×10^{-2}
ZOO 5	9.75×10^{-3}	N.D.	1.24×10^{-2}	N.D.	N.D.	N.D.	5.75×10^{-2}
ZOO 6	2.15×10^{-1}	N.D.	1.64×10^{-1}	8.84×10^{-2}	N.D.	N.D.	1.13
	158	178/129	175	187	183	128	185

ZOO 1	4.30×10^{-3}	2.07×10^{-2}	6.93×10^{-4}	3.12×10^{-2}	8.63×10^{-3}	2.72×10^{-3}	1.81×10^{-3}
ZOO 2	7.21×10^{-3}	2.13×10^{-2}	N.D.	2.62×10^{-2}	1.71×10^{-2}	1.12×10^{-3}	N.D.
ZOO 3	6.68×10^{-3}	1.38×10^{-2}	N.D.	4.08×10^{-2}	1.44×10^{-2}	1.14×10^{-2}	N.D.
ZOO 4	2.54×10^{-3}	8.26×10^{-3}	1.71×10^{-3}	1.17×10^{-2}	4.06×10^{-3}	3.88×10^{-3}	N.D.
ZOO 5	N.D.	N.D.	N.D.	1.36×10^{-2}	6.31×10^{-3}	N.D.	N.D.
ZOO 6	N.D.	N.D.	N.D.	2.32×10^{-1}	9.16×10^{-2}	5.85×10^{-2}	N.D.
	174	177	171/156	201/157	172/197	180	193
ZOO 1	2.41×10^{-2}	8.12×10^{-3}	3.08×10^{-3}	N.D.	N.D.	2.71×10^{-2}	2.75×10^{-3}
ZOO 2	3.45×10^{-2}	1.60×10^{-2}	N.D.	N.D.	N.D.	3.40×10^{-2}	3.37×10^{-3}
ZOO 3	3.25×10^{-2}	2.39×10^{-2}	N.D.	N.D.	N.D.	3.88×10^{-2}	4.30×10^{-3}
ZOO 4	1.45×10^{-2}	8.09×10^{-3}	N.D.	N.D.	N.D.	1.19×10^{-2}	N.D.
ZOO 5	1.72×10^{-2}	1.06×10^{-2}	N.D.	N.D.	N.D.	1.10×10^{-2}	N.D.
ZOO 6	3.12×10^{-1}	1.82×10^{-1}	N.D.	N.D.	N.D.	2.25×10^{-1}	N.D.

	191	200	170	190	198	199	196/203
ZOO 1	N.D.	N.D.	3.28×10^{-3}	N.D.	N.D.	6.24×10^{-3}	2.39×10^{-3}
ZOO 2	N.D.	N.D.	4.61×10^{-3}	2.39×10^{-3}	N.D.	5.27×10^{-3}	6.04×10^{-3}
ZOO 3	N.D.	N.D.	1.25×10^{-2}	N.D.	N.D.	9.74×10^{-3}	8.73×10^{-3}
ZOO 4	N.D.	N.D.	N.D.	N.D.	N.D.	2.14×10^{-3}	5.58×10^{-3}
ZOO 5	N.D.	N.D.	N.D.	N.D.	N.D.	N.D.	N.D.
ZOO 6	N.D.	N.D.	N.D.	N.D.	N.D.	N.D.	N.D.
	189	208	195	207	194	205	206
ZOO 1	N.D.	N.D.	N.D.	N.D.	2.75×10^{-3}	N.D.	1.98×10^{-3}
ZOO 2	N.D.	N.D.	N.D.	N.D.	N.D.	N.D.	N.D.
ZOO 3	N.D.	N.D.	N.D.	N.D.	N.D.	N.D.	N.D.
ZOO 4	N.D.	N.D.	N.D.	N.D.	N.D.	N.D.	N.D.
ZOO 5	N.D.	N.D.	N.D.	N.D.	N.D.	N.D.	N.D.

ZOO 6	N.D.	N.D.	N.D.	N.D.	N.D.	N.D.	N.D.	
	209	TL						
ZOO 1	N.D.	1.95						
ZOO 2	N.D.	1.87						
ZOO 3	N.D.	2.03						
ZOO 4	N.D.	2.01						
ZOO 5	N.D.	2.03						
ZOO 6	N.D.	2.11						

Turbot		Recovery %	Recovery %	PCB concentrations (ng/g) wet weight			
Samples	Lipid %	PCB 30	PCB 204	1	3	4/10	7
TB 4	1.16×10 ¹	4.08×10 ¹	7.13×10 ¹	N.D.	N.D.	N.D.	N.D.
TB 12	9.83	4.78×10 ¹	8.28×10 ¹	N.D.	N.D.	N.D.	N.D.
TB 28	1.29×10 ¹	6.33×10 ¹	7.63×10 ¹	N.D.	N.D.	N.D.	1.15×10 ⁻²
TB 29	8.18	5.19×10 ¹	4.44×10 ¹	N.D.	N.D.	2.21×10 ⁻¹	1.75×10 ⁻²
TB 30	1.26×10 ¹	1.16×10 ²	1.20×10 ²	N.D.	N.D.	2.23×10 ⁻¹	N.D.
TB 31	9.60	1.28×10 ²	1.35×10 ²	N.D.	N.D.	N.D.	N.D.
TB 32	1.21×10 ¹	9.94×10 ¹	1.21×10 ²	N.D.	N.D.	N.D.	N.D.
TB 33	1.45×10 ¹	7.55×10 ¹	7.64×10 ¹	N.D.	N.D.	N.D.	N.D.
	6	8/5	19	18	17	24/27	16/32
TB 4	1.64×10 ⁻¹	N.D.	N.D.	N.D.	3.28×10 ⁻²	N.D.	1.12×10 ⁻¹
TB 12	N.D.	N.D.	N.D.	N.D.	N.D.	N.D.	N.D.

TB 28	N.D.	N.D.	N.D.	5.62×10^{-2}	6.40×10^{-2}	5.62×10^{-2}	1.09×10^{-1}
TB 29	6.66×10^{-1}	N.D.	2.02×10^{-1}	4.92×10^{-2}	4.54×10^{-2}	4.43×10^{-2}	N.D.
TB 30	2.94×10^{-1}	N.D.	1.29×10^{-1}	3.31×10^{-2}	4.22×10^{-2}	5.76×10^{-2}	4.10×10^{-4}
TB 31	N.D.	N.D.	N.D.	6.34×10^{-2}	1.08×10^{-1}	N.D.	6.01×10^{-2}
TB 32	N.D.	N.D.	N.D.	4.21×10^{-2}	1.18×10^{-1}	N.D.	4.77×10^{-3}
TB 33	N.D.	N.D.	N.D.	8.82×10^{-2}	1.03×10^{-1}	N.D.	N.D.
	26	25	31	28	33	22	45
TB 4	N.D.	7.42×10^{-2}	2.42×10^{-1}	2.16×10^{-1}	N.D.	N.D.	N.D.
TB 12	N.D.	5.13×10^{-2}	1.35×10^{-1}	1.32×10^{-1}	N.D.	N.D.	N.D.
TB 28	2.25×10^{-2}	3.07×10^{-2}	1.94×10^{-1}	1.89×10^{-1}	1.81×10^{-2}	1.74×10^{-2}	4.71×10^{-1}
TB 29	4.53×10^{-2}	3.27×10^{-2}	1.52	1.67×10^{-1}	1.56×10^{-2}	3.77×10^{-2}	2.93×10^{-1}
TB 30	7.00×10^{-2}	5.35×10^{-2}	1.68	2.53×10^{-1}	4.81×10^{-2}	7.68×10^{-2}	3.66×10^{-1}
TB 31	4.38×10^{-2}	6.22×10^{-2}	3.95	4.50×10^{-1}	1.24×10^{-1}	4.44×10^{-1}	7.18×10^{-1}

TB 32	2.63×10^{-2}	7.14×10^{-2}	1.78	3.24×10^{-1}	5.33×10^{-2}	1.95×10^{-2}	4.97×10^{-1}
TB 33	4.24×10^{-2}	3.23×10^{-2}	2.99	3.99×10^{-1}	1.22×10^{-1}	3.47×10^{-2}	7.55×10^{-1}
	46	52	49	47	48	44	42
TB 4	1.55×10^{-1}	3.30×10^{-1}	1.90×10^{-1}	6.36×10^{-2}	N.D.	1.33×10^{-1}	9.92×10^{-2}
TB 12	N.D.	3.17×10^{-1}	2.12×10^{-1}	5.48×10^{-2}	N.D.	1.49×10^{-1}	8.87×10^{-2}
TB 28	6.02×10^{-1}	3.91×10^{-1}	1.10×10^{-1}	3.78×10^{-2}	9.14×10^{-2}	1.70×10^{-1}	1.79×10^{-1}
TB 29	3.81×10^{-1}	2.79×10^{-1}	8.67×10^{-2}	1.55×10^{-2}	6.54×10^{-2}	9.22×10^{-2}	1.17×10^{-1}
TB 30	6.47×10^{-1}	4.55×10^{-1}	2.32×10^{-1}	1.28×10^{-1}	N.D.	1.52×10^{-1}	1.49×10^{-1}
TB 31	1.04	8.25×10^{-1}	5.00×10^{-1}	1.92×10^{-1}	5.23×10^{-3}	2.37×10^{-1}	2.15×10^{-1}
TB 32	6.64×10^{-1}	4.34×10^{-1}	1.59×10^{-1}	1.04×10^{-1}	2.56×10^{-2}	1.24×10^{-1}	1.21×10^{-1}
TB 33	3.24×10^{-1}	7.55×10^{-1}	2.97×10^{-1}	1.64×10^{-1}	2.12×10^{-1}	2.19×10^{-1}	1.75×10^{-1}
	41/71	64	40	74	70/76	66	95
TB 4	N.D.	1.97×10^{-1}	N.D.	2.35×10^{-2}	2.88×10^{-1}	N.D.	5.69×10^{-1}

TB 12	1.81×10^{-1}	1.70×10^{-1}	N.D.	6.86×10^{-2}	2.34×10^{-1}	4.45×10^{-2}	7.55×10^{-1}
TB 28	2.45×10^{-1}	1.43×10^{-1}	2.07×10^{-2}	2.99×10^{-1}	4.26×10^{-1}	N.D.	6.74×10^{-1}
TB 29	N.D.	1.06×10^{-1}	3.83×10^{-3}	1.54×10^{-1}	2.41×10^{-1}	1.23×10^{-1}	4.51×10^{-1}
TB 30	N.D.	2.53×10^{-1}	3.80×10^{-2}	3.72×10^{-1}	5.54×10^{-1}	1.12×10^{-1}	3.61×10^{-1}
TB 31	3.99×10^{-1}	3.36×10^{-1}	7.69×10^{-2}	7.04×10^{-1}	9.17×10^{-1}	1.21	8.00×10^{-1}
TB 32	2.30×10^{-1}	1.70×10^{-1}	3.07×10^{-2}	4.16×10^{-1}	4.79×10^{-1}	6.95×10^{-1}	6.45×10^{-1}
TB 33	N.D.	2.76×10^{-1}	7.61×10^{-2}	2.56×10^{-1}	5.26×10^{-1}	8.21×10^{-1}	6.30×10^{-1}
	56/60	91	84/89	101	99	83	97
TB 4	6.33×10^{-1}	1.68×10^{-2}	1.41	8.43×10^{-1}	8.40×10^{-1}	N.D.	1.26×10^{-1}
TB 12	2.89×10^{-1}	6.24×10^{-2}	2.70×10^{-1}	5.00×10^{-1}	4.99×10^{-1}	N.D.	3.56×10^{-1}
TB 28	6.71×10^{-1}	4.11×10^{-2}	1.18	8.08×10^{-1}	8.08×10^{-1}	6.64×10^{-2}	2.26×10^{-1}
TB 29	3.68×10^{-1}	2.85×10^{-2}	5.93×10^{-1}	3.74×10^{-1}	3.89×10^{-1}	4.51×10^{-3}	1.64×10^{-1}
TB 30	6.44×10^{-1}	3.93×10^{-2}	7.88×10^{-1}	7.16×10^{-1}	1.48	3.35×10^{-2}	1.69×10^{-1}

TB 31	5.70×10^{-1}	3.04×10^{-1}	7.19×10^{-1}	1.20	1.20	7.57×10^{-1}	2.83×10^{-1}
TB 32	2.98×10^{-1}	1.74×10^{-1}	3.22×10^{-1}	6.27×10^{-1}	6.27×10^{-1}	6.72×10^{-1}	2.39×10^{-1}
TB 33	2.15×10^{-1}	1.09×10^{-1}	3.44×10^{-1}	6.01×10^{-1}	1.22	4.40×10^{-1}	1.08×10^{-1}
	87	85	136	110	82	151	144/135
TB 4	2.36×10^{-1}	N.D.	N.D.	5.59×10^{-1}	N.D.	1.33×10^{-1}	2.16×10^{-1}
TB 12	4.11×10^{-1}	N.D.	1.21×10^{-2}	6.33×10^{-1}	N.D.	1.36×10^{-1}	2.11×10^{-1}
TB 28	6.76×10^{-1}	3.24×10^{-1}	2.05×10^{-2}	2.20×10^{-2}	1.95×10^{-2}	1.55×10^{-1}	N.D.
TB 29	4.85×10^{-1}	1.87×10^{-1}	2.36×10^{-2}	3.58×10^{-1}	2.52×10^{-2}	1.06×10^{-1}	1.91×10^{-1}
TB 30	2.51×10^{-1}	4.59×10^{-1}	N.D.	7.33×10^{-1}	3.33×10^{-2}	1.76×10^{-1}	3.33×10^{-1}
TB 31	6.81×10^{-1}	7.47×10^{-1}	7.27×10^{-2}	1.48	2.82×10^{-2}	3.43×10^{-1}	3.55×10^{-1}
TB 32	4.88×10^{-1}	3.91×10^{-1}	N.D.	1.30	8.98×10^{-2}	1.90×10^{-1}	1.90×10^{-1}
TB 33	5.53×10^{-1}	5.08×10^{-1}	N.D.	8.86×10^{-1}	2.91×10^{-2}	1.96×10^{-1}	2.25×10^{-1}
	149	118	134	114	131	146	153

TB 4	6.07×10^{-1}	6.56	N.D.	2.66×10^{-1}	4.98×10^{-2}	3.78×10^{-2}	6.81×10^{-1}
TB 12	1.55×10^{-1}	5.33	N.D.	8.64×10^{-1}	1.43×10^{-1}	3.80×10^{-2}	6.38×10^{-1}
TB 28	3.94×10^{-1}	5.83	N.D.	8.13×10^{-2}	1.37×10^{-1}	1.48×10^{-1}	4.22×10^{-1}
TB 29	3.05×10^{-1}	5.07	N.D.	3.17×10^{-2}	1.17×10^{-1}	9.02×10^{-2}	3.41×10^{-1}
TB 30	7.79×10^{-1}	7.73	N.D.	2.55×10^{-1}	3.10×10^{-2}	2.12×10^{-1}	1.38
TB 31	1.29	1.05×10^1	N.D.	6.68×10^{-1}	1.53×10^{-1}	3.09×10^{-1}	1.97
TB 32	1.05	5.94	1.99×10^{-2}	3.75×10^{-1}	6.73×10^{-2}	2.56×10^{-1}	1.94
TB 33	6.46×10^{-1}	5.44	N.D.	2.45×10^{-1}	1.43×10^{-2}	4.89×10^{-1}	1.18
	132	105	141	179	137	130/176	138
TB 4	2.38×10^{-1}	4.00×10^{-1}	6.24×10^{-2}	N.D.	9.54×10^{-2}	N.D.	1.56
TB 12	5.18×10^{-1}	3.68×10^{-1}	7.16×10^{-2}	1.54×10^{-2}	8.28×10^{-2}	5.50×10^{-1}	1.32
TB 28	7.39×10^{-2}	3.27×10^{-1}	6.08×10^{-2}	2.36×10^{-2}	2.17×10^{-1}	N.D.	9.34×10^{-1}
TB 29	3.29×10^{-2}	2.14×10^{-1}	6.16×10^{-2}	1.88×10^{-2}	1.08×10^{-1}	3.70×10^{-1}	7.34×10^{-1}

TB 30	4.15×10^{-1}	3.03×10^{-1}	1.39×10^{-1}	4.47×10^{-2}	1.33×10^{-1}	N.D.	1.94
TB 31	8.58×10^{-1}	4.77×10^{-1}	1.75×10^{-1}	7.15×10^{-2}	1.38×10^{-1}	7.56×10^{-1}	2.73
TB 32	7.68×10^{-1}	7.09×10^{-1}	2.14×10^{-1}	4.97×10^{-2}	1.06×10^{-1}	4.90×10^{-1}	3.77
TB 33	4.35×10^{-1}	N.D.	1.14×10^{-1}	3.61×10^{-2}	6.18×10^{-2}	2.84×10^{-1}	1.70
	158	178/129	175	187	183	128	185
TB 4	1.31×10^{-1}	1.33×10^{-1}	N.D.	1.49×10^{-1}	6.13×10^{-2}	5.98×10^{-2}	N.D.
TB 12	5.84×10^{-2}	8.75×10^{-2}	N.D.	1.82×10^{-1}	6.25×10^{-2}	6.19×10^{-2}	N.D.
TB 28	6.18×10^{-2}	1.90×10^{-1}	N.D.	8.92×10^{-2}	5.50×10^{-2}	3.23×10^{-2}	8.06×10^{-3}
TB 29	6.95×10^{-2}	1.28×10^{-1}	4.62×10^{-3}	7.47×10^{-2}	6.04×10^{-2}	6.48×10^{-2}	1.09×10^{-2}
TB 30	1.79×10^{-1}	9.72×10^{-2}	5.46×10^{-3}	1.98×10^{-1}	9.39×10^{-2}	9.36×10^{-2}	1.51×10^{-2}
TB 31	1.25×10^{-1}	2.10×10^{-1}	N.D.	2.67×10^{-1}	1.13×10^{-1}	1.99×10^{-1}	3.09×10^{-2}
TB 32	1.93×10^{-1}	1.40×10^{-1}	N.D.	1.80×10^{-1}	8.75×10^{-2}	2.77×10^{-1}	2.38×10^{-2}
TB 33	9.71×10^{-2}	8.07×10^{-2}	1.06×10^{-2}	1.53×10^{-1}	7.03×10^{-2}	1.82×10^{-1}	1.85×10^{-2}

	174	177	171/156	201/157	172/197	180	193
TB 4	5.78×10^{-2}	2.27×10^{-1}	N.D.	N.D.	N.D.	1.05×10^{-1}	4.32×10^{-2}
TB 12	7.10×10^{-2}	1.03×10^{-1}	N.D.	N.D.	N.D.	1.05×10^{-1}	5.01×10^{-2}
TB 28	2.60×10^{-2}	2.37×10^{-1}	7.42×10^{-2}	4.14×10^{-2}	N.D.	5.31×10^{-2}	4.21×10^{-2}
TB 29	8.24×10^{-3}	8.55×10^{-2}	5.53×10^{-2}	3.52×10^{-2}	N.D.	5.02×10^{-2}	3.55×10^{-2}
TB 30	3.93×10^{-2}	3.28×10^{-2}	6.42×10^{-2}	3.96×10^{-2}	N.D.	1.42×10^{-1}	2.76×10^{-2}
TB 31	1.50×10^{-1}	8.83×10^{-2}	1.16×10^{-1}	5.74×10^{-2}	4.91×10^{-2}	1.51×10^{-1}	1.48×10^{-2}
TB 32	1.04×10^{-1}	7.77×10^{-2}	1.55×10^{-1}	2.10×10^{-2}	8.08×10^{-2}	3.04×10^{-2}	6.90×10^{-3}
TB 33	1.22×10^{-1}	3.08×10^{-2}	2.87×10^{-2}	3.95×10^{-2}	N.D.	9.92×10^{-2}	2.86×10^{-2}
	191	200	170	190	198	199	196/203
TB 4	N.D.	N.D.	6.15×10^{-2}	N.D.	N.D.	N.D.	N.D.
TB 12	N.D.	N.D.	4.65×10^{-2}	N.D.	N.D.	N.D.	N.D.
TB 28	N.D.	N.D.	1.48×10^{-2}	N.D.	N.D.	8.77×10^{-3}	N.D.

TB 29	4.98×10^{-2}	N.D.	5.42×10^{-2}	4.98×10^{-3}	N.D.	8.73×10^{-3}	1.10×10^{-2}
TB 30	N.D.	N.D.	4.94×10^{-2}	4.52×10^{-4}	N.D.	1.86×10^{-2}	1.14×10^{-2}
TB 31	N.D.	1.79×10^{-2}	2.36×10^{-2}	2.07×10^{-3}	N.D.	3.16×10^{-2}	1.39×10^{-2}
TB 32	N.D.	4.16×10^{-3}	3.08×10^{-2}	3.41×10^{-4}	4.43×10^{-3}	2.15×10^{-2}	N.D.
TB 33	N.D.	N.D.	2.39×10^{-2}	3.40×10^{-3}	N.D.	2.30×10^{-2}	N.D.
	189	208	195	207	194	205	206
TB 4	N.D.	N.D.	N.D.	N.D.	N.D.	N.D.	N.D.
TB 12	N.D.	N.D.	N.D.	N.D.	N.D.	N.D.	N.D.
TB 28	N.D.	N.D.	N.D.	N.D.	N.D.	N.D.	N.D.
TB 29	3.10×10^{-2}	N.D.	N.D.	3.42×10^{-2}	1.41×10^{-2}	N.D.	N.D.
TB 30	N.D.	N.D.	N.D.	N.D.	N.D.	N.D.	N.D.
TB 31	N.D.	N.D.	N.D.	N.D.	N.D.	N.D.	N.D.
TB 32	N.D.	N.D.	1.78×10^{-2}	N.D.	N.D.	N.D.	N.D.

TB 33	N.D.	N.D.	N.D.	N.D.	N.D.	N.D.	N.D.
	209	TL					
TB 4	N.D.	3.48					
TB 12	N.D.	3.47					
TB 28	N.D.	3.35					
TB 29	N.D.	3.47					
TB 30	N.D.	3.89					
TB 31	N.D.	3.81					
TB 32	N.D.	3.91					
TB 33	N.D.	3.78					

Char		Recovery %	Recovery %	PCB concentrations (ng/g) wet weight			
Samples	Lipid %	PCB 30	PCB 204	1	3	4/10	7
CH 1	7.57	7.36×10 ¹	1.21×10 ²	N.D.	N.D.	N.D.	N.D.
CH 2	3.62	8.17×10 ¹	1.04×10 ²	N.D.	N.D.	6.14×10 ⁻²	3.16×10 ⁻²
CH 3	2.88	8.46×10 ¹	8.64×10 ¹	N.D.	N.D.	4.68×10 ⁻²	1.62×10 ⁻²
CH 6	1.88	7.02×10 ¹	8.76×10 ¹	N.D.	N.D.	4.48×10 ⁻²	N.D.
CH 8	1.69	7.76×10 ¹	9.40×10 ¹	N.D.	N.D.	N.D.	N.D.
	6	8/5	19	18	17	24/27	16/32
CH 1	N.D.	N.D.	N.D.	3.50×10 ⁻²	N.D.	1.35×10 ⁻²	1.58×10 ⁻²
CH 2	N.D.	N.D.	5.52×10 ⁻²	5.54×10 ⁻²	3.38×10 ⁻²	N.D.	1.29×10 ⁻²
CH 3	N.D.	N.D.	3.16×10 ⁻²	4.24×10 ⁻²	4.68×10 ⁻²	N.D.	1.10×10 ⁻²
CH 6	N.D.	N.D.	1.58×10 ⁻²	2.05×10 ⁻²	1.43×10 ⁻²	N.D.	1.31×10 ⁻²
CH 8	N.D.	N.D.	N.D.	2.69×10 ⁻²	N.D.	N.D.	1.88×10 ⁻²

	26	25	31	28	33	22	45
CH 1	N.D.	N.D.	1.14×10^{-1}	1.28×10^{-1}	N.D.	N.D.	5.56×10^{-2}
CH 2	5.07×10^{-2}	N.D.	1.10×10^{-1}	1.06×10^{-1}	1.46×10^{-2}	6.89×10^{-2}	2.67×10^{-1}
CH 3	N.D.	1.38×10^{-2}	6.49×10^{-1}	7.34×10^{-2}	4.78×10^{-2}	6.41×10^{-2}	6.32×10^{-2}
CH 6	6.45×10^{-3}	1.43×10^{-2}	4.18×10^{-1}	3.12×10^{-2}	2.15×10^{-2}	2.82×10^{-2}	5.41×10^{-2}
CH 8	N.D.	N.D.	4.18×10^{-1}	6.09×10^{-2}	3.70×10^{-2}	3.38×10^{-2}	6.54×10^{-2}
	46	52	49	47	48	44	42
CH 1	1.47×10^{-1}	1.73×10^{-1}	1.15×10^{-1}	3.05×10^{-2}	N.D.	8.31×10^{-2}	3.81×10^{-2}
CH 2	7.50×10^{-2}	1.88×10^{-1}	1.27×10^{-1}	5.37×10^{-2}	8.40×10^{-2}	1.11×10^{-1}	5.26×10^{-2}
CH 3	8.55×10^{-2}	1.56×10^{-1}	9.29×10^{-2}	4.27×10^{-2}	1.12×10^{-2}	9.44×10^{-2}	3.80×10^{-2}
CH 6	7.52×10^{-2}	7.24×10^{-2}	4.82×10^{-2}	3.77×10^{-2}	N.D.	4.99×10^{-2}	2.47×10^{-2}
CH 8	7.19×10^{-2}	7.65×10^{-2}	5.95×10^{-2}	4.18×10^{-2}	3.40×10^{-2}	5.09×10^{-2}	3.45×10^{-2}
	41/71	64	40	74	70/76	66	95

CH 1	N.D.	5.18×10^{-2}	N.D.	4.01×10^{-2}	1.41×10^{-1}	N.D.	3.52×10^{-1}
CH 2	N.D.	6.14×10^{-2}	2.05×10^{-2}	5.90×10^{-2}	1.41×10^{-1}	N.D.	3.50×10^{-1}
CH 3	5.34×10^{-2}	6.00×10^{-2}	1.30×10^{-2}	6.18×10^{-2}	1.41×10^{-1}	N.D.	2.82×10^{-1}
CH 6	N.D.	4.86×10^{-2}	3.70×10^{-2}	4.17×10^{-2}	1.07×10^{-1}	N.D.	1.42×10^{-1}
CH 8	2.19×10^{-2}	4.34×10^{-2}	N.D.	4.17×10^{-2}	9.74×10^{-2}	1.02×10^{-1}	9.48×10^{-2}
	56/60	91	84/89	101	99	83	97
CH 1	6.02×10^{-2}	2.72×10^{-2}	2.28×10^{-1}	2.72×10^{-1}	2.71×10^{-1}	N.D.	1.16×10^{-1}
CH 2	1.04×10^{-1}	3.14×10^{-2}	1.41×10^{-1}	2.33×10^{-1}	1.10×10^{-1}	1.32×10^{-1}	1.45×10^{-1}
CH 3	9.58×10^{-2}	1.55×10^{-2}	5.96×10^{-2}	1.51×10^{-1}	1.50×10^{-1}	2.89×10^{-2}	6.04×10^{-2}
CH 6	N.D.	N.D.	4.61×10^{-2}	9.71×10^{-2}	1.20×10^{-1}	3.78×10^{-2}	6.72×10^{-2}
CH 8	3.42×10^{-2}	1.77×10^{-2}	6.54×10^{-2}	1.06×10^{-1}	1.06×10^{-1}	5.05×10^{-2}	5.71×10^{-2}
	87	85	136	110	82	151	144/135
CH 1	1.65×10^{-1}	N.D.	N.D.	2.27×10^{-1}	N.D.	7.45×10^{-2}	1.11×10^{-1}

CH 2	2.15×10^{-1}	1.18×10^{-1}	1.62×10^{-2}	4.82×10^{-1}	1.89×10^{-1}	N.D.	7.43×10^{-2}
CH 3	1.01×10^{-1}	2.92×10^{-2}	1.08×10^{-2}	2.83×10^{-1}	1.77×10^{-2}	5.67×10^{-2}	4.76×10^{-2}
CH 6	1.01×10^{-1}	3.13×10^{-2}	1.67×10^{-2}	3.39×10^{-1}	2.87×10^{-2}	4.46×10^{-2}	N.D.
CH 8	8.52×10^{-2}	2.48×10^{-2}	1.34×10^{-2}	1.83×10^{-1}	1.40×10^{-2}	3.76×10^{-2}	8.17×10^{-3}
	149	118	134	114	131	146	153
CH 1	2.86×10^{-1}	3.50	N.D.	1.98×10^{-1}	6.24×10^{-2}	2.61×10^{-2}	3.61×10^{-1}
CH 2	3.41×10^{-1}	2.50	6.88×10^{-2}	4.27×10^{-2}	2.99×10^{-2}	1.46×10^{-1}	5.51×10^{-1}
CH 3	2.15×10^{-1}	1.22	N.D.	6.26×10^{-2}	2.02×10^{-2}	6.90×10^{-2}	3.44×10^{-1}
CH 6	2.29×10^{-1}	8.53×10^{-1}	1.11×10^{-2}	5.64×10^{-2}	2.86×10^{-2}	8.22×10^{-2}	4.14×10^{-1}
CH 8	1.48×10^{-1}	6.33×10^{-1}	N.D.	6.86×10^{-3}	6.02×10^{-3}	3.27×10^{-2}	1.82×10^{-1}
	132	105	141	179	137	130/176	138
CH 1	2.10×10^{-1}	2.95×10^{-2}	3.64×10^{-2}	9.49×10^{-3}	3.31×10^{-2}	2.21×10^{-1}	6.51×10^{-1}
CH 2	2.69×10^{-1}	1.96×10^{-1}	5.67×10^{-2}	N.D.	3.88×10^{-2}	1.39×10^{-1}	7.84×10^{-1}

CH 3	1.47×10^{-1}	9.32×10^{-2}	4.45×10^{-2}	1.46×10^{-2}	1.82×10^{-2}	1.04×10^{-1}	6.22×10^{-1}
CH 6	2.26×10^{-1}	1.85×10^{-1}	7.82×10^{-2}	1.96×10^{-2}	3.19×10^{-2}	1.18×10^{-1}	9.50×10^{-1}
CH 8	1.04×10^{-1}	7.23×10^{-2}	3.14×10^{-2}	1.28×10^{-2}	1.64×10^{-2}	6.37×10^{-2}	3.85×10^{-1}
	158	178/129	175	187	183	128	185
CH 1	2.36×10^{-2}	6.78×10^{-2}	N.D.	9.59×10^{-2}	3.41×10^{-2}	3.07×10^{-2}	N.D.
CH 2	2.67×10^{-2}	3.74×10^{-2}	N.D.	5.75×10^{-2}	2.43×10^{-2}	7.04×10^{-2}	1.19×10^{-2}
CH 3	6.26×10^{-2}	3.17×10^{-2}	N.D.	4.41×10^{-2}	2.44×10^{-2}	5.39×10^{-2}	N.D.
CH 6	6.51×10^{-2}	4.85×10^{-2}	N.D.	3.57×10^{-2}	2.60×10^{-2}	1.08×10^{-1}	8.74×10^{-3}
CH 8	2.62×10^{-2}	2.31×10^{-2}	N.D.	2.43×10^{-2}	1.57×10^{-2}	3.82×10^{-2}	N.D.
	174	177	171/156	201/157	172/197	180	193
CH 1	5.90×10^{-2}	9.19×10^{-2}	N.D.	N.D.	N.D.	6.83×10^{-3}	4.98×10^{-2}
CH 2	4.01×10^{-2}	6.13×10^{-3}	1.57×10^{-2}	9.75×10^{-3}	4.00×10^{-3}	3.42×10^{-2}	1.98×10^{-2}
CH 3	4.01×10^{-2}	N.D.	N.D.	3.12×10^{-3}	N.D.	3.54×10^{-2}	1.57×10^{-2}

CH 6	5.69×10^{-2}	1.27×10^{-2}	3.18×10^{-2}	1.03×10^{-2}	N.D.	3.26×10^{-2}	1.87×10^{-2}
CH 8	2.79×10^{-2}	9.73×10^{-3}	N.D.	1.18×10^{-2}	N.D.	2.19×10^{-2}	2.19×10^{-3}
	191	200	170	190	198	199	196/203
CH 1	N.D.	N.D.	1.36×10^{-2}	N.D.	N.D.	1.01×10^{-2}	5.80×10^{-3}
CH 2	N.D.	2.20×10^{-3}	7.14×10^{-3}	8.60×10^{-4}	N.D.	6.44×10^{-3}	1.33×10^{-3}
CH 3	N.D.	N.D.	6.43×10^{-3}	N.D.	N.D.	5.42×10^{-3}	N.D.
CH 6	N.D.	N.D.	8.73×10^{-3}	N.D.	N.D.	2.57×10^{-3}	4.32×10^{-4}
CH 8	N.D.	N.D.	4.71×10^{-3}	N.D.	N.D.	N.D.	N.D.
	189	2.08×10^2	1.95×10^2	2.07×10^2	1.94×10^2	2.05×10^2	2.06×10^2
CH 1	N.D.	N.D.	N.D.	N.D.	N.D.	N.D.	N.D.
CH 2	N.D.	N.D.	N.D.	N.D.	N.D.	N.D.	N.D.
CH 3	N.D.	N.D.	N.D.	N.D.	N.D.	N.D.	N.D.
CH 6	N.D.	N.D.	N.D.	N.D.	N.D.	N.D.	N.D.

CH 8	N.D.	N.D.	N.D.	N.D.	N.D.	N.D.	N.D.
	209	TL					
CH 1	N.D.	3.06					
CH 2	N.D.	2.93					
CH 3	N.D.	3.07					
CH 6	N.D.	2.92					
CH 8	N.D.	2.98					

Harp seal		Recovery %	Recovery %	PCB concentrations (ng/g) wet weight			
Samples	Lipid %	PCB 30	PCB 204	1	3	4/10	7
HS 02	8.85×10 ¹	6.11×10 ¹	6.88×10 ¹	N.D.	N.D.	N.D.	N.D.
HS 02 DUP	8.83×10 ¹	8.53×10 ¹	1.06×10 ²	N.D.	N.D.	4.90×10 ⁻¹	1.11
HS 03	1.03×10 ²	7.67×10 ¹	9.15×10 ¹	N.D.	N.D.	N.D.	2.96×10 ⁻¹
HS 04	8.92×10 ¹	5.38×10 ¹	6.98×10 ¹	N.D.	N.D.	N.D.	4.59
HS 06	9.57×10 ¹	1.01×10 ²	1.01×10 ²	N.D.	N.D.	1.87	1.36
	6	8/5	19	18	17	24/27	16/32
HS 02	N.D.	N.D.	6.71×10 ⁻¹	3.22	N.D.	N.D.	1.99
HS 02 DUP	7.94×10 ⁻¹	N.D.	N.D.	3.43	2.68×10 ⁻¹	N.D.	5.38×10 ⁻¹
HS 03	6.95×10 ⁻¹	6.60	5.46×10 ⁻¹	8.32×10 ⁻¹	6.82×10 ⁻¹	N.D.	N.D.
HS 04	5.93	6.66	1.30×10 ¹	N.D.	1.11×10 ¹	N.D.	9.09
HS 06	N.D.	N.D.	4.35×10 ⁻¹	N.D.	N.D.	N.D.	N.D.

	26	25	31	28	33	22	45
HS 02	4.05	2.51×10^{-2}	4.94	1.91	9.24×10^{-1}	2.24	7.61
HS 02 DUP	9.52×10^{-1}	2.91×10^{-1}	4.63	6.75×10^{-1}	1.89	4.25	1.57×10^1
HS 03	2.11	N.D.	3.75	3.54	7.44×10^{-1}	N.D.	1.05×10^1
HS 04	5.11	6.08	7.24	1.65	1.23	5.17×10^{-1}	7.18
HS 06	2.89	1.18	4.99	1.69	1.26	N.D.	5.12
	46	52	49	47	48	44	42
HS 02	N.D.	9.90	3.53	4.49	4.64	2.74	1.16
HS 02 DUP	N.D.	1.55×10^1	6.97	6.11	7.94	3.33	1.30
HS 03	4.55×10^{-1}	6.04	1.57	3.53	3.37	4.64×10^{-1}	6.53×10^{-1}
HS 04	2.49	1.19×10^1	3.05	3.89	4.61	3.32	1.16
HS 06	N.D.	1.75×10^1	5.48	7.52	6.71	6.81	1.68
	41/71	64	40	74	70/76	66	95

HS 02	N.D.	3.62	N.D.	6.22	5.14	3.59	1.99×10 ¹
HS 02 DUP	4.48×10 ⁻¹	4.24	N.D.	6.56	5.07	3.63	1.43×10 ¹
HS 03	N.D.	1.25	N.D.	2.34	1.24	1.63	1.11×10 ¹
HS 04	5.99×10 ⁻¹	1.49	7.25×10 ⁻¹	4.64	3.18	1.44	9.46
HS 06	N.D.	2.22	N.D.	8.82	5.96	1.61	1.76×10 ¹
	56/60	91	84/89	101	99	83	97
HS 02	3.63	1.11	N.D.	1.31×10 ¹	1.32×10 ¹	1.57×10 ¹	1.46
HS 02 DUP	5.82	1.77	1.66	2.38×10 ¹	2.41×10 ¹	1.28×10 ¹	3.55
HS 03	1.23	1.60	8.42	9.26	6.39×10 ¹	5.23	2.81×10 ⁻¹
HS 04	1.27	N.D.	N.D.	7.89	3.07×10 ¹	7.53	9.19×10 ⁻¹
HS 06	2.46	1.02	N.D.	1.82×10 ¹	4.91×10 ¹	7.22	3.91
	87	85	136	110	82	151	144/135
HS 02	8.06	5.20	N.D.	3.92	N.D.	3.55	4.64

HS 02 DUP	5.38	9.96	9.23×10^{-1}	6.84	N.D.	7.30	6.88
HS 03	2.43	7.68	N.D.	5.23	N.D.	1.28	3.49
HS 04	3.24	6.78	5.27×10^{-1}	2.57	N.D.	2.48	7.04×10^{-1}
HS 06	4.27	9.32	N.D.	3.98	N.D.	3.70	8.18×10^{-1}
	149	118	134	114	131	146	153
HS 02	1.46×10^1	2.82×10^1	2.83	1.23	9.69×10^{-1}	2.32×10^1	8.68×10^1
HS 02 DUP	1.96×10^1	3.95×10^1	N.D.	1.70	1.42	3.73×10^1	1.98×10^2
HS 03	8.46	1.77×10^1	1.66	4.54×10^{-1}	5.29×10^{-1}	1.17×10^1	1.04×10^2
HS 04	4.65	1.78×10^1	N.D.	3.66×10^{-1}	N.D.	1.10×10^1	6.24×10^1
HS 06	1.27×10^1	3.07×10^1	N.D.	3.93×10^{-1}	N.D.	1.24×10^1	7.98×10^1
	132	105	141	179	137	130/176	138
HS 02	2.73	3.99	N.D.	2.46×10^{-1}	2.59	1.00×10^1	6.84×10^1
HS 02 DUP	2.63	6.47	2.03	5.27×10^{-1}	4.11	2.20×10^1	1.42×10^2

HS 03	9.58×10^{-1}	1.76	N.D.	1.09×10^{-1}	1.53	8.70	7.16×10^1
HS 04	2.77	1.73	8.89×10^{-1}	7.70×10^{-1}	1.37	3.37	4.46×10^1
HS 06	1.41	6.19	1.38	2.88×10^{-1}	1.87	6.38	6.99×10^1
	158	178/129	175	187	183	128	185
HS 02	1.89	2.88×10^1	7.41×10^{-1}	2.27×10^1	1.05×10^1	1.16×10^1	N.D.
HS 02 DUP	3.72	4.66×10^1	1.61	5.24×10^1	2.69×10^1	2.95×10^1	4.19×10^{-1}
HS 03	1.11	9.14	1.02×10^{-1}	7.85	4.79	1.06×10^1	N.D.
HS 04	1.05	8.85	6.27×10^{-1}	9.31	4.93	5.92	N.D.
HS 06	1.34	1.65×10^1	3.70×10^{-1}	1.15×10^1	5.47	7.16	1.96×10^{-1}
	174	177	171/156	201/157	172/197	180	193
HS 02	1.56	1.24×10^1	3.73	3.05×10^{-1}	4.96	4.10×10^1	4.07
HS 02 DUP	2.33	2.55×10^1	9.21	9.46×10^{-1}	1.27×10^1	1.01×10^2	9.47
HS 03	4.30×10^{-1}	5.06	1.38	2.96×10^{-1}	2.32	2.83×10^1	3.04

HS 04	1.16	4.69	1.40	5.61×10^{-2}	2.27	2.13×10^1	2.10
HS 06	5.12×10^{-1}	5.78	2.82	2.80×10^{-1}	2.14	1.87×10^1	1.68
	191	200	170	190	198	199	196/203
HS 02	3.04×10^{-1}	N.D.	1.45×10^1	3.46×10^{-2}	3.70×10^{-1}	1.44×10^1	6.18
HS 02 DUP	1.13	N.D.	3.47×10^1	3.30	1.70	4.50×10^1	1.82×10^1
HS 03	2.14×10^{-1}	N.D.	1.07×10^1	1.91	N.D.	5.81	2.40
HS 04	N.D.	N.D.	8.22	1.19	N.D.	6.67	1.93
HS 06	N.D.	N.D.	8.02	1.60	1.84×10^{-1}	4.85	1.77
	189	208	195	207	194	205	206
HS 02	5.36×10^{-1}	8.48×10^{-1}	2.23	N.D.	8.74	2.78×10^{-1}	2.82
HS 02 DUP	1.12	3.05	5.79	9.59×10^{-2}	2.44×10^1	1.29	1.03×10^1
HS 03	5.03×10^{-1}	2.74×10^{-1}	7.80×10^{-1}	N.D.	4.32	2.48×10^{-1}	1.48
HS 04	5.14×10^{-1}	3.04×10^{-1}	8.87×10^{-1}	N.D.	4.39	1.54×10^{-2}	1.21

HS 06	2.39×10^{-1}	N.D.	5.05×10^{-1}	N.D.	2.16	N.D.	5.21×10^{-1}
	209	TL					
HS 02	9.97×10^{-1}	3.58					
HS 02 DUP	3.00	2.79					
HS 03	4.46×10^{-1}	2.94					
HS 04	3.88×10^{-1}	2.84					
HS 06	2.38×10^{-1}	2.86					

Ringed seal		Recovery %	Recovery %	PCB concentrations (ng/g) wet weight			
Samples	Lipid %	PCB 30	PCB 204	1	3	4/10	7
RS 01	8.89×10 ¹	6.58×10 ¹	6.67×10 ¹	N.D.	N.D.	N.D.	N.D.
RS 01 DUP	9.20×10 ¹	7.79×10 ¹	1.03×10 ²	N.D.	N.D.	N.D.	N.D.
RS 02	9.18×10 ¹	6.22×10 ¹	6.57×10 ¹	N.D.	N.D.	3.87×10 ⁻¹	7.26×10 ⁻¹
RS 04	9.51×10 ¹	7.63×10 ¹	8.17×10 ¹	N.D.	N.D.	4.06×10 ⁻¹	1.17
RS 11	8.95×10 ¹	N/A	N/A	N.D.	N.D.	N.D.	N.D.
RS 12	8.40×10 ¹	9.60×10 ¹	6.80×10 ¹	N.D.	N.D.	4.83×10 ⁻¹	N.D.
	6	8/5	19	18	17	24/27	16/32
RS 01	N.D.	N.D.	N.D.	N.D.	N.D.	N.D.	N.D.
RS 01 DUP	N.D.	N.D.	N.D.	N.D.	N.D.	N.D.	N.D.
RS 02	N.D.	N.D.	N.D.	N.D.	N.D.	N.D.	N.D.
RS 04	1.05	N.D.	1.24	8.34×10 ⁻¹	3.74×10 ⁻¹	N.D.	4.20×10 ⁻¹

RS 11	N.D.	N.D.	N.D.	N.D.	N.D.	N.D.	9.33×10 ⁻²
RS 12	N.D.	N.D.	5.16×10 ⁻¹	3.42×10 ⁻¹	1.18	N.D.	N.D.
	26	25	31	28	33	22	45
RS 01	N.D.	N.D.	4.56	6.89	1.04	3.56	1.63×10 ¹
RS 01 DUP	N.D.	N.D.	6.13	7.74	6.01×10 ⁻¹	3.56	1.35×10 ¹
RS 02	1.63	N.D.	2.31	5.91	N.D.	3.65	1.99
RS 04	N.D.	N.D.	4.09	5.52	N.D.	4.65	5.07
RS 11	7.83×10 ⁻¹	5.26×10 ⁻¹	1.96	4.54	4.94×10 ⁻¹	2.76	4.88
RS 12	6.44×10 ⁻¹	3.01×10 ⁻¹	2.19	1.43	1.77×10 ⁻¹	5.84×10 ⁻²	1.46
	46	52	49	47	48	44	42
RS 01	5.30×10 ⁻¹	3.08×10 ¹	8.69	1.06×10 ¹	2.96	2.37	1.61
RS 01 DUP	N.D.	3.25×10 ¹	1.08×10 ¹	1.14×10 ¹	3.02	2.94	1.72
RS 02	N.D.	6.98	4.24	3.25	1.06	8.05×10 ⁻¹	5.89×10 ⁻¹

RS 04	1.77	1.41×10^1	4.58	5.86	3.84	1.58	2.09
RS 11	N.D.	1.05×10^1	1.84	3.75	1.14	1.08	3.10×10^{-1}
RS 12	1.11	2.26	1.49×10^{-1}	8.32×10^{-1}	1.17	4.94×10^{-1}	9.46×10^{-1}
	41/71	64	40	74	70/76	66	95
RS 01	N.D.	3.81	N.D.	1.77×10^1	3.00	1.26×10^1	3.17×10^1
RS 01 DUP	N.D.	4.23	N.D.	1.77×10^1	4.08	1.44×10^1	3.23×10^1
RS 02	N.D.	8.29×10^{-1}	1.53	5.63	1.89	4.33	1.04×10^1
RS 04	N.D.	1.74	6.57×10^{-1}	8.18	1.51	3.31	2.07×10^1
RS 11	N.D.	1.83	1.45	8.37	2.19	1.16×10^1	2.50×10^1
RS 12	2.12×10^{-1}	8.45×10^{-1}	N.D.	1.41	4.48×10^{-1}	1.58	1.69
	56/60	91	84/89	101	99	83	97
RS 01	1.03×10^1	1.93	5.89×10^{-1}	4.96×10^1	5.14×10^1	3.36	1.60
RS 01 DUP	1.15×10^1	1.00	7.86×10^{-1}	5.46×10^1	5.46×10^1	3.51	2.00

RS 02	2.42	N.D.	3.05×10^{-1}	9.73	9.71	5.16×10^{-1}	3.97×10^{-1}
RS 04	3.39	6.62×10^{-1}	3.55×10^{-1}	1.77×10^1	1.76×10^1	2.83	4.08×10^{-1}
RS 11	4.77	7.94×10^{-1}	1.21	1.68×10^1	1.65×10^1	6.01×10^{-1}	2.72×10^{-1}
RS 12	5.87×10^{-1}	2.32×10^{-1}	N.D.	2.82	2.80	N.D.	9.15×10^{-2}
	87	85	136	110	82	151	144/135
RS 01	9.26	1.41×10^1	N.D.	1.61×10^1	N.D.	6.13	1.64
RS 01 DUP	1.04×10^1	1.48×10^1	N.D.	1.86×10^1	N.D.	5.75	1.54
RS 02	1.30	1.86	N.D.	3.65	N.D.	5.35×10^{-1}	N.D.
RS 04	1.91	4.62	N.D.	4.24	N.D.	1.86	4.14×10^{-1}
RS 11	2.20	2.83	N.D.	5.40	N.D.	8.40×10^{-1}	N.D.
RS 12	2.28×10^{-1}	5.53×10^{-1}	N.D.	1.11	N.D.	4.61×10^{-1}	N.D.
	149	118	134	114	131	146	153
RS 01	3.25×10^1	5.84×10^1	N.D.	2.42	6.93×10^{-1}	2.70×10^1	1.13×10^2

RS 01 DUP	3.33×10^1	6.24×10^1	N.D.	2.51	7.50×10^{-1}	2.44×10^1	1.24×10^2
RS 02	1.52×10^1	1.07×10^1	N.D.	4.06×10^{-1}	N.D.	3.67	1.91×10^1
RS 04	1.83×10^1	1.42×10^1	N.D.	5.53×10^{-1}	N.D.	8.48	4.07×10^1
RS 11	2.14×10^1	2.37×10^1	N.D.	6.86×10^{-1}	N.D.	5.78	3.36×10^1
RS 12	1.84	3.75	N.D.	8.78×10^{-2}	5.15×10^{-2}	1.11	7.15
	132	105	141	179	137	130/176	138
RS 01	2.61	1.90×10^1	5.08	2.57×10^{-1}	7.13	1.66×10^1	1.04×10^2
RS 01 DUP	3.21	2.02×10^1	5.19	4.63×10^{-1}	7.05	1.80×10^1	1.12×10^2
RS 02	3.61×10^{-1}	3.72	9.67×10^{-1}	2.62×10^{-1}	8.46×10^{-1}	2.12	1.91×10^1
RS 04	8.98×10^{-1}	4.84	8.20×10^{-1}	2.65×10^{-1}	1.75	4.65	4.15×10^1
RS 11	6.91×10^{-1}	7.78	1.11	N.D.	1.44	3.05	3.08×10^1
RS 12	N.D.	1.28	1.22×10^{-1}	3.39×10^{-2}	1.65×10^{-1}	8.21×10^{-1}	5.04
	158	178/129	175	187	183	128	185

RS 01	4.64	1.83×10^1	2.60×10^{-1}	1.77×10^1	1.10×10^1	2.05×10^1	2.39×10^{-1}
RS 01 DUP	5.11	1.78×10^1	2.46×10^{-1}	2.10×10^1	1.21×10^1	2.54×10^1	8.86×10^{-1}
RS 02	1.03	4.60	N.D.	2.65	9.61×10^{-1}	6.25	N.D.
RS 04	1.48	8.00	N.D.	8.77	2.95	4.89	N.D.
RS 11	9.06×10^{-1}	6.49	N.D.	4.03	1.60	3.84	N.D.
RS 12	1.37×10^{-1}	8.24×10^{-1}	5.40×10^{-2}	8.14×10^{-1}	4.21×10^{-1}	6.74×10^{-1}	N.D.
	174	177	171/156	201/157	172/197	180	193
RS 01	1.25	1.29	5.98	7.30×10^{-1}	3.37	2.48×10^1	2.35
RS 01 DUP	1.44	1.91	6.85	7.76×10^{-1}	3.83	2.87×10^1	3.26
RS 02	5.77×10^{-1}	2.82×10^{-1}	6.85×10^{-1}	N.D.	N.D.	2.20	8.21×10^{-1}
RS 04	1.07	1.26	1.62	9.43×10^{-2}	1.00	7.10	1.20
RS 11	3.79×10^{-1}	N.D.	8.20×10^{-1}	1.37×10^{-1}	3.15×10^{-1}	4.06	4.19×10^{-1}
RS 12	N.D.	1.06×10^{-1}	9.09×10^{-2}	N.D.	1.22×10^{-1}	9.14×10^{-1}	1.50×10^{-1}

	191	200	170	190	198	199	196/203
RS 01	1.97×10 ⁻¹	N.D.	1.00×10 ¹	9.98×10 ⁻¹	N.D.	4.16	2.71
RS 01 DUP	3.45×10 ⁻¹	N.D.	1.29×10 ¹	2.49	N.D.	5.28	3.56
RS 02	N.D.	N.D.	2.14	4.10×10 ⁻¹	N.D.	4.75×10 ⁻¹	1.39×10 ⁻¹
RS 04	N.D.	N.D.	4.85	2.05	N.D.	1.62	8.26×10 ⁻¹
RS 11	N.D.	N.D.	2.89	4.57×10 ⁻¹	N.D.	5.15×10 ⁻¹	2.12×10 ⁻¹
RS 12	N.D.	N.D.	2.54×10 ⁻¹	6.05×10 ⁻²	N.D.	1.48×10 ⁻¹	7.14×10 ⁻²
	189	208	195	207	194	205	206
RS 01	2.20×10 ⁻¹	N.D.	5.25×10 ⁻¹	N.D.	2.35	N.D.	2.98×10 ⁻¹
RS 01 DUP	N.D.	N.D.	6.71×10 ⁻¹	2.69×10 ⁻¹	3.02	N.D.	3.88×10 ⁻¹
RS 02	N.D.	N.D.	N.D.	N.D.	1.93×10 ⁻¹	N.D.	N.D.
RS 04	N.D.	N.D.	1.09×10 ⁻¹	N.D.	4.55×10 ⁻¹	N.D.	N.D.
RS 11	N.D.	N.D.	N.D.	N.D.	3.10×10 ⁻¹	N.D.	N.D.

RS 12	N.D.	N.D.	N.D.	N.D.	4.03×10^{-2}	N.D.	N.D.
	209	TL					
RS 01	N.D.	2.87					
RS 01 DUP	N.D.	2.87					
RS 02	N.D.	2.95					
RS 04	N.D.	3.14					
RS 11	N.D.	3.06					
RS 12	N.D.	3.48					

Greenland shark		Recovery %	Recovery %	PCB concentrations (ng/g) wet weight			
Samples	Lipid %	PCB 30	PCB 204	1	3	4/10	7
GS 01	2.93×10 ¹	7.31×10 ¹	5.18×10 ¹	N.D.	N.D.	2.31	2.45
GS 02	1.58×10 ¹	6.83×10 ¹	6.64×10 ¹	N.D.	N.D.	1.12	2.03
GS 03	2.79×10 ¹	7.49×10 ¹	7.70×10 ¹	N.D.	N.D.	1.63	5.49
GS 04	2.44×10 ¹	8.07×10 ¹	1.00×10 ²	N.D.	N.D.	1.46	2.73
GS 05	2.91×10 ¹	8.78×10 ¹	6.33×10 ¹	N.D.	N.D.	6.59×10 ⁻²	6.38×10 ⁻¹
GS 08	2.53×10 ¹	1.03×10 ²	8.16×10 ¹	N.D.	N.D.	1.98	9.97
GS 09	1.95×10 ¹	8.78×10 ¹	8.68×10 ¹	N.D.	N.D.	2.03	3.69
GS 11	2.48×10 ¹	1.10×10 ²	1.15×10 ²	N.D.	N.D.	4.04	5.74
GS 12	2.66×10 ¹	1.08×10 ²	9.43×10 ¹	N.D.	N.D.	N.D.	2.13
GS 15	2.28×10 ¹	9.51×10 ¹	7.58×10 ¹	N.D.	N.D.	4.08×10 ⁻¹	3.38×10 ⁻¹
GS 16	2.89×10 ¹	7.78×10 ¹	9.87×10 ¹	N.D.	N.D.	5.09	3.52

	6	8/5	19	18	17	24/27	16/32
GS 01	N.D.	9.00	N.D.	1.44	N.D.	N.D.	N.D.
GS 02	N.D.	N.D.	1.18	7.59×10^{-1}	5.93×10^{-1}	N.D.	N.D.
GS 03	N.D.	N.D.	1.49	2.52	3.13	N.D.	5.25×10^{-1}
GS 04	N.D.	1.47	3.70	2.09	N.D.	N.D.	N.D.
GS 05	N.D.	4.63×10^{-1}	5.01×10^{-1}	N.D.	3.56×10^{-1}	N.D.	N.D.
GS 08	N.D.	N.D.	1.31	5.42	4.63	N.D.	9.28×10^{-1}
GS 09	N.D.	N.D.	5.93	5.98	4.29	N.D.	N.D.
GS 11	1.86	N.D.	4.90	5.71	1.93	N.D.	N.D.
GS 12	3.94	1.60×10^1	6.12	1.92	4.57	N.D.	N.D.
GS 15	N.D.	1.97×10^1	1.86	1.56	1.33×10^1	N.D.	N.D.
GS 16	1.87	N.D.	3.12	2.65	N.D.	N.D.	N.D.
	26	25	31	28	33	22	45

GS 01	6.92	N.D.	1.38×10^1	4.82	2.88	2.19	2.00×10^1
GS 02	9.60×10^{-1}	N.D.	1.39	2.99	8.73×10^{-1}	7.26×10^{-1}	6.56
GS 03	2.91	N.D.	9.61	3.77	2.30	1.57	1.62×10^1
GS 04	3.54	5.51×10^{-1}	8.39	5.47	2.96	N.D.	1.76×10^1
GS 05	N.D.	N.D.	7.69×10^{-1}	1.69×10^{-1}	7.70×10^{-2}	5.42×10^{-1}	1.14
GS 08	5.24	1.69×10^{-1}	1.03×10^1	6.73	5.22	1.83	2.75×10^1
GS 09	2.85	N.D.	8.53	2.91	1.31	9.53×10^{-1}	1.59×10^1
GS 11	1.45	N.D.	1.95×10^1	6.03	N.D.	1.85	1.51×10^1
GS 12	4.82	N.D.	1.76×10^1	5.27	1.87	2.29	3.03×10^1
GS 15	4.96	7.56×10^{-1}	8.70	7.68	1.35	2.23	2.06×10^1
GS 16	9.61	1.41	2.05×10^1	1.11	3.35	3.79	2.71×10^1
	46	52	49	47	48	44	42
GS 01	N.D.	2.75×10^1	7.37	8.37	8.24	3.78	1.14

GS 02	1.50	1.09×10^1	1.06	3.39	3.51	1.33	2.57×10^{-1}
GS 03	2.22	1.89×10^1	5.28	7.07	1.02×10^1	4.02	5.05
GS 04	N.D.	3.28×10^1	8.52	6.71	8.61	7.20	2.58
GS 05	N.D.	1.12	4.69×10^{-2}	2.40×10^{-1}	1.68×10^{-1}	1.80×10^{-1}	1.20×10^{-1}
GS 08	4.78	4.29×10^1	8.83	1.40×10^1	1.45×10^1	4.55	2.61
GS 09	3.31	1.25×10^1	6.04	5.82	7.08	1.22	2.00
GS 11	5.21	3.50×10^1	9.43	8.92	4.64	5.21	1.54
GS 12	8.27	3.54×10^1	1.61×10^1	1.07×10^1	7.82	6.75	2.37
GS 15	2.12	2.19×10^1	5.02	7.87	3.13	2.31	N.D.
GS 16	5.02	5.69×10^1	1.33×10^1	1.92×10^1	1.05×10^1	5.08	7.48
	41/71	64	40	74	70/76	66	95
GS 01	N.D.	5.47	N.D.	1.42×10^1	3.73	1.01×10^1	3.56×10^1
GS 02	N.D.	1.93	1.03	7.22	5.96×10^{-1}	3.29×10^{-1}	1.19×10^1

GS 03	5.83×10^{-1}	4.68	1.20	9.22	4.17	6.49	2.06×10^1
GS 04	9.51×10^{-1}	4.85	1.21	1.02×10^1	4.19	8.89	2.47×10^1
GS 05	N.D.	2.38×10^{-1}	N.D.	3.02×10^{-1}	1.39	N.D.	7.81×10^{-1}
GS 08	1.53	6.46	1.07	1.89×10^1	3.10	N.D.	3.60×10^1
GS 09	7.80×10^{-1}	3.94	N.D.	1.24×10^1	9.61	4.76	1.43×10^1
GS 11	N.D.	4.65	N.D.	1.06×10^1	4.98	1.39×10^1	3.90×10^1
GS 12	N.D.	7.79	1.36	1.56×10^1	6.37	1.02×10^1	4.81×10^1
GS 15	N.D.	1.61	N.D.	1.32×10^1	2.41	1.17×10^1	2.70×10^1
GS 16	1.10	7.47	1.64	2.78×10^1	4.04	1.63×10^1	5.46×10^1
	56/60	91	84/89	101	99	83	97
GS 01	9.41	5.54	N.D.	5.64×10^1	5.64×10^1	1.42×10^1	4.76
GS 02	4.22	2.12	6.86	1.98×10^1	1.98×10^1	2.36	1.01
GS 03	5.78	5.88	N.D.	2.98×10^1	3.04×10^1	1.19×10^1	3.04

GS 04	5.91	6.50	1.50×10^1	2.88×10^1	2.88×10^1	5.53	2.76
GS 05	2.44×10^{-1}	8.85×10^{-2}	N.D.	1.02	1.93	8.13×10^{-2}	5.01×10^{-2}
GS 08	1.08×10^1	6.08	N.D.	6.19×10^1	6.19×10^1	1.40×10^1	6.03
GS 09	4.02	2.63	N.D.	2.59×10^1	2.59×10^1	1.06×10^1	N.D.
GS 11	1.02×10^1	7.28	N.D.	5.32×10^1	5.68×10^1	1.30×10^1	3.00
GS 12	9.91	8.45	N.D.	6.18×10^1	6.92×10^1	8.42	2.91
GS 15	5.63	2.73	N.D.	3.47×10^1	3.47×10^1	1.26×10^1	1.06
GS 16	1.56×10^1	1.25×10^1	N.D.	8.99×10^1	9.19×10^1	1.25×10^1	4.51
	87	85	136	110	82	151	144/135
GS 01	1.19×10^1	1.32×10^1	3.12	3.59×10^1	N.D.	1.19×10^1	4.93
GS 02	1.70	5.82	8.18×10^{-1}	8.08	N.D.	4.03	8.76×10^{-1}
GS 03	7.57	7.72	1.57	1.91×10^1	N.D.	7.14	5.35
GS 04	6.27	6.77	2.15	1.80×10^1	N.D.	7.36	3.34

GS 05	1.06×10^{-1}	3.99×10^{-1}	2.04×10^{-1}	5.92×10^{-1}	N.D.	3.56×10^{-1}	8.50×10^{-2}
GS 08	1.70×10^1	2.02×10^1	2.39	3.26×10^1	N.D.	1.40×10^1	7.71
GS 09	2.61	9.79	1.57	1.78×10^1	N.D.	4.76	1.16
GS 11	9.46	1.04×10^1	4.66	2.57×10^1	N.D.	1.71×10^1	6.77
GS 12	7.29	1.17×10^1	9.19	7.43×10^1	N.D.	1.79×10^1	4.04
GS 15	1.10×10^1	9.38	2.07	1.46×10^1	N.D.	8.66	1.08
GS 16	1.79×10^1	1.96×10^1	3.79	4.42×10^1	N.D.	1.81×10^1	7.21
	149	118	134	114	131	146	153
GS 01	3.82×10^1	5.97×10^1	N.D.	1.49×10^1	5.24	2.24×10^1	1.22×10^2
GS 02	1.12×10^1	2.43×10^1	1.02	5.03	1.23	7.54	5.81×10^1
GS 03	2.00×10^1	5.01×10^1	N.D.	7.57	4.69	1.16×10^1	7.52×10^1
GS 04	2.55×10^1	4.77×10^1	6.76	8.07	2.83	1.22×10^1	7.81×10^1
GS 05	1.47	1.25	N.D.	1.85×10^{-1}	N.D.	5.19×10^{-1}	3.08

GS 08	3.25×10^1	6.83×10^1	N.D.	1.65×10^1	1.33×10^1	2.49×10^1	1.58×10^2
GS 09	1.26×10^1	3.88×10^1	3.03	3.11	1.71	1.61×10^1	9.68×10^1
GS 11	3.74×10^1	6.57×10^1	N.D.	7.49	8.64	1.19×10^1	6.43×10^1
GS 12	4.27×10^1	7.18×10^1	N.D.	1.08×10^1	7.00	3.27×10^1	8.75×10^1
GS 15	1.94×10^1	4.81×10^1	2.46	8.24	1.10	1.47×10^1	8.03×10^1
GS 16	5.45×10^1	1.12×10^2	4.07	1.93×10^1	9.22	2.90×10^1	1.60×10^2
	132	105	141	179	137	130/176	138
GS 01	2.98×10^1	1.30×10^1	3.94	1.47	5.67	1.77×10^1	1.19×10^2
GS 02	8.03	6.38	1.69	3.77×10^{-1}	2.30	5.97	3.96×10^1
GS 03	1.47×10^1	1.27×10^1	2.04	7.83×10^{-1}	2.00	1.03×10^1	6.88×10^1
GS 04	1.39×10^1	6.71	2.09	7.15×10^{-1}	2.62	9.98	6.91×10^1
GS 05	1.24×10^{-1}	4.18×10^{-1}	1.43×10^{-1}	N.D.	6.96×10^{-2}	2.03×10^{-1}	2.66
GS 08	9.94	2.20×10^1	3.89	1.12	6.01	2.17×10^1	1.40×10^2

GS 09	9.63	5.93	2.46	N.D.	3.68	1.24×10 ¹	8.16×10 ¹
GS 11	2.47×10 ¹	1.13×10 ¹	2.98	2.12	3.06	9.97	7.28×10 ¹
GS 12	2.99×10 ¹	1.29×10 ¹	5.60	2.24	4.65	1.31×10 ¹	9.39×10 ¹
GS 15	1.82×10 ¹	8.67	2.80	7.02×10 ⁻¹	2.67	9.58	7.78×10 ¹
GS 16	3.13×10 ¹	2.21×10 ¹	6.41	1.71	8.14	2.21×10 ¹	1.50×10 ²
	158	178/129	175	187	183	128	185
GS 01	7.45	2.18×10 ¹	1.77	3.19×10 ¹	1.38×10 ¹	1.24×10 ¹	6.48×10 ⁻¹
GS 02	1.66	7.07	8.36×10 ⁻¹	1.13×10 ¹	4.46	4.22	N.D.
GS 03	1.67	1.38×10 ¹	2.02×10 ⁻¹	1.65×10 ¹	9.08	7.77	3.00×10 ⁻¹
GS 04	2.04	9.32	1.09	1.51×10 ¹	8.07	7.41	N.D.
GS 05	1.95×10 ⁻¹	4.46×10 ⁻¹	1.32×10 ⁻²	6.86×10 ⁻¹	3.20×10 ⁻¹	2.57×10 ⁻¹	N.D.
GS 08	5.11	2.44×10 ¹	1.79	3.21×10 ¹	1.78×10 ¹	1.77×10 ¹	1.64×10 ⁻¹
GS 09	2.72	1.41×10 ¹	1.72	2.64×10 ¹	1.38×10 ¹	6.48	N.D.

GS 11	6.99	1.63×10^1	1.52	2.41×10^1	9.26	7.56	4.58×10^{-1}
GS 12	8.23	2.06×10^1	1.80	3.58×10^1	1.21×10^1	1.11×10^1	9.61×10^{-1}
GS 15	3.28	1.50×10^1	3.07×10^{-1}	1.90×10^1	7.67	5.90	2.08×10^{-1}
GS 16	5.77	3.22×10^1	2.26	3.86×10^1	2.01×10^1	1.29×10^1	3.47×10^{-1}
	174	177	171/156	201/157	172/197	180	193
GS 01	6.65	9.20	5.90	1.26	3.56	2.79×10^1	2.29
GS 02	2.64	2.41	2.11	3.38×10^{-1}	1.21	9.55	8.20×10^{-1}
GS 03	3.35	5.95	4.55	8.89×10^{-1}	1.79	1.81×10^1	1.51
GS 04	2.84	4.92	3.23	5.12×10^{-1}	1.85	1.73×10^1	1.13
GS 05	1.34×10^{-1}	1.40×10^{-1}	8.02×10^{-2}	N.D.	1.34×10^{-1}	7.40×10^{-1}	6.78×10^{-2}
GS 08	6.22	1.02×10^1	7.08	1.27	4.83	3.64×10^1	3.48
GS 09	2.20	9.04	7.28	4.62×10^{-1}	5.60	4.05×10^1	3.51
GS 11	6.82	6.88	2.98	1.58	1.01	1.51×10^1	1.95

GS 12	1.02×10^1	1.06×10^1	5.56	1.32	3.12	2.48×10^1	3.30
GS 15	4.09	6.99	3.15	3.31×10^{-1}	2.46	2.05×10^1	1.44
GS 16	7.67	1.32×10^1	8.02	2.48	5.12	4.14×10^1	3.52
	191	200	170	190	198	199	196/203
GS 01	1.52×10^{-1}	N.D.	1.16×10^1	2.05	N.D.	8.48	4.37
GS 02	1.14×10^{-1}	N.D.	3.91	N.D.	5.24×10^{-1}	3.28	1.68
GS 03	3.25×10^{-1}	N.D.	6.24	7.33×10^{-1}	N.D.	4.05	2.35
GS 04	N.D.	N.D.	6.13	2.74×10^{-1}	N.D.	5.15	2.39
GS 05	N.D.	N.D.	2.16×10^{-1}	N.D.	N.D.	2.49×10^{-1}	1.30×10^{-1}
GS 08	1.22×10^{-1}	2.01×10^{-1}	1.28×10^1	1.79	2.12×10^{-1}	1.02×10^1	5.62
GS 09	4.83×10^{-1}	N.D.	8.88	N.D.	5.37×10^{-1}	1.95×10^1	8.87
GS 11	2.33	N.D.	7.27	N.D.	N.D.	4.94	2.03
GS 12	7.31×10^{-1}	N.D.	9.86	N.D.	N.D.	8.84	4.08

GS 15	1.99×10^{-1}	N.D.	9.22	N.D.	1.13	5.89	2.93
GS 16	5.78×10^{-1}	N.D.	1.53×10^1	3.72	1.24	1.60×10^1	8.12
	189	208	195	207	194	205	206
GS 01	N.D.	4.30×10^{-1}	7.68×10^{-1}	N.D.	2.57	N.D.	6.33×10^{-1}
GS 02	N.D.	1.23×10^{-1}	2.52×10^{-1}	6.77×10^{-2}	9.62×10^{-1}	N.D.	3.45×10^{-1}
GS 03	1.58×10^{-1}	N.D.	4.21×10^{-1}	1.26×10^{-1}	1.80	N.D.	4.72×10^{-1}
GS 04	N.D.	N.D.	N.D.	N.D.	1.31	N.D.	N.D.
GS 05	N.D.	N.D.	N.D.	N.D.	6.09×10^{-2}	N.D.	N.D.
GS 08	8.52×10^{-1}	4.15×10^{-1}	1.22	N.D.	4.20	N.D.	1.58
GS 09	4.79×10^{-1}	1.26	1.32	N.D.	7.71	N.D.	4.50
GS 11	N.D.	N.D.	N.D.	N.D.	1.68	N.D.	5.29×10^{-1}
GS 12	N.D.	2.11×10^{-1}	6.56×10^{-1}	1.21×10^{-1}	2.72	N.D.	6.25×10^{-1}
GS 15	N.D.	1.88×10^{-1}	5.16×10^{-1}	N.D.	2.04	N.D.	2.62×10^{-1}

GS 16	N.D.	8.83×10^{-1}	1.29	N.D.	5.40	N.D.	2.59
	209	TL					
GS 01	N.D.	3.59					
GS 02	N.D.	3.35					
GS 03	N.D.	3.39					
GS 04	N.D.	3.54					
GS 05	N.D.	3.45					
GS 08	N.D.	3.80					
GS 09	N.D.	3.66					
GS 11	N.D.	3.59					
GS 12	N.D.	3.56					
GS 15	N.D.	3.57					
GS 16	N.D.	3.63					

Beluga		Recovery %	Recovery %	PCB concentrations (ng/g) wet weight			
Samples	Lipid %	PCB 30	PCB 204	1	3	4/10	7
APRG 1314	8.97×10 ¹	1.03×10 ²	1.07×10 ²	N.D.	N.D.	N.D.	1.24×10 ¹
ARPG 1314 Dup	7.64×10 ¹	9.59×10 ¹	8.89×10 ¹	N.D.	N.D.	2.29	1.69×10 ¹
ARPG 1317	8.49×10 ¹	1.24×10 ²	9.37×10 ¹	N.D.	N.D.	1.16	7.32
ARPG 1323	9.33×10 ¹	9.69×10 ¹	9.46×10 ¹	N.D.	N.D.	2.40	2.38×10 ¹
ARPG 1323 Dup	8.97×10 ¹	6.60×10 ¹	6.06×10 ¹	N.D.	N.D.	2.23	1.69×10 ¹
ARPG 1328	6.53×10 ¹	1.00×10 ²	9.43×10 ¹	N.D.	N.D.	1.36	1.80×10 ¹
	6	8/5	19	18	17	24/27	16/32
APRG 1314	8.25	N.D.	8.93	5.92	6.83	N.D.	6.26×10 ⁻¹
ARPG 1314 Dup	1.10×10 ¹	1.87	6.68	9.54	1.78×10 ¹	N.D.	1.50
ARPG 1317	1.21×10 ¹	5.95	5.14×10 ⁻¹	4.26	1.09×10 ¹	N.D.	N.D.
ARPG 1323	1.21×10 ¹	N.D.	4.21	1.39×10 ¹	1.31×10 ¹	N.D.	2.59

ARPG 1323 Dup	N.D.	6.14	9.03	1.09×10^1	2.27×10^1	5.22×10^{-1}	N.D.
ARPG 1328	3.11	4.24×10^1	7.52	2.05×10^1	2.17×10^1	5.08×10^{-1}	4.61
	26	25	31	28	33	22	45
APRG 1314	N.D.	1.41	6.00×10^1	7.46	2.12	5.97	2.84×10^1
ARPG 1314 Dup	7.57	7.43×10^{-1}	5.43×10^1	5.56	4.33×10^{-1}	4.50	2.14×10^1
ARPG 1317	6.76	N.D.	3.17×10^1	3.69	2.54×10^{-1}	N.D.	4.41×10^1
ARPG 1323	1.17×10^1	1.31	6.20×10^1	5.86	2.48	4.19	3.30×10^1
ARPG 1323 Dup	5.93	1.13×10^{-1}	3.22×10^1	3.01	6.10×10^{-1}	2.80	2.42×10^1
ARPG 1328	4.91×10^1	2.42	1.01×10^2	8.65	1.39×10^1	1.84×10^1	1.40×10^2
	46	52	49	47	48	44	42
APRG 1314	7.73	3.59×10^1	6.24	7.21	1.25×10^1	5.43	5.56
ARPG 1314 Dup	1.34×10^1	2.96×10^1	7.86	4.70	1.52×10^1	1.50×10^1	1.41×10^1
ARPG 1317	1.46×10^1	2.89×10^1	8.76	2.20	5.70	5.76	5.41

ARPG 1323	1.33×10^1	6.73×10^1	2.37×10^1	1.41×10^1	1.94×10^1	1.88×10^1	8.91
ARPG 1323 Dup	1.09	4.17×10^1	1.02×10^1	6.06	1.08×10^1	1.06×10^1	1.49×10^1
ARPG 1328	8.02	3.01×10^2	9.99×10^1	5.77×10^1	4.76×10^1	6.33×10^1	2.10×10^1
	41/71	64	40	74	70/76	66	95
APRG 1314	8.07×10^{-1}	4.85	N.D.	9.05	6.68	6.20	4.74×10^1
ARPG 1314 Dup	2.16	7.10	N.D.	5.43	6.24	6.06	3.75×10^1
ARPG 1317	N.D.	N.D.	2.28	6.17	5.53	N.D.	4.52×10^1
ARPG 1323	3.31	8.92	N.D.	1.09×10^1	9.48	4.53	6.82×10^1
ARPG 1323 Dup	3.83	9.83	N.D.	6.45	5.62	5.40	5.66×10^1
ARPG 1328	3.29	2.32×10^1	6.52×10^{-1}	3.46×10^1	1.73×10^1	N.D.	3.26×10^2
	56/60	91	84/89	101	99	83	97
APRG 1314	6.65	6.50	1.12	2.67×10^1	2.77×10^1	4.02×10^1	5.90
ARPG 1314 Dup	5.86	3.86	4.86	2.11×10^1	2.63×10^1	3.07×10^1	6.50

ARPG 1317	7.48	3.93	N.D.	3.28×10^1	3.89×10^1	1.50×10^1	5.33
ARPG 1323	1.26×10^1	7.48	N.D.	5.46×10^1	6.39×10^1	3.34×10^1	9.89
ARPG 1323 Dup	7.32	4.92	N.D.	3.23×10^1	3.84×10^1	3.55×10^1	9.25
ARPG 1328	5.42×10^1	4.00×10^1	N.D.	2.84×10^2	3.10×10^2	6.80×10^1	1.70×10^1
	87	85	136	110	82	151	144/135
APRG 1314	6.26	5.16	3.49	1.40×10^1	N.D.	2.12×10^1	2.44
ARPG 1314 Dup	1.15×10^1	3.89	4.00	1.69×10^1	2.94×10^{-1}	1.29×10^1	3.95
ARPG 1317	6.06	5.28	3.34	1.05×10^1	N.D.	2.28×10^1	2.12
ARPG 1323	1.72×10^1	7.48	6.51	2.32×10^1	N.D.	3.12×10^1	N.D.
ARPG 1323 Dup	1.52×10^1	6.40	4.61	2.22×10^1	N.D.	1.77×10^1	3.26
ARPG 1328	7.76×10^1	3.89×10^1	2.47×10^1	1.22×10^2	N.D.	1.26×10^2	5.95
	149	118	134	114	131	146	153
APRG 1314	4.43×10^1	4.11×10^1	2.16	6.81	1.68	1.12×10^1	4.86×10^1

ARPG 1314 Dup	3.52×10^1	2.81×10^1	N.D.	1.08×10^1	1.45	1.01×10^1	3.22×10^1
ARPG 1317	3.54×10^1	3.35×10^1	1.69	5.96	1.70	1.21×10^1	5.58×10^1
ARPG 1323	5.30×10^1	3.34×10^1	N.D.	9.84	6.90	1.60×10^1	6.54×10^1
ARPG 1323 Dup	4.46×10^1	4.46×10^1	2.79×10^{-1}	5.93	1.27	8.90	4.26×10^1
ARPG 1328	2.46×10^2	1.57×10^2	N.D.	4.15×10^1	4.91	7.54×10^1	3.27×10^2
	132	105	141	179	137	130/176	138
APRG 1314	2.35×10^1	7.16	2.14	3.78	2.23	9.14	6.48×10^1
ARPG 1314 Dup	1.96×10^1	5.99	1.88	2.42	3.56×10^{-1}	7.80	5.49×10^1
ARPG 1317	9.92	7.64	2.48	2.83	2.56	6.97	5.44×10^1
ARPG 1323	1.96×10^1	6.76	1.96	2.30	6.24×10^{-1}	3.77	6.74×10^1
ARPG 1323 Dup	2.36×10^1	1.06×10^1	5.67×10^{-1}	1.87	1.46	8.45	6.74×10^1
ARPG 1328	9.86×10^1	4.44×10^1	1.26×10^1	1.31×10^1	1.04×10^1	4.54×10^1	3.18×10^2
	158	178/129	175	187	183	128	185

APRG 1314	1.68	1.89×10 ¹	2.75×10 ⁻¹	2.58×10 ¹	7.98	9.55	1.08
ARPG 1314 Dup	1.32	1.48×10 ¹	N.D.	1.58×10 ¹	5.45	9.61	2.05
ARPG 1317	2.13	1.07×10 ¹	8.92×10 ⁻¹	1.98×10 ¹	6.18	8.82	5.60×10 ⁻¹
ARPG 1323	2.46	1.21×10 ¹	N.D.	1.50×10 ¹	5.53	1.18×10 ¹	1.39
ARPG 1323 Dup	2.44	1.31×10 ¹	N.D.	1.24×10 ¹	4.21	6.95	N.D.
ARPG 1328	1.41×10 ¹	5.45×10 ¹	2.27	7.99×10 ¹	2.21×10 ¹	4.06×10 ¹	1.38
	174	177	171/156	201/157	172/197	180	193
APRG 1314	9.66	9.04	3.30	5.27×10 ⁻¹	2.75	1.43×10 ¹	1.48
ARPG 1314 Dup	4.56	3.20	2.20	3.81×10 ⁻¹	2.34	1.14×10 ¹	1.59
ARPG 1317	6.10	5.31	3.06	5.55×10 ⁻¹	2.24	9.94	1.36
ARPG 1323	7.40	3.52	2.96	3.51×10 ⁻¹	1.57	1.11×10 ¹	1.44
ARPG 1323 Dup	4.33	3.47	7.99×10 ⁻¹	N.D.	1.06	6.38	5.91×10 ⁻¹
ARPG 1328	3.55×10 ¹	3.08×10 ¹	4.11	2.24	5.47	3.89×10 ¹	4.43

	191	200	170	190	198	199	196/203
APRG 1314	N.D.	N.D.	5.35	6.50×10^{-1}	N.D.	6.37	2.69
ARPG 1314 Dup	N.D.	N.D.	2.74	1.57×10^{-1}	N.D.	4.83	1.96
ARPG 1317	N.D.	N.D.	3.46	6.84×10^{-1}	N.D.	3.43	1.77
ARPG 1323	N.D.	N.D.	3.23	1.52×10^{-2}	N.D.	2.81	1.02
ARPG 1323 Dup	N.D.	N.D.	2.45	N.D.	N.D.	1.78	6.53×10^{-1}
ARPG 1328	N.D.	3.99×10^{-1}	1.63×10^1	N.D.	1.12×10^{-1}	1.31×10^1	4.85
	189	208	195	207	194	205	206
APRG 1314	1.71×10^{-1}	N.D.	3.98×10^{-1}	N.D.	1.54	N.D.	N.D.
ARPG 1314 Dup	1.53×10^{-1}	N.D.	4.09×10^{-1}	N.D.	1.17	N.D.	2.01×10^{-1}
ARPG 1317	3.97×10^{-1}	2.98×10^{-1}	5.39×10^{-1}	2.68×10^{-1}	1.16	N.D.	3.37×10^{-1}
ARPG 1323	1.07×10^{-1}	N.D.	1.02	9.34×10^{-2}	1.24	N.D.	N.D.
ARPG 1323 Dup	N.D.	N.D.	N.D.	N.D.	3.06×10^{-1}	N.D.	N.D.

ARPG 1328	2.66×10^{-1}	1.78×10^{-1}	7.29×10^{-1}	2.60×10^{-1}	2.80	3.61×10^{-1}	4.30×10^{-1}
	209	TL					
APRG 1314	N.D.	3.46					
ARPG 1314 Dup	N.D.	3.46					
ARPG 1317	N.D.	3.38					
ARPG 1323	N.D.	3.25					
ARPG 1323 Dup	N.D.	3.25					
ARPG 1328	N.D.	3.57					

Narwhal		Recovery %	Recovery %	PCB concentrations (ng/g) wet weight			
Samples	Lipid %	PCB 30	PCB 204	1	3	4/10	7
ARPG 1330	8.85×10 ¹	1.12×10 ²	8.64×10 ¹	N.D.	N.D.	2.05	1.52×10 ¹
ARPG1337	6.49×10 ¹	1.03×10 ²	9.84×10 ¹	N.D.	N.D.	2.89	2.11×10 ¹
ARPG 1339	8.57×10 ¹	1.04×10 ²	8.62×10 ¹	N.D.	N.D.	1.04	1.94×10 ¹
ARPG 1341	8.40×10 ¹	9.35×10 ¹	6.90×10 ¹	N.D.	N.D.	2.21	1.65×10 ¹
ARPG 1342	7.22×10 ¹	1.09×10 ²	1.01×10 ²	N.D.	N.D.	1.75	1.37×10 ¹
ARPG 1343	7.36×10 ¹	1.17×10 ²	9.11×10 ¹	N.D.	N.D.	2.17	1.55×10 ¹
ARPG 1350	6.86×10 ¹	1.03×10 ²	8.49×10 ¹	N.D.	N.D.	9.85×10 ⁻¹	8.04
	6	8/5	19	18	17	24/27	16/32
ARPG 1330	8.07	3.48×10 ¹	6.27	1.79×10 ¹	1.20×10 ¹	N.D.	3.16
ARPG1337	1.77×10 ¹	N.D.	6.62	1.67×10 ¹	1.55×10 ¹	1.37	2.53
ARPG 1339	6.82	1.70×10 ¹	4.20	1.68×10 ¹	2.80×10 ¹	N.D.	2.20

ARPG 1341	8.08	2.81×10^1	N.D.	1.96×10^1	1.27×10^1	1.49	2.76
ARPG 1342	1.80	2.76×10^1	3.01	1.89×10^1	2.84×10^1	N.D.	2.98
ARPG 1343	8.42	1.34	4.41	2.07×10^1	2.06×10^1	N.D.	2.91
ARPG 1350	4.40	N.D.	2.28	1.10×10^1	7.94	N.D.	1.40
	26	25	31	28	33	22	45
ARPG 1330	3.04×10^1	2.44	4.20×10^1	2.13×10^1	7.76	1.35×10^1	1.11×10^2
ARPG1337	3.29×10^1	1.50	5.45×10^1	2.40×10^1	4.09	1.59×10^1	9.93×10^1
ARPG 1339	3.06×10^1	6.62×10^{-1}	4.13×10^1	2.29×10^1	3.61	1.42×10^1	8.33×10^1
ARPG 1341	3.82×10^1	3.02	3.86×10^1	1.33×10^1	5.79	1.43×10^1	1.28×10^2
ARPG 1342	1.96×10^1	N.D.	4.33×10^1	2.38	5.19	1.11×10^1	7.97×10^1
ARPG 1343	3.57×10^1	2.97	5.37×10^1	2.51×10^1	8.31	1.81×10^1	1.54×10^2
ARPG 1350	2.00×10^1	9.07×10^{-1}	2.21×10^1	1.17×10^1	3.39	9.01	7.56×10^1
	46	52	49	47	48	44	42

ARPG 1330	1.17×10^1	2.03×10^2	6.58×10^1	4.22×10^1	4.15×10^1	5.72×10^1	2.26×10^1
ARPG1337	1.19×10^1	1.83×10^2	5.07×10^1	3.20×10^1	2.70×10^1	4.00×10^1	1.32×10^1
ARPG 1339	1.49×10^1	1.76×10^2	4.88×10^1	3.05×10^1	3.08×10^1	4.66×10^1	2.20×10^1
ARPG 1341	1.23×10^1	2.44×10^2	7.34×10^1	4.96×10^1	4.11×10^1	5.14×10^1	2.52×10^1
ARPG 1342	1.31×10^1	1.53×10^2	4.54×10^1	2.59×10^1	2.81×10^1	4.93×10^1	2.02×10^1
ARPG 1343	1.18×10^1	2.49×10^2	6.24×10^1	4.41×10^1	3.57×10^1	5.27×10^1	2.89×10^1
ARPG 1350	8.04	1.30×10^2	3.52×10^1	2.19×10^1	1.99×10^1	3.48×10^1	1.68×10^1
	41/71	64	40	74	70/76	66	95
ARPG 1330	3.29	1.16×10^1	2.25	4.41×10^1	8.97	3.47×10^1	2.75×10^2
ARPG1337	4.53	8.65	3.76	3.63×10^1	7.91	5.31×10^1	1.90×10^2
ARPG 1339	9.86×10^{-1}	7.29	3.55	3.35×10^1	7.41	2.14×10^1	2.16×10^2
ARPG 1341	3.66	1.09×10^1	2.65	4.49×10^1	7.40	4.51	3.41×10^2
ARPG 1342	3.26	8.30	N.D.	3.33×10^1	7.88	1.34	2.23×10^2

ARPG 1343	1.96	1.11×10^1	5.10	5.07×10^1	8.29	N.D.	3.88×10^2
ARPG 1350	2.45	5.78	N.D.	2.20×10^1	4.63	1.62×10^{-1}	2.04×10^2
	56/60	91	84/89	101	99	83	97
ARPG 1330	4.20×10^1	2.72×10^1	8.89	1.75×10^2	2.14×10^2	6.48×10^1	1.89×10^1
ARPG1337	3.05×10^1	2.06×10^1	4.39	1.29×10^2	1.73×10^2	7.25×10^1	9.10
ARPG 1339	3.00×10^1	1.89×10^1	4.37×10^1	1.28×10^2	1.56×10^2	6.80×10^1	1.82×10^1
ARPG 1341	4.31×10^1	3.10×10^1	3.64	1.80×10^2	2.34×10^2	1.28×10^2	1.19×10^1
ARPG 1342	3.12×10^1	1.86×10^1	1.42×10^1	1.27×10^2	1.53×10^2	5.87×10^1	1.81×10^1
ARPG 1343	5.33×10^1	3.37×10^1	3.16×10^1	2.02×10^2	2.64×10^2	8.54×10^1	2.88×10^1
ARPG 1350	2.63×10^1	1.56×10^1	1.25×10^1	9.73×10^1	1.29×10^2	4.59×10^1	1.28×10^1
	87	85	136	110	82	151	144/135
ARPG 1330	6.52×10^1	3.07×10^1	2.03×10^1	7.59×10^1	N.D.	9.76×10^1	1.70×10^1
ARPG1337	4.93×10^1	2.16×10^1	1.44×10^1	1.16×10^1	N.D.	7.41×10^1	1.04×10^1

ARPG 1339	3.18×10^1	2.57×10^1	1.33×10^1	4.11×10^1	N.D.	6.77×10^1	8.64
ARPG 1341	6.74×10^1	2.91×10^1	2.04×10^1	7.12×10^1	N.D.	1.08×10^2	1.28×10^1
ARPG 1342	4.96×10^1	2.64×10^1	1.39×10^1	4.63×10^1	N.D.	6.91×10^1	1.34×10^1
ARPG 1343	7.10×10^1	3.99×10^1	2.34×10^1	9.51×10^1	1.89	1.19×10^2	2.29×10^1
ARPG 1350	4.18×10^1	1.78×10^1	1.16×10^1	4.29×10^1	N.D.	5.87×10^1	1.23×10^1
	149	118	134	114	131	146	153
ARPG 1330	1.85×10^2	1.75×10^2	6.37	3.26×10^1	7.61	4.89×10^1	2.24×10^2
ARPG1337	1.36×10^2	1.32×10^2	6.04	3.27×10^1	3.62	5.26×10^1	1.61×10^2
ARPG 1339	1.37×10^2	1.36×10^2	6.93	2.77×10^1	3.03	3.44×10^1	1.56×10^2
ARPG 1341	1.94×10^2	1.79×10^2	7.17	3.29×10^1	5.44	5.01×10^1	2.23×10^2
ARPG 1342	1.38×10^2	1.30×10^2	4.33	2.53×10^1	4.34	3.80×10^1	1.77×10^2
ARPG 1343	2.31×10^2	2.02×10^2	8.60	3.63×10^1	1.03×10^1	5.47×10^1	2.62×10^2
ARPG 1350	1.18×10^2	1.07×10^2	4.38	1.93×10^1	3.83	2.93×10^1	1.35×10^2

	132	105	141	179	137	130/176	138
ARPG 1330	1.11×10^2	4.21×10^1	6.90	1.16×10^1	1.15×10^1	7.81×10^1	2.97×10^2
ARPG1337	7.18×10^1	2.39×10^1	4.07	7.20	7.20	3.00×10^1	2.27×10^2
ARPG 1339	9.24×10^1	2.63×10^1	5.63	7.18	7.22	2.62×10^1	2.29×10^2
ARPG 1341	1.34×10^2	4.35×10^1	6.82	1.24×10^1	1.32×10^1	3.51×10^1	3.14×10^2
ARPG 1342	6.85×10^1	2.71×10^1	4.84	7.89	9.02	2.73×10^1	2.30×10^2
ARPG 1343	1.50×10^2	4.46×10^1	5.36	1.27×10^1	1.35×10^1	4.15×10^1	3.55×10^2
ARPG 1350	8.22×10^1	1.94×10^1	3.58	6.55	6.97	2.08×10^1	1.97×10^2
	158	178/129	175	187	183	128	185
ARPG 1330	1.09×10^1	4.79×10^1	2.47×10^{-1}	6.84×10^1	2.17×10^1	3.82×10^1	2.48
ARPG1337	6.46	4.94×10^1	1.20	4.57×10^1	1.28×10^1	2.48×10^1	1.76
ARPG 1339	6.31	3.59×10^1	1.09	4.77×10^1	1.36×10^1	2.43×10^1	9.31×10^{-1}
ARPG 1341	1.06×10^1	4.83×10^1	2.55	6.82×10^1	2.16×10^1	3.51×10^1	2.67

ARPG 1342	7.39	3.59×10^1	1.55	5.33×10^1	1.69×10^1	2.98×10^1	1.95
ARPG 1343	1.27×10^1	5.57×10^1	1.20	7.69×10^1	2.48×10^1	4.15×10^1	1.48
ARPG 1350	5.49	3.12×10^1	1.09	3.87×10^1	1.21×10^1	2.13×10^1	7.76×10^{-1}
	174	177	171/156	201/157	172/197	180	193
ARPG 1330	3.48×10^1	2.64×10^1	1.23×10^1	1.74	7.07	4.15×10^1	4.03
ARPG1337	2.08×10^1	1.43×10^1	6.60	7.61×10^{-1}	4.47	2.23×10^1	2.44
ARPG 1339	2.13×10^1	1.44×10^1	7.70	9.13×10^{-1}	4.52	2.61×10^1	2.46
ARPG 1341	3.35×10^1	2.54×10^1	1.12×10^1	1.62	6.42	3.86×10^1	3.60
ARPG 1342	2.46×10^1	1.95×10^1	8.95	1.25	5.62	3.34×10^1	3.20
ARPG 1343	3.34×10^1	2.76×10^1	1.36×10^1	1.85	6.92	4.19×10^1	4.06
ARPG 1350	1.90×10^1	8.61	5.84	7.62×10^{-1}	3.71	2.24×10^1	2.16
	191	200	170	190	198	199	196/203
ARPG 1330	N.D.	7.41×10^{-1}	1.66×10^1	1.70	2.89×10^{-1}	1.43×10^1	6.14

ARPG1337	N.D.	N.D.	9.88	9.68×10^{-1}	N.D.	6.99	2.42
ARPG 1339	N.D.	2.21×10^{-1}	1.12×10^1	7.42×10^{-1}	N.D.	8.73	3.25
ARPG 1341	3.98×10^{-1}	4.81×10^{-1}	1.55×10^1	2.14	N.D.	1.36×10^1	5.66
ARPG 1342	3.29×10^{-1}	N.D.	1.37×10^1	1.22	N.D.	1.13×10^1	4.40
ARPG 1343	1.39	4.70×10^{-2}	1.88×10^1	1.01	N.D.	1.32×10^1	5.76
ARPG 1350	N.D.	1.59×10^{-1}	9.67	5.38×10^{-1}	N.D.	6.79	3.20
	189	208	195	207	194	205	206
ARPG 1330	1.07	5.09×10^{-1}	1.24	3.04×10^{-1}	3.33	2.39	8.28×10^{-1}
ARPG1337	N.D.	N.D.	4.48×10^{-1}	N.D.	1.21	2.44×10^{-1}	N.D.
ARPG 1339	N.D.	N.D.	4.22×10^{-1}	N.D.	1.74	N.D.	N.D.
ARPG 1341	2.62×10^{-1}	2.20×10^{-1}	9.41×10^{-1}	N.D.	2.47	1.96	4.18×10^{-1}
ARPG 1342	3.92×10^{-1}	2.65×10^{-1}	7.53×10^{-1}	N.D.	2.51	1.26	6.63×10^{-1}
ARPG 1343	5.31×10^{-1}	3.13×10^{-1}	1.08	1.69×10^{-1}	3.26	2.41	5.96×10^{-1}

ARPG 1350	2.93×10^{-1}	N.D.	4.02×10^{-1}	N.D.	1.47	1.26	2.32×10^{-1}
	209	TL					
ARPG 1330	N.D.	3.07					
ARPG1337	N.D.	3.39					
ARPG 1339	N.D.	3.22					
ARPG 1341	N.D.	3.30					
ARPG 1342	N.D.	3.31					
ARPG 1343	N.D.	3.28					
ARPG 1350	N.D.	3.10					

Appendix 5

PCB Concentrations in Greenland Sharks Collected from Cumberland Sound (Canada) from 1998 to 1999

Appendix 5. PCB concentrations of Greenland sharks in Cumberland. Concentration data was provided by Dr. Aaron T. Fisk. N.D. = not detected. PCB congeners are presented as **bold** numbers.

Samples	%lipid	PCB concentrations (ng/g) wet weight					
		19	18	17	24/27	16/32	26
GS 001	5.80×10 ¹	N.D.	9.90×10 ⁻¹	6.30×10 ⁻¹	N.D.	N.D.	N.D.
GS 002	4.95×10 ¹	N.D.	1.33	N.D.	N.D.	N.D.	4.80×10 ⁻¹
GS 003	5.57×10 ¹	N.D.	1.35	6.10×10 ⁻¹	N.D.	N.D.	7.80×10 ⁻¹
GS 004	6.02×10 ¹	N.D.	3.92	2.39	N.D.	9.10×10 ⁻¹	8.20×10 ⁻¹
GS 005	4.87×10 ¹	N.D.	2.58	9.60×10 ⁻¹	N.D.	N.D.	9.60×10 ⁻¹
GS 006	5.19×10 ¹	N.D.	4.67	1.69	N.D.	N.D.	4.50×10 ⁻¹
GS 007	6.39×10 ¹	N.D.	9.69	3.19	N.D.	1.11	5.50×10 ⁻¹
GS 008	5.85×10 ¹	N.D.	1.24	N.D.	N.D.	N.D.	1.08
GS 009	4.05×10 ¹	N.D.	1.39	N.D.	N.D.	N.D.	5.40×10 ⁻¹
GS 010	6.75×10 ¹	N.D.	2.73	1.56	N.D.	N.D.	8.50×10 ⁻¹
GS 011	5.40×10 ¹	N.D.	1.86	N.D.	N.D.	N.D.	9.00×10 ⁻¹

GS 012	6.96×10^1	N.D.	1.50	6.50×10^{-1}	N.D.	N.D.	5.90×10^{-1}
GS 013	6.30×10^1	N.D.	4.53	2.72	N.D.	1.34	8.30×10^{-1}
GS 014	4.60×10^1	N.D.	N.D.	N.D.	N.D.	N.D.	N.D.
GS 015	5.20×10^1	N.D.	1.97	5.70×10^{-1}	N.D.	N.D.	N.D.
	25	31	28	33/20	22	45	46
GS 001	N.D.	1.68	9.33	N.D.	N.D.	4.10×10^{-1}	N.D.
GS 002	N.D.	7.40×10^{-1}	4.99	N.D.	N.D.	N.D.	N.D.
GS 003	N.D.	1.58	1.32×10^1	N.D.	N.D.	N.D.	N.D.
GS 004	N.D.	1.39	1.96×10^1	N.D.	N.D.	2.95	N.D.
GS 005	N.D.	2.17	1.39×10^1	N.D.	N.D.	1.25	N.D.
GS 006	N.D.	2.25	2.27×10^1	N.D.	N.D.	2.65	N.D.
GS 007	N.D.	3.30	2.95×10^1	3.80×10^{-1}	N.D.	5.04	N.D.
GS 008	N.D.	2.23	1.39×10^1	N.D.	N.D.	N.D.	N.D.

GS 009	N.D.	2.22	6.90	N.D.	N.D.	N.D.	N.D.
GS 010	N.D.	1.65	1.80×10^1	N.D.	N.D.	1.53	N.D.
GS 011	N.D.	4.37	1.57×10^1	N.D.	N.D.	8.60×10^{-1}	N.D.
GS 012	N.D.	2.81	7.45	N.D.	N.D.	9.20×10^{-1}	N.D.
GS 013	N.D.	3.81	2.71×10^1	N.D.	N.D.	3.09	N.D.
GS 014	N.D.	2.38	1.36×10^1	N.D.	N.D.	N.D.	N.D.
GS 015	N.D.	9.40×10^{-1}	1.28×10^1	N.D.	N.D.	9.80×10^{-1}	N.D.
	52	49	47/48	44	42	64/41/71	40
GS 001	1.94×10^1	6.26	5.42	2.80	2.00×10^{-2}	3.83	N.D.
GS 002	1.90×10^1	5.68	4.65	2.95	2.28	2.74	N.D.
GS 003	4.31×10^1	1.23×10^1	1.25×10^1	4.93	2.17	4.54	N.D.
GS 004	1.88×10^2	5.12×10^1	4.34×10^1	2.66×10^1	3.04	9.37	N.D.
GS 005	6.54×10^1	2.10×10^1	1.48×10^1	1.02×10^1	2.15	7.59	N.D.

GS 006	1.22×10^2	3.54×10^1	2.41×10^1	1.99×10^1	6.80	6.91	N.D.
GS 007	3.41×10^2	8.85×10^1	7.96×10^1	5.26×10^1	6.94	6.84	1.73
GS 008	3.66×10^1	1.07×10^1	9.79	4.48	4.85	6.29	N.D.
GS 009	2.64×10^1	8.65	8.40	4.10	N.D.	3.73	N.D.
GS 010	1.31×10^2	3.39×10^1	4.17×10^1	2.05×10^1	2.77	1.04×10^1	N.D.
GS 011	5.55×10^1	1.66×10^1	1.51×10^1	6.41	6.00×10^{-2}	6.07	N.D.
GS 012	4.63×10^1	1.36×10^1	8.60	6.27	2.15	3.94	N.D.
GS 013	1.89×10^2	6.33×10^1	5.55×10^1	2.96×10^1	1.10×10^1	1.75×10^1	N.D.
GS 014	5.73×10^1	1.62×10^1	1.31×10^1	4.65	9.75	N.D.	N.D.
GS 015	5.90×10^1	1.62×10^1	1.37×10^1	7.73	1.20	7.37	N.D.
	74	70/76	66	56/60	95	91	92
GS 001	1.22×10^1	4.12	3.07×10^1	4.02	5.95	1.80	4.57
GS 002	7.29	3.19	1.62×10^1	1.77	5.92	2.01	4.27

GS 003	2.53×10^1	5.12	2.58×10^1	5.52	1.20×10^1	3.68	1.26×10^1
GS 004	5.50×10^1	6.60	8.78×10^1	1.41×10^1	1.07×10^2	2.89×10^1	5.39×10^1
GS 005	2.34×10^1	7.72	4.69×10^1	6.38	3.30×10^1	8.56	1.85×10^1
GS 006	3.61×10^1	7.24	7.90×10^1	1.04×10^1	6.76×10^1	1.98×10^1	3.37×10^1
GS 007	8.93×10^1	4.90	1.36×10^2	2.29×10^1	1.78×10^2	4.10×10^1	9.63×10^1
GS 008	1.87×10^1	6.50	3.33×10^1	5.25	1.11×10^1	3.57	1.18×10^1
GS 009	1.36×10^1	4.72	1.71×10^1	2.34	9.81	3.44	7.48
GS 010	5.90×10^1	6.81	1.06×10^2	1.55×10^1	6.55×10^1	1.59×10^1	4.35×10^1
GS 011	2.70×10^1	7.61	4.37×10^1	6.32	2.23×10^1	7.41	1.58×10^1
GS 012	1.25×10^1	4.82	3.11×10^1	3.56	1.73×10^1	4.82	9.90
GS 013	8.25×10^1	1.08×10^1	1.20×10^2	1.86×10^1	7.69×10^1	2.58×10^1	4.87×10^1
GS 014	3.35×10^1	7.92	4.46×10^1	9.67	1.90×10^1	1.16×10^1	1.59×10^1
GS 015	1.98×10^1	2.07	3.64×10^1	5.47	3.80×10^1	9.17	1.71×10^1

	84	101/90	99	97	87	85	110
GS 001	9.60×10 ⁻¹	2.50×10 ¹	2.46×10 ¹	N.D.	8.22	5.97	9.99
GS 002	1.10	1.99×10 ¹	1.86×10 ¹	N.D.	6.43	4.36	7.40
GS 003	1.31	6.83×10 ¹	7.70×10 ¹	1.01	1.71×10 ¹	1.43×10 ¹	1.78×10 ¹
GS 004	1.92×10 ¹	2.11×10 ²	2.16×10 ²	3.67	6.23×10 ¹	6.32	4.05×10 ¹
GS 005	6.86	8.77×10 ¹	6.75×10 ¹	N.D.	2.60×10 ¹	4.75	3N.D.
GS 006	1.31×10 ¹	1.54×10 ²	1.18×10 ²	7.73	4.73×10 ¹	6.02	3.84×10 ¹
GS 007	3.09×10 ¹	3.75×10 ²	3.11×10 ²	1.02×10 ¹	1.06×10 ²	8.88	5.62×10 ¹
GS 008	2.99	5.56×10 ¹	5.50×10 ¹	1.76	1.62×10 ¹	1.18×10 ¹	2.02×10 ¹
GS 009	1.66	3.38×10 ¹	4.50×10 ¹	N.D.	1.13×10 ¹	1.96	1.24×10 ¹
GS 010	7.41	2.16×10 ²	2.19×10 ²	7.48	5.56×10 ¹	6.24	3.90×10 ¹
GS 011	4.70	8.41×10 ¹	8.00×10 ¹	N.D.	2.30×10 ¹	3.91	2.47×10 ¹
GS 012	3.15	4.36×10 ¹	3.02×10 ¹	1.69	1.32×10 ¹	8.04	1.11×10 ¹

GS 013	1.66×10^1	2.49×10^2	2.51×10^2	8.07	7.54×10^1	1.33×10^1	8.47×10^1
GS 014	2.00×10^{-2}	1.03×10^2	1.24×10^2	N.D.	2.84×10^1	N.D.	2.69×10^1
GS 015	7.10	6.84×10^1	5.52×10^1	1.96	2.32×10^1	2.98	1.86×10^1
	82	118	105	136	151	144/135	149
GS 001	N.D.	2.65×10^1	1.08×10^1	1.36	N.D.	N.D.	1.33×10^1
GS 002	N.D.	1.58×10^1	6.33	1.46	N.D.	3.97	1.21×10^1
GS 003	N.D.	5.42×10^1	2.26×10^1	2.22	N.D.	5.26	3.04×10^1
GS 004	N.D.	1.87×10^2	7.33×10^1	2.72×10^1	N.D.	4.72×10^1	2.32×10^2
GS 005	N.D.	7.42×10^1	3.57×10^1	9.32	N.D.	1.34×10^1	6.97×10^1
GS 006	N.D.	1.24×10^2	5.81×10^1	1.76×10^1	N.D.	2.92×10^1	1.33×10^2
GS 007	N.D.	3.63×10^2	1.18×10^2	3.89×10^1	N.D.	6.98×10^1	3.80×10^2
GS 008	N.D.	5.36×10^1	2.07×10^1	1.96	N.D.	4.39	2.83×10^1
GS 009	N.D.	3.56×10^1	1.33×10^1	2.31	N.D.	4.27	2.08×10^1

GS 010	N.D.	2.61×10^2	9.94×10^1	1.38×10^1	N.D.	2.29×10^1	1.49×10^2
GS 011	N.D.	7.71×10^1	3.76×10^1	6.10	N.D.	8.31	5.54×10^1
GS 012	N.D.	3.21×10^1	1.15×10^1	4.32	N.D.	9.93	3.36×10^1
GS 013	N.D.	2.27×10^2	8.96×10^1	1.89×10^1	N.D.	2.99×10^1	1.48×10^2
GS 014	N.D.	1.04×10^2	4.06×10^1	N.D.	N.D.	N.D.	5.75×10^1
GS 015	N.D.	7.62×10^1	2.78×10^1	1.08×10^1	N.D.	1.60×10^1	7.40×10^1
	134	146	153	141	130	137	138/163
GS 001	N.D.	9.19	7.04×10^1	2.32	2.99	1.45	4.51×10^1
GS 002	N.D.	6.87	5.52×10^1	2.11	1.55	1.24	3.61×10^1
GS 003	6.60×10^{-1}	2.73×10^1	1.78×10^2	5.23	5.01	2.16	1.37×10^2
GS 004	6.85	7.55×10^1	5.58×10^2	1.58×10^1	2.30×10^1	2.63×10^1	4.39×10^2
GS 005	3.33	2.50×10^1	2.17×10^2	1.02×10^1	4.60	5.03	1.29×10^2
GS 006	5.91	4.41×10^1	2.87×10^2	9.91	1.21×10^1	1.60×10^1	2.30×10^2

GS 007	1.28×10^1	1.35×10^2	6.76×10^2	2.06×10^1	3.24×10^1	2.81×10^1	6.16×10^2
GS 008	N.D.	1.82×10^1	1.17×10^2	5.48	3.75	1.68	9.97×10^1
GS 009	1.20×10^{-1}	1.52×10^1	1.43×10^2	4.58	2.57	3.59	8.31×10^1
GS 010	5.22	8.15×10^1	4.90×10^2	1.62×10^1	2.35×10^1	1.68×10^1	4.14×10^2
GS 011	N.D.	3.13×10^1	2.72×10^2	8.01	5.66	9.44	1.59×10^2
GS 012	N.D.	1.09×10^1	7.40×10^1	2.60	N.D.	N.D.	5.16×10^1
GS 013	6.39	7.37×10^1	6.96×10^2	2.03×10^1	1.95×10^1	1.91×10^1	4.38×10^2
GS 014	N.D.	5.06×10^1	2.82×10^2	1.15×10^1	1.46	5.67	1.33×10^2
GS 015	2.64	2.24×10^1	1.02×10^2	6.97	5.50	5.03	1.09×10^2
	158	128	156/202	157/200	169	179	176
GS 001	3.37	5.35	4.15	N.D.	N.D.	N.D.	N.D.
GS 002	2.92	4.67	3.48	1.44	N.D.	N.D.	N.D.
GS 003	1.10	1.49×10^1	1.23×10^1	2.93	N.D.	N.D.	N.D.

GS 004	2.50×10 ¹	6.77×10 ¹	3.14×10 ¹	1.75×10 ¹	N.D.	N.D.	6.95
GS 005	1.15×10 ¹	2.11×10 ¹	1.46×10 ¹	8.82	N.D.	N.D.	N.D.
GS 006	1.58×10 ¹	2.92×10 ¹	2.03×10 ¹	1.59×10 ¹	N.D.	N.D.	4.61
GS 007	3.20×10 ¹	6.28×10 ¹	3.85×10 ¹	2.22×10 ¹	N.D.	N.D.	9.12
GS 008	8.80×10 ⁻¹	1.52×10 ¹	8.33	4.02	N.D.	N.D.	N.D.
GS 009	6.78×10 ¹	1.77×10 ¹	5.71	N.D.	N.D.	N.D.	N.D.
GS 010	2.27×10 ¹	2.76×10 ¹	3.19×10 ¹	1.82×10 ¹	N.D.	N.D.	3.44
GS 011	1.06×10 ¹	1.64×10 ¹	1.34×10 ¹	8.41	N.D.	N.D.	N.D.
GS 012	6.22	7.18	4.05	1.43	N.D.	N.D.	N.D.
GS 013	3.02×10 ¹	5.19×10 ¹	5.42×10 ¹	1.79×10 ¹	N.D.	N.D.	3.41
GS 014	1.83	2.66×10 ¹	N.D.	N.D.	N.D.	N.D.	N.D.
GS 015	6.60	1.33×10 ¹	1.30×10 ¹	N.D.	N.D.	N.D.	N.D.
	178	187/182	183	185	174	177	171

GS 001	3.70×10^1	1.22×10^1	3.92	N.D.	9.20×10^{-1}	1.73	N.D.
GS 002	3.04×10^1	1.08×10^1	2.59	N.D.	1.18	1.36	9.20×10^{-1}
GS 003	6.05×10^1	3.49×10^1	1.47×10^1	N.D.	3.43	8.67	3.25
GS 004	2.03×10^2	1.63×10^2	5.26×10^1	4.72	3.89×10^1	3.63×10^1	2.00×10^1
GS 005	5.26×10^1	4.88×10^1	1.49×10^1	2.10	1.09×10^1	9.99	5.17
GS 006	1.39×10^2	1.10×10^2	3.01×10^1	4.03	2.53×10^1	2.30×10^1	1.05×10^1
GS 007	3.18×10^2	2.31×10^2	7.04×10^1	6.46	5.80×10^1	5.29×10^1	1.65×10^1
GS 008	3.61×10^1	2.64×10^1	9.77	N.D.	3.00	6.74	1.81
GS 009	2.37×10^1	1.85×10^1	8.43	N.D.	2.02	3.97	2.31
GS 010	2.27×10^2	1.58×10^2	4.73×10^1	3.79	2.87×10^1	2.77×10^1	1.02×10^1
GS 011	8.72×10^1	5.96×10^1	2.23×10^1	N.D.	7.67	1.24×10^1	6.28
GS 012	5.36×10^1	1.75×10^1	3.65	3.30×10^{-1}	3.51	2.78	1.21
GS 013	1.41×10^2	1.04×10^2	3.52×10^1	N.D.	1.80×10^1	2.51×10^1	1.12×10^1

GS 014	7.35×10^1	6.66×10^1	2.23×10^1	N.D.	6.12	1.29×10^1	N.D.
GS 015	5.46×10^1	4.39×10^1	1.17×10^1	N.D.	1.18×10^1	9.00	3.13
	172	180	193	191	170/190	202	200
GS 001	7.90×10^{-1}	1.27×10^1	5.20×10^{-1}	N.D.	4.90	3.48	N.D.
GS 002	5.10×10^{-1}	1.03×10^1	5.60×10^{-1}	N.D.	4.40	2.64	N.D.
GS 003	3.65	5.39×10^1	3.03	N.D.	2.08×10^1	7.87	N.D.
GS 004	1.71×10^1	1.45×10^2	1.17×10^1	N.D.	5.70×10^1	2.11×10^1	1.25×10^1
GS 005	2.67	4.45×10^1	4.90×10^{-1}	N.D.	1.73×10^1	7.52	4.20
GS 006	8.02	8.48×10^1	3.89	N.D.	3.30×10^1	1.89×10^1	1.45×10^1
GS 007	9.62	1.82×10^2	9.48	5.63	6.98×10^1	2.57×10^1	2.11×10^1
GS 008	2.52	3.05×10^1	1.25	N.D.	1.11×10^1	4.46	N.D.
GS 009	1.92	2.21×10^1	3.40×10^{-1}	N.D.	7.13	N.D.	N.D.
GS 010	8.85	1.56×10^2	5.34	2.76	5.44×10^1	2.66×10^1	1.51×10^1

GS 011	6.53	7.23×10^1	1.03	N.D.	2.62×10^1	1.25×10^1	4.17
GS 012	2.60×10^{-1}	1.00×10^1	6.10×10^{-1}	N.D.	3.99	2.77	N.D.
GS 013	8.58	1.12×10^2	7.09	N.D.	5.10×10^1	1.31×10^1	5.68
GS 014	N.D.	8.86×10^1	7.96	N.D.	4.71×10^1	N.D.	N.D.
GS 015	2.26	3.13×10^1	1.60×10^1	N.D.	1.22×10^1	5.84	5.91
	201	199	196/203	195	194	205	208
GS 001	N.D.	1.35	6.17	N.D.	3.92	N.D.	N.D.
GS 002	N.D.	7.80×10^{-1}	2.61	N.D.	2.34	N.D.	N.D.
GS 003	N.D.	3.01	7.14	N.D.	5.90	N.D.	N.D.
GS 004	N.D.	5.65	1.60×10^1	1.73	1.04×10^1	N.D.	N.D.
GS 005	N.D.	2.92	1.09×10^1	N.D.	5.30	N.D.	N.D.
GS 006	N.D.	6.07	1.98×10^1	1.32	1.03×10^1	N.D.	N.D.
GS 007	N.D.	1.36×10^1	4.19×10^1	6.18	2.72×10^1	N.D.	N.D.

GS 008	N.D.	3.10	7.35	N.D.	5.16	N.D.	N.D.
GS 009	N.D.	1.28	2.93	N.D.	2.33	N.D.	N.D.
GS 010	N.D.	1.06×10^1	3.52×10^1	4.97	2.25×10^1	N.D.	N.D.
GS 011	N.D.	3.62	1.57×10^1	2.82	9.78	N.D.	N.D.
GS 012	N.D.	1.22	3.67	N.D.	1.46	N.D.	N.D.
GS 013	N.D.	4.51	1.57×10^1	N.D.	1.04×10^1	N.D.	N.D.
GS 014	N.D.	5.13	1.83×10^1	N.D.	N.D.	N.D.	N.D.
GS 015	N.D.	2.26	6.64	N.D.	N.D.	N.D.	N.D.
	206	209					
GS 001	N.D.	N.D.					
GS 002	N.D.	N.D.					
GS 003	N.D.	N.D.					
GS 004	N.D.	N.D.					

GS 005	N.D.	N.D.
GS 006	N.D.	N.D.
GS 007	N.D.	N.D.
GS 008	N.D.	N.D.
GS 009	N.D.	N.D.
GS 010	N.D.	N.D.
GS 011	N.D.	N.D.
GS 012	N.D.	N.D.
GS 013	N.D.	N.D.
GS 014	N.D.	N.D.
GS 015	N.D.	N.D.

Appendix 6

PCB Concentrations in Greenland Sharks Collected from Svalbard (Norway) from 2008 to 2009

Appendix 6. PCB concentrations of Greenland sharks in Svalbard. Concentration data was provided by Dr. Aaron T. Fisk. N.D. = not detected. PCB congeners are presented as **bold** numbers.

Table A6-1: SVGS01L--- SVGS015L, liver samples

Samples	Lipid %	PCB concentrations (ng/g) wet weight					
		18/17	31/28	33	52	49	44
SVGS01L	4.34×10 ¹	2.55	1.98×10 ¹	N.D.	1.02×10 ²	2.17×10 ¹	1.55×10 ¹
SVGS02L	4.74×10 ¹	1.97	8.38	N.D.	2.35×10 ¹	7.51	3.75
SVGS03L	4.90×10 ¹	9.87	2.68×10 ¹	N.D.	1.78×10 ²	4.79×10 ¹	3.38×10 ¹
SVGS04L	5.08×10 ¹	1.81	1.05×10 ¹	N.D.	3.47×10 ¹	1.08×10 ¹	5.19
SVGS05L	4.45×10 ¹	1.26	1.08×10 ¹	N.D.	2.43×10 ¹	7.32	3.30
SVGS06L	4.66×10 ¹	5.12	2.03×10 ¹	N.D.	9.82×10 ¹	3.26×10 ¹	2.14×10 ¹
SVGS07L	4.74×10 ¹	1.18	5.57	N.D.	1.98×10 ¹	5.96	4.59
SVGS08L	4.02×10 ¹	1.13	9.95	1.39	2.95×10 ¹	7.71	4.56
SVGS09L	3.84×10 ¹	1.38	7.04	N.D.	1.73×10 ¹	4.76	3.42
SVGS10L	4.39×10 ¹	1.77	1.04×10 ¹	N.D.	4.41×10 ¹	1.19×10 ¹	8.27

SVGS11L	4.89×10^1	4.08	1.94×10^1	N.D.	1.64×10^2	2.89×10^1	1.83×10^1
SVGS12L	5.14×10^1	3.25	2.50×10^1	N.D.	9.57×10^1	2.04×10^1	1.27×10^1
SVGS13L	5.12×10^1	2.69	1.09×10^1	N.D.	5.34×10^1	1.36×10^1	8.60
SVGS14L	4.87×10^1	4.90	9.12	N.D.	4.27×10^1	1.06×10^1	7.16
SVGS15L	4.69×10^1	3.58	1.28×10^1	N.D.	9.15×10^1	2.64×10^1	1.33×10^1
	74	70	95	101	99	87	110
SVGS01L	1.34×10^2	2.31×10^1	1.28×10^2	1.48×10^2	2.54×10^2	1.47×10^2	1.07×10^2
SVGS02L	3.68×10^1	4.20	3.07×10^1	4.07×10^1	5.30×10^1	5.94	1.72×10^1
SVGS03L	1.02×10^2	1.51×10^1	2.08×10^2	2.51×10^2	2.77×10^2	5.59×10^1	1.00×10^2
SVGS04L	2.52×10^1	5.59	4.39×10^1	7.16×10^1	8.70×10^1	7.11×10^1	2.39×10^1
SVGS05L	2.89×10^1	4.09	3.58×10^1	4.80×10^1	8.38×10^1	6.69	1.84×10^1
SVGS06L	7.76×10^1	1.45×10^1	1.62×10^2	2.01×10^2	1.84×10^2	4.31×10^1	6.95×10^1
SVGS07L	1.41×10^2	2.80	1.88×10^1	2.25×10^1	3.72×10^1	2.24×10^1	1.26×10^1

SVGS08L	3.84×10^1	5.96	3.43×10^1	5.18×10^1	6.80×10^1	5.14×10^1	2.06×10^1
SVGS09L	1.70×10^1	3.91	2.03×10^1	2.79×10^1	2.32×10^1	4.78	1.15×10^1
SVGS10L	3.44×10^1	7.63	5.84×10^1	5.58×10^1	1.16×10^2	5.53×10^1	3.97×10^1
SVGS11L	5.68×10^1	1.48×10^1	2.03×10^2	1.99×10^2	4.01×10^2	1.97×10^2	1.43×10^2
SVGS12L	4.96×10^1	1.46×10^1	1.34×10^2	1.47×10^2	2.97×10^2	1.47×10^1	6.72×10^1
SVGS13L	7.19×10^1	1.05×10^1	5.92×10^1	5.18×10^1	1.17×10^2	5.14×10^1	2.78×10^1
SVGS14L	1.62×10^2	5.65	5.11×10^1	3.93×10^1	1.01×10^2	3.90×10^1	2.12×10^1
SVGS15L	8.61×10^1	7.75	1.01×10^2	1.09×10^2	2.00×10^2	1.08×10^2	8.81×10^1
	151/82	149	118	153	105/132	138	158
SVGS01L	5.09×10^1	2.88×10^2	3.17×10^2	6.78×10^2	1.23×10^2	7.24×10^2	4.68×10^1
SVGS02L	6.50	4.06×10^1	7.10×10^1	1.43×10^2	2.54×10^1	1.32×10^2	6.38
SVGS03L	6.26×10^1	2.67×10^2	3.02×10^2	5.58×10^2	1.36×10^2	5.70×10^2	3.20×10^1
SVGS04L	9.70	5.99×10^1	9.54×10^1	1.76×10^2	3.13×10^1	1.64×10^2	7.76

SVGS05L	5.23	5.10×10^1	9.33×10^1	2.53×10^2	2.82×10^1	2.16×10^2	7.06
SVGS06L	6.12×10^1	2.43×10^2	3.19×10^2	4.99×10^2	1.63×10^2	5.39×10^2	3.70×10^1
SVGS07L	5.12	2.63×10^1	5.07×10^1	8.21×10^1	1.90×10^1	7.44×10^1	3.28
SVGS08L	8.48	5.55×10^1	1.06×10^2	2.41×10^2	4.41×10^1	2.24×10^2	1.52×10^1
SVGS09L	5.53	2.45×10^1	2.92×10^1	6.28×10^1	1.98×10^1	5.35×10^1	2.50
SVGS10L	2.06×10^1	7.66×10^1	1.11×10^2	2.23×10^2	4.51×10^1	2.18×10^2	1.68×10^1
SVGS11L	9.51×10^1	4.36×10^2	2.97×10^2	1.08×10^3	1.77×10^2	1.06×10^3	6.07×10^1
SVGS12L	4.10×10^1	2.13×10^2	2.18×10^2	8.94×10^2	8.99×10^1	8.43×10^2	2.93×10^1
SVGS13L	1.50×10^1	6.45×10^1	1.22×10^2	2.70×10^2	4.53×10^1	2.65×10^2	1.74×10^1
SVGS14L	1.25×10^1	6.52×10^1	1.04×10^2	1.43×10^2	3.60×10^1	1.30×10^2	5.52
SVGS15L	3.93×10^1	1.65×10^2	2.21×10^2	3.34×10^2	9.23×10^1	3.63×10^2	2.97×10^1
	187	183	128	177	156/171	180	191
SVGS01L	2.02×10^2	8.75×10^1	6.53×10^1	4.42×10^1	7.97×10^1	2.94×10^2	4.39

SVGS02L	2.72×10^1	1.34×10^1	1.52×10^1	6.60	1.32×10^1	4.93×10^1	5.50×10^{-1}
SVGS03L	1.06×10^2	5.24×10^1	7.35×10^1	2.45×10^1	4.51×10^1	1.63×10^2	2.82
SVGS04L	3.68×10^1	1.86×10^1	1.89×10^1	9.57	1.84×10^1	5.90×10^1	1.17
SVGS05L	3.97×10^1	2.03×10^1	2.38×10^1	9.73	2.08×10^1	8.98×10^1	1.09
SVGS06L	1.42×10^2	6.33×10^1	6.34×10^1	3.47×10^1	4.49×10^1	2.02×10^2	2.52
SVGS07L	3.73×10^1	1.29×10^1	9.53	3.51	8.38	2.63×10^1	5.90×10^{-1}
SVGS08L	5.24×10^1	2.72×10^1	2.18×10^1	6.78	2.26×10^1	9.84×10^1	1.48
SVGS09L	1.42×10^1	8.42	6.88	2.44	7.52	2.00×10^1	9.70×10^{-1}
SVGS10L	5.57×10^1	2.27×10^1	2.48×10^1	1.29×10^1	2.16×10^1	8.63×10^1	1.42
SVGS11L	2.97×10^2	1.17×10^2	8.76×10^1	9.81×10^1	8.72×10^1	4.25×10^2	9.09
SVGS12L	1.60×10^2	7.86×10^1	9.01×10^1	3.60×10^1	5.60×10^1	3.12×10^2	3.74
SVGS13L	5.69×10^1	2.49×10^1	3.12×10^1	1.32×10^1	2.52×10^1	9.02×10^1	1.28
SVGS14L	8.32×10^1	2.93×10^1	1.80×10^1	6.92	1.47×10^1	4.45×10^1	8.80×10^{-1}

SVGS15L	9.92×10^1	4.33×10^1	4.35×10^1	2.36×10^1	3.78×10^1	1.26×10^2	1.81
	170	201	195/208	194	205	206	209
SVGS01L	1.02×10^2	3.36×10^1	1.08×10^1	2.90×10^1	1.74	8.65	7.55
SVGS02L	1.81×10^1	6.29	2.10	5.47	4.60×10^{-1}	2.32	1.66
SVGS03L	5.69×10^1	1.65×10^1	6.26	1.43×10^1	1.27	4.86	2.52
SVGS04L	2.05×10^1	6.73	2.29	5.95	5.20×10^{-1}	2.22	1.71
SVGS05L	3.26×10^1	1.08×10^1	2.93	9.96	6.30×10^{-1}	3.25	1.92
SVGS06L	6.83×10^1	2.60×10^1	6.61	1.84×10^1	1.04	4.91	2.52
SVGS07L	8.78	2.99	1.05	2.31	6.40×10^{-1}	8.10×10^{-1}	4.50×10^{-1}
SVGS08L	9.62	4.87	1.25×10^1	6.30×10^{-1}	4.96	2.26	2.39
SVGS09L	6.61	2.10	8.70×10^{-1}	2.04	3.60×10^{-1}	8.40×10^{-1}	5.70×10^{-1}
SVGS10L	1.10×10^1	4.23	1.02×10^1	7.30×10^{-1}	3.28	1.83	1.94
SVGS11L	1.54×10^2	4.68×10^1	1.67×10^1	3.94×10^1	2.15	1.09×10^1	8.40

SVGS12L	1.13×10^2	3.35×10^1	7.64	2.93×10^1	1.83	5.80	3.19
SVGS13L	3.17×10^1	9.94	2.99	7.78	4.60×10^{-1}	2.47	1.40
SVGS14L	1.43×10^1	4.72	1.54	4.03	9.10×10^{-1}	1.06	8.40×10^{-1}
SVGS15L	4.26×10^1	2.02×10^1	5.61	1.24×10^1	1.00	4.85	2.98

Table A6-2: SVGS16L- SVGS32L, liver samples.

Samples	Lipid %	18/17	31/28	33	52	49	44
SVGS16L	5.34×10 ¹	2.07	1.38×10 ¹	N.D.	6.68×10 ¹	1.14×10 ¹	5.65
SVGS17L	4.66×10 ¹	2.42	1.28×10 ¹	N.D.	3.90×10 ¹	1.15×10 ¹	6.35
SVGS18L	4.46×10 ¹	1.86	9.49	N.D.	6.30×10 ¹	1.26×10 ¹	7.41
SVGS19L	5.71×10 ¹	2.96	1.41×10 ¹	N.D.	4.61×10 ¹	1.19×10 ¹	7.35
SVGS20L	5.59×10 ¹	1.37	7.43	N.D.	2.41×10 ¹	6.31	3.30
SVGS20LD	4.68×10 ¹	3.72	1.15×10 ¹	N.D.	3.18×10 ¹	1.35×10 ¹	9.39
SVGS21L	4.67×10 ¹	3.17	9.92	N.D.	3.39×10 ¹	1.13×10 ¹	9.07
SVGS22L	4.83×10 ¹	3.27	1.68×10 ¹	N.D.	8.66×10 ¹	1.89×10 ¹	1.44×10 ¹
SVGS23L	3.55×10 ¹	N.D.	4.39	N.D.	7.48	2.56	1.88
SVGS24L	4.41×10 ¹	1.01×10 ¹	2.35×10 ¹	N.D.	6.77	4.65×10 ¹	3.72×10 ¹
SVGS25L	3.82×10 ¹	3.04	1.12×10 ¹	N.D.	9.46×10 ¹	2.48×10 ¹	1.50×10 ¹

SVGS26L	4.41×10^1	1.57	8.76	N.D.	5.20×10^1	1.30×10^1	8.31
SVGS27L	4.49×10^1	2.75	1.59×10^1	N.D.	8.50×10^1	1.80×10^1	1.16×10^1
SVGS29L	4.07×10^1	4.78	2.40×10^1	N.D.	1.69×10^2	4.81×10^1	2.50×10^1
SVGS30L	1.10×10^1	N.D.	8.42	N.D.	2.42×10^1	6.87	4.93
SVGS31L	5.43×10^1	2.29	1.69×10^1	N.D.	8.62×10^1	2.11×10^1	1.43×10^1
SVGS32L	3.02×10^1	2.98	1.56×10^1	N.D.	2.88×10^2	4.83×10^1	1.21×10^1
	74	70	95	101	99	87	110
SVGS16L	5.87×10^1	8.60	7.88×10^1	8.71×10^1	1.82×10^2	1.22×10^1	3.87×10^1
SVGS17L	8.36×10^1	5.95	4.16×10^1	6.53×10^1	8.23×10^1	6.48×10^1	3.28×10^1
SVGS18L	2.50×10^1	4.83	7.74×10^1	6.41×10^1	1.53×10^2	6.35×10^1	4.38×10^1
SVGS19L	3.26×10^1	6.66	5.46×10^1	5.71×10^1	1.15×10^2	1.31×10^1	2.92×10^1
SVGS20L	1.17×10^1	4.37	2.70×10^1	4.26×10^1	5.23×10^1	6.26	1.32×10^1
SVGS20LD	2.59×10^1	1.02×10^1	4.63×10^1	6.47×10^1	9.17×10^1	6.42×10^1	3.85×10^1

SVGS21L	5.95×10^1	7.06	4.68×10^1	6.09×10^1	9.27×10^1	6.04×10^1	3.74×10^1
SVGS22L	2.12×10^2	8.84	9.74×10^1	1.07×10^2	1.93×10^2	1.06×10^2	5.18×10^1
SVGS23L	3.13×10^1	1.51	1.17×10^1	9.86	2.31×10^1	9.79	7.73
SVGS24L	5.38×10^1	1.13×10^1	2.15×10^2	2.20×10^2	4.27×10^2	2.18×10^2	1.22×10^2
SVGS25L	4.95×10^1	7.18	1.20×10^2	1.02×10^2	2.37×10^2	1.02×10^2	7.45×10^1
SVGS26L	4.73×10^1	4.91	6.38×10^1	5.89×10^1	1.26×10^2	5.84×10^1	4.33×10^1
SVGS27L	4.86×10^1	9.48	9.76×10^1	8.90×10^1	1.93×10^2	8.83×10^1	6.13×10^1
SVGS29L	9.85×10^1	1.40×10^1	2.15×10^2	2.64×10^2	4.26×10^2	2.62×10^2	9.13×10^1
SVGS30L	1.91×10^1	5.01	2.88×10^1	3.08×10^1	5.71×10^1	3.06×10^1	1.76×10^1
SVGS31L	2.78×10^1	1.01×10^1	9.85×10^1	1.56×10^2	1.94×10^2	2.07×10^1	5.67×10^1
SVGS32L	1.29×10^2	1.26×10^1	2.87×10^2	4.09×10^2	8.09×10^2	8.93	1.03×10^2
	151/82	149	118	153	105/132	138	158
SVGS16L	2.64×10^1	1.26×10^2	1.34×10^2	4.92×10^2	5.15×10^1	4.66×10^2	1.79×10^1

SVGS17L	1.09×10^1	7.06×10^1	1.50×10^2	2.49×10^2	5.77×10^1	2.44×10^2	1.73×10^1
SVGS18L	2.83×10^1	1.23×10^2	1.39×10^2	3.43×10^2	6.80×10^1	3.43×10^2	2.48×10^1
SVGS19L	1.40×10^1	7.60×10^1	1.36×10^2	2.62×10^2	4.36×10^1	2.56×10^2	1.24×10^1
SVGS20L	8.60	4.02×10^1	8.20×10^1	1.24×10^2	2.71×10^1	1.22×10^2	6.53
SVGS20LD	1.87×10^1	6.59×10^1	8.78×10^1	1.51×10^2	3.82×10^1	1.46×10^2	8.70
SVGS21L	1.71×10^1	5.93×10^1	9.92×10^1	1.46×10^2	3.95×10^1	1.37×10^2	8.80
SVGS22L	3.06×10^1	1.28×10^2	1.79×10^2	2.68×10^2	7.73×10^1	2.58×10^2	1.76×10^1
SVGS23L	1.99	1.65×10^1	3.51×10^1	6.96×10^1	1.12×10^1	5.48×10^1	1.86
SVGS24L	7.13×10^1	2.67×10^2	2.63×10^2	5.05×10^2	1.47×10^2	5.35×10^2	3.40×10^1
SVGS25L	5.11×10^1	1.76×10^2	2.07×10^2	3.32×10^2	9.61×10^1	3.53×10^2	2.77×10^1
SVGS26L	2.67×10^1	9.89×10^1	1.16×10^2	1.95×10^2	4.97×10^1	1.97×10^2	1.19×10^1
SVGS27L	4.42×10^1	1.63×10^2	1.59×10^2	4.21×10^2	7.45×10^1	4.21×10^2	2.59×10^1
SVGS29L	7.37×10^1	3.29×10^2	3.26×10^2	6.15×10^2	1.59×10^2	6.43×10^2	3.80×10^1

SVGS30L	7.41	3.97×10^1	7.11×10^1	1.35×10^2	2.59×10^1	1.19×10^2	3.44
SVGS31L	3.00×10^1	1.54×10^2	1.96×10^2	5.02×10^2	1.03×10^2	4.71×10^2	2.74×10^1
SVGS32L	1.09×10^2	6.04×10^2	5.37×10^2	1.84×10^3	2.52×10^2	1.84×10^3	1.05×10^2
	187	183	128	177	156/171	180	191
SVGS16L	8.97×10^1	4.38×10^1	5.34×10^1	2.36×10^1	3.41×10^1	1.77×10^2	2.08
SVGS17L	5.72×10^1	2.72×10^1	2.82×10^1	1.07×10^1	2.67×10^1	8.89×10^1	1.77
SVGS18L	9.07×10^1	3.65×10^1	4.00×10^1	2.43×10^1	3.07×10^1	1.33×10^2	1.97
SVGS19L	4.69×10^1	2.76×10^1	3.41×10^1	1.16×10^1	2.51×10^1	8.37×10^1	1.82
SVGS20L	2.56×10^1	1.47×10^1	1.68×10^1	5.24	9.68	3.79×10^1	9.10×10^{-1}
SVGS20LD	4.04×10^1	2.02×10^1	2.18×10^1	1.21×10^1	1.80×10^1	6.87×10^1	1.69
SVGS21L	4.42×10^1	2.15×10^1	1.77×10^1	9.56	1.93×10^1	6.88×10^1	1.07
SVGS22L	7.17×10^1	3.62×10^1	3.26×10^1	1.26×10^1	2.85×10^1	9.57×10^1	2.42
SVGS23L	4.93×10^1	1.15×10^1	7.64	2.05	6.09	2.32×10^1	5.30×10^{-1}

SVGS24L	1.36×10^2	5.87×10^1	6.71×10^1	2.23×10^1	5.05×10^1	1.50×10^2	2.91
SVGS25L	1.17×10^2	4.40×10^1	4.60×10^1	2.56×10^1	3.71×10^1	1.45×10^2	3.53
SVGS26L	6.57×10^1	2.68×10^1	2.43×10^1	1.62×10^1	2.23×10^1	8.45×10^1	2.24
SVGS27L	9.77×10^1	4.29×10^1	5.36×10^1	2.42×10^1	3.50×10^1	1.41×10^2	2.70
SVGS29L	1.80×10^2	7.34×10^1	6.95×10^1	4.42×10^1	6.24×10^1	2.64×10^2	4.27
SVGS30L	5.18×10^1	2.37×10^1	1.77×10^1	6.85	1.41×10^1	4.59×10^1	9.60×10^{-1}
SVGS31L	1.04×10^2	5.97×10^1	5.89×10^1	1.94×10^1	4.07×10^1	1.76×10^2	2.87
SVGS32L	4.19×10^2	1.89×10^2	2.19×10^2	9.29×10^1	1.11×10^2	6.66×10^2	6.55
	170	201	195/208	194	205	206	209
SVGS16L	6.12×10^1	2.07×10^1	5.08	1.79×10^1	1.52	4.01	2.18
SVGS17L	3.02×10^1	1.09×10^1	3.33	9.45	7.40×10^{-1}	3.30	2.28
SVGS18L	1.47×10^1	5.68	1.41×10^1	6.90×10^{-1}	3.27	1.81	1.92
SVGS19L	2.92×10^1	8.83	2.79	7.96	6.50×10^{-1}	2.33	1.40

SVGS20L	1.26×10^1	4.16	1.18	3.54	3.40×10^{-1}	1.22	9.30×10^{-1}
SVGS20LD	2.33×10^1	1.12×10^1	4.32	1.05×10^1	6.20×10^{-1}	4.01	1.97
SVGS21L	2.32×10^1	1.10×10^1	4.58	9.69	6.90×10^{-1}	3.94	2.38
SVGS22L	3.20×10^1	1.30×10^1	4.49	1.12×10^1	9.50×10^{-1}	4.27	3.06
SVGS23L	7.51	2.88	9.80×10^{-1}	2.79	2.60×10^{-1}	9.30×10^{-1}	5.30×10^{-1}
SVGS24L	5.11×10^1	1.68×10^1	4.86	1.26×10^1	1.04	3.04	2.00
SVGS25L	2.09×10^1	7.20	1.78×10^1	7.90×10^{-1}	4.97	2.66	2.82
SVGS26L	1.18×10^1	4.11	9.67	5.90×10^{-1}	2.72	1.59	1.68
SVGS27L	1.46×10^1	5.48	1.33×10^1	9.70×10^{-1}	3.53	2.04	2.16
SVGS29L	9.03×10^1	3.67×10^1	9.87	3.13×10^1	1.75	8.68	5.46
SVGS30L	1.51×10^1	5.75	1.79	5.07	8.00×10^{-1}	1.69	1.19
SVGS31L	5.42×10^1	1.98×10^1	6.07	1.74×10^1	1.22	6.61	4.03
SVGS32L	2.24×10^2	9.19×10^1	2.07×10^1	6.08×10^1	2.11	1.91×10^1	1.13×10^1

Table A6-3: SM09-01Li--SM09-13Li, liver samples.

Samples	Lipid %	PCB concentrations (ng/g) wet weight					
		18/17	31/28	33	52	49	44
SM09-01Li	4.73×10 ¹	4.73	2.22×10 ¹	N.D.	1.21×10 ²	2.87×10 ¹	1.76×10 ¹
SM09-02Li	4.75×10 ¹	1.41	1.06×10 ¹	N.D.	3.48×10 ¹	1.09×10 ¹	7.38
SM09-03Li	3.80×10 ¹	3.62	1.53×10 ¹	N.D.	7.83×10 ¹	1.91×10 ¹	8.43
SM09-04Li	4.61×10 ¹	6.40	1.23×10 ¹	N.D.	4.87×10 ¹	1.43×10 ¹	6.41
SM09-05Li	3.45×10 ¹	3.54	1.26×10 ¹	N.D.	7.67×10 ¹	2.05×10 ¹	1.36×10 ¹
SM09-06Li	4.37×10 ¹	1.75	8.77	N.D.	2.28×10 ¹	6.74	4.37
SM-09-07Lii	3.57×10 ¹	2.32	1.03×10 ¹	N.D.	5.37×10 ¹	1.27×10 ¹	9.49
SM-09-08Lii	4.04×10 ¹	9.90×10 ⁻¹	8.46	N.D.	2.12×10 ¹	6.11	3.19
SM-09-09Lii	4.24×10 ¹	1.68	9.30	N.D.	9.09×10 ¹	1.26×10 ¹	8.56
SM-09-10Lii	4.65×10 ¹	3.95	1.80×10 ¹	N.D.	8.60×10 ¹	2.01×10 ¹	1.36×10 ¹

SM-09-11Lii	3.35×10^1	4.07	1.35×10^1	N.D.	1.17×10^2	3.28×10^1	1.56×10^1
SM-09-12Lii	3.50×10^1	1.20	7.65	N.D.	2.26×10^1	6.75	4.19
SM09-13Lii	4.03×10^1	7.50×10^{-1}	8.14	N.D.	1.47×10^1	5.40	4.47
	74	70	95	101	99	87	110
SM09-01Li	7.18×10^1	9.81	1.04×10^2	1.55×10^2	1.88×10^2	3.60×10^1	8.35×10^1
SM09-02Li	5.05×10^1	6.39	3.58×10^1	6.54×10^1	8.50×10^1	1.05×10^1	3.05×10^1
SM09-03Li	6.53×10^1	5.99	7.68×10^1	1.13×10^2	1.28×10^2	3.41×10^1	4.78×10^1
SM09-04Li	3.51×10^1	6.80	6.41×10^1	8.94×10^1	9.66×10^1	1.72×10^1	7.19×10^1
SM09-05Li	5.71×10^1	6.20	7.02×10^1	9.82×10^1	1.15×10^2	1.44×10^1	5.65×10^1
SM09-06Li	4.27×10^1	6.52	2.04×10^1	4.42×10^1	7.57×10^1	1.00×10^1	1.56×10^1
SM-09-07Lii	4.33×10^1	6.83	6.13×10^1	8.12×10^1	8.48×10^1	1.54×10^1	4.08×10^1
SM-09-08Lii	3.27×10^1	5.22	3.01×10^1	5.48×10^1	5.18×10^1	9.00	2.44×10^1
SM-09-09Lii	6.43×10^1	7.37	1.05×10^2	1.40×10^2	1.98×10^2	1.19×10^1	6.54×10^1

SM-09-10Lii	8.08×10^1	1.16×10^1	9.49×10^1	1.28×10^2	1.46×10^2	2.71×10^1	5.89×10^1
SM-09-11Lii	8.76×10^1	1.05×10^1	1.61×10^2	1.88×10^2	1.89×10^2	2.69×10^1	9.93×10^1
SM-09-12Lii	2.10×10^1	4.03	2.45×10^1	4.12×10^1	4.14×10^1	6.41	1.87×10^1
SM09-13Lii	2.31×10^1	5.10	1.88×10^1	2.87×10^1	3.02×10^1	4.97	2.38×10^1
	151/82	149	118	153	105/132	138	158
SM09-01Li	4.46×10^1	1.78×10^2	2.07×10^2	4.68×10^2	8.99×10^1	4.60×10^2	2.08×10^1
SM09-02Li	9.88	5.49×10^1	1.10×10^2	2.55×10^2	4.35×10^1	1.85×10^2	8.47
SM09-03Li	4.11×10^1	1.48×10^2	1.46×10^2	3.26×10^2	7.40×10^1	3.23×10^2	1.99×10^1
SM09-04Li	3.43×10^1	1.21×10^2	1.69×10^2	2.66×10^2	7.61×10^1	2.63×10^2	1.69×10^1
SM09-05Li	2.68×10^1	1.05×10^2	1.40×10^2	2.25×10^2	6.43×10^1	2.35×10^2	1.52×10^1
SM09-06Li	7.88	4.37×10^1	8.36×10^1	2.14×10^2	2.31×10^1	1.89×10^2	6.19
SM-09-07Lii	1.93×10^1	7.37×10^1	1.16×10^2	1.97×10^2	4.70×10^1	1.93×10^2	1.04×10^1
SM-09-08Lii	7.59	4.02×10^1	6.59×10^1	1.39×10^2	2.42×10^1	1.27×10^2	5.74

SM-09-09Lii	4.78×10^1	1.94×10^2	1.85×10^2	5.69×10^2	8.82×10^1	5.71×10^2	2.83×10^1
SM-09-10Lii	3.20×10^1	1.22×10^2	1.88×10^2	3.30×10^2	7.96×10^1	3.38×10^2	1.69×10^1
SM-09-11Lii	6.66×10^1	2.62×10^2	2.81×10^2	4.66×10^2	1.28×10^2	5.01×10^2	2.80×10^1
SM-09-12Lii	8.86	4.06×10^1	6.90×10^1	9.98×10^1	2.51×10^1	9.50×10^1	5.11
SM09-13Lii	6.51	3.31×10^1	6.85×10^1	7.56×10^1	2.65×10^1	6.85×10^1	3.96
	187	183	128	177	156/171	180	191
SM09-01Li	9.81×10^1	5.17×10^1	5.90×10^1	2.26×10^1	4.13×10^1	1.74×10^2	1.89
SM09-02Li	3.84×10^1	2.28×10^1	1.97×10^1	7.15	2.54×10^1	1.28×10^2	1.93
SM09-03Li	9.38×10^1	4.12×10^1	3.82×10^1	2.20×10^1	3.19×10^1	1.35×10^2	2.47
SM09-04Li	9.12×10^1	3.99×10^1	3.73×10^1	2.00×10^1	3.21×10^1	1.16×10^2	2.22
SM09-05Li	4.87×10^1	2.61×10^1	3.53×10^1	8.51	2.39×10^1	7.03×10^1	1.19
SM09-06Li	3.50×10^1	1.84×10^1	2.63×10^1	8.92	1.82×10^1	7.44×10^1	1.30
SM-09-07Lii	4.01×10^1	2.07×10^1	2.40×10^1	8.69	2.01×10^1	6.90×10^1	1.29

SM-09-08Lii	2.84×10^1	1.41×10^1	1.31×10^1	5.66	1.32×10^1	4.98×10^1	6.60×10^{-1}
SM-09-09Lii	1.35×10^2	6.49×10^1	6.07×10^1	3.04×10^1	4.57×10^1	2.34×10^2	3.31
SM-09-10Lii	7.64×10^1	3.99×10^1	4.15×10^1	1.92×10^1	3.24×10^1	1.18×10^2	1.64
SM-09-11Lii	1.49×10^2	6.80×10^1	6.18×10^1	3.25×10^1	5.04×10^1	1.99×10^2	2.30
SM-09-12Lii	2.53×10^1	1.30×10^1	1.15×10^1	5.42	1.10×10^1	3.53×10^1	5.70×10^{-1}
SM09-13Lii	2.32×10^1	1.18×10^1	1.03×10^1	5.42	1.05×10^1	2.79×10^1	8.70×10^{-1}
	170	201	195/208	194	205	206	209
SM09-01Li	6.09×10^1	2.13×10^1	5.84	1.79×10^1	1.12	4.78	3.06
SM09-02Li	6.59×10^1	7.18	2.41	5.24×10^1	2.34	7.74	4.06
SM09-03Li	4.68×10^1	2.20×10^1	5.54	1.51×10^1	9.10×10^{-1}	4.04	1.94
SM09-04Li	3.94×10^1	2.08×10^1	5.38	1.31×10^1	8.00×10^{-1}	5.42	3.55
SM09-05Li	2.53×10^1	8.51	2.44	7.05	7.20×10^{-1}	1.74	1.11
SM09-06Li	2.64×10^1	8.20	2.43	7.23	7.00×10^{-1}	2.40	1.41

SM-09-07Lii	2.39×10^1	8.26	2.70	6.98	5.10×10^{-1}	2.50	1.83
SM-09-08Lii	1.77×10^1	6.34	1.96	5.23	4.90×10^{-1}	1.74	1.09
SM-09-09Lii	8.21×10^1	2.96×10^1	6.72	2.18×10^1	1.03	4.83	2.96
SM-09-10Lii	3.97×10^1	1.65×10^1	4.40	1.24×10^1	8.10×10^{-1}	3.91	2.48
SM-09-11Lii	6.80×10^1	2.97×10^1	7.30	2.07×10^1	1.36	5.18	2.68
SM-09-12Lii	1.21×10^1	4.92	1.49	3.86	3.00×10^{-1}	1.50	1.16
SM09-13Lii	9.19	4.08	1.13	2.81	3.40×10^{-1}	9.30×10^{-1}	5.80×10^{-1}

Table A6-4: Plasma samples of Greenland sharks.

Samples	Lipid %	PCB concentrations (ng/g) wet weight					
		18/17	31/28	33	52	49	44
SVGS 08 01 BP	5.00×10^{-2}	2.00×10^{-1}	2.90×10^{-1}	N.D.	8.10×10^{-1}	1.70×10^{-1}	1.20×10^{-1}
SVGS 08 02 BP	6.70×10^{-1}	N.D.	1.90×10^{-1}	N.D.	8.80×10^{-1}	1.80×10^{-1}	1.10×10^{-1}
SVGS 08 03 BP	9.10×10^{-1}	4.90×10^{-1}	1.09	N.D.	2.69	7.70×10^{-1}	4.70×10^{-1}
SVGS 08 04 BP	1.47	N.D.	N.D.	1.90×10^{-1}	N.D.	1.35	2.30×10^{-1}
SVGS 08 05 BP	2.70×10^{-1}	1.40×10^{-1}	2.00×10^{-1}	1.00×10^{-1}	N.D.	6.60×10^{-1}	1.40×10^{-1}
SVGS 08 06 BP	4.10×10^{-1}	8.00×10^{-2}	1.10×10^{-1}	2.00×10^{-1}	N.D.	8.20×10^{-1}	2.20×10^{-1}
SVGS 08 07 BP	5.10×10^{-1}	N.D.	N.D.	1.10×10^{-1}	N.D.	6.80×10^{-1}	1.30×10^{-1}
SVGS 08 08 BP	3.80×10^{-1}	N.D.	N.D.	9.00×10^{-2}	N.D.	6.30×10^{-1}	1.30×10^{-1}
SVGS 08 09 BP	1.50×10^{-1}	N.D.	N.D.	N.D.	N.D.	5.00×10^{-1}	6.00×10^{-2}
SVGS 08 10 BP	1.50×10^{-1}	N.D.	N.D.	6.00×10^{-2}	N.D.	1.17	2.30×10^{-1}

SVGS 08 11 BP	7.50×10^{-1}	N.D.	N.D.	8.00×10^{-2}	N.D.	1.86	2.80×10^{-1}
SVGS 08 12 BP	1.24	N.D.	N.D.	N.D.	N.D.	2.23	4.10×10^{-1}
SVGS 08 13 BP	6.00×10^{-1}	8.00×10^{-2}	1.20×10^{-1}	4.00×10^{-2}	N.D.	9.10×10^{-1}	1.70×10^{-1}
SVGS 08 14 BP	4.60×10^{-1}	N.D.	N.D.	9.00×10^{-2}	N.D.	7.70×10^{-1}	1.30×10^{-1}
SVGS 08 15 BP	6.30×10^{-1}	N.D.	N.D.	8.00×10^{-2}	N.D.	1.20	2.60×10^{-1}
SVGS 08 16 BP	5.00×10^{-1}	N.D.	N.D.	1.00×10^{-1}	N.D.	8.80×10^{-1}	1.90×10^{-1}
SVGS 08 17 BP	3.10×10^{-1}	N.D.	N.D.	6.00×10^{-2}	N.D.	6.10×10^{-1}	8.00×10^{-2}
SVGS 08 18 BP	4.70×10^{-1}	N.D.	N.D.	1.40×10^{-1}	N.D.	1.76	2.30×10^{-1}
SVGS 08 19 BP	5.60×10^{-1}	N.D.	N.D.	1.70×10^{-1}	N.D.	8.10×10^{-1}	1.90×10^{-1}
SVGS 08 20 BP	9.50×10^{-1}	N.D.	N.D.	4.00×10^{-2}	N.D.	5.60×10^{-1}	1.30×10^{-1}
SVGS 08 21 BP	3.20×10^{-1}	N.D.	N.D.	5.00×10^{-2}	N.D.	6.50×10^{-1}	9.00×10^{-2}
SVGS 08 22 BP	3.20×10^{-1}	N.D.	N.D.	1.20×10^{-1}	N.D.	7.80×10^{-1}	1.40×10^{-1}
SVGS 08 23 BP	3.60×10^{-1}	N.D.	N.D.	2.00×10^{-1}	N.D.	4.70×10^{-1}	1.20×10^{-1}

SVGS 08 24 BP	4.40×10^{-1}	N.D.	N.D.	2.10×10^{-1}	N.D.	1.95	4.50×10^{-1}
SVGS 08 25 BP	6.10×10^{-1}	N.D.	N.D.	8.00×10^{-2}	N.D.	8.20×10^{-1}	1.70×10^{-1}
SVGS 08 26 BP	8.50×10^{-1}	N.D.	N.D.	1.30×10^{-1}	N.D.	1.24	2.60×10^{-1}
SVGS 08 27 BP	6.40×10^{-1}	N.D.	N.D.	1.30×10^{-1}	N.D.	1.48	2.00×10^{-1}
SVGS 08 29 BP	1.03	N.D.	N.D.	3.10×10^{-1}	N.D.	3.04	7.90×10^{-1}
SVGS 08 30 BP	2.30×10^{-1}	N.D.	N.D.	8.00×10^{-2}	N.D.	6.40×10^{-1}	1.20×10^{-1}
SVGS 08 31 BP	3.10×10^{-1}	N.D.	N.D.	1.40×10^{-1}	N.D.	7.60×10^{-1}	2.00×10^{-1}
SVGS 08 32 BP	1.11	N.D.	N.D.	1.60×10^{-1}	N.D.	3.90	7.10×10^{-1}
SM09 01 BP	8.70×10^{-1}	N.D.	N.D.	1.70×10^{-1}	N.D.	1.96	4.10×10^{-1}
SM09 02 BP	5.20×10^{-1}	N.D.	N.D.	N.D.	N.D.	7.10×10^{-1}	1.20×10^{-1}
SM09 03 BP	1.19	N.D.	N.D.	N.D.	N.D.	2.07	4.10×10^{-1}
SM09 04 BP	3.00×10^{-1}	N.D.	N.D.	N.D.	N.D.	9.80×10^{-1}	1.80×10^{-1}
SM09 05 BP	7.90×10^{-1}	2.60×10^{-1}	3.60×10^{-1}	2.40×10^{-1}	N.D.	2.39	4.50×10^{-1}

SM09 06 BP	8.20×10^{-1}	N.D.	N.D.	N.D.	N.D.	6.80×10^{-1}	1.00×10^{-1}
SM09 07 BP	4.50×10^{-1}	N.D.	N.D.	N.D.	N.D.	7.80×10^{-1}	1.00×10^{-1}
SM09 09 BP	5.40×10^{-1}	N.D.	N.D.	N.D.	N.D.	1.48	1.70×10^{-1}
SM09 10 BP	4.10×10^{-1}	N.D.	N.D.	6.00×10^{-2}	N.D.	9.00×10^{-1}	1.20×10^{-1}
SM09 11 BP	6.60×10^{-1}	N.D.	N.D.	1.40×10^{-1}	1.60×10^{-1}	2.25	4.50×10^{-1}
SM09 12 BP	2.40×10^{-1}	N.D.	N.D.	N.D.	N.D.	6.90×10^{-1}	9.00×10^{-2}
SM09 13 BP	3.80×10^{-1}	N.D.	N.D.	N.D.	N.D.	1.01	1.40×10^{-1}
	74	70	95	101	99	87	110
SVGS 08 01 BP	5.20×10^{-1}	2.60×10^{-1}	7.60×10^{-1}	1.00	9.50×10^{-1}	1.70×10^{-1}	6.90×10^{-1}
SVGS 08 02 BP	2.70×10^{-1}	1.30×10^{-1}	5.70×10^{-1}	1.02	9.30×10^{-1}	1.70×10^{-1}	5.90×10^{-1}
SVGS 08 03 BP	1.38	3.30×10^{-1}	2.51	4.00	3.64	7.30×10^{-1}	1.77
SVGS 08 04 BP	1.20×10^{-1}	1.50×10^{-1}	7.80×10^{-1}	1.23	1.59	1.90×10^{-1}	6.20×10^{-1}
SVGS 08 05 BP	2.00×10^{-1}	2.00×10^{-1}	4.60×10^{-1}	5.70×10^{-1}	4.80×10^{-1}	1.30×10^{-1}	3.40×10^{-1}

SVGS 08 06 BP	1.90×10^{-1}	1.60×10^{-1}	8.00×10^{-1}	1.18	1.02	1.90×10^{-1}	6.20×10^{-1}
SVGS 08 07 BP	1.30×10^{-1}	1.20×10^{-1}	3.50×10^{-1}	5.20×10^{-1}	4.00×10^{-1}	9.00×10^{-2}	2.70×10^{-1}
SVGS 08 08 BP	1.00×10^{-1}	1.30×10^{-1}	4.00×10^{-1}	7.20×10^{-1}	7.30×10^{-1}	1.00×10^{-1}	3.30×10^{-1}
SVGS 08 09 BP	9.00×10^{-2}	1.10×10^{-1}	2.80×10^{-1}	3.50×10^{-1}	1.90×10^{-1}	1.00×10^{-1}	2.30×10^{-1}
SVGS 08 10 BP	2.40×10^{-1}	2.50×10^{-1}	1.14	1.47	1.04	2.30×10^{-1}	9.40×10^{-1}
SVGS 08 11 BP	1.50×10^{-1}	1.80×10^{-1}	1.89	1.69	2.46	N.D.	1.51
SVGS 08 12 BP	2.10×10^{-1}	2.40×10^{-1}	1.79	3.04	6.52	N.D.	1.56
SVGS 08 13 BP	1.40×10^{-1}	1.60×10^{-1}	6.40×10^{-1}	9.30×10^{-1}	1.14	2.00×10^{-1}	4.10×10^{-1}
SVGS 08 14 BP	1.40×10^{-1}	1.40×10^{-1}	5.90×10^{-1}	7.70×10^{-1}	6.80×10^{-1}	1.30×10^{-1}	4.50×10^{-1}
SVGS 08 15 BP	1.60×10^{-1}	1.40×10^{-1}	1.10	1.45	1.46	1.80×10^{-1}	1.21
SVGS 08 16 BP	9.00×10^{-2}	1.50×10^{-1}	6.40×10^{-1}	7.70×10^{-1}	1.59	N.D.	5.10×10^{-1}
SVGS 08 17 BP	9.00×10^{-2}	1.00×10^{-1}	3.50×10^{-1}	5.50×10^{-1}	5.40×10^{-1}	1.00×10^{-1}	3.20×10^{-1}
SVGS 08 18 BP	2.60×10^{-1}	2.50×10^{-1}	1.11	1.36	1.12	2.00×10^{-1}	1.06

SVGS 08 19 BP	1.20×10^{-1}	1.60×10^{-1}	5.60×10^{-1}	6.70×10^{-1}	1.01	1.60×10^{-1}	4.40×10^{-1}
SVGS 08 20 BP	9.00×10^{-2}	1.50×10^{-1}	4.20×10^{-1}	5.90×10^{-1}	7.00×10^{-1}	1.20×10^{-1}	4.50×10^{-1}
SVGS 08 21 BP	1.00×10^{-1}	1.10×10^{-1}	3.50×10^{-1}	4.40×10^{-1}	3.10×10^{-1}	1.10×10^{-1}	3.10×10^{-1}
SVGS 08 22 BP	1.00×10^{-1}	9.00×10^{-2}	5.50×10^{-1}	6.20×10^{-1}	6.00×10^{-1}	1.00×10^{-1}	4.70×10^{-1}
SVGS 08 23 BP	8.00×10^{-2}	1.10×10^{-1}	2.90×10^{-1}	3.90×10^{-1}	3.50×10^{-1}	1.00×10^{-1}	2.70×10^{-1}
SVGS 08 24 BP	3.80×10^{-1}	2.40×10^{-1}	1.73	2.08	2.25	4.10×10^{-1}	1.79
SVGS 08 25 BP	1.10×10^{-1}	1.70×10^{-1}	6.90×10^{-1}	9.30×10^{-1}	9.20×10^{-1}	2.00×10^{-1}	6.80×10^{-1}
SVGS 08 26 BP	2.20×10^{-1}	2.40×10^{-1}	1.11	1.41	1.25	1.80×10^{-1}	1.12
SVGS 08 27 BP	2.50×10^{-1}	2.60×10^{-1}	1.20	1.52	1.78	2.30×10^{-1}	1.06
SVGS 08 29 BP	4.30×10^{-1}	3.60×10^{-1}	3.10	4.20	4.14	N.D.	2.44
SVGS 08 30 BP	1.70×10^{-1}	2.00×10^{-1}	4.40×10^{-1}	5.90×10^{-1}	4.00×10^{-1}	1.40×10^{-1}	3.50×10^{-1}
SVGS 08 31 BP	1.40×10^{-1}	1.50×10^{-1}	5.80×10^{-1}	8.30×10^{-1}	8.60×10^{-1}	1.90×10^{-1}	6.00×10^{-1}
SVGS 08 32 BP	1.90×10^{-1}	3.00×10^{-1}	3.23	5.12	9.62	N.D.	3.98

SM09 01 BP	3.40×10^{-1}	2.80×10^{-1}	1.69	2.37	2.52	4.50×10^{-1}	1.54
SM09 02 BP	1.50×10^{-1}	1.30×10^{-1}	5.10×10^{-1}	7.80×10^{-1}	7.90×10^{-1}	1.60×10^{-1}	4.80×10^{-1}
SM09 03 BP	3.60×10^{-1}	3.50×10^{-1}	1.88	2.44	2.66	4.30×10^{-1}	1.36
SM09 04 BP	3.20×10^{-1}	3.30×10^{-1}	8.30×10^{-1}	7.80×10^{-1}	4.50×10^{-1}	2.40×10^{-1}	7.10×10^{-1}
SM09 05 BP	6.30×10^{-1}	4.70×10^{-1}	1.90	2.59	2.04	4.90×10^{-1}	1.69
SM09 06 BP	1.60×10^{-1}	1.90×10^{-1}	5.30×10^{-1}	8.30×10^{-1}	1.28	2.00×10^{-1}	4.30×10^{-1}
SM09 07 BP	2.20×10^{-1}	2.50×10^{-1}	6.70×10^{-1}	7.80×10^{-1}	6.00×10^{-1}	1.80×10^{-1}	6.40×10^{-1}
SM09 09 BP	2.70×10^{-1}	2.80×10^{-1}	1.34	1.70	2.06	2.30×10^{-1}	1.08
SM09 10 BP	1.90×10^{-1}	2.10×10^{-1}	7.90×10^{-1}	1.00	1.00	2.20×10^{-1}	6.50×10^{-1}
SM09 11 BP	3.30×10^{-1}	3.00×10^{-1}	2.67	3.27	3.17	4.60×10^{-1}	2.29
SM09 12 BP	1.80×10^{-1}	2.50×10^{-1}	5.50×10^{-1}	7.30×10^{-1}	3.70×10^{-1}	1.60×10^{-1}	4.30×10^{-1}
SM09 13 BP	2.30×10^{-1}	3.10×10^{-1}	7.40×10^{-1}	6.60×10^{-1}	4.30×10^{-1}	2.70×10^{-1}	6.40×10^{-1}
	151/82	149	118	153	105/132	138	158

SVGS 08 01 BP	3.40×10^{-1}	1.34	1.64	2.90	6.90×10^{-1}	2.99	2.00×10^{-1}
SVGS 08 02 BP	2.40×10^{-1}	7.60×10^{-1}	1.26	2.47	3.70×10^{-1}	2.06	9.00×10^{-2}
SVGS 08 03 BP	1.00	3.60	4.56	7.07	1.89	7.05	3.60×10^{-1}
SVGS 08 04 BP	2.50	1.23	2.04	3.64	5.70×10^{-1}	3.28	1.50×10^{-1}
SVGS 08 05 BP	9.00×10^{-2}	2.70×10^{-1}	4.30×10^{-1}	9.70×10^{-1}	1.90×10^{-1}	7.80×10^{-1}	4.00×10^{-2}
SVGS 08 06 BP	3.30×10^{-1}	1.22	1.72	2.35	6.70×10^{-1}	2.34	1.30×10^{-1}
SVGS 08 07 BP	9.00×10^{-2}	2.80×10^{-1}	5.00×10^{-1}	7.10×10^{-1}	1.70×10^{-1}	6.70×10^{-1}	4.00×10^{-2}
SVGS 08 08 BP	8.00×10^{-2}	5.10×10^{-1}	9.30×10^{-1}	1.85	3.00×10^{-1}	1.63	8.00×10^{-2}
SVGS 08 09 BP	8.00×10^{-2}	1.70×10^{-1}	2.70×10^{-1}	2.80×10^{-1}	1.30×10^{-1}	2.60×10^{-1}	2.00×10^{-2}
SVGS 08 10 BP	4.40×10^{-1}	1.42	1.44	2.24	7.00×10^{-1}	2.22	1.20×10^{-1}
SVGS 08 11 BP	1.03	4.21	2.18	9.80	1.58	8.91	5.30×10^{-1}
SVGS 08 12 BP	1.12	4.70	4.28	2.15×10^1	1.55	1.85×10^1	7.20×10^{-1}
SVGS 08 13 BP	2.10×10^{-1}	7.50×10^{-1}	9.90×10^{-1}	2.59	2.80×10^{-1}	2.08	7.00×10^{-2}

SVGS 08 14 BP	1.60×10^{-1}	6.70×10^{-1}	1.04	N.D.	3.60×10^{-1}	1.14	4.00×10^{-2}
SVGS 08 15 BP	3.60×10^{-1}	1.59	2.05	2.97	8.30×10^{-1}	2.95	1.60×10^{-1}
SVGS 08 16 BP	2.80×10^{-1}	1.18	1.10	4.06	4.20×10^{-1}	3.57	1.50×10^{-1}
SVGS 08 17 BP	1.10×10^{-1}	3.80×10^{-1}	6.30×10^{-1}	1.14	2.40×10^{-1}	1.00	5.00×10^{-2}
SVGS 08 18 BP	4.90×10^{-1}	1.46	1.16	2.69	5.80×10^{-1}	2.43	1.40×10^{-1}
SVGS 08 19 BP	1.40×10^{-1}	7.10×10^{-1}	1.10	2.16	3.40×10^{-1}	1.98	9.00×10^{-2}
SVGS 08 20 BP	1.50×10^{-1}	6.40×10^{-1}	1.06	1.53	3.20×10^{-1}	1.38	5.00×10^{-2}
SVGS 08 21 BP	1.40×10^{-1}	3.30×10^{-1}	4.80×10^{-1}	6.60×10^{-1}	1.80×10^{-1}	5.80×10^{-1}	3.00×10^{-2}
SVGS 08 22 BP	2.00×10^{-1}	7.00×10^{-1}	7.90×10^{-1}	1.16	3.40×10^{-1}	1.10	7.00×10^{-2}
SVGS 08 23 BP	1.30×10^{-1}	2.90×10^{-1}	4.40×10^{-1}	8.10×10^{-1}	1.50×10^{-1}	6.40×10^{-1}	2.00×10^{-2}
SVGS 08 24 BP	6.90×10^{-1}	2.33	2.09	3.91	1.12	3.83	2.50×10^{-1}
SVGS 08 25 BP	2.40×10^{-1}	9.50×10^{-1}	1.20	2.34	4.80×10^{-1}	2.10	9.00×10^{-2}
SVGS 08 26 BP	4.30×10^{-1}	1.56	1.77	2.87	8.00×10^{-1}	2.85	1.90×10^{-1}

SVGS 08 27 BP	5.10×10^{-1}	1.87	1.82	4.35	8.60×10^{-1}	4.04	2.30×10^{-1}
SVGS 08 29 BP	1.15	4.97	5.13	9.11	2.31	9.24	4.80×10^{-1}
SVGS 08 30 BP	1.50×10^{-1}	3.00×10^{-1}	4.20×10^{-1}	6.60×10^{-1}	2.00×10^{-1}	5.90×10^{-1}	4.00×10^{-2}
SVGS 08 31 BP	1.60×10^{-1}	6.60×10^{-1}	1.08	1.77	3.90×10^{-1}	1.58	1.00×10^{-1}
SVGS 08 32 BP	1.48	6.97	8.05	2.29×10^1	2.90	2.25×10^1	1.06
SM09 01 BP	7.30×10^{-1}	2.43	2.67	5.94	1.17	5.79	3.20×10^{-1}
SM09 02 BP	1.30×10^{-1}	5.20×10^{-1}	8.20×10^{-1}	1.99	3.00×10^{-1}	1.45	8.00×10^{-2}
SM09 03 BP	8.40×10^{-1}	2.99	2.73	5.94	1.28	5.83	3.20×10^{-1}
SM09 04 BP	2.40×10^{-1}	4.80×10^{-1}	5.40×10^{-1}	6.90×10^{-1}	2.50×10^{-1}	7.20×10^{-1}	4.00×10^{-2}
SM09 05 BP	5.30×10^{-1}	1.89	2.03	3.66	1.02	3.59	1.90×10^{-1}
SM09 06 BP	1.60×10^{-1}	7.30×10^{-1}	1.12	3.09	3.00×10^{-1}	2.67	1.30×10^{-1}
SM09 07 BP	2.40×10^{-1}	5.20×10^{-1}	7.60×10^{-1}	1.18	3.30×10^{-1}	1.19	7.00×10^{-2}
SM09 09 BP	5.10×10^{-1}	1.85	1.77	5.29	8.30×10^{-1}	5.17	2.50×10^{-1}

SM09 10 BP	3.40×10^{-1}	9.20×10^{-1}	1.24	1.96	4.40×10^{-1}	1.97	9.00×10^{-2}
SM09 11 BP	1.19	4.00	4.30	7.10	1.76	7.26	3.70×10^{-1}
SM09 12 BP	1.90×10^{-1}	3.60×10^{-1}	5.20×10^{-1}	6.20×10^{-1}	2.10×10^{-1}	6.40×10^{-1}	5.00×10^{-2}
SM09 13 BP	2.30×10^{-1}	3.40×10^{-1}	5.80×10^{-1}	6.50×10^{-1}	3.70×10^{-1}	6.30×10^{-1}	6.00×10^{-2}
	187	183	128	177	156/171	180	191
SVGS 08 01 BP	8.80×10^{-1}	4.00×10^{-1}	3.20×10^{-1}	2.20×10^{-1}	3.70×10^{-1}	1.27	4.00×10^{-2}
SVGS 08 02 BP	4.20×10^{-1}	2.60×10^{-1}	2.30×10^{-1}	1.00×10^{-1}	2.20×10^{-1}	9.90×10^{-1}	3.00×10^{-2}
SVGS 08 03 BP	1.53	7.20×10^{-1}	1.01	3.30×10^{-1}	6.30×10^{-1}	2.07	5.00×10^{-2}
SVGS 08 04 BP	6.80×10^{-1}	3.50×10^{-1}	4.00×10^{-1}	1.90×10^{-1}	3.00×10^{-1}	1.22	N.D.
SVGS 08 05 BP	1.20×10^{-1}	7.00×10^{-2}	1.10×10^{-1}	5.00×10^{-2}	9.00×10^{-2}	3.20×10^{-1}	N.D.
SVGS 08 06 BP	6.80×10^{-1}	3.00×10^{-1}	3.10×10^{-1}	1.50×10^{-1}	3.30×10^{-1}	9.80×10^{-1}	N.D.
SVGS 08 07 BP	1.30×10^{-1}	7.00×10^{-2}	8.00×10^{-2}	5.00×10^{-2}	4.00×10^{-2}	2.30×10^{-1}	N.D.
SVGS 08 08 BP	3.60×10^{-1}	1.90×10^{-1}	1.80×10^{-1}	6.00×10^{-2}	1.70×10^{-1}	7.40×10^{-1}	N.D.

SVGS 08 09 BP	5.00×10^{-2}	3.00×10^{-2}	5.00×10^{-2}	N.D.	N.D.	1.00×10^{-1}	N.D.
SVGS 08 10 BP	7.00×10^{-1}	2.70×10^{-1}	2.90×10^{-1}	1.60×10^{-1}	2.30×10^{-1}	9.40×10^{-1}	N.D.
SVGS 08 11 BP	2.82	1.12	7.70×10^{-1}	9.90×10^{-1}	7.10×10^{-1}	3.53	6.00×10^{-2}
SVGS 08 12 BP	4.07	2.02	1.92	1.02	1.42	8.32	1.70×10^{-1}
SVGS 08 13 BP	4.50×10^{-1}	2.10×10^{-1}	1.90×10^{-1}	9.00×10^{-2}	1.80×10^{-1}	8.30×10^{-1}	N.D.
SVGS 08 14 BP	2.30×10^{-1}	1.40×10^{-1}	1.60×10^{-1}	6.00×10^{-2}	1.50×10^{-1}	3.60×10^{-1}	N.D.
SVGS 08 15 BP	9.20×10^{-1}	3.50×10^{-1}	4.10×10^{-1}	2.10×10^{-1}	3.50×10^{-1}	1.10	3.00×10^{-2}
SVGS 08 16 BP	7.50×10^{-1}	3.40×10^{-1}	4.60×10^{-1}	2.10×10^{-1}	2.70×10^{-1}	1.46	3.00×10^{-2}
SVGS 08 17 BP	2.10×10^{-1}	1.10×10^{-1}	1.30×10^{-1}	5.00×10^{-2}	1.10×10^{-1}	3.90×10^{-1}	N.D.
SVGS 08 18 BP	6.40×10^{-1}	2.80×10^{-1}	3.00×10^{-1}	1.80×10^{-1}	2.20×10^{-1}	9.30×10^{-1}	N.D.
SVGS 08 19 BP	3.30×10^{-1}	2.10×10^{-1}	2.60×10^{-1}	9.00×10^{-2}	2.10×10^{-1}	7.10×10^{-1}	N.D.
SVGS 08 20 BP	2.50×10^{-1}	1.20×10^{-1}	2.30×10^{-1}	8.00×10^{-2}	1.40×10^{-1}	4.60×10^{-1}	N.D.
SVGS 08 21 BP	1.50×10^{-1}	7.00×10^{-2}	9.00×10^{-2}	5.00×10^{-2}	7.00×10^{-2}	2.60×10^{-1}	N.D.

SVGS 08 22 BP	2.60×10^{-1}	1.20×10^{-1}	1.40×10^{-1}	5.00×10^{-2}	1.10×10^{-1}	3.90×10^{-1}	N.D.
SVGS 08 23 BP	1.10×10^{-1}	7.00×10^{-2}	9.00×10^{-2}	N.D.	5.00×10^{-2}	2.50×10^{-1}	N.D.
SVGS 08 24 BP	8.90×10^{-1}	4.10×10^{-1}	5.10×10^{-1}	2.00×10^{-1}	3.60×10^{-1}	1.11	N.D.
SVGS 08 25 BP	5.40×10^{-1}	2.60×10^{-1}	2.80×10^{-1}	1.30×10^{-1}	2.30×10^{-1}	8.80×10^{-1}	N.D.
SVGS 08 26 BP	8.90×10^{-1}	3.50×10^{-1}	3.80×10^{-1}	2.40×10^{-1}	3.40×10^{-1}	1.19	N.D.
SVGS 08 27 BP	9.40×10^{-1}	4.20×10^{-1}	5.30×10^{-1}	2.50×10^{-1}	3.40×10^{-1}	1.42	4.00×10^{-2}
SVGS 08 29 BP	2.61	1.08	1.11	6.90×10^{-1}	9.80×10^{-1}	3.74	6.00×10^{-2}
SVGS 08 30 BP	1.00×10^{-1}	7.00×10^{-2}	1.00×10^{-1}	5.00×10^{-2}	N.D.	2.10×10^{-1}	N.D.
SVGS 08 31 BP	3.70×10^{-1}	1.80×10^{-1}	2.40×10^{-1}	9.00×10^{-2}	2.20×10^{-1}	6.50×10^{-1}	N.D.
SVGS 08 32 BP	5.46	2.33	2.70	1.33	1.97	8.15	1.30×10^{-1}
SM09 01 BP	1.62	6.30×10^{-1}	9.60×10^{-1}	2.90×10^{-1}	5.20×10^{-1}	2.12	7.00×10^{-2}
SM09 02 BP	1.17	4.90×10^{-1}	2.30×10^{-1}	6.00×10^{-2}	1.50×10^{-1}	9.40×10^{-1}	N.D.
SM09 03 BP	2.01	6.30×10^{-1}	8.50×10^{-1}	3.90×10^{-1}	5.10×10^{-1}	2.21	8.00×10^{-2}

SM09 04 BP	2.10×10^{-1}	8.00×10^{-2}	1.10×10^{-1}	6.00×10^{-2}	8.00×10^{-2}	3.00×10^{-1}	N.D.
SM09 05 BP	1.86	8.80×10^{-1}	7.40×10^{-1}	1.50×10^{-1}	3.20×10^{-1}	1.07	N.D.
SM09 06 BP	4.70×10^{-1}	2.50×10^{-1}	4.20×10^{-1}	1.20×10^{-1}	2.40×10^{-1}	1.00	N.D.
SM09 07 BP	2.60×10^{-1}	1.10×10^{-1}	1.70×10^{-1}	5.00×10^{-2}	1.10×10^{-1}	4.20×10^{-1}	N.D.
SM09 09 BP	1.35	5.80×10^{-1}	6.60×10^{-1}	3.00×10^{-1}	3.90×10^{-1}	2.16	4.00×10^{-2}
SM09 10 BP	4.50×10^{-1}	1.90×10^{-1}	2.90×10^{-1}	1.10×10^{-1}	1.90×10^{-1}	7.00×10^{-1}	N.D.
SM09 11 BP	2.39	9.10×10^{-1}	1.05	5.40×10^{-1}	7.30×10^{-1}	2.95	5.00×10^{-2}
SM09 12 BP	2.00×10^{-1}	6.00×10^{-2}	9.00×10^{-2}	4.00×10^{-2}	7.00×10^{-2}	1.80×10^{-1}	N.D.
SM09 13 BP	1.70×10^{-1}	9.00×10^{-2}	1.20×10^{-1}	N.D.	N.D.	2.40×10^{-1}	N.D.
	170	201	195/208	194	205	206	209
SVGS 08 01 BP	4.70×10^{-1}	1.50×10^{-1}	5.00×10^{-2}	1.50×10^{-1}	3.00×10^{-2}	4.00×10^{-2}	4.00×10^{-2}
SVGS 08 02 BP	3.30×10^{-1}	1.40×10^{-1}	6.00×10^{-2}	1.50×10^{-1}	2.00×10^{-2}	5.00×10^{-2}	3.00×10^{-2}
SVGS 08 03 BP	7.70×10^{-1}	2.30×10^{-1}	7.00×10^{-2}	1.90×10^{-1}	3.00×10^{-2}	8.00×10^{-2}	4.00×10^{-2}

SVGS 08 04 BP	4.40×10^{-1}	1.50×10^{-1}	5.00×10^{-2}	1.10×10^{-1}	N.D.	4.00×10^{-2}	6.00×10^{-2}
SVGS 08 05 BP	1.30×10^{-1}	5.00×10^{-2}	N.D.	5.00×10^{-2}	N.D.	2.00×10^{-2}	N.D.
SVGS 08 06 BP	3.40×10^{-1}	1.50×10^{-1}	2.00×10^{-2}	1.00×10^{-1}	N.D.	3.00×10^{-2}	N.D.
SVGS 08 07 BP	8.00×10^{-2}	N.D.	N.D.	3.00×10^{-2}	N.D.	N.D.	N.D.
SVGS 08 08 BP	2.30×10^{-1}	9.00×10^{-2}	2.00×10^{-2}	9.00×10^{-2}	N.D.	5.00×10^{-2}	3.00×10^{-2}
SVGS 08 09 BP	3.00×10^{-2}	N.D.	N.D.	N.D.	N.D.	N.D.	N.D.
SVGS 08 10 BP	3.40×10^{-1}	1.60×10^{-1}	5.00×10^{-2}	1.00×10^{-1}	N.D.	4.00×10^{-2}	3.00×10^{-2}
SVGS 08 11 BP	1.26	4.50×10^{-1}	1.50×10^{-1}	3.10×10^{-1}	N.D.	1.20×10^{-1}	1.00×10^{-1}
SVGS 08 12 BP	3.03	1.15	3.10×10^{-1}	9.30×10^{-1}	N.D.	2.50×10^{-1}	2.00×10^{-1}
SVGS 08 13 BP	2.90×10^{-1}	1.00×10^{-1}	4.00×10^{-2}	7.00×10^{-2}	N.D.	3.00×10^{-2}	3.00×10^{-2}
SVGS 08 14 BP	1.40×10^{-1}	4.00×10^{-2}	N.D.	6.00×10^{-2}	N.D.	N.D.	N.D.
SVGS 08 15 BP	4.10×10^{-1}	2.00×10^{-1}	8.00×10^{-2}	1.30×10^{-1}	N.D.	4.00×10^{-2}	4.00×10^{-2}
SVGS 08 16 BP	5.00×10^{-1}	2.00×10^{-1}	6.00×10^{-2}	1.40×10^{-1}	N.D.	6.00×10^{-2}	N.D.

SVGS 08 17 BP	1.30×10^{-1}	6.00×10^{-2}	2.00×10^{-2}	4.00×10^{-2}	N.D.	3.00×10^{-2}	N.D.
SVGS 08 18 BP	3.20×10^{-1}	1.40×10^{-1}	N.D.	8.00×10^{-2}	N.D.	N.D.	N.D.
SVGS 08 19 BP	2.40×10^{-1}	8.00×10^{-2}	N.D.	6.00×10^{-2}	N.D.	3.00×10^{-2}	N.D.
SVGS 08 20 BP	1.60×10^{-1}	6.00×10^{-2}	N.D.	4.00×10^{-2}	N.D.	3.00×10^{-2}	3.00×10^{-2}
SVGS 08 21 BP	8.00×10^{-2}	4.00×10^{-2}	N.D.	4.00×10^{-2}	N.D.	N.D.	N.D.
SVGS 08 22 BP	1.40×10^{-1}	6.00×10^{-2}	3.00×10^{-2}	4.00×10^{-2}	N.D.	3.00×10^{-2}	N.D.
SVGS 08 23 BP	8.00×10^{-2}	3.00×10^{-2}	N.D.	3.00×10^{-2}	N.D.	N.D.	N.D.
SVGS 08 24 BP	3.80×10^{-1}	1.70×10^{-1}	N.D.	1.00×10^{-1}	1.00×10^{-1}	6.00×10^{-2}	N.D.
SVGS 08 25 BP	3.20×10^{-1}	1.20×10^{-1}	6.00×10^{-2}	9.00×10^{-2}	N.D.	4.00×10^{-2}	4.00×10^{-2}
SVGS 08 26 BP	4.10×10^{-1}	2.00×10^{-1}	7.00×10^{-2}	1.40×10^{-1}	N.D.	5.00×10^{-2}	4.00×10^{-2}
SVGS 08 27 BP	5.10×10^{-1}	1.80×10^{-1}	6.00×10^{-2}	1.30×10^{-1}	N.D.	4.00×10^{-2}	5.00×10^{-2}
SVGS 08 29 BP	1.39	5.70×10^{-1}	1.60×10^{-1}	4.60×10^{-1}	N.D.	1.50×10^{-1}	9.00×10^{-2}
SVGS 08 30 BP	8.00×10^{-2}	4.00×10^{-2}	N.D.	N.D.	N.D.	N.D.	N.D.

SVGS 08 31 BP	2.40×10^{-1}	9.00×10^{-2}	5.00×10^{-2}	7.00×10^{-2}	N.D.	5.00×10^{-2}	N.D.
SVGS 08 32 BP	2.87	1.24	2.90×10^{-1}	8.00×10^{-1}	6.00×10^{-2}	2.60×10^{-1}	1.60×10^{-1}
SM09 01 BP	7.90×10^{-1}	2.80×10^{-1}	1.10×10^{-1}	2.20×10^{-1}	N.D.	8.00×10^{-2}	7.00×10^{-2}
SM09 02 BP	4.40×10^{-1}	1.10×10^{-1}	4.00×10^{-2}	3.70×10^{-1}	4.00×10^{-2}	6.00×10^{-2}	5.00×10^{-2}
SM09 03 BP	5.40×10^{-1}	4.00×10^{-1}	1.30×10^{-1}	2.60×10^{-1}	N.D.	1.10×10^{-1}	N.D.
SM09 04 BP	7.00×10^{-2}	5.00×10^{-2}	N.D.	4.00×10^{-2}	N.D.	3.00×10^{-2}	N.D.
SM09 05 BP	3.50×10^{-1}	1.40×10^{-1}	6.00×10^{-2}	1.10×10^{-1}	N.D.	5.00×10^{-2}	N.D.
SM09 06 BP	2.70×10^{-1}	1.20×10^{-1}	6.00×10^{-2}	8.00×10^{-2}	N.D.	5.00×10^{-2}	4.00×10^{-2}
SM09 07 BP	1.50×10^{-1}	6.00×10^{-2}	N.D.	4.00×10^{-2}	N.D.	N.D.	N.D.
SM09 09 BP	7.90×10^{-1}	3.00×10^{-1}	8.00×10^{-2}	2.10×10^{-1}	N.D.	4.00×10^{-2}	3.00×10^{-2}
SM09 10 BP	2.50×10^{-1}	1.00×10^{-1}	3.00×10^{-2}	7.00×10^{-2}	N.D.	3.00×10^{-2}	N.D.
SM09 11 BP	1.06	4.90×10^{-1}	1.40×10^{-1}	3.30×10^{-1}	N.D.	1.00×10^{-1}	4.00×10^{-2}
SM09 12 BP	7.00×10^{-2}	4.00×10^{-2}	N.D.	3.00×10^{-2}	N.D.	N.D.	N.D.

SM09 13 BP	1.00×10^{-1}	7.00×10^{-2}	N.D.	N.D.	N.D.	N.D.	N.D.
------------	-----------------------	-----------------------	------	------	------	------	------

Appendix 7

Enantiomer Fractions (EFs) of PCBs in Cumberland Sound (Canada) and Svalbard (Norway) Biota

Collected from 1998 to 2009

Appendix 7

Table A7-1: EFs of chiral PCBs of organisms collected from Cumberland in 2007-2008. A blank value means not detected.

Samples	ID	PCB 95	PCB 91	PCB 136	PCB 149	PCB 176	PCB 174
Standard	A	0.498	0.503	0.505	0.495	0.497	0.502
SRM1945 control	33	0.406	0.456	0.536			
	37	0.424	0.490	0.520	0.535	0.542	0.541
Greenland shark	017	0.537			0.412		
	018				0.485		
	019	0.520			0.481		
	020	0.523			0.490		
	021						
	022	0.505			0.431		
	027	0.510			0.443		

	028	0.513			0.390		
	029	0.524			0.462		
	030						
	035	0.586			0.407		
	038	0.502	0.317	0.533	0.456		0.565
	039	0.540	0.261	0.526	0.450		0.523
	043	0.502	0.329	0.481	0.479		
	044	0.509	0.286	0.565	0.416		0.565
Beluga	001	0.502	0.407	0.406	0.416		0.556
	034	0.497	0.382	0.455	0.434		
	037						
	038	0.466	0.431	0.421	0.436		
	040	0.523	0.414	0.411	0.395	0.486	0.548

Narwhal	009	0.461	0.368	0.482	0.454		
	010						
	011	0.480	0.381	0.521	0.453		0.442
	012	0.460	0.364	0.460	0.478		0.556
	039	0.460	0.352	0.495	0.482		0.514
	040	0.459	0.411	0.461	0.468		0.487
Harp seal	023	0.626					
	024	0.588					
	025	0.535			0.502		
	26	0.544			0.476		
	036	0.575			0.412		
	41	0.612			0.495		
	42	0.586			0.405		

Rinded seal	013	0.812			0.508		
	014	0.839			0.538		
	015	0.603			0.489		
	016						
	031						
	032						
Skate	29						
	30	0.478			0.515		
	31	0.552					
	32	0.542					
	33	0.479			0.482		
Snail	26	0.475			0.542		
	27	0.494			0.498		

	28	0.504			0.503		
Zooplankton	20	0.522			0.480		
	21	0.491			0.509		
	22	0.499		0.472	0.489		
	23						
	24	0.483					
	25	0.505			0.471		
Capelin	03	0.487			0.494		
	04						
	05	0.495			0.465		
	06	0.467			0.524		
	07	0.475			0.524		
Scallop	01	0.493			0.475		

	02	0.528			0.512		
	17	0.448			0.518		
	18						
	34	0.508			0.521		
	35	0.463			0.471		
	36	0.545			0.524		
Sculpin	09						
	10	0.488			0.519		
	11	0.526			0.471		
	12	0.508			0.478		
	14	0.471			0.510		
	15	0.556			0.521		
	16	0.488			0.513		

	19	0.512			0.519		
Char	CH01	0.430			0.570		
Herring	08	0.478			0.482		

Table A7-2: EFs of chiral PCBs of Greenland sharks collected from Cumberland in 1998-1999. A blank value means not detected. EF data was provided by Dr. Charles S. Wong and Dr. Aaron T. Fisk.

Samples	PCB 91	PCB 95	PCB 136	PCB 149
01	0.448	0.567	0.460	0.389
02	0.507		0.460	0.467
03	0.308	0.653	0.347	0.395
04	0.492	0.495	0.438	0.386
05	0.53	0.496	0.482	0.425
06	0.572	0.503	0.474	0.414
07	0.484	0.446	0.461	0.486
08	0.344	0.578	0.455	0.442
09	0.461	0.541	0.466	0.409
10	0.345	0.449	0.451	0.454

11	0.443	0.519	0.483	0.389
12	0.533	0.509	0.465	0.417
13	0.282	0.61	0.481	0.357
14	0.51	0.504	0.470	0.347

Table A7-3: EFs of chiral PCBs of Greenland sharks collected from Svalbard in 2008-2009. A blank value means not detected.

L—liver samples; P-plasma samples; B-blank control.

Samples	PCB 95	PCB 91	PCB 136	PCB 149	PCB 176	PCB 174
Standard	0.500	0.500	0.500	0.498	0.498	0.499
01L(a)	0.501			0.429		
01L(b)	0.504			0.410		
06L	0.439			0.523		
07L						
08L						
09L						
10L	0.465			0.466		
13L	0.471			0.535		
14L	0.380			0.554		

15L	0.480		0.594	0.376		
17L	0.563			0.413		
18L	0.492			0.439		
20L	0.446					
23L						
24L	0.472	0.370	0.396	0.439		
25L	0.485		0.531	0.428		
26L	0.442			0.446		
27L	0.453			0.523		
30L	0.445					
31L	0.460			0.483		
32L	0.509		0.547	0.377		
H1	0.472	0.393	0.512	0.546		0.453

H2	0.461	0.415	0.515	0.557		0.488
H3	0.457	0.445	0.522	0.545		0.485
H4	0.457	0.399	0.546	0.564		0.497
B1						
B2						
B3						
B4						
04L	0.491			0.501		
02P	0.485			0.526		
03P	0.488	0.333	0.448	0.489		
05P	0.541			0.410		
11P	0.617		0.573	0.306		
12P	0.496			0.484		

16P	0.530			0.506		
19P	0.488			0.507		
20P	0.453			0.531		
21P	0.492			0.519		
22P	0.481			0.430		
29P	0.474	0.241	0.547	0.418		
H7	0.462	0.428	0.573	0.541		0.483
H8	0.461	0.449	0.525	0.548		0.464
B7						
B8						
SM-01L	0.442			0.509		
SM-02L						
SM-03L	0.485			0.458		

SM-04L	0.465			0.402		
SM-05L	0.465			0.426		
SM-06L	0.465			0.423		
SM-07L	0.480			0.436		
SM-08L						
SM-09L	0.487			0.463		
SM-10L	0.444			0.499		
SM-11L	0.456	0.245	0.596	0.430		
SM-12L						
SM-13L						
SM-H09	0.463	0.439	0.567	0.546		0.513
SM-H10	0.468	0.431	0.546	0.547		0.477
SM-H11	0.468	0.433	0.569	0.548		0.496

SM-B09						
SM-B10						
SM-B11						